MATHEMATICAL MODELING ICE-HULL INTERACTION FOR REAL TIME SIMULATIONS OF SHIP MANOEUVRING IN LEVEL ICE

JIANCHENG LIU


CENTRE FOR NFLD. STUDIES
MEMORIAL UNIVERSITY
OF NEWFOUNDLAND

MATHEMATICAL MODELING ICE-HULL INTERACTION FOR REAL TIME SIMULATIONS OF SHIP MANOEUVRING IN LEVEL ICE

By

© Jiancheng Liu, B. Eng, M.Eng

A THESIS SUBMITTED TO THE SCHOOL OF GRADUATE STUDENT IN PARTIAL FULFILMENT OF THE REQUIREMENTS FOR THE DEGREE OF DOCTOR OF PHILOSOPHY IN ENGINEERING

FACULTY OF ENGINEERING AND APPLIED SCIENCE

MEMORIAL UNIVERSITY OF NEWFOUNDLAND

SEPTEMBER 2009

ST. JOHN'S NEWFOUNDLAND CANADA

Abstract

A new ice-hull interaction (IHI) model for the real-time simulations of ship manoeuvring in level ice was developed as a basic and necessary step towards the final target of the research of Institute for Ocean Technology (NRC/IOT): a general model that reliably simulates a ship's arbitrary manoeuvres in any ice conditions, which is to be integrated into the training simulator at the Centre for Marine Simulation (CMS) as an internal ice force module of the numerical framework.

Using an analytical approach and its numerical implementation, the model was built on a detailed analysis of hull-ice interaction mechanics. The model considered the breaking force, buoyancy force and clearing force. The whole hull was divided into ten or more segments and the global ice forces were calculated through vectorially adding the forces on the segments. The hull-ice contacts were calculated based on the ship motion and ice edge in time domain and the channel was tracked using a simple house-keeping method. A multi-failure model was adopted to calculate ice failures along the hull waterline. A flat-plate model was used for the buoyancy force calculation. Both viscous and inertial effects were incorporated into the clearing force. The adoption of the analytical approach yielded a short calculation time that is essential for simulator application. Since the forces were calculated at each new time increment of any prescribed motion,

the resulting simulation had the capacity to respond to arbitrary control inputs and hence arbitrary manoeuvres in ice.

The model was coded using MatLab. Two PMM test series carried out at IOT, using Terry Fox and R-Class scale models, were used to verify the IHI model. The ice force distributions along the waterline of the hull were benchmarked using test data from the National Maritime Research Institute (NMRI) of Japan. It is the first time such an extensive experimental database is used for mathematical model verification, which enables separate component validation.

Investigations of ice-hull interaction including parametric analysis and simulations of specific manoeuvres was carried out using the IHI model and the experiments, which also served as further checks and verifications of the IHI model. Some general conclusions on the ship-ice interaction were drawn up, which were of high value to the modeling of ship manoeuvres and operations in ice.

This thesis also provides recommendations for future IHI model refinements and benchmarks.

Acknowledgements

I would firstly like to express my sincere gratitude to my supervisor, Dr M. Williams, for all ways she helped me. Dr. M. Williams continuously oriented me in the correct research direction, concretely guided and substantially helped me to finish the whole research work. Her insightful supervision, kindly encouragement and understanding are vital for me to complete this study.

I would like to express my sincere thanks to Dr. M. Lau, who directly took care of me with many valuable guidance and constructive comments throughout the whole study. His continuous supervision and friendly supports have made this Ph.D study possible.

I would like to say heartfelt thanks to Dr. S. Bruneau for the thoughtful guidance and valuable discussions with me at the key points during this study. I shall never forget his kindly helps forever.

I am sincerely thankful to Dr. C. Daley, Dr. C. Williams and Dr. A. Derradji for the expert advice and professional assistance with valuable discussions during the study. I also would like to acknowledge the valuable suggestions and generous helps from other people of Memorial University of Newfoundland and Institute for Ocean Technology, Dr. S. J. Jones, Dr. Ian Jordaan, Dr. D. Molyneux, Dr. R.

Gagon, Dr. W. Qiu, Mr. B. Hill, Mr. G. Wong, Mr. R. Wadman and all associated faculties, staffs, tech experts and friends, which made this PhD study a rewarding one.

The financial support from the Institute for Ocean Technology (NRC/IOT), NSERC and the Atlantic Innovation Fund, under the project "Modeling and Simulation of Harsh Environments", is gratefully acknowledged.

Lastly, and far from least, thank you to my loving wife Haiyan, my parents Zhensheng and Shuan, my brothers Jianli and Jiandong and my sister Cuiling for their continuous love, supports and patience. No words can enough describe my gratitude to them and I shall deeply love them forever.

Table of Contents

List of Tables

List of Figures

Nomenclature

A_c , A_{crush}	Nominal area of the ice crushed by the hull
A_{Ice}	Nominal are of the ice piece
$A_{projected}$	Projected area of the ice sheet
$\tilde{A}$, $\tilde{R}$, Γ, Λ	Temporary variables during algebraic derivations from equations from 3-67 to 3-71
B	Waterline beam
C_D	The water drag coefficient
$C_{R\_add\_mass}$	The water added mass coefficient during the ice floe rotary motion
$C_{T\_add\_mass}$	The water added mass coefficient during the ice floe translational motion
C_{V0} , C_V	Empirical coefficients in Equation 3-31
C_{add_mass}	The water added mass coefficient
C_{br}	Constant coefficients for breaking force calculation defined in Spencer et al. (IOT) resistance model
C_{dg}	A constant which value is dependent to static pressure distribution and the ice cusp geometrics adopted in Equation 3-50
C_{cl}	Constant coefficients for clearing force calculation defined in Spencer et al. (1993) IOT resistance model
C_s	Constant coefficients for submersion force calculation defined in Spencer et al. (1993) IOT resistance model
C_0 , C_1 , C_2	Constant coefficients defined in Lewis et al. resistance model
D	Ice cusp depth
D_{plate}	Characteristic ice cusp depth defined by Equation 3-30

D_0	Ice cusp depth proportional to the characteristic length of ice without considering the ship velocity effects
D_1	The length between the low edge of rotating ice floe and its rounded axis
E	Strain modulus of ice
E_k	Kinetic energy Kinetic energy
E_r	gy caused by the rotary motion
F_H	Ice force component in horizontal direction
F_N	Ice force on the hull in the direction normal to hull surface
F_V	Ice force component in vertical direction
F_{buoya}	The ice buoyancy force
F_{break}	The ice breaking force
F_c, F_{crush}	The ice crushing failure force
F_{clear}	The ice clearing force
F_f, F_{flex}	The ice flexural bending failure force
F_{shear}	The ice shearing force
F_{sp}	The water static pressure force on the turning floe
F_{nbuoya}	The force normal to the hull due to the buoyancy force
F_{nw}	The force normal to hull surface due to water drag on the turning ice floe
F_{xbuoya}	Surge force on the hull due to the buoyancy force
F_{xcrush}	Surge force caused by ice crushing failure
F_{xw}	The surge force caused by the water drag on the turning ice floe
F_{ybuoya}	Sway force on the hull due to the buoyancy force
F_{yw}	The surge force caused by the water drag on the turning ice

	floe
G_{br}, G_{cl}, G_s	Empirical coefficients for calculating the ice yaw moment defined in Williams and Waclawek's model (1996)
H_s	The depth where the water pressure is regarded as the average pressure on the whole turning ice piece
H_w	The wave height during the ice piece turning
J_i	The rotational moment of inertia of the rotating ice floe
L	Waterline length
M_{ice}	Mass of ice
M_{w_add}	Water added mass
$M_{T\_w\_add}$	Water added mass due to the ice floe translational motion
$M_{R\_w\_add}$	Water added mass due to the ice floe rotary motion
$M_{\max}$	Maximum moment
N	Yaw Moment defined in Menon et al model (1986)
$N_v, N_r, N_{\dot{v}}, N_{\dot{r}}, N_\delta$	Yaw moment derivatives to sway velocity, yaw rate, sway acceleration, yaw acceleration and rudder angle
N_i, N_{ice}	Ice induced yaw moment
N_{br}	Yaw moment by breaking force component
N_s	Yaw moment by submersion force component
N_{cl}	Yaw moment caused by clearing force component
N_{break}, N_{buoya}, N_{clear}	Representing ice breaking contribution, the ice buoyancy contribution and the ice clearing contribution to yaw moment respectively
P_H	Ice force component in horizontal direction on unit width
P_N	Ice force on the hull in the direction normal to hull surface on unit width

P_V	Ice force component in vertical direction on unit width
P_{buoya}	Buoyancy force on the ice pieces on unit width
P_{impact}	The ice force due is impact phenomena between rotating ice floe and hull during the icebreaking cycle on unit width hull
P_k	Mass force of ice on unit width of the hull
P_{nsw}	The force normal to hull surface on the unit width cause by bow wave and water static pressure on the turning ice cusp
P_{xsw}	Surge force on unit width of the hull caused by the wave height and water static pressure on each turning ice cusp
P_{ysw}	Sway force on unit width of the hull caused by the wave height and water static pressure on each turning ice cusp
R	Ice resistance
R_b	Bending failure force defined in Lindqvist's model (1989)
R_c	Crushing failure force defined in Lindqvist's model (1989)
R_{br}	Resistance caused by breaking force component
R_{cl}	Resistance caused by clearing force component
R_s	Resistance caused by submersion force component
R_{speed}	Speed dependent force defined in Lindqvist's model (1989)
S_1, S_2	The surface areas of the bow on respective sides of the mid-longitudinal plane as shown in Figure 3.30
U	Ship surge velocity
V	Ship speed
V_n	Ship velocity component in normal hull surface direction
$\vec{V}$	Translational motion vector of the ship mass center in global coordinate system
V_i	Velocity of the sliding ice piece
$\vec{V}_0$	Velocity vector of origin point of the global coordinate

	system
$\vec{V}_{\tilde{X}\tilde{Y}\tilde{Z}}$	Velocity vector of any point in the global coordinate system
V_h'	The horizontal velocity of the sliding ice piece relative to the moving hull
V_z'	The vertical velocity of the sliding ice piece relative to the moving hull
W	Ice cusp width
W_{crush}	The crushed width of the ice wedge
X_{ice}	Ice caused surge force
$X_{break}, X_{buoya}, X_{clear}$	Representing ice breaking contribution, the ice buoyancy contribution and ice clearing contribution to surge force respectively
$\tilde{X}, \tilde{Y}, \tilde{Z}$	Coordinates of point in the global coordinate system for the coordinate transferring
Y	Sway Force defined in Menon et al. model (1986)
$Y_{break}, Y_{buoya}, Y_{clear}$	Representing ice breaking contribution, the ice buoyancy contribution and the ice clearing contribution to sway force respectively
Y_{ice}	Ice caused sway force
$Y_v, Y_r, Y_{\dot{v}}, Y_{\dot{r}}, Y_\delta$	Sway force derivatives to sway velocity, yaw rate, sway acceleration, yaw acceleration and rudder angle
a	Horizontal displacement of the hull from ice-hull contact moment until ice broken due to flexural failure
c	The virtual mass per unit area defined in Lindstrom model (1989)
e	The restitution coefficient defined in Equation 3-72
g	Gravity acceleration
h	Ice thickness

$\hbar$	Constant coefficient empirically decided by the statistical data of the full-scale observations by Kotras et al. (1983)
l_c	Characteristic length of ice
l_b	Length of the breaking piece in beam theory
l_1, l_2	The widths of the covered area of the respective sides, S_1 and S_2
$\vec{i}$, $\vec{j}$, $\vec{k}$	Representing the $\tilde{X}$ axial direction, $\tilde{Y}$ axial direction and $\tilde{Z}$ axial direction of the global coordinate system respectively
$\vec{i}'$, $\vec{j}'$, $\vec{k}'$	Representing the $\tilde{x}$ axial direction, $\tilde{y}$ axial direction and $\tilde{z}$ axial direction of the moving coordinate system respectively
n	Number of radical cracks
r	Yaw rate
$\dot{r}$	Yaw acceleration
$\vec{r}_{\tilde{x}\tilde{y}\tilde{z}}$	Position vector of any point in the moving coordinate system
$\vec{r}_{\tilde{X}\tilde{Y}\tilde{Z}}$	Position vector of any point in global coordinate system
$\vec{r}_0$	Position vector of origin point of the moving coordinate system in global coordinate system
$\tilde{t}$	Period of one ice breaking force cycle
v	Sway velocity
$\vec{v}$	Translational motion vector of the ship mass center in moving coordinate system
$\dot{v}$	Sway acceleration
w	The vertical deflection of the ice sheet
$\tilde{x}$, $\tilde{y}$, $\tilde{z}$	Coordinates of point in the moving coordinate system for the coordinate transferring
z	Vertical deflection of ice before it is broken due to flexural

	failure
ρ_i	Ice mass density
ρ_w	Water mass density
σ_f	Ice flexural strength
σ_c	Compressive strength of ice
τ_ϑ	The shear stress along the shear plane
τ_{max}	The maximum shear stress
α	Waterline entrance angle
$\tilde{\alpha}$, $\tilde{\beta}$,$\tilde{\gamma}$	Euler angles as shown in Figure 3.4
ω_i	The rotary angle velocity of rotating ice floe
δ	Rudder angle
ψ	Angle between the vertical direction and the normal direction of the hull surface as shown in Figure 3.6
ψ'	The angle between the ice piece velocity and vertical direction as shown in Figure 3.26
φ	The opening angle of the ice wedge
φ_n	The opening angle of the ice wedge
ϕ	Stem angle
η	Frame angle of the hull
μ	Frictional coefficient between ice and hull
χ	The angle between the frictional force and the tangent of the hull in a vertical plane normal to the surface of the hull
γ	Angle between the turning ice piece and hull surface
$\tilde{\gamma}_w$	Weight density of water
$\tilde{\gamma}$	Weight density of ice
ν	Poisson's ratio of ice
ϑ	Inclination angle between vertical direction and the tangent

	of shear plane as shown in the Figure 3.11
ϑ_0	The inclination angle of the shear plane corresponding to the max shear stress
$\tilde{\vartheta}$	The sloping angle of the structure
Θ	The flexural rigidity of the ice plate defined in Lindstrom model
λ	The ratio between the pressure from the underneath water and the deflection of the ice
Φ	Vector normal to the hull surface, ζ, as shown in Figure 3.7
Φ_1, Φ_2, Φ_3	Angles between Vector Φ and the x-, y- and z-axis of the moving coordinate system
$\vec{\Omega}$	Vector matrix of the angular velocities of the moving coordinate system
∇	Total ice volume on the bow as shown in Figure 3.30
∇_1, ∇_2	The ice volumes on the respective sides, S_1 and S_2
$\Delta\rho$	The density difference between ice and water

Chapter 1 Introduction

1.1 Introduction

Precise manoeuvring of a ship in ice is necessary in confined passageways and in the presence of navigation hazards. Navigation simulators, training simulators and autopilot systems are valuable tools to achieve precise control of a ship in a particular set of ice conditions. Institute for Ocean Technology of National Research Council (NRC/IOT) is developing a real time simulator for the ship's navigation in harsh environments, as one of its research strategies. As part of the whole research, this thesis presented a physically-based ice-hull force model designed to serve as the key ice component for the real-time simulator for ship navigation in level ice, which was the basic and necessary step towards realistic simulation of ship manoeuvres in any ice conditions.

This thesis first presents a literature review of the existing mathematical models for ship manoeuvring in ice. Then, a new analytically based ice-hull interaction model and its numerical and computational implementations for continuous shipping transit through level ice are described. The adoption of the analytical approach yields a short calculation time, which made the model very suitable for real-time simulations. Since the forces are calculated at each time increment in any

prescribed motion, the resulting simulation had the capacity to respond to arbitrary control inputs and hence arbitrary manoeuvres in ice.

The Planar Motion Mechanism (PMM) model test series, Terry Fox model and R-Class tests, were selected for the mathematical model benchmark study (Hoffmann, 1998; Lau et al., 2007; Molyneux et al., 1998, 1998a, 1998b, 1998c; Newbury, 1988, 1989, 1991, 1992; Newbury et al., 1986a, 1986b; Derradji et al., 2002, 2004a, 2004b, 2005). The tests included resistance runs, constant radius runs and sinusoidal runs. In addition, data from tests by National Maritime Research Institute (NMRI) of Japan (Izumiyama et al., 1998, 1999, 2001, 2005) were adopted for the model benchmark task in particular on the ice force distribution along the waterline.

The ice-hull interaction was investigated through parametric analysis and specific manevuer simulations based on the developed IHI model, which also served as a further check of the model.

This research was carried out under a collaborative project between IOT and Center for Marine Simulation of Memorial University of Newfoundland (MUN/CMS): in which the real time modeling technology of ship manoeuvring in ice is under development. As the model's first application, it will be integrated

into the numerical framework of the CMS Training Simulator as an internal ice force module.

This thesis summarizes the progress and achievements of the research. The conception and the corresponding theories of the model can also be introduced in previous publications (Lau et al., 2004; Liu et al., 2006, 2007a, 2007b).

1.2 Objectives

The main objectives of this research are:

- Developing a new ice-hull interaction (IHI) model that reliably calculates the ice forces on the hull during the ship's arbitrary manoeuvres. The model firstly satisfies the simulation requirements, which means the model can correctly feel the ship's motions. The resulted model not only has good universality, for different ships with a variety of manoeuvres in Canadian waters or other ice regions in the world, but also good numerical efficiency, estimating ice forces on the hull within a short time.

- To further understand the ice-ship interaction physical processes through parametric analysis and specific manoeuvre simulations based on the developed ice-hull interaction model.

In Canadian waters, ships may encounter ice in many forms, i.e., level ice, pack ice, ridge ice, etc (Aboulazm and Muggeridge , 1989; Bruneau, 1996; Williams et al., 1992; Molyneux and Williams, 1999; Wadhams, 2000). Solid level ice presents a serious challenge for ship manoeuvring. It is also a condition that may be unambiguously defined in engineering terms. Hence, level ice provides a reference condition for this research. The surge force, sway force and yaw moment caused by ice-induced forces on the hull for the simulations of continuous ship manoeuvring in level ice were calculated using the ice-hull interaction model developed. With appropriate definition of the ice conditions, the resulting model is applicable to Arctic regions, the Baltic, the Caspian and the Antarctic.

1.3 Approach and Methodology

1.3.1 Engineering Requirements

In ship manoeuvring simulations, the ship can be regarded as a rigid body, whose motions are calculated based on a function of global forces on its hull. The ship manoeuvring process can be simulated through numerically solving the ship motion equations with predetermined load functions. The external forces include forces from the hull, the thruster, the rudder, and other appendages. During ship ice navigation, forces on the hull are mainly composed of ice forces,

hydrodynamic forces, current forces and wind forces. Among them, the ice force on the hull is focused on in this study, as shown in Figure 1.1.

The surge force, sway force and yaw moment are the three major global forces to determine the ship's manoeuvring motions. Therefore, determination of these force components due to ice action on the hull is the focus for this thesis research. Cargo ships operating in ice may break the ice cover by themselves without an escort icebreaker. Therefore, the resulting model will have to be applied not only to general icebreaker navigation, but also to large ship manoeuvres in level ice.

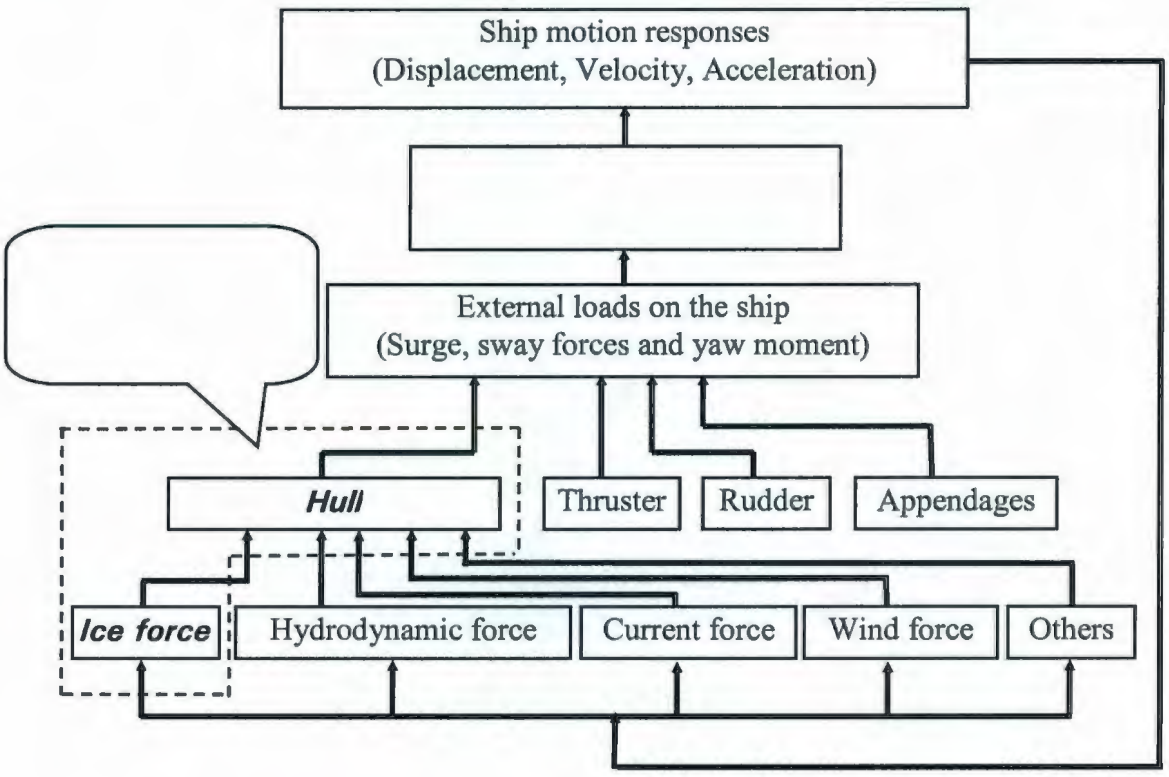

Figure 1.1 Ice-Hull Interaction (IHI) model as a module in the numerical framework of ship-ice navigation simulation

For engineering applications such as training simulators and automatic pilot systems, the manoeuvring model should satisfy the following requirements:

- **Simulation accuracy** --- The model should be sufficiently detailed and accurate enough, to provide the correct 'feel' to the ship operators.

- **Numerical efficiency** --- In those applications, the simulations are usually in real-time. Therefore, the model also needs to be able to provide the results in real time.

- **Application Universality** --- An ideal model should be general enough to simulate the arbitrary specified manoeuvres. The final developed model should be applicalbe not only for Canadian waters, but also for the Antarctic, the Arctic and other ice regions in the world.

1.3.2 IHI Model Brief Description

Analytical approach with numerical implementation was adopted to build the ice-hull interaction model. Its simple physical detail and short computation time made the model very suitable for real-time simulations.

In the model, the ice force was equal to the linear sum of three independent force components, breaking force, buoyancy force and clearing force, which respectively represented the physical phenomena during the ice breaking process in time domain.

At each calculation step, the ice-hull contact area is calculated in the time domain and the channel geometry is tracked through a simple house-keeping method, which means the ice channel is kept using a channel matrix during the simulation. The resulting channel edge by the ship in one calculation step is used as the initial channel edge for next calculation step. As the ship turns, more parts of the hull may contact the unbroken level ice. Different ice failures, i.e., bending failure, crushing failure and shear failure, may simultaneously occur from stem to stern at the water line of the hull due to the change in flare angle at the ice contact surface of the hull. Therefore, a multi-failure ice model considered of the bending failure, shear failure and crushing failure is used to calculate the ice breaking forces and the failure mode associated with minimum failure force is identified. A cusp ice crack pattern consistent with a 3-D plate theory governed the flexural failure and the channel formation.

A flat-plate model was used for the buoyancy force calculation and the volume of ice covering on each surface of the flat-plate model is calculated in the time

domain. The buoyancy force is calculated by multiplying the ice volume on each wet surface of the hull with density difference between ice and water.

The ice clearing force is a velocity dependent term governed by the movements of the ice pieces. The physical motion of the ice pieces around the hull, ice piece rotation, ventilation of the rotating ice pieces, ice piece acceleration and water viscous drag on the sliding ice pieces, are considered and their contributions to the total force calculated.

The whole hull is divided into more than ten segments and the ice forces on each segment separately calculated based on the ice-hull contact area and ship motions. The global ice forces on the whole hull are obtained through vectorially adding those forces and moments.

1.3.3 IHI Model Benchmark

Two PMM model test series carried out in IOT, Terry Fox tests and R-Class tests, were used to verify the developed IHI model. The force components of the IHI model, breaking force, buoyancy force and clearing force, were separately verified through comparing them with the measured forces in the different test conditions: open water, level ice and pre-sawn ice. The ice force distributions along the waterline of the R-Class model were calculated using IHI model and compared

with NMRI's tests (Izumiyama et al., 2005) in qualitative. Besides the ice forces on the hull, the validation of the model also included the ice-hull contact, ship motions, ice edge, channel shape and width, etc. Several technical details like drift angles effects in PMM tests, jamming effects at the hull shoulder were also studied and discussed in the thesis.

1.3.4 Investigation of Ice-Hull Interaction

The mechanics of ship-ice interaction was studied through parametric analysis and specific manoeuvring simulations based on the IHI model. A parametric study provided results for a comprehensive evaluation of the influence of various relevant factors to the ice forces. The specific manoeuvring simulations showcased the developed model's capability in simulating the ship's arbitrary manoeuvres in ice. Several curves of ice loads due to ice properties, ship motions and geometries were developed, which were also used for assessing the model's accuracy through compares with the experimental data. Several conclusions on ship manoeuvrability in ice were drawn. The above research was of great value for mathematical modeling of ship-ice interaction and operation in ice.

1.4 Thesis Layout

This thesis documented a new ice-hull interaction (IHI) model for the real-time simulations of ship manoeuvring in level ice.

Chapter 1 provides the introduction to the whole thesis including background and objective of this research, approach and methodology adopted in the development of the model, numerical implementation of the model, benchmarking and calibration of the model and investigation of ship-ice interaction.

Chapter 2 documents a literature review on mathematical modeling of ship manoeuvres in the level ice. The review showed that none of the existing mathematical ship-ice models could entirely satisfy the CMS training simulator's requirements.

Chapter 3 introduces theoretical basis of the developed IHI model with details. The model was built on a detailed analysis of hull-ice interaction mechanics. Analytical approach with numerical implementation was adopted.

Chapter 4 presents a stand-alone numerical simulation software developed using MatLab, which provided an independent numerical simulation platform for developing and benchmarking the desired IHI model.

Chapter 5 introduces the process of benchmarking and calibrating the Ice-Hull Interaction (IHI) model using PMM ship model test data.

Chapters 6 and 7 respectively presented benchmarking of the IHI model using Terry Fox model test series and R-Class model test series respectively. The selected tests included resistance runs, constant radius runs and sinusoidal runs.

Chapter 8 presents the IHI model benchmark using Izumiyama's tests. The ice force distributions around the R-Class model hull were calculated using IHI model and qualitatively compared with Izumiyama's tests.

Chapters 9 and 10 describes on ice-hull interaction study through parametric analysis and specific maneuvering simulation using the IHI model. Through detailed parametric check and analysis of the IHI model, the accuracy of the model was further verified.

In Chapter 11, conclusions and recommendations for future research on real-time mathematical modeling of ship-ice interaction are provided. A brief instruction of the developed IHI model software is provided in Appendix A. Appendix B includes the recorded movies for the selected IHI model simulations presented in this thesis.

Chapter 2 Literature Review

2.1 Introduction

Ship-ice navigation has attracted mariner's attention for many years and considerable efforts have been made to modeling ship performance in ice. Some of these models estimate the ice forces on the hull due to the ship's navigation in level ice, but most of the models focus on resistance forces only (Jones, 1989 & 2004; Daley and Riska, 1990).

The previous literature reviews include Jansson (1956a & 1956b), in which he discussed the history of icebreaking up to the end of 1956, and Jones (1989 & 2004), in which he reviewed the literature mainly on ship resistance in level ice from 1888 to 2004. This chapter presents a literature review of mathematically modeling ship navigation in ice including resistance model and manoeuvring model. Typical existing models for ice-hull interaction in the continuous ice breaking mode were collected and critically evaluated. The advantages and disadvantages of each model are discussed.

Two categories, **Analytical Approach** and **Numerical Approach**, are used to classify the existing models of ice-ship interaction process and are respectively reviewed in the following sections.

2.2 Analytical Approach

The analytical category is also subdivided into empirical, semi-empirical and theoretical models.

2.2.1 Analytical Models Using Empirical Formulae

In a large proportion of the available studies, some reasonable simplifications are made and empirical formulas are applied to model the complicated ice-hull interaction process, i.e. Lewis et al's model (Lewis and Edwards, 1970, 1982, Roderick and Edwards, 1979), Menon's time domain model (Menon et al., 1986, 1988, 1991; Majid and Menon, 1983), Williams and Waclawek's model (Williams et al., 1996, 1998; Spencer, 1992, 1993, 1998; Spencer et al., 1992, 1993; Colbourne., 1987a, 1987b; Colbourne et al., 1992),.....

Jansson (1956a, 1956b) gave a very simple empirical formula for the total ship ice resistance. Lewis and Edwards (1970) reviewed previous ship-ice research and presented an engineering framework for ship resistance in level ice based on some full-scale ice trials and model tests of Wind-class, Raritan, M-9 and M-15. An empirical formula was proposed for estimating ship resistance in level ice conditions. Later, many researchers contributed to and improved the ice resistance calculation using empirical approaches and several formulae were developed

based on model test data or trials data (Crago et al., 1971; Vance, 1975; Edwards, et al. 1972, 1976).

Kashtelyan, et al. (1968) first analyzed level ice resistance in details. In their research, the total ice resistance is divided into several force components: resistance due to breaking the ice, resistance due to forces connected with weight (i.e. submersion of broken ice, turning of broken ice, change of position of icebreaker, and dry friction resistance), resistance due to passage through broken ice, and water friction and wave making resistance. Based on model and full-scale tests, an empirical equation was developed by calculating each component separately.

Menon, et al (1983, 1986) built a time domain model for ship maneuvers in ice based on conventional maneuvering equations. The Taylor's series expressions with coefficients obtained from model tests were adopted to estimate the ice forces on the hull due to the ship motion in the level ice. The maneuvering equations were sufficiently general and applicable to conventional icebreaker maneuvers. The shortcomings of the Menon's Time Domain Model are mainly that its application is limited due to the absence of sufficient and appropriate model tests or trial results that can be used to derive the ice force coefficients. The reasonability of using simplified Taylor series expansions with only the first power terms to estimate the ice force still needs rigorous verification based on

sufficient experimental results. Through regression and neural network analyses on their R-Class data, Shi (2002) estimated the values for the coefficients and pointed out that the coefficients are not linear with small variations in ice condition.

Colbourne (1987) proposed that the total ice resistance could be split into three components: an open water component, an ice clearing component and a breaking component. Spencer, et al. (1992) modified and improved Colbourne's theory and proposed an IOT model for ship resistance in level ice, which separated the buoyancy force component from ice clearing component in Colbourne's model. Jones et al. (2000, 2002, 2005,2006) applied that resistance model to a detailed study of the ice resistance of USCGC Healy and also formulated standard test methods for resistance in ice of IOT based on it. Williams, et al (1996) proposed an ice-hull force model for ship maneuvers in level ice from a series of PMM model tests. As the first approximation, the sway velocity and acceleration was assumed to be zero because the sway motion would be very small due to the large force acting along the side of the ship opposing sway. The surge force was assumed to be the same as the ship resistance force. The empirical formulae were derived for calculating the ice induced yaw moment and the corresponding empirical constants can be derived from experiments. In their models, the total ice force consists of breaking force, clearing force and buoyancy force and the empirical formulae were derived to estimate the individual force component.

In the analytical models using empirical formulae, the empirical coefficients were derived through fitting the formulae to data from model tests and full-scale trials. Due to the limited data available from model tests and sea trials, the expressions are usually simple, with few empirical constants. Hence, there is a limitation in scope with various degrees of accuracy.

2.2.2 Analytical Model Using Semi-Empirical Approaches

The analytical models using semi-empirical approaches can take into account more details of the pertinent ship-ice interaction processes, i.e. Lindqvist's model (1989), Canmar's steady turning model (Tue-Fee, et al, 1986, 1987), etc.

Lindqvist (1989) proposed an ice resistance model, in which the total force was divided into two groups of components. The speed-independent force terms, ice bending, crushing and submersion (buoyancy), are calculated theoretically from mechanical principles. The speed-dependent force terms were assumed to be linear to ship speed and calculated using simple empirical formulas. The Lindqvist model was tested through estimating the resistances of several icebreakers, Jelppari, Otso, Vladivostok, Mergus, Warc, Valpas and Silma, in ice. The results showed fairly good accuracy. The model took account of both friction and the shape of the hull and can be a tool in the early design process. The Lindqvist

model's shortcomings are that it proved to be reliable only for larger ships. It appears that the formula for speed-dependent terms is too simple and refinement is required.

Tue-Fee, et al. (1986) proposed a semi-empirical model for predicting the ship's steady turning maneuvers in level, unbroken, homogeneous ice fields. The formulas for calculating sway force and yaw moment caused by pure ice forces are theoretically derived from basic assumptions. The asymmetric ice force on the bow in the transverse direction is assumed to be proportional to the difference in the volume of ice broken by the bow per unit time. In order to calculate the ice forces randomly distributed on the outboard side of the ship, the contact force distribution is idealized as point load at the end of the parallel mid-body. The model was used to simulate the USCGC POLAR STAR's performance in level ice and the results showed that the model correctly predicts the expected trend of the turning radii in ice. The Tue-Fee model mainly has the following shortcomings: The resistance in turning motion was equal to the resistance in ahead motion with the same speed, which is an approximate treatment (Tue-Fee et al., 1986). The location of the mid-body side force is usually difficult to predict for a specific new ship design. The coefficients for calculating the bow asymmetric forces are still empirically determined by test results. The present model cannot be used for maneuvers other than constant radius turns.

2.2.3 Analytical Model Using Fully Derived Mechanical Formulae

The analytical models adopting fully derived mechanical formulae, i.e., Milano's model (1973, 1975, 1980) and Kotras et al's model (1983).

Enkvist (1972) considered the total ice resistance as the sum of three components: breaking of ice, submersion of ice, and velocity dependent resistance. He studied the ice resistance in level ice conditions by a combination of analytical work, dimensional analysis, and a few assumptions. Another important contribution by Enkvist is that he first described the details of isolating those three terms in model tests and applied scaling techniques. Enkvist also carried out research on the relationship between model tests and full-scale trials. Through dimensionless resistance equation based on the model tests, the full-scale resistance can be predicted.

Milano (1973) considered the energy needed for a ship moving through level ice. The total energy loss due to ship motion is from the ship moving through the ice-filled channel, impacting the unbroken ice sheet, causing local crushing, climbing onto the ice, causing ice fracture and submersion of the broken ice. The explicit analytical expression for each of energy term was derived. He also proposed the speed dependent phenomena, named "Milano hump", which he explained using different mechanisms in the energy equations.

Naegle (1980) developed an algorithm predicting ship resistance in level ice. He studied ice resistance as a mechanical problem and divided the ice resistance into several components related to the breaking of ice, the turning of ice floes and the submersion of ice floes. His model provided results and trends that agree reasonably well with full-scale trials and model tests. Based on Naegle's research, Kotras et al. (1983) set up a model for ship resistance, in which the total ice resistance is divided into the following phenomena in ice-ship interaction process: ice breaking, ice floe turning force and ice sliding on the wet hull surface. Two breaking failures, initial crushing and flexural bending, were considered in the ice breaking force model. The wedge-shaped ice crack pattern was originally proposed to represent the broken ice shape and corresponding plate theories were used to estimate the ice force due to flexural bending failure. Four independent force components, buoyancy force, ventilation of rotating ice pieces, viscous drag and acceleration of ice pieces, were considered in calculating force due to the ice. The Kotras model is a cost-effective model that can be a valuable tool for the designer during the early design stages. The model regards ship resistance in level ice as a mechanical problem that adopts physical considerations of the ice-hull interaction process. It provides a more accurate analysis than Lewis's theories. Good agreement is obtained by comparing the full-scale trial data and the model calculation results. The main shortcoming for Kotras model is the assumption of the ice breaking pattern. Edwards thought there should be only one characteristic

failure shape rather than two ice failure types, one row of semi-ellipses ice piece and one row of wedge ice piece (Kotras et al., 1983).

The models using fully derived mechanical formulae are usually more complicated and require more work to apply, but they are more universal. The physical processes of ice-hull interaction provide basis for further model refinements.

2.3 Numerical Model

Numerical approaches have advanced with the development of the computer technology. They can be used to solve analytical equations, i.e. Lindstrom's model (1990, 1991), or to simulate the continuous ship-ice interaction process, i.e., Daley's chaotic ice failure process model (Daley, 1991, 1998). In particular, two numerical approaches, finite element method (FEM) and discrete element method (DEM), which divide the continuous ice material into many small elements, are widely applied in ice mechanics problem (Heinonen, 1999, 2004; Jebaraj et al., 1988, 1989; Sand et. al., 1998, 2001; Swamidas et al., 1991; Varsta, 1983; Vinogradov, 1986; Goldstein et al., 1989; Derradji, 2003; Valanto P. 2001a, 2001b, 2006; Hopkins et al., 1994, 1996, 1998; Hamza, 1989; Murray et al., 1997; Lau, 2006b).

Lindstrom (1990) built a framework for simulating ship manoeuvring in ice, in which the hydrodynamic hull forces, rudder forces, propulsion forces and forces due to the interaction between ship and ice are considered and calculated. For the calculation of ice forces on the hull, Lindstrom adopted the dynamic equation for an elastic plate on an elastic foundation and obtained its approximate solution using numerical methods. Lindstrom's model considers nearly all factors of ship navigation in ice, however, according to available publications (Lindstrom, 1990, 1991), for the calculation of ice forces on the hull, the following aspects were not addressed, i.e., the ice-hull contact area calculation, the ice edges and the ice crack shape. The bending failure solution for a line-load on the edge of the semi-infinite ice sheet was adopted, which may be different from the actual process of the ship breaking ice. The crushing failure and shear failure were not included. His model was benchmarked with several sea-trials in simple turning manoeuvres through comparison of the simulated ship tracks and the measured tracks. No detailed benchmark, especially on ice force calculation model, was presented. He also mentioned that the model only applied for ships where sloping sides directly break the level ice, which limited the model's universality.

Varsta, et al. (Varsta, et al., 1977; Varsta, 1983) studied the ship-ice contact process. A finite element model with the Tsai-Wu failure criterion was proposed to calculate the crushing failure at the ice edge during the ship ice interaction process. Jebaraj, et al. (1988, 1989) studied the failure loads and the total stress

and deformation states of the ice during the ship-ice interaction process. The ice sheet was modeled with finite elements and the ice failure was described by a Tsai-Wu criterion. McKenna, et al. (Jordaan, et al., 1991; Swamidas, et al., 1991; McKenna, et al. 1993a, 1993b) developed a finite element model to investigate the damage and stress progression during ship contact with the thick ice. A viscoelastic model coupled with damage mechanics was proposed to simulate ice creeping under the external loads.

Valanto (1987, 1989, 1993, 1997, 2001a, 2001b, 2006) set up a numerical model to estimate ship resistance in level ice. The ice was treated as a linearly elastic homogeneous and isotropic material with a simple failure criterion and the ice cover's deformation due to ice force is calculated using finite difference method (FDM).

With an added element of complexity in ice failure, Lau (2006b) applied the discrete element method software, DECICE, in simulating a series of PMM ship model tests in level ice conditions. Analysis of the numerical results showed the effects of ice conditions and ship motions to the global forces and moments on the hull when the Terry Fox model is advancing and turning in level ice conditions. Although Lau's model simplified the problem, the simulation results still showed good prediction compared with the experiments.

These FEM and DEM models have good potential due to their more detailed modeling capability and good universality; however, there is more to be learned about the mechanical properties of sea ice before a satisfactory simulation of the ice cover breaking process is achieved. Moreover, the hardware requirements and the large calculation time present a challenge for real-time simulations.

2.4 CMS Training Simulator

Shipping experience in the Arctic has told us that human factors usually played a significant role in marine emergencies and human error might lead to costly accidents. Shipping in icy waters has some unique characters compared with open-water navigation, therefore, effective and safe cold-ocean transportation needs special ice training for ship officers and crew. Many countries where shipping operations are conducted at high latitudes, i.e., Canada, Finland, Russia, etc., require the ship operator to be skilled in ice navigation (Marton, 2000, 2001; Bos et. al., 2005; Sinder, 2005; Tucker et. al., 2006).

With the development of computer technology in recent years, simulation and modeling have become the low-cost, readily available and vital tools for people to gain training, knowledge and experience in the field of ice navigation, which is also an essential step to offset the impacts of new technology on human performance and improve the ship operator's professional judgment and reduce

human error. Ice navigation training courses have been provided at Memorial University of Newfoundland (MUN) and directly delivered by the university's Center for Marine Simulation (MUN/CMS) with its innovative simulation tools for the students (Website: http://www.mi.mun.ca/cms). The CMS undertook a major project, Modeling and Simulation of Harsh Environments – Ice Management in the Offshore, in order to improve the safety and efficiency of oil and gas operations in harsh maritime environments, in which the innovative modeling and simulation capabilities are being developed and explored in order to satisfy the industry demand including personnel training, development and testing of operational procedures, risk analysis, route selection, port development, evaluation of ice navigation technology and development and testing of improved vessel and equipment design. (Patterson, 2002, 2003; Tucker et. al., 2006).

The existing work by Tue-Fee, et al. (1986, 1987), Lindstrom (1990, 1991), Williams, et al. (1996), Menon, et al. (1988, 1991), etc, has shown that the ship ice navigation may be simulated using the numerical approach. As part of the project, a collaborative project between the NRC/IOT and MUN/CMS was set up and carried out at IOT, in which a reliable ice-hull interaction model for simulating ship's arbitrary manoeuvres in level ice is being developed. The model is to be integrated into the existing CMS real-time simulator for water navigation as an ice force module within the whole numerical framework. This will extend the CMS simulator to ice navigation.

2.5 Discussion

A summary of the existing mathematical models for a ship continuously breaking level ice with some brief notes is given in Table 2.1 at the end of this chapter. Lewis' model, Spencer's model, Milano's model, Kotras et al's model and Lindqvist's model are for ice resistance only. Lindstrom's model considered only the bending failure of the ice. Canmar's model is restricted to constant radius turns. Menon's time domain model and Williams and Waclawek's model are both limited in accuracy and universality. The high hardware requirements and long calculation time present a large challenge to applying FEM model and DEM model in real-time simulations.

The CMS simulator requires real-time simulation of the ship's arbitrary manoeuvres in ice, therefore, none of the existing mathematical ship-ice models can entirely satisfy the simulator's requirements. A new reliable ice-hull interaction model for real-time ship-ice simulations is required and is developed in this doctorial research.

2.6 Ship-Ice Experiments

Experiments can provide reliable verification data sources for the development of modeling theories and insight into the ice-ship interaction mechanism. The total ship-ice manoeuvre experiments can be classified into two categories: **Full-scale Trials** and **Model Tests**.

Full-scale ship voyage trials constitute a very valid assessment of ship-ice performance and provide the necessary data for the validation of model test measurements and analytical predictions. The disadvantages of full-scale trials are mainly the high cost of planning to execution. It is difficult to accurately determine the forces on the ship, and the ice properties must be measured at a sufficient number of locations to reasonably characterize the ice along the track. Finding a large enough test area with homogeneous ice condition for ship manoeuvring and keeping the ship velocity steady for a sufficiently long period are also both difficult (Abkowitz et al., 1988; Kendrick et al., 1984; Kivimaa, 1992, 1993; Menon et al., 1986; Riska et al., 1990, 2001; Williams et al., 1992).

Due to the complication of ship-ice interaction, physical model tests have played a very important role in studying ship manoeuvrability in ice. Model experiments can be used to study more details of ship-ice interaction or determine corresponding derivatives for numerical formulations. In model tests, controlling

of manoeuvres and measuring ship motions are much easier and more accurate than full-scale trials. The costs of model tests are also more affordable compared to the full-scale trials. The main shortcomings of model tests are the uncertainty of the various scaling requirements imposed by ice and hydrodynamic efforts. Those shortcomings can be reduced through improvements in modeling technologies and refinements of data treatments based on test experience. For instance, IOT has achieved good correlation between model test results and sea trial results (Spencer et al., 1992a, 1992b, 2001; Jones et al., 1994, 2002, 2006).

Generally, there are two types of model tests: **Free-running Model Tests** and **Captive Model Tests**. Free-running Model Tests make use of a self-propelled model fitted with all appendages and a remote control. Actual manoeuvres can be performed and manoeuvrability can be directly evaluated. One of the disadvantages of free-running model tests is usually the large space required to perform the experiments, which limits the scale of the model. In captive model tests, the ship model is moved using the external apparatus in exact, pre-programmed patterns. At the same time, forces on the model and the motions of model and ice around the model are measured and recorded. The obtained results can be directly used to determine hull force and moment derivatives for empirical formulae. Captive model tests are usually used to calibrate and refine theoretical models. Captive model tests include: the Straight-line Oblique Tow Model Test,

the oscillator Test, the Rotating-Arm Test, the Impulse Test, the Planar Motion Mechanism (PMM) Test, and other method tests.

The model tests, especially PMM model tests, carried out in IOT include different models, and different test runs in different ice conditions and open water conditions. Experiment substantially provides a basic set of data for verification of mathematical ice-hull interaction model of ship maneuvers in ice.

2.7 Summary and Conclusions

A literature review on the modeling of ship maneuvers in ice, especially in level ice, was given in this chapter in order to illustrate the theoretical basis and engineering background for modeling the ice-hull interaction processes for real-time simulations. The following conclusions are summarized.

1) Ship navigation in ice has been of interest to mariners and considerable efforts have been made to model ship performance in ice. Some of these models estimate ice forces on the hull due to the ship moving through level ice, but most of them focus on resistance forces only.

2) At the CMS, a training simulator is used for the ship's arbitrary maneuvers in level ice in real-time. However, it seems that none of the existing models can

satisfy its requirements, i.e., Lewis' model, Kotras' model and Lindqvist's model are for resistance estimation only. Lindstrom's model considered only the bending failure of the ice. Canmar's model is restricted to constant radius turns. Menon's time domain model and Williams and Waclawek's model are both limited in accuracy and universality. Valanto's model and Lau's model respectively adopted the FDM and DEM to calculate the response of the level ice due to ship's contact. However, its hardware requirements and the long calculation time required present a challenge for real-time simulations. A new reliable ice-hull interaction model is required to satisfy the requirements of real-time ship-ice navigation simulators like the CMS training simulator.

3) In the exiting models, analytical approach and numerical approach are both applied in modeling ship maneuvers in ice. Analytical approach is a classical approach, which treat ice-hull interaction process in a cost-effective manner with rapid estimating capability. Numerical approaches have advanced with the development of the computer technology, which has the advantage of solving the problem for the continuous process. Therefore, analytical approach with numerical implementation is more appropriate to build up the ice-hull interaction model for the real-time simulator.

4) Ship maneuvering in level ice is actually a problem of solid-solid interaction. The ice undergoes a similar physical process for each ice piece in both ship

advance (resistance) and ship turning. From the macroscopic point of view, the amounts of the breaking ice on two sides of the longitudinal center section plane are different when the ship turns in ice. This causes an asymmetric force on the hull. Also, more parts of the hull may directly contact the unbroken ice compared to the ship straight-ahead advance case, which also affects the global ice forces on the hull. The actual ice crack patterns due to ship's motions are very complicated and stochastically changing, usually, the cusp pattern with the corresponding plate theories shown more frequent and reasonable among the assumptions of the existing models. Different ice failure modes may occurs simultaneously from the stem to the stern along the waterline when the ship turns in the various level ice conditions due to the changing flare angle of the contact surface of the hull. Therefore a multi-failure ice model is more appropriate. The ice-hull contact area, ice-breaking pattern, ice pieces sliding on underwater part of the hull and frictional effects should all be considered in the ice-hull interaction model.

5) The Ship-Ice Experiments including full-scale trials and model tests were briefly viewed and discussed. The IOT database for ship manoeuvring in ice, especially PMM model tests, provides substantially a very useful benchmark source for the mathematical ice-hull interaction model.

Table 2. 1 Summary of some existing mathematical models of continuous icebreaking by ships

Developer	Subject/topic	Approach	Brief Description of the Model	Reference
Lewis J.W., Edwards R.Y., et al.	Resistance	Empirical analytical forms	$\frac{R}{\rho_w g B h^2} = C_0 + C_1 \frac{\sigma_f}{\rho_w g h} + C_2 \frac{V}{\sqrt{gh}} \frac{(L/h)}{(B/h)^{1/2}}$ Where R is ice resistance on ship; C_0, C_1 and C_2 are the constant coefficients; B is the waterline beam at the ship operating condition; L is waterline length at the ship operating condition; V is ship speed; g is the acceleration of gravity; ρ_w is mass density of water; h is ice thickness; σ_f is ice flexural strength.	Lewis, et al., 1970, 1982
			Note: The first term accounts for the ice force from the buoyancy, the second term represents ice breaking and the third one accounts for all resistance forces attributable to momentum interchange between the ship and the broken ice.	

Table 2.1 Summary of existing mathematical models for continuous icebreaking by ships (continued)

Developer	Subject/topic	Approach	Brief Description of the Model		Reference
Lindqvist G.	Resistance	Semi-empirical analytical forms	Total ice force	Breaking force: crushing failure R_c and bending failure R_b	Lindqvist, 1989
				Submersion R_s: 1) Assuming the ice distribution covered on wet surface of the hull; 2) The energy method adopted.	
				Speed dependent force: Empirical constants are adopted $R_{speed} = 1.4*(R_c + R_b)*V/\sqrt{g*h} + 9.4*R_s*V/\sqrt{g*L}$ Where h is ice thickness; V is ship speed; g is the acceleration of gravity; L is waterline length at the ship operating condition.	
			Note: 1) The formula only fairly reliable for larger ships 2) The speed dependent force calculation is too simple.		

Table 2.1 Summary of existing mathematical models for continuous icebreaking by ships (continued)

Developer	Subject/topic	Approach	Brief Description of the Model		Reference
Spencer D. et al. (IOT)	Resistance	Empirical analytical forms	Total ice force	Breaking force: $R_{br} = C_{br}\rho_i BhV^2\left(\frac{\sigma_f h}{\rho_i BV^2}\right)^b$ Submersion force: $R_s = C_s \Delta\rho BhDr$ Clearing: $R_{cl} = C_{cl}\rho_i BhV^2\left(\frac{gh}{V^2}\right)^c$ Where the coefficients, C_{br}, C_{cl}, C_s, b and c are determined through the tests; B is the maximum beam at the operating waterline; V is ship speed; g is the acceleration of gravity; h is ice thickness; σ_f is ice flexural strength; ρ_i is mass density of ice; $\Delta\rho$ is mass density difference between ice and water; D is draft, r is the yaw rate.	Colbourne, 1987a, 1987b; Spencer, 1993
			Note: The empirical approach is adopted and the corresponding coefficients are derived based on the data source from experiments.		

Table 2.1 Summary of existing mathematical models for continuous icebreaking by ships (continued)

Developer	Subject/topic	Approach	Brief Description of the Model		Reference
Milano V.	Resistance	Theoretically derived forms using energy method	Total ice energy	1) Ship moving through the ice-filled channel 2) Local crushing at the contacted ice (thick ice) or ice bending failure (thin ice). 3) Ship climbing the ice (thick ice) or the strain for the bow and cusp ice wedge (thin ice). 4) The ship falling after the ice fractures. 5) Ship forcing ice downward 6) Energy lost due to frictional force, etc.	Milano., 1973, 1975, 1980
			Note: 1) The ice resistance may be taken as the total energy lost divided by the ship moving distance in a load cycle. 2) The model's advantage is that it considers many details of the ice breaking process during the ship continuously navigating in solid ice (thick ice, thin ice or very thin ice), however, which also causes the arguments on the model's assumptions: i.e., the actual dynamic ice force constitutions, the actual ship's oscillation motion, the hydrodynamic force, etc.		

Table 2.1 Summary of existing mathematical models for continuous icebreaking by ships (continued)

Developer	Subject/topic	Approach	Brief Description of the Model		Reference
Kotras V. et al.	Resistance	Theoretically derived forms using ice mechanics	Total ice force	Icebreaking resistance model: 1) The wedge-shaped ice crack pattern was originally proposed to represent the broken ice shape. The ice cusp broken force was calculated based on the approximate solution of the semi-infinite plate on elastic foundation given by Nevel (1965). 2) Two breaking failures, initial crushing and flexural bending, were considered.	Kotras, et al., 1983
				Turning resistance model: Hull-induced pressure by bow wave and ventilation above rotating ice piece; Viscous drag; Mass forces to accelerate ice pieces.	
				Submergence resistance model: $R_s = \Delta\rho g h \cdot A_{projected}$ Where $\Delta\rho$ is mass density difference between ice and water; g is the acceleration of gravity; h is ice thickness; $A_{projected}$ is the projected area of the ice.	
			Note: 1) It provides more accurate prediction than Lewis's theories. 2) The shortcomings of his model are mainly the selection of the ice breaking pattern.		

Table 2.1 Summary of existing mathematical models for continuous icebreaking by ships (continued)

Developer	Subject/topic	Approach	Brief Description of the Model	Reference
Lindstrom et al.	Turning	Theoretically derived forms using ice mechanics	The following dynamic equation for an elastic plate on an elastic foundation was adopted in his work: $\nabla^4 w + \frac{c\partial^2 w}{\Theta \partial t^2} + \frac{\lambda}{\Theta} w = 0$ Where w is the vertical deflection of the ice sheet; c is the virtual mass per unit area; Θ is the flexural rigidity of the ice plate; λ is the relation between the pressure from the underneath water and the deflection of the ice.	Lindstrom, 1990, 1991; Sorensen, 1978
			Note: 1) Numerical approach used to solve above equation. 2) Only the bending failure of the ice was considered.	
Menon et al.	Any Maneuvers	Empirical analytical forms	Sway Force: $Y = Y_v v + Y_r r + Y_{\dot{v}} \dot{v} + Y_{\dot{r}} \dot{r} + Y_\delta \delta$ Yaw Moment: $N = N_v v + N_r r + N_{\dot{v}} \dot{v} + N_{\dot{r}} \dot{r} + N_\delta \delta$ Where $Y_v, Y_r, Y_{\dot{v}}, Y_{\dot{r}}, Y_\delta$, are sway force derivatives to sway velocity, yaw rate, sway acceleration, yaw acceleration and rudder angle ; $N_v, N_r, N_{\dot{v}}, N_{\dot{r}}$ *and* N_δ are yaw moment derivatives to sway velocity, yaw rate, sway acceleration, yaw acceleration and rudder angle; δ is rudder angle; v is sway velocity; r is yaw velocity.	Menon, et al., 1986, 1988, 1991
			Note: 1) The sway force and yaw moment are expressed as linear combinations of terms involving the first power velocities and accelerations neglecting second and higher order terms by Taylor series expansion of the forcing functions. 2) The linearity of ice forces on the hull to small variations of ship motions needs verifications.	

Table 2.1 Summary of existing mathematical models for continuous icebreaking by ships (continued)

Developer	Subject/topic	Approach	Brief Description of the Model	Reference
Tue-Fee K.K. et al.	Steady Turning	Semi-sempirical Approach	1) It is assumed that the asymmetric ice force on the bow in the transverse direction is proportional to the difference in the volume of ice broken by the bow per unit time. 2) In order to calculate the ice forces randomly distributed on the outboard side of the ship, the contact force distribution is idealized as point load at the end of the parallel mid-body, ellipsoidal force distribution for the ship with a long effective parallel mid-body, triangular or trapezoidal force distribution for short effective parallel mid-body.	Tue-Fee et al., 1986, 1987
			Note: 1) Only applied to steady turning. 2) Deciding the load point position is difficult 3) Deciding the coefficient between force and broken ice volumes.	

Table 2.1 Summary of existing mathematical models for continuous icebreaking by ships (continued)

Developer	Subject/topic	Approach	Brief Description of the Model	Reference
Williams M., Waclawek P. et al.	Any Maneuvers	Empirical analytical forms	The yaw moment from the total ice loads, $N_i = N_s + N_{cl} + N_{br}$ The yaw moment from ice loads due to breaking, $N_{br} = G_{br}\sigma_f h^2 r L^2 \sin r / U$; The yaw moment from ice loads due to submergence, $N_s = G_s \Delta\rho g h L^2 D r \sin r$; The yaw moment from ice loads due to clearing, $N_{cl} = G_{cl}\rho_i h L^3 r\sqrt{gh}$; Where G_{br} , G_{cl} and G_s are empirical coefficients; L is ship length at the operating waterline; g is the acceleration of gravity; h is ice thickness; σ_f is ice flexural strength; U is sway velocity; ρ_i is mass density of ice; $\Delta\rho$ is mass density difference between ice and water; D is draft, r is the yaw rate.	Williams and Waclawek, 1996
			Note: The model was designed for the numerical ship navigation simulators like the NavSim software and the empirical coefficients can be derived from the model tests.	

Table 2.1 Summary of existing mathematical models for continuous icebreaking by ships (continued)

Developer	Subject/topic	Approach	Brief Description of the Model	Reference
Valanto P.	Resistance and Turning	Numerical approach	The ice regarded as a linearly elastic homogeneous and isotropic material with a simple failure criterion. A 3-D numerical model of the icebreaking process on the waterline of a ship advancing in level ice was developed to simulate the response of a floating ice cover and the surrounding fluid. The ice's deformation due to ice force is calculated using finite difference method (FDM)	Valanto, 1993, 1997, 2001, 2006
			Note: Detailed simulation capability and good universality An expensive approach with high requirements of computer hardware/software technology and computation time for some real-time simulators.	

Chapter 3 Theories of IHI Model

3.1 Introduction

The simulation of ship's manoeuvres in ice is a problem that involves solid-solid and fluid-solid interaction processes. For each small ice piece, similar physical processes apply to ship motions in straight-ahead advancing and in turning. From the macro point of view, for ship advancing, roughly equal amounts of broken ice pass along both sides of the hull; however, different amounts of broken ice pass along both sides when the ship turns in ice. This difference in how the ice is pushed aside can cause asymmetric clearing loading on the hull. Furthermore, one side of the hull may contact more intact ice during turning, which also leads to asymmetric load on the hull. The ice breaking pattern during ship transit is complex and stochastic. Most existing models estimate the cusp pattern with elastic plate theories. Various ice failure modes may happen simultaneously from the stem to the stern along the waterline when the ship turns due to the varying flare angle of the hull in contact with the ice cover. Therefore, a multi-ice failure model should be employed in the model treatment. The ice-hull contact area, ice-breaking patterns, ice piece sliding and submergence along the underwater part of the hull and the ice-hull friction should also be considered in the ice-hull interaction model.

The ice-hull interaction model developed is a physically-based ice-hull force distribution model designed to serve as the key ice component for a real-time ship simulator in ice. This chapter focuses on the model's theories with its corresponding theoretical backgrounds. The model is built on a detailed mechanics analysis of the hull-ice interaction in level ice. It considers the distributions of the breaking force, buoyancy force and clearing force separately. A multi-failure ice model is adopted to represent the ice failure process along the waterline of the hull from the bow to the stern. Both viscous and inertial effects are incorporated into the clearing force. The hull-ice contact area is calculated in time domain at each calculation step. The ice channel is tracked using a simple house-keeping method in the model. The resulting IHI model is direct and numerically efficient. Since the forces are calculated at each new increment of any prescribed motion, the resulting simulation has the capacity to respond to arbitrary control inputs and hence arbitrary maneuvers in ice.

3.2 Brief Description of IHI Model

Normally, an icebreaker is designed so that it can break level ice of a certain thickness in the continuous mode at a desired speed. When a ship navigates at low speed in continuous unbroken level ice, the resonance between the ship's rigid motions and the global ice forces on the hull rarely occurs and the dynamic trimming motions are usually small (Ettema et al, 1991; Daley, 1984; Thomas et

al., 1983; Lee et al, 1987). In this case, the ship resistance can be approximated by considering ship motions only in the horizontal plane, i.e., surge, sway and yaw. This simplification doesn't greatly affect the accuracy of the ice loads on the hull (Enkvist, 1972, 1979; Kotras, et al., 1983; Akexander, et al., 1997; Puntigliano, 1997). During the ship continuous breaking the level ice, the average ice breaking force over large distance is of more interest because the kinetic energy of ship is normally large enough to overcome any ice resistance temporarily exceeding the available thrust force. For this reason, the IHI model uses the average load approach and neglects the high frequency cyclical nature of ice load due to ice breaking. The model calculates the equivalent local ice force along the hull according to ship motion and local ice condition.

The model treats ice-hull interaction analytically based on ice mechanics and faithfully follows the details of the interaction process. This approach leads to a more realistic force prediction for any prescribed motion, and, hence, arbitrary manoeuvres in ice. The adoption of the analytical approach yields a short computation time that makes the model particularly suitable for real-time simulations.

An overview of the ice-hull interaction model is given in Figure 3.1. The model works as an ice force module of the ship navigation simulator as shown in Figure 1.1.

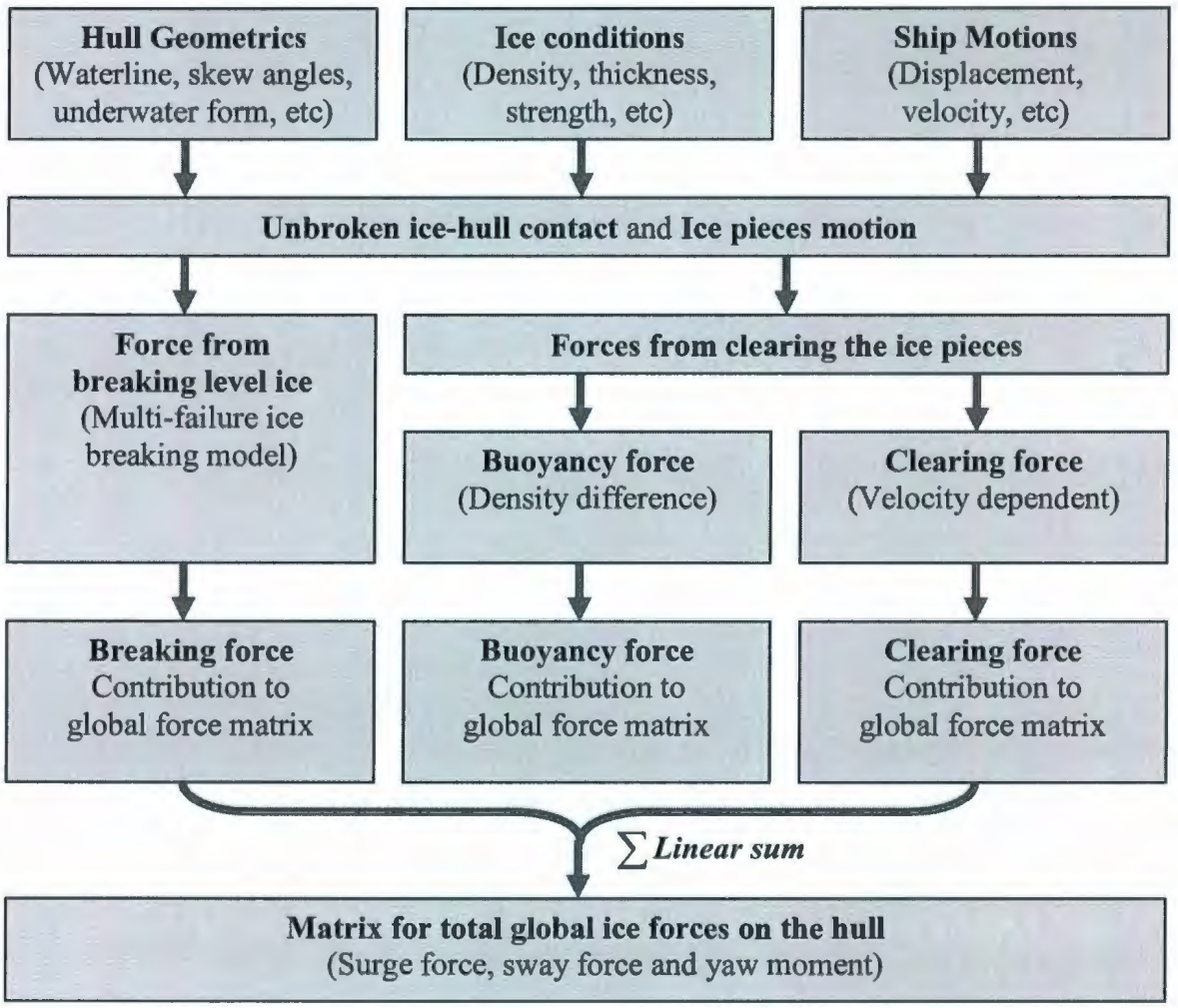

Figure 3.1 Overview of Ice-Hull Interaction (IHI) model

During ship manoeuvring in level ice, not only does the bow directly contact the unbroken level ice, the aft-hull may also directly break ice. The ice-hull contact area directly affects the ice force distribution on the hull, which determines the final global forces on the whole ship for its manoeuvring motions. The IHI model first calculates the ice-hull contact area based on the current ice edge and ship motion, then the ice generated loads on the hull are calculated using the applicable ice-structure interaction mechanics theories. The total ice force is equal to the

linear sum of three independent force components: breaking force, buoyancy force and clearing force.

3.3 Theoretical Description of IHI Model

3.3.1 Coordinate Systems

In the present development of the IHI model, the ship motion is considered in the horizontal plane with three degrees of the freedom (DOF). However, for completeness, we begin by considering the general case of a six DOF rigid body's motion. To describe the ship's motion, two coordinate systems, i.e., a global coordinate system and a moving local coordinate system, are used (Lewis, 1989). Based on the ship position and motion, the motion of the ice floe relative to the hull for the ice force calculation are determined and discussed in latter sections.

Figures 3.2 and 3.3 show the global coordinate system and the local coordinate system depicting the ship's motion and ice force in 2-dimensions and 3-dimensions, respectively. These systems use the standard right-hand rule convention. The global coordinate system is fixed to an arbitrary earth location, and the local coordinate system moves with the ship with its origin fixed at the center of gravity (cg) of the ship. In this version of the model, only the planar motion is considered, and the local $\tilde{x}$- and $\tilde{y}$-axes form a right-hand orthogonal system. The $\tilde{x}$-axis is along the center-plane of the hull, coincident with the

longitudinal axis of inertia, which may be assumed with very small error, to be parallel to the baseline of the ship. Its positive direction is forward. The direction of the $\tilde{x}$ axis is referred to as the heading. The $\tilde{z}$ -axis is also located on the center-plane of the ship, but is perpendicular to the $\tilde{x}$ axis and positive upward. The $\tilde{y}$ -axis is normal to the $\tilde{x}$ - and $\tilde{z}$ -axes and is positive towards starboard.

The corresponding forces and moments, i.e., surge force, sway force, heave force, roll moment, pitch moment and yaw moment, are also defined in Figure 3.3.

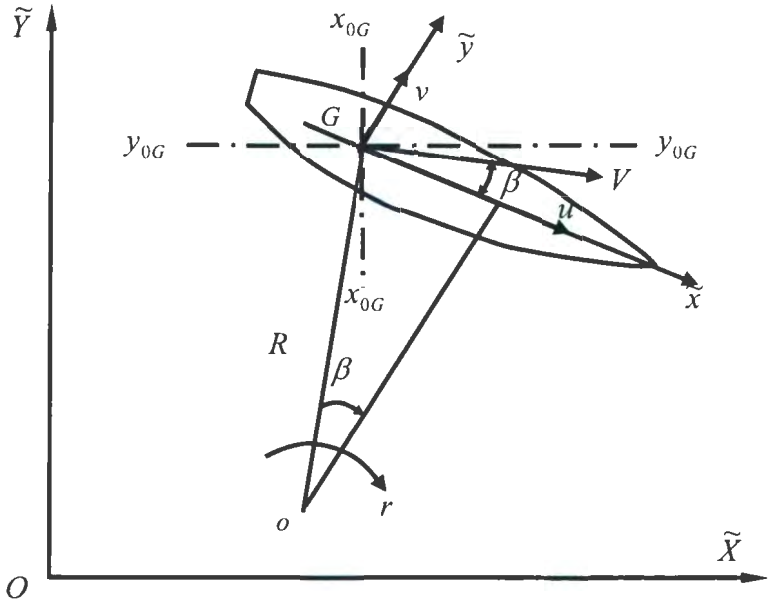

Figure 3.2 Coordinate systems (2-Dimensional view)

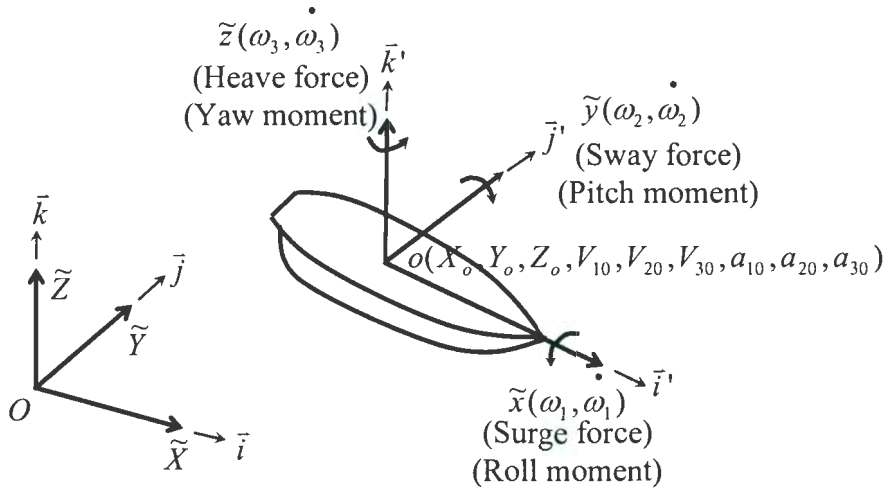

Figure 3.3 Coordinate systems (3-Dimensional view)

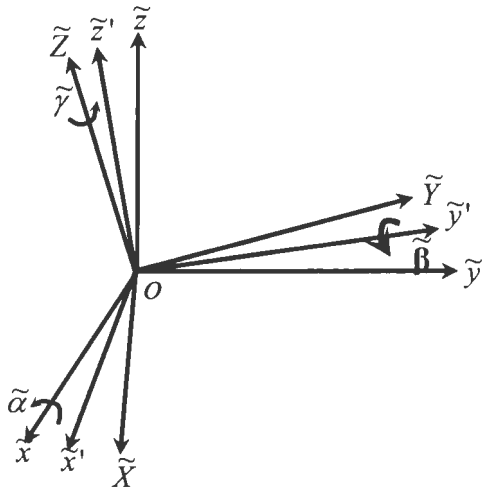

Figure 3.4 Euler angles

(3-Dimensional view. The $\tilde{x}\tilde{y}\tilde{z}$ coordinate system first rotates $\tilde{\alpha}$ angle along $\tilde{x}$ axis to become $\tilde{x}\tilde{y}'\tilde{z}'$ coordinate system, then $\tilde{x}\tilde{y}'\tilde{z}'$ coordinate system rotates $\tilde{\beta}$ angle along $\tilde{y}$ axis to become $\tilde{x}'\tilde{y}'Z$ coordinate system. Finally, $\tilde{x}'\tilde{y}'Z$ coordinate system rotates γ angle along Z axis to become the XYZ coordinate system. Accordingly, any rotation may be described using three Euler angles.)

In the IHI model, the following transfer matrix is derived for the global coordinate system and the moving coordinate system.

$$\begin{Bmatrix} \tilde{X} \\ \tilde{Y} \\ \tilde{Z} \end{Bmatrix} = \begin{bmatrix} \cos\tilde{\beta}\cos\tilde{\gamma} & -\cos\tilde{\beta}\sin\tilde{\gamma} & \sin\tilde{\beta} \\ \sin\tilde{\alpha}\sin\tilde{\beta}\cos\tilde{\gamma}+\cos\tilde{\alpha}\sin\tilde{\gamma} & -\sin\tilde{\alpha}\sin\tilde{\beta}\sin\tilde{\gamma}+\cos\tilde{\alpha}\cos\tilde{\gamma} & -\sin\tilde{\alpha}\cos\tilde{\beta} \\ -\cos\tilde{\alpha}\sin\tilde{\beta}\cos\tilde{\gamma}+\sin\tilde{\alpha}\sin\tilde{\gamma} & -\cos\tilde{\alpha}\sin\tilde{\beta}\sin\tilde{\gamma}+\sin\tilde{\alpha}\cos\tilde{\gamma} & \cos\tilde{\alpha}\cos\tilde{\beta} \end{bmatrix} \begin{Bmatrix} \tilde{x} \\ \tilde{y} \\ \tilde{z} \end{Bmatrix}$$

(3-1)

Where $\tilde{\alpha}$, $\tilde{\beta}$ and $\tilde{\gamma}$ are the Euler angles, as shown in Figure 3.4, representing roll, pitch and yaw angles respectively in the model. $\tilde{x}$, $\tilde{y}$ and $\tilde{z}$ are the point coordinates in the moving coordinate system, and $\tilde{X}$, $\tilde{Y}$ and $\tilde{Z}$ are the point coordinates in the global coordinate system.

The translating motion vector of the center mass of the ship, $\vec{V} = V_1\vec{i} + V_2\vec{j} + V_3\vec{k}$, in global coordinate system is expressed as, $\vec{v} = v_1\vec{i}' + v_2\vec{j}' + v_3\vec{k}'$, in the moving coordinate system fixed to the ship. They have the following relationship.

$$\begin{Bmatrix} V_1 \\ V_2 \\ V_3 \end{Bmatrix} = \begin{bmatrix} \cos\tilde{\beta}\cos\tilde{\gamma} & -\cos\tilde{\beta}\sin\tilde{\gamma} & \sin\tilde{\beta} \\ \sin\tilde{\alpha}\sin\tilde{\beta}\cos\tilde{\gamma}+\cos\tilde{\alpha}\sin\tilde{\gamma} & -\sin\tilde{\alpha}\sin\tilde{\beta}\sin\tilde{\gamma}+\cos\tilde{\alpha}\cos\tilde{\gamma} & -\sin\tilde{\alpha}\cos\tilde{\beta} \\ -\cos\tilde{\alpha}\sin\tilde{\beta}\cos\tilde{\gamma}+\sin\tilde{\alpha}\sin\tilde{\gamma} & -\cos\tilde{\alpha}\sin\tilde{\beta}\sin\tilde{\gamma}+\sin\tilde{\alpha}\cos\tilde{\gamma} & \cos\tilde{\alpha}\cos\beta \end{bmatrix} \begin{Bmatrix} v_1 \\ v_2 \\ v_3 \end{Bmatrix}$$

(3-2)

The angular velocities, ω_1, ω_2 and ω_3, of the ship can be expressed using the following equation in the moving coordinate system.

$$\begin{Bmatrix} \omega_1 \\ \omega_2 \\ \omega_3 \end{Bmatrix} = \begin{bmatrix} \cos\tilde{\beta}\cos\tilde{\gamma} & \sin\tilde{\gamma} & 0 \\ -\cos\tilde{\beta}\sin\tilde{\alpha} & \cos\tilde{\gamma} & 0 \\ \sin\tilde{\beta} & 0 & 1 \end{bmatrix} \begin{Bmatrix} \dot{\tilde{\alpha}} \\ \dot{\tilde{\beta}} \\ \dot{\tilde{\gamma}} \end{Bmatrix} \tag{3-3}$$

If $\tilde{\alpha}$, $\tilde{\beta}$ and $\tilde{\gamma}$ are small, then,

$$\begin{Bmatrix} \tilde{X} \\ \tilde{Y} \\ \tilde{Z} \end{Bmatrix} = \begin{bmatrix} 1 & -\tilde{\gamma} & \tilde{\beta} \\ \tilde{\gamma} & 1 & -\tilde{\alpha} \\ -\tilde{\beta} & -\tilde{\alpha} & 1 \end{bmatrix} \begin{Bmatrix} \tilde{x} \\ \tilde{y} \\ \tilde{z} \end{Bmatrix} \tag{3-4}$$

and

$$\begin{Bmatrix} v_1 \\ v_2 \\ v_3 \end{Bmatrix} = \begin{bmatrix} 1 & -\tilde{\gamma} & \tilde{\beta} \\ \tilde{\gamma} & 1 & -\tilde{\alpha} \\ -\tilde{\beta} & -\tilde{\alpha} & 1 \end{bmatrix} \begin{Bmatrix} V_1 \\ V_2 \\ V_3 \end{Bmatrix} \tag{3-5}$$

and

$$\begin{Bmatrix} \omega_1 \\ \omega_2 \\ \omega_3 \end{Bmatrix} = \begin{bmatrix} 1 & 0 & 0 \\ 0 & 1 & 0 \\ 0 & 0 & 1 \end{bmatrix} \begin{Bmatrix} \dot{\tilde{\alpha}} \\ \dot{\tilde{\beta}} \\ \dot{\tilde{\gamma}} \end{Bmatrix} \tag{3-6}$$

The coordinates of any point and the associated velocities referenced to the two coordinate systems satisfy the following vectorial formulas:

$$\vec{r}_{\tilde{X}\tilde{Y}\tilde{Z}} = \vec{r}_o + \vec{r}_{\tilde{x}\tilde{y}\tilde{z}} \tag{3-7}$$

$$\vec{V}_{\tilde{X}\tilde{Y}\tilde{Z}} = \vec{V}_o + \vec{\Omega} \times \vec{r}_{\tilde{x}\tilde{y}\tilde{z}} \tag{3-8}$$

Where $\vec{r}_{\tilde{X}\tilde{Y}\tilde{Z}}$ is the position vector of any point in global coordinate system.

$$\vec{r}_{\tilde{X}\tilde{Y}\tilde{Z}} = \tilde{X}\vec{i} + \tilde{Y}\vec{j} + \tilde{Z}\vec{k} \tag{3-9}$$

$\vec{i}$, $\vec{j}$ and $\vec{k}$ represent the $\tilde{X}$ axial direction, $\tilde{Y}$ axial direction and $\tilde{Z}$ axial direction of the global coordinate system respectively.

$\vec{r}_0$ is the position vector of the origin of the moving coordinate system in global coordinate system:

$$\vec{r}_0 = X_0\vec{i} + Y_0\vec{j} + Z_0\vec{k} \tag{3-10}$$

$\vec{r}_{\tilde{x}\tilde{y}\tilde{z}}$ is the position vector of any point in the moving coordinate system:

$$\vec{r}_{\tilde{x}\tilde{y}\tilde{z}} = \tilde{x}\vec{i}' + \tilde{y}\vec{j}' + \tilde{z}\vec{k}' \tag{3-11}$$

$\vec{i}'$, $\vec{j}'$ and $\vec{k}'$ represent the $\tilde{x}$ axial direction, $\tilde{y}$ axial direction and $\tilde{z}$ axial direction of the moving coordinate system respectively. $\vec{\Omega}$ is the vector matrix of the

angular velocities of the moving coordinate system. Its value is given by the following equation:

$$\vec{\Omega} = \omega_1 \vec{i}' + \omega_2 \vec{j}' + \omega_3 \vec{k}' \tag{3-12}$$

$\vec{V}_{\tilde{X}\tilde{Y}\tilde{Z}}$ is the velocity vector of any point in the global coordinate system.

$$\vec{V}_{XYZ} = V_1 \vec{i} + V_2 \vec{j} + V_3 \vec{k} \tag{3-13}$$

$\vec{V}_0$ is the velocity vector of origin point of the global coordinate system.

$$\vec{V}_0 = V_{10} \vec{i} + V_{20} \vec{j} + V_{30} \vec{k} \tag{3-14}$$

For the sloping surface ζ as shown in figure 3.5 and figure 3.6, the following geometrical relationship equations can be derived:

$$\tan\psi = \frac{\tan\eta}{\cos\alpha} \tag{3-15}$$

$$\tan\psi = \frac{\tan\phi}{\sin\alpha} \tag{3-16}$$

$$\tan\phi = \tan\alpha * \tan\eta \tag{3-17}$$

Where, ψ is angle between the vertical direction and the normal direction of the hull surface; ϕ is the stem angle; η is the frame angle of the hull; α is the waterline entrance angle.

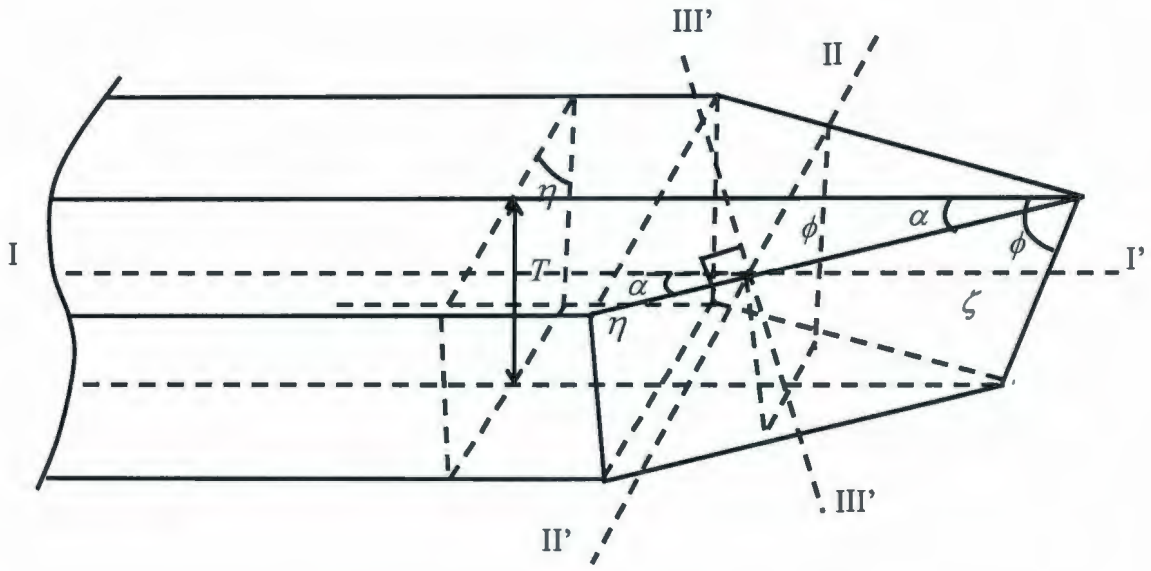

Figure 3.5 Geometry of the hull surface

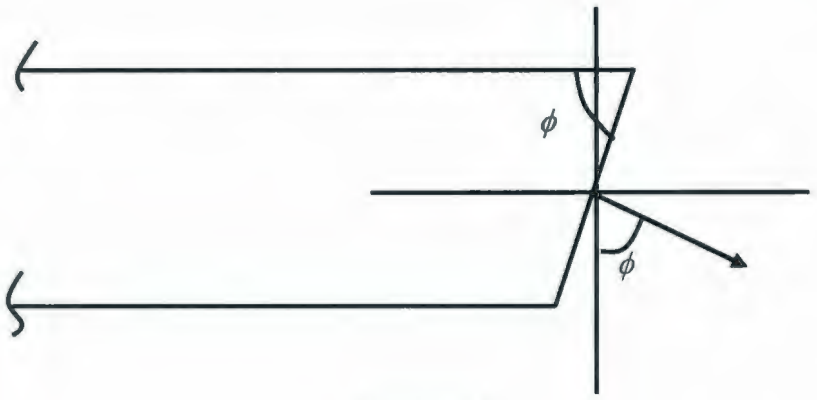

Section I-I'

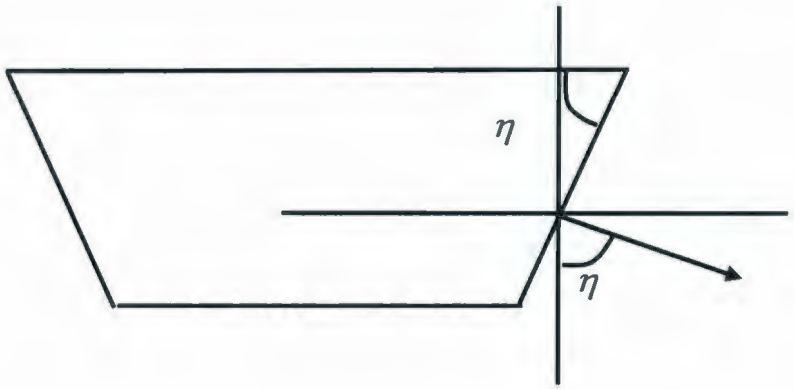

Section II-II'

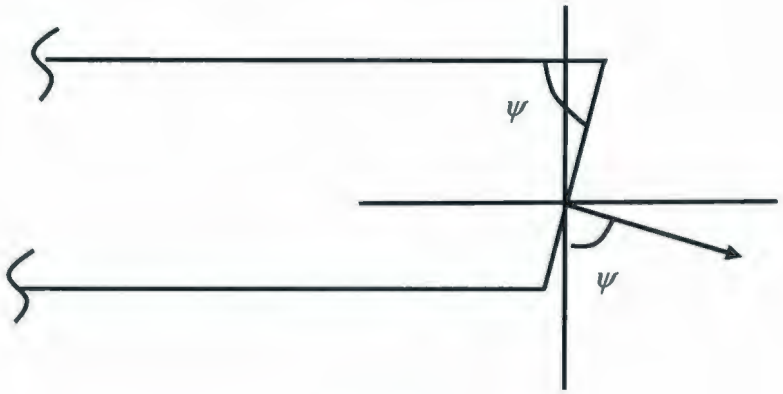

Section III-III'

Figure 3.6 Section surfaces of the hull

3.3.2 Vectors Normal to Hull Surface

The angles between the direction of the hull surface, ζ, and the x axis, y axis and z axis of the coordinate system as shown in figure 3.7, can be calculated using the following equations:

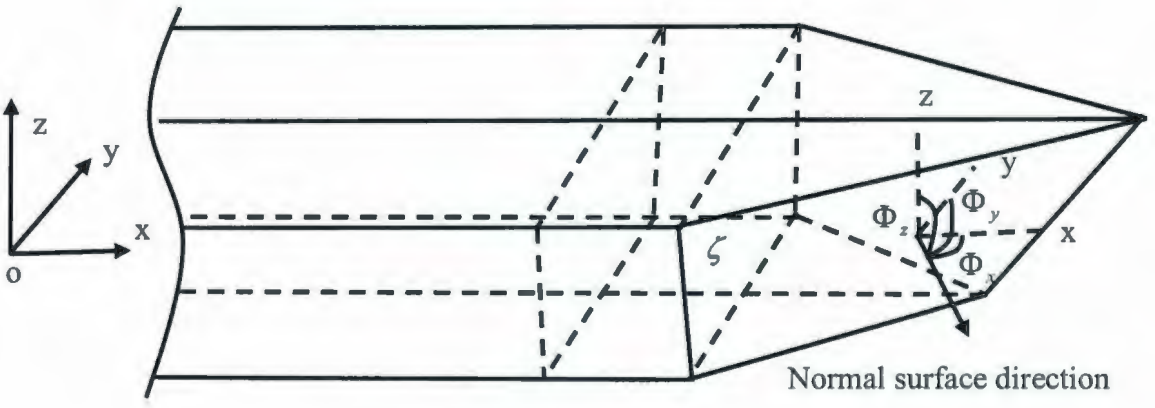

Figure 3.7 The direction normal to the hull surface

$$\cos\Phi_x = \frac{\tan\alpha}{\sqrt{1+\tan^2\alpha+\left(\frac{1}{\tan^2\eta}\right)}} \tag{3-18}$$

$$\cos\Phi_y = \frac{-1}{\sqrt{1+\tan^2\alpha+\left(\frac{1}{\tan^2\eta}\right)}} \tag{3-19}$$

$$\cos\Phi_z = \frac{-\left(\frac{1}{\tan\eta}\right)}{\sqrt{1+\tan^2\alpha+\left(\frac{1}{\tan^2\eta}\right)}} \qquad (3\text{-}20)$$

3.3.3 Ice Force Component Analysis

The ice broken by a ship during continuous transit introduces of the following processes:

Firstly, the ice deforms with relatively small deflection and initial crushing at the ice edge. The vertical force on the ice increases until flexural failure of ice occurs and an ice cusp forms. In the case of thick ice or a structure with a large sloping angle, the ice cover may be broken due to shear failure before the flexural capacity is reached.

Secondly, the broken ice piece is then rotated until it is tangential to the wet surface of the hull. Ventilation may occur due to the inability of the water to fill the void above the rotating ice piece.

Finally, some ice pieces slide along the wetted surface of the hull reaching the hull bottom and leave the hull eventually. Others may be cleared to the sides of the

ship. All ice pieces may further act upon the hull, its appendages and propulsion system.

The methodology in which the total ice force is divided into several independent force components that represent the corresponding physical processes during the continuous ship transit in level ice has been widely used (Poznyak et al., 1981; Jones et al., 1987, 2000; Spencer et al., 1992, 2001; Williams M. et al., 1996).

Each ice piece undergoes a similar physical process during ship advance and turning. For ship advancing, the amounts of ice acting on each side of the hull are the same resulting in symmetrical loading along the longitudinal center plane of the ship; whereas the amounts of ice acting on each side of the hull are different during ship turning causing an asymmetric loading on the hull. Considering the fore-mentioned interaction processes, the analytical model also divides the total ice force on the hull into three independent ice force components, i.e., the breaking, buoyancy and clearing force components. The global ice force is equal to the linear sum of the three force components:

$$X_{ice} = X_{break} + X_{buoy} + X_{clear} \tag{3-21}$$

$$Y_{ice} = Y_{break} + Y_{buoy} + Y_{clear} \tag{3-22}$$

$$N_{ice} = N_{break} + N_{buoy} + N_{clear} \tag{3-23}$$

Where, X , Y and N are the surge force, sway force and yaw moment respectively, and the subscripts "ice, break, buoy, and clear" refer to the total ice force, the ice breaking contribution, the ice buoyancy contribution and the ice clearing contribution, respectively. The ice breaking forces components are mainly dependent on ice thickness, ice flexural failure strength, ice crushing failure strength, ice shear failure strength, ice elastic modulus, hull frame angles near the waterline and ship velocity. The ice clearing force components are mainly dependent on ice thickness, hull wetted surface and ship velocity. The buoyancy force component is mainly dependent on the ice-water density difference, hull wetted surface and ice thickness.

3.3.4 Ice-Hull Contact and Channel Configuration

The process of ship navigating in ice is represented numerically in time domain. A time domain methodology is adopted to calculate the contact area between the hull and the unbroken ice and the channel is tracked through a simple house-keeping method, which means the ice channel is kept using a channel matrix during the simulation. The resulting channel edge by the ship in one calculation step is used as the initial channel edge for next calculation step.

The IHI model estimates the ice-hull contact area for the current time step based on the channel configuration and prescribed ship motions (displacement, velocity and acceleration) of the preceding time step, as shown in Figure 3.8. Then, it calculates the ice breaking force based on the contact area.

The ice was broken by the hull where the hull directly contacts unbroken level ice. At each calculation step, the newly broken ice area is overlapped to the channel left in previous step, which generates the new channel. That new channel is tracked using the channel matrix and kept as the initial ice channel edge for next calculation step.

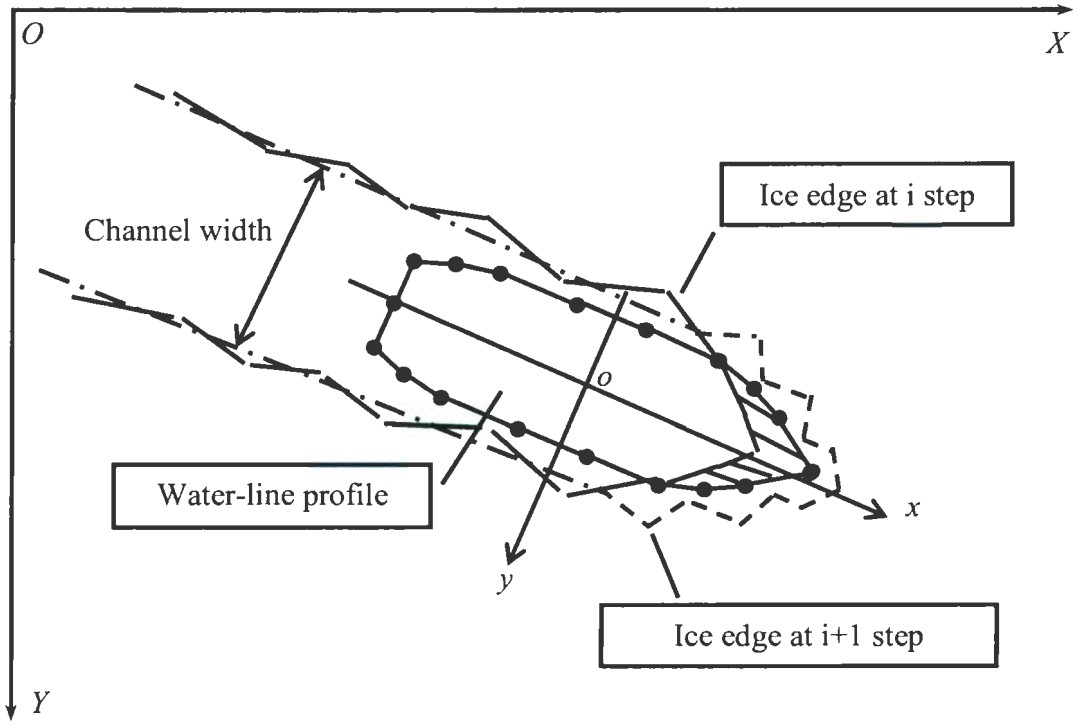

Figure 3.8 Schematic ice-hull contact in IHI model

3.3.5 Breaking Force Component

The ice breaking force component represents the contributions from the ice breaking process. Based on the ice-hull contact conditions, the ice breaking force distribution along the hull's water line is determined and integrated to give the global ice breaking force.

When the ship turns in the various level ice conditions, more parts of the hull may directly contact the unbroken ice compared to the ship advance case. Different ice failure modes, i.e., bending, crushing and shear failures, may occur simultaneously along the waterline from the stem to the stern of the hull due to the changing flare angle of the contact surface of the hull.

Upon the first contact with the hull, local crushing of the ice edge occurs. The crushing continues with increasing contact area until the contact force is large enough to initiate macro cracking due to flexural failure and a cusp of ice is generated. For thick ice or large flare angles, ice may fail in shear or crushing before the bending capacity of ice is exceeded.

The IHI model adopts a multi-mode ice failure model to calculate the ice breaking force in which the load capacity associated with each mode is assessed and the ice

is assumed to fail in the mode with minimum load capacity, as shown in Figure 3.9.

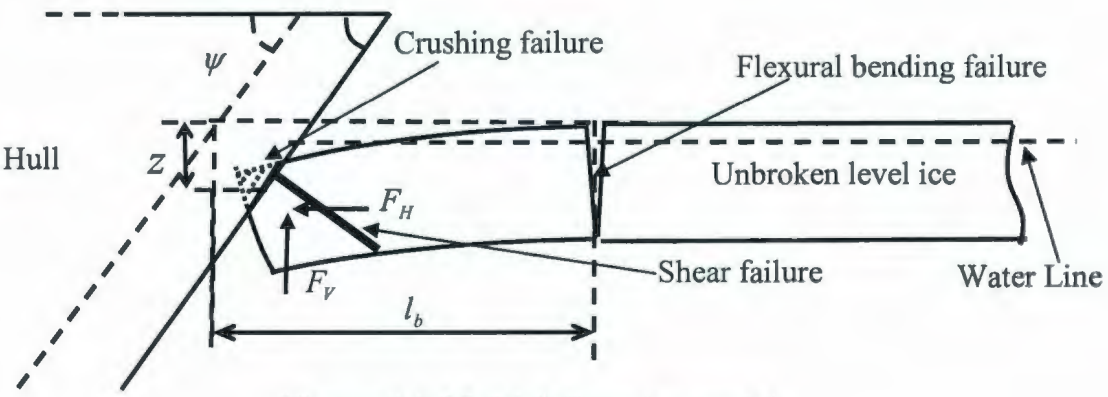

Figure 3.9 Multi-failure ice model

3.3.5.1 Bending Failure Pattern

The ice breaking process during ship manoeuvres is stochastic in nature resulting in irregular icebreaking pattern with high degree of uncertainty in predictability. This is mainly caused by the non-uniformity of the mechanical properties of ice even within a small ice extent. The icebreaking and hence the size and shape of the broken ice pieces are influenced by ice properties, such as ice thickness, elastic modulus and ice breaking strength, and by the ship related parameters such as ship speed, form, and surface friction. Due to the complexity of the interaction and ice failure process, there is not yet a universally accepted icebreaking model that can be applied to ship transit; although many models have been developed by individual researchers based on simplified treatments of the icebreaking process

(Envist, 1972; Michel, 1978; Cammaert, et al., 1988; Volanto, 1993, 2001b; Yamaguchi et al., 1994, 1997a, 1997b).

According to field observation of continuous icebreaking process, Kashteljan (1968) depicted a sketch of the ice-breaking pattern around the bow as shown in Figure 3.10.

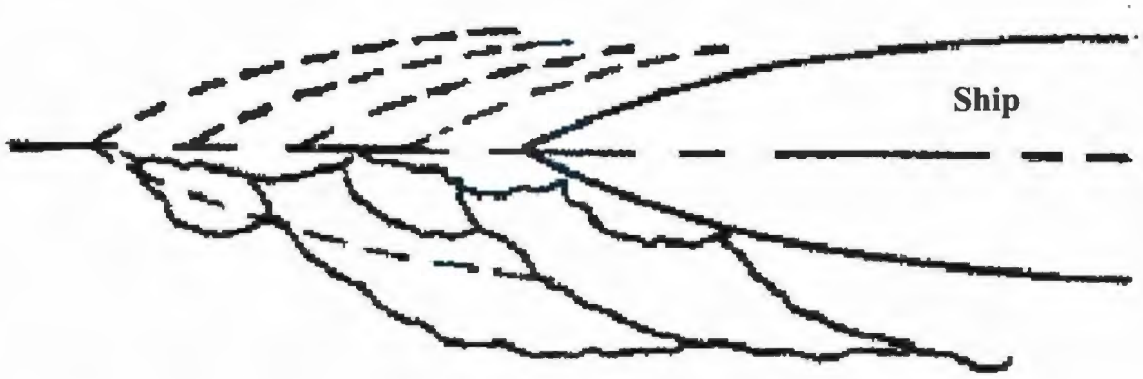

Figure 3.10 Sketch of icebreaking process by the bow of an icebreaker (Kashteljan, 1968)

Considering the complexity of the ice breaking process, Enkvist (1972) idealized the ice breaking patterns at the bow with the constant radius semicircles as shown in Figure 3.11. The number of cusps along the bow waterline is B/l. The distance travelled for each cusps is equal to l. His idealization was based on observations from model tests or full-scale trials.

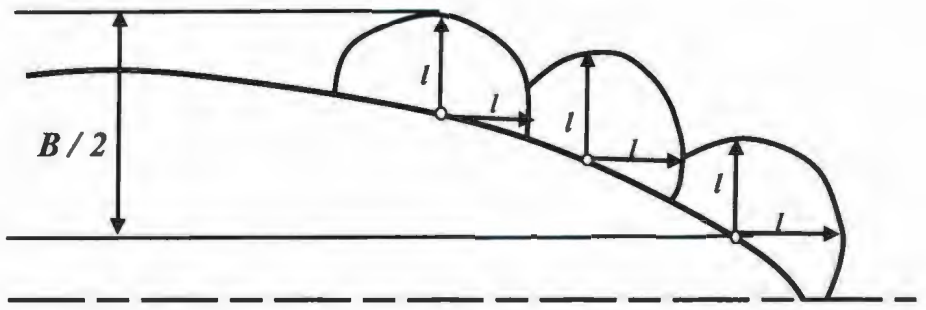

Figure 3.11 Schematic of breaking pattern (Enkvist, 1972)

Kotras et al. (1983) discussed in details various idealization of ice breaking pattern used by other researchers and proposed a more detailed idealization of the ice breaking pattern, in which the shape of the cracking pattern was expressed by a series of semi-ellipses with varying radius due to the varying hull curvature and angle along the hull's waterline as shown in Figure 3.12.

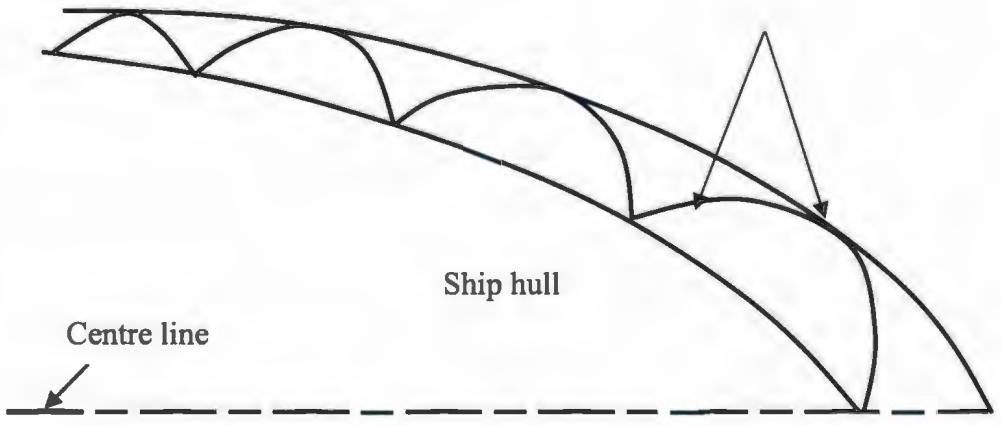

Figure 3.12 Breaking pattern used by Kotras et al. (1983)

Based on a large number of observations in full-scale sea trails, Edwards gave his opinion on the ice pattern around an icebreaker (Kotras et al., 1983). He pointed out that there should be only one characteristic failure shape and "the failed ice cover consisted of row pieces that resemble the superposition of a cusp on a segment".

During ship turning in level ice, the ice-hull contact condition is complex and any parts of the hull from the bow to the stern may directly contact the intact ice edges with the contact angle, and interaction velocity varied along the ship hull. Even during a steady motion, the momentary local ice-hull contact condition is still stochastic and there are still big local variations. Based on the discussions presented in Section 3.1, the proposed IHI model neglects the high frequency ice force fluctuation (due to cyclical icebreaking) and integrates ice force over a large time interval consisting of at least a few ice breaking cycles to arrive at an equivalent local ice resistance. The IHI model does not attempt to calculate the actual shape and position of each ice piece. Instead, the IHI model assumes an ice cusp pattern similar to that proposed by Edwards (Kotras et al., 1983) as shown in Figure 3.13, and a 3-dimensional plate theory is used to calculate the flexural icebreaking force.

The crushing failure of the intact ice edge is also considered. The cusp parameters, D and W, are determined by the ice properties, ship velocity and ship geometry, i.e. flare angle at the ice-hull contact point.

The average breaking depth, D, is taken as a function of the characteristic length of ice, and is computed according to Lau et al (1999). The width, W, is proportional to the semi-ellipse cusp depth based on the full-scale trials (Kotras et al., 1983), and is defined as follows

$$\frac{W}{L_D} = \sqrt{\frac{\hbar}{h}} \tag{3-25}$$

Figure 3.13 Sketch of ice cusp pattern adopted in IHI model

Where h is the ice thickness in meters, $\hbar$ is an empirical constant determined from the statistical data of full-scale observations. According to Kotras et al (1983), $\hbar$

is defined as 10.0m in the model. According to the geometrical relationship, it can be derived that D, as shown in figure 3.13, is about equal to the double length of L_D.

In Kotras's model, the ice crack is modeled as the combination of semi-ellipse cusp and wedges. The Nevel's solution for edge-loaded semi-infinite ice sheet was adopted for calculating the flexural bending failure force to form a semi-ellipse cusp. In the ice-hull interaction model presented in this thesis, a complete ice cusp model was adopted as shown in figure 3.15. When the hull breaks the level ice, the crushing failure first happens at the contact edge. The ice-hull contact force is loaded at the ice-hull crushing area. Since the crushing depth is very small (crushing strength is much bigger than bending strength of ice) comparing to the ice cusp width, globally the ice-hull contact load can still be treated as a concentrated load rather than a line load on the ice edge. Many researchers have made contributions on calculating the bearing capacity of the floating ice plates subjected to concentrated static or quasi-static loads such as Black (1958), Kashtelyan (Kashtelyan, 1960; Kashtelyan et al., 1969), Kerr (Kerr, 1975, 1976, 1996; Kerr et al., 1972, 1988), Michel (1978), and so on.

Kashtelyan's equations for calculating the bearing capacity values of the semi-infinite ice plate including the water pressure (from the 'elastic foundation') were verified by the results of 150 tests on floating ice plates and analyzed by Kerr

(1976). From the Kashtelyan's solution, the ice load for the ice wedge with any opening angle can be calculated using relative simple formulas. It can be more easily implemented into the multi-failure model with crushing failure, flexural failure and shear failure that was adopted by the IHI model. The theoretical solution by Kashtelyan (Kashtelyan, 1960; Kashtelyan et al., 1969) was adopted in the presently developed IHI model.

According to Kashtelyan (1960; Kashtelyan et al., 1969), the corresponding flexural bending failure load, F_f, for producing a cusp by bending from a semi-infinite ice plate is given as follows:

$$F_f = 0.518\sigma_f h^2 \tag{3-26}$$

Where σ_f is the flexural strength of ice; h is the ice thickness.

Kashtelyan also gave the flexural bending failure load for an infinite plate using the following expression:

$$F_f = 2.08\left(\frac{\varphi_n}{\pi}\right)\sigma_f h^2 \tag{3-27}$$

Where φ_n is the opening angle of the ice wedge and is equal to $\varphi_n = 2\pi/n$ and n is the number of radial cracks.

Then, the maximum deflection for producing a cusp by bending failure was (1960, Kashtelyan et al., 1969):

$$\delta = \frac{0.518\sigma_f h^2}{\tilde{\gamma}_w l_c^2} \tag{3-28}$$

Where the weight density of water, $\tilde{\gamma}_w$, is defined by

$$\tilde{\gamma}_w = \rho_w g \tag{3-29}$$

l_c is characteristic length for the plate defined by

$$l_c = \left[\frac{Eh^3}{12.0\rho_w g(1-\nu^2)}\right]^{0.25} \tag{3-30}$$

ν is Poisson's ratio of ice, E is elastic modulus of ice, h is the ice thickness and g is the acceleration due to gravility.

3.3.5.2 Ship Velocity Effects on Ice Piece Size

The average size of broken ice pieces depends on ship speed, the ice thickness and ice mechanical properties. The ship velocity effects on ice piece size are taken into consideration using the results of Varsta (1983), Enkvist (1972) and Yamaguchi et al. (1994). The ice cusp depth, D, as a function of ship velocity may be expressed as:

$$D = \frac{D_0}{(C_{V0} + C_V V)} \tag{3-31}$$

where the ice cusp depth, D_0, is 0.2 times the characteristic length of ice according to Lau et al (1999) and is independent of velocity. V is the velocity of the ship breaking ice. C_{V0} and C_V are two constants determined from experimental data. The IHI model uses a value of 0.75 for C_{V0} and 0.3 for C_V in order to make the equation 3-31 fit the experimental data provided by Varsta (1983).

3.3.5.3 Initial Crushing Failure

The ice crushing process starts upon ice-hull contact. A crushing process exists before the ice macro cracks appear due to the ice bending failure or shear failure . The crushing force and the corresponding contact area increase with the

penetration of the hull. Once the ice-hull contact load is large enough to initiate flexural or shear ice failures, the crushing process ends and an ice cusp is generated. A new ice breaking cycle begins as soon as the hull contacts the intact ice edge again.

The crushing failure mechanism on the ice edge during ship-ice interaction has been studied by Varsta (1983; Varsta et al., 1977), Linqvist (1989), Arunachalam et al. (1993), Kujala (1994a, 1994b, 1996), Jordaan and McKenna (Jordaan, 2001; Jordaan et al., 1991; Fuglem, 1999) and Daley (1992, 1999; Daley et al., 1990, 1997), among others. All of these approaches use a reference crushing strength, with the details of the model representing details at the failure surface. In the present IHI model, only the average global load is required. Hence the crushing force, F_{crush}, normal to the ice-hull contact surface is simplified and calculated using the following equation (Sanderson, 1988):

$$F_{crush} = \sigma_c \cdot A_c \tag{3-32}$$

where σ_c is the crushing strength of ice. A_c is the hull-ice contact area, which is noted in the following section 3.3.5.4.

The contact between the ice and the hull surface is assumed to remain perfect during the initial crushing process. In each icebreaking cycle, the ice-hull contact force increases from zero with the increase of the crushing surface area until the contact force is large enough to cause a microscopic crack due to bending bending failure or shear failure, then the ice breaking force drops to zero. The average force for each icebreaking cycle is calculated using an energy method.

3.3.5.4 Shear Failure

For a thick ice sheet, the ice may fail in shear through the depth of the ice sheet before its flexural capacity is exceeded. The local crushing of the ice, spalling at the ice edge and shear through the depth of the ice sheet may happen simultaneously when the ice is thick or when the hull surface contacting ice is nearly vertical (Varsta et al., 1977; Daley, et al., 1998; Jordaan, 2001). The simplified shear failure model given by Mckenna (1993a, 1993b) for the shear failure of an ice wedge was adopted in the IHI model. The local crushing and spalling is modeled as a constant contact pressure. Friction between the ice and hull is modelled using a constant coefficient. A simple shear failure criterion is also included. Then, the formula for calculating the shear stress in a shear plane with an inclination angle ϑ, as shown in the Figure 3.14, can be derived as

$$\tau_{\vartheta} \approx \frac{\sigma_c \dfrac{h}{\sin\psi}\left[W_{crush} - h\cot(\psi) * \tan(\frac{\varphi}{2})\right](\cos\psi\cos\vartheta + \sin\psi\sin\vartheta)\cos\vartheta}{\left[W_{crush} + h\tan\vartheta\tan\left(\dfrac{\varphi}{2}\right)\right]h} \qquad (3\text{-}33)$$

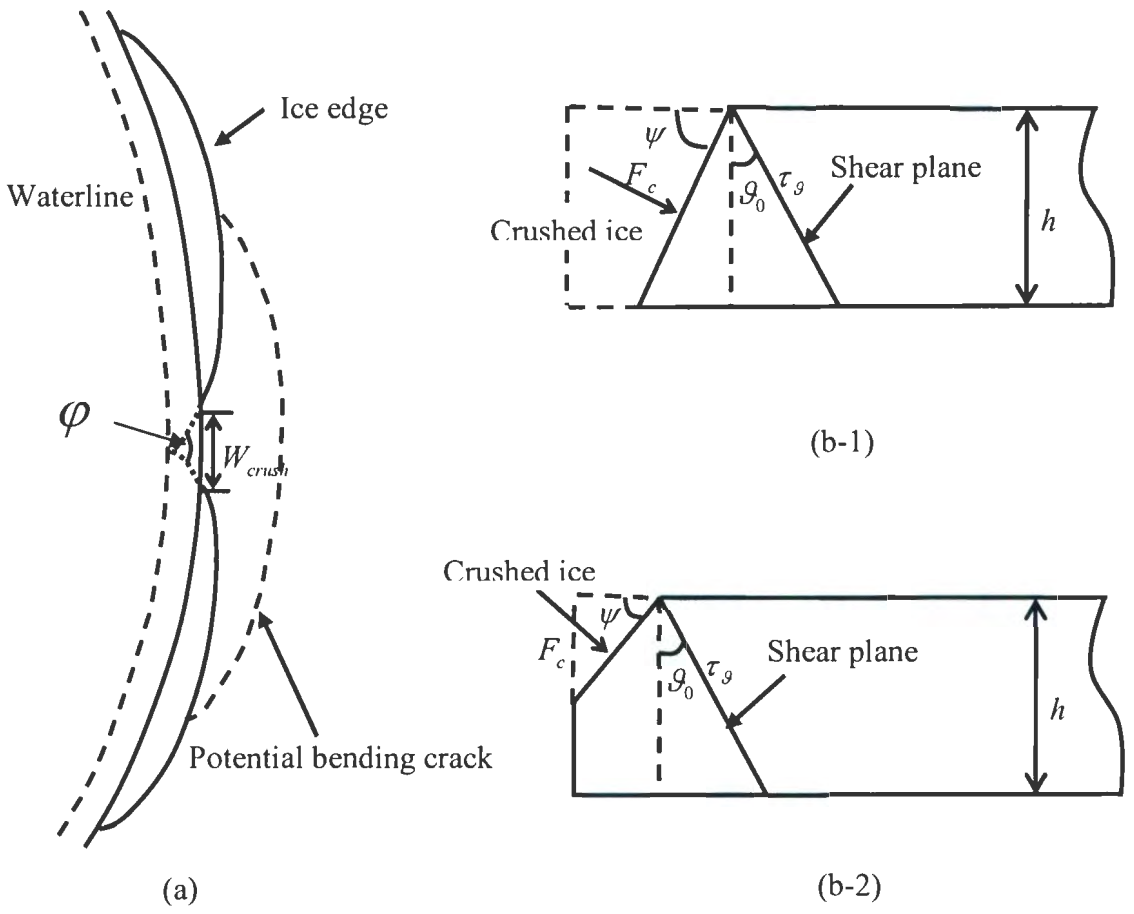

Figure 3. 14 Sketch of initial crushing at the edge of the ice cusp acted on by the inclined force

Equation 3-33 is valid when the crushing surface completely penetrates through the whole ice profile as shown in b-1 of Figure 3.14. In this case, the ice-hull contact area, A_c, is equal to $\frac{h}{\sin\psi}\left[W_{crush} - h\cot(\psi) * \tan(\frac{\varphi}{2})\right]$.

In the case where the crushing surface does not penetrate through the ice sheet, as shown in b-2 of figure 3.14,

$$\tau_{\vartheta} \approx \frac{0.25\sigma_c W_{crush}^2 * (\cos\psi\cos\vartheta + \sin\psi\sin\vartheta)\cos\vartheta}{\tan\frac{\varphi}{2}\cos\psi\left[W_{crush} + h\tan\vartheta\tan\left(\frac{\varphi}{2}\right)\right]h} \tag{3-34}$$

In this case, the ice-hull contact area, A_c, is equal to $\frac{0.25W_{crush}^2}{\tan\frac{\varphi}{2}\cos\psi}$.

In equations 3-33 and 3-34, τ_{ϑ} is the shear stress along the shear plane; h is the ice thickness; the angle, ψ, is the sloping angle of the structure; W_{crush} is the width of the wedge at the intersection line of the shear plane and the level ice surface; φ is the opening angle of the ice wedge.

The inclination angle, ϑ_0, of the shear plane corresponding to the maximum shear stress is determined by solving the following theoretically derived formula:

$$\left.\frac{d\tau_{\vartheta}}{d\vartheta}\right|_{\vartheta=\vartheta_0} = \frac{d\left(\frac{(F_c\cos\psi\cos\vartheta + F_c\sin\psi\sin\vartheta)\cos\vartheta}{\left[W_{crush} + h\tan\vartheta\tan\left(\frac{\varphi}{2}\right)\right]h}\right)}{d\vartheta}_{\vartheta=\vartheta_0} = 0 \tag{3-35}$$

where F_c is the crushing force acting on the hull.

The IHI model computes the shear failure load by checking the maximum shear stress, $\tau_{\max}$, corresponding to the shear strength of ice, τ_c, i.e.,

$$\tau_{\max} = \tau(\vartheta_0) \geq \tau_c \tag{3-36}$$

Compared to the crushing width, $h \tan\vartheta \tan\left(\frac{\varphi}{2}\right)$ is a small amount and can be neglected. Hence the complicated formula, Equation 3-34, can be simplified into the following relationship:

$$\psi = 2.0 * \vartheta_0 \tag{3-37}$$

Combining Equations 3-33, 3-34, 3-35 and 3-36, the shear failure happens when one of the following equations are satisfied:

$$\frac{\sigma_c \frac{h}{\sin\psi}\left[W_{crush} - h\cot(\psi) * \tan(\frac{\varphi}{2})\right]\left(\cos\psi\cos\frac{\psi}{2} + \sin\psi\sin\frac{\psi}{2}\right)\cos\frac{\psi}{2}}{\left[W_{crush} + h\tan\frac{\psi}{2}\tan\left(\frac{\varphi}{2}\right)\right]h} = \tau_s \tag{3-38}$$

or

$$\frac{0.25\sigma_c W_{crush}^2 * \left(\cos\psi\cos\frac{\psi}{2}+\sin\psi\sin\frac{\psi}{2}\right)\cos\frac{\psi}{2}}{\tan\frac{\varphi}{2}\cos\psi\left[W_{crush}+h\tan\frac{\psi}{2}\tan\left(\frac{\varphi}{2}\right)\right]h}=\tau_s \tag{3-39}$$

The Equations 3-37 and 3-38 can be respectively transferred into the following forms:

$$W_{crush}=\frac{h\left(\tan\frac{\psi}{2}\tan\frac{\varphi}{2}+0.5\frac{\sigma_c}{\tau_s}\frac{\tan\frac{\varphi}{2}}{\tan\frac{\psi}{2}\tan\psi}\right)}{0.5\frac{\sigma_c}{\tau_s}\frac{1}{\tan\frac{\psi}{2}}-1.0} \tag{3-40}$$

and

$$W_{crush}=2h\frac{\tau_s}{\sigma_c}\frac{\tan\frac{\varphi}{2}\cos\psi}{\cos^2\frac{\psi}{2}}+2h\sqrt{\frac{\tau_s}{\sigma_c}\frac{\tan\frac{\varphi}{2}\cos\psi}{\cos^2\frac{\psi}{2}}\left(\frac{\tau_s}{\sigma_c}\frac{\tan\frac{\varphi}{2}\cos\psi}{\cos^2\frac{\psi}{2}}+\tan\frac{\psi}{2}\tan\frac{\varphi}{2}\right)} \tag{3-41}$$

3.3.5.5 Effects of In-Plane Force

The contents of this section consider the research by Croasdale (1980, 1994) and Mckenna (1993). A hull surface with the sloping angle, ψ, breaks an ice sheet of thickness h, as shown in Figure 3.15. The ice is broken in flexure by the hull, which submerges the broken ice along the hull surface. The frictional force from

the hull acts on the ice opposite to the ice piece sliding direction. The force normal to the hull surface on the unit width level ice, P_N, can be divided into two components: P_V acting vertically and P_H acting horizontally. If the frictional coefficient between ice and hull is μ, these components can be written using the following equations (Croasdale, 1980),

$$P_V = P_N(\cos\psi - \mu\sin\psi) - P_{buoya}\sin\psi(\sin\psi + \mu\cos\psi) \tag{3-42}$$

$$P_H = P_N(\sin\psi + \mu\cos\psi) + P_{buoya}\cos\psi(\sin\psi + \mu\cos\psi) \tag{3-43}$$

P_{buoya} is the buoyancy force acting on the submerged ice. The above equations can also translated into the following forms,

$$P_H = P_V\frac{(\sin\psi + \mu\cos\psi)}{(\cos\psi - \mu\sin\psi)} + P_{buoya}\frac{(\sin\psi + \mu\cos\psi)}{(\cos\psi - \mu\sin\psi)} \tag{3-44}$$

$$P_V = P_H\frac{(\cos\psi - \mu\sin\psi)}{(\sin\psi - \mu\cos\psi)} - P_{buoya} \tag{3-45}$$

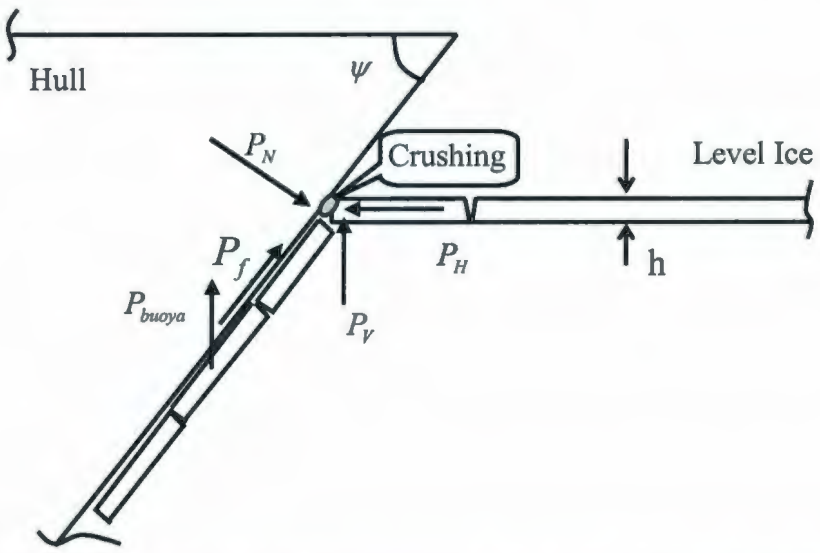

Figure 3.15 Geometry for 2-dimensional analysis of forces on a sloping structure

McKenna (1993) used the following equation to approximately calculate the maximum flexural stress in the bending ice wedge,

$$\sigma_f = \frac{6M_{\max}}{Wh^2} - \frac{P_H}{Wh} \tag{3-46}$$

Here, it is applied to approximately estimate flexural stress of the bending ice cusp. $M_{\max}$ is the bending moment on the ice, which is dependent on the vertical force, P_V and the horizontal force, P_H, on the ice cusp. The vertical force P_V is dependent on the ice flexural strength. It is calculated based on the corresponding plate mechanics, the vertical force, F_v, given in Equation 3-26, divided by cusp width W. P_H is calculated through Equation 3-44. Using the equations, 3-42 and

3-43, the normal force on the ice-contact hull surface, P_N, can be calculated. The bending moment to fail an ice sheet increases due to its balance partly by the in-plane force.

3.3.6 Clearing Force Component

The clearing force component is developed mainly in the ice piece rotating process. The sources of the clearing force are complex including the physical processes of the broken ice rotating at the water surface, sliding along the hull surface, and its eventual movement away from the hull.

The IHI model calculates the clearing force component by considering the force imposed by the motion of an ensemble of ice pieces rotating and sliding along the submerged surface of the hull. The clearing force component includes viscous drag and inherent buoyancy for the rotating ice floes, forces caused by wave pressure and ventilation of the rotating ice floes, and inertial forces due to the ice acceleration. The IHI model computes the force associated with each phenomenon by considering the physical process involved.

The IHI model adopts an energy method to calculate the force imposed by the motion of the ice mass during the ice floe turning process. The force due to ventilation, the static pressure and bow wave on the ice piece turning at the water

surface is estimated according to Enkvist (1972), Kotras, et al. (1983) and Lindstrom (1990, 1991) as shown in Figure 3.16.

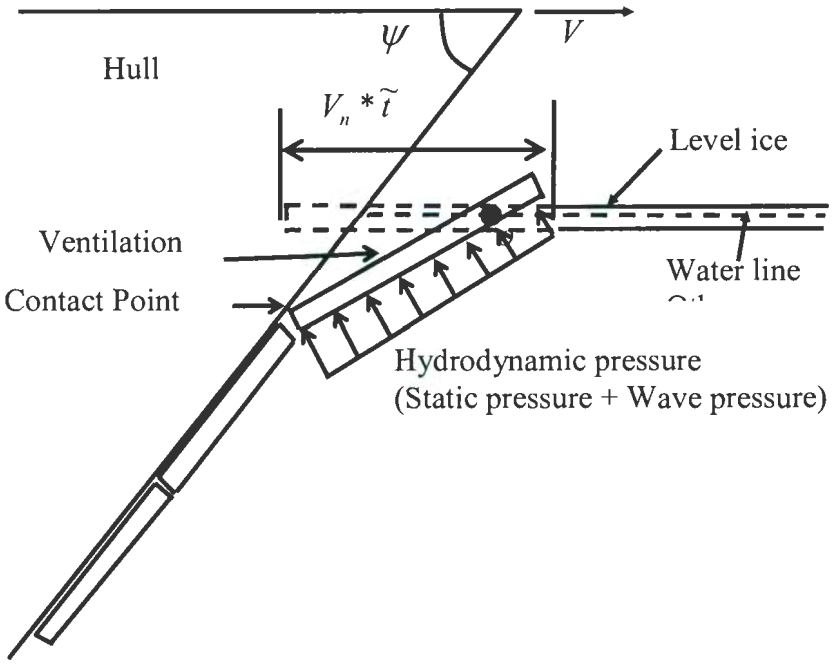

Figure 3.16 Sketch of ice pieces turning and sliding (view in horizontal direction)

3.3.6.1 Modeling of Ice Piece Rotation

The following content on the modeling of ice cusp turning process refers to the research by Enkvist (1972), Kotras, et al. (1983), Lindstrom (1990, 1991) and Valanto (2001a, 2001b, 2006).

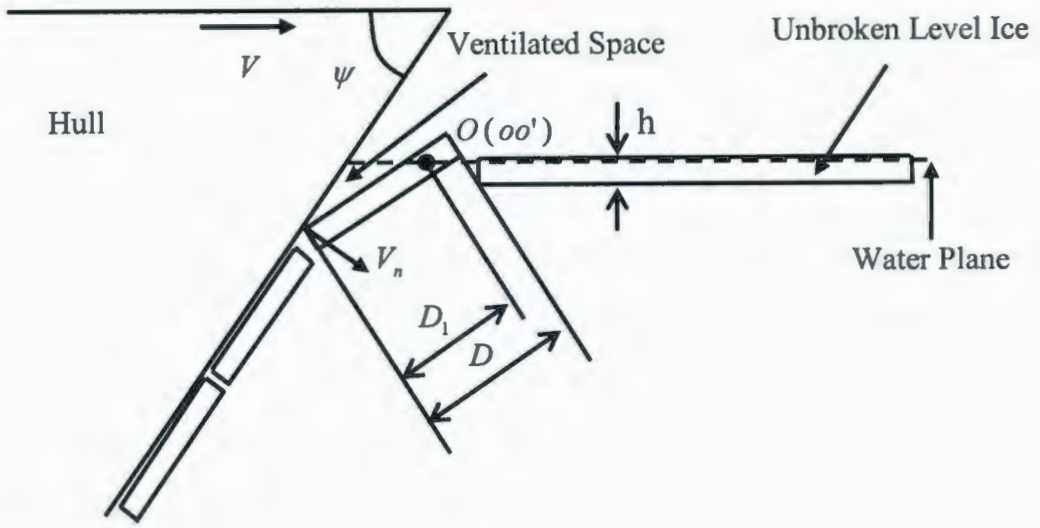

Figure 3.17 Sketch of turning ice cusp pieces (view in horizontal direction)

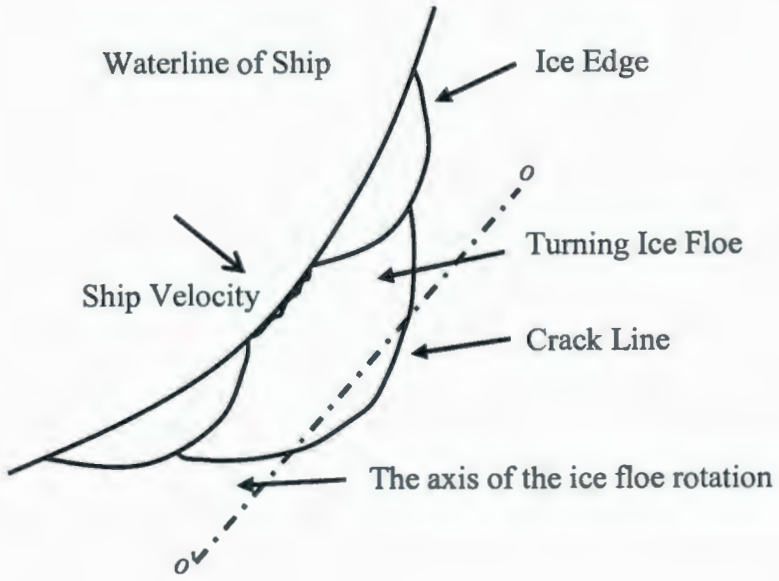

Figure 3.18 Sketch of turning ice cusp pieces at the side of a ship (view in vertical direction)

After the level ice cusp is broken, the newly generated ice piece is accelerated and rotated by the hull, and resisted by the wave and hydrostatic pressures. The floe first turns about the end of the intact ice edge until the vertical force on the ice floe exceeds the friction force that can hold the end of the floe at its original place. The ventilation happens during rapid floe turning, as shown in Figure 3.17 and 3.18. The floe rotates until it is parallel to the hull surface. It is then pushed further downward along the wet surface of the hull by other newly generated floes.

3.3.6.2 Hydrodynamic Force on Ice Pieces

The hydrodynamic force is a result of viscous drag on the turning ice floe and a combined effect of potential ventilation and bow wave.

The viscous drag and inherent buoyancy and the forces caused by wave pressure and ventilation of the rotating ice pieces are all considered as the hydrodynamic force in the IHI model.

3.3.6.2.1 Viscous Drag

During the ice piece turning process, it also is acted on by water viscous drag as shown in Figure 3.19. The viscous drag calculation is taken from Kotras (1983) and Lindstrom (1991).

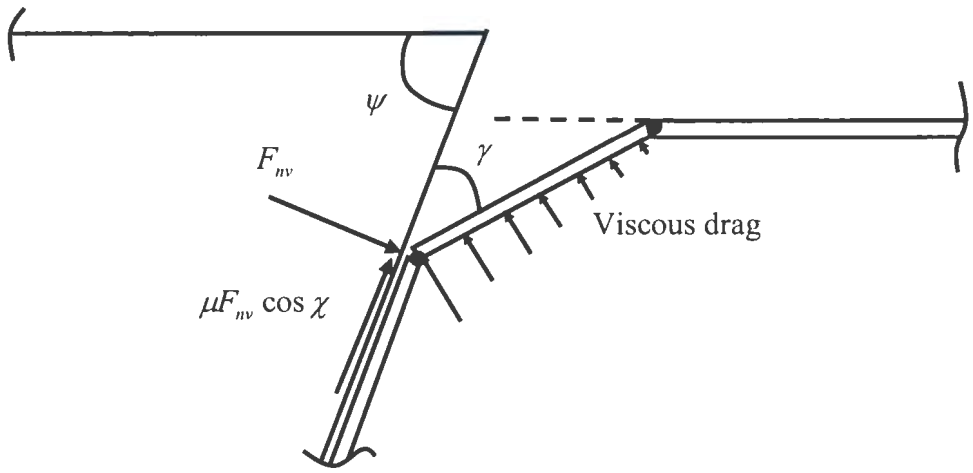

Figure 3.19 Viscous drag force

It is assumed that the floe is rotating around its rear edge for calculation of the hydrodynamic drag force. Integrating the velocity over the ice floe and solving the moment equation, the following equation can be derived for the force normal to hull surface due to water drag on the turning ice cusp (Lindstrom, 1991):

$$F_{nv} \approx \frac{0.1675\rho_w C_d V^2 DW}{\cos(\gamma) - \mu\cos(\chi)\sin(\gamma)} \tag{3-47}$$

Where, V is the velocity of the front edge of the ice cusp floe; The drag coefficient, C_d, was assumed equal to 1.0 after Kotras et al (1983).

3.3.6.2.2 Static Pressure Due to Ventilation and Bow Wave Pressure

In the IHI model, ventilation above the roting ice floe is assumed in order to calculate the force on the hull caused by the static water pressure and wave pressure under the roting ice floe. The force due to the ventilation, static pressure and bow wave associated to the turning ice piece, as shown in Figure 3.20, was estimated referring to the theories by Lindstrom (1991) and Enkvist (1972). The water static pressure under the turning piece is

$$F_{ns} = \frac{A_{ice} * \rho_w g * H_s \zeta_s}{[\cos\gamma - \mu \cos\chi \sin\gamma]} \tag{3-48}$$

Where A_{ice} is the area of the ice piece and is about equal to $0.5 * DW$; H_s is the depth of the whole turning ice cusp; ξ_s is a constant whose value is dependent on the static pressure distribution and the ice cusp geometries. In the model, an ice cusp pattern was adopted as shown Figure 3.18 and its ξ_s value is between that of a regular triangle plate and a rectangle plate. As we know, the ξ_s value for regular triangle plate is 0.4 and the rectangle plate 0.67. Therefore, its value for the ice cusp is approximately adopted as 0.45 considering the geometries of the ice cusp with its static pressure distribution and the ice crushing at end edge of the ice cusp.

The wave height during the ice piece turning is approximated by (Enkvist, 1972), which was obtained from model tests.

$$H_w = 0.5\frac{V^2}{2g} \tag{3-49}$$

Where, V is the velocity of the hull at the ice-hull contacted point normal to the contacted surface.

It should be noted that Kotras, et al. (1983) adopted one more complicated formula from other researchers to calculate the wave pressure in his ice resistance model, which considers the length between the calculated point and the stem. Because his work is only based on the simple resistance case whether those formulas are still valid is unknown when the ship turns in the ice. Therefore, in the model for the ship manoeuvring, the simplified treatment of this problem was adopted as described above (Enkvist, 1972).

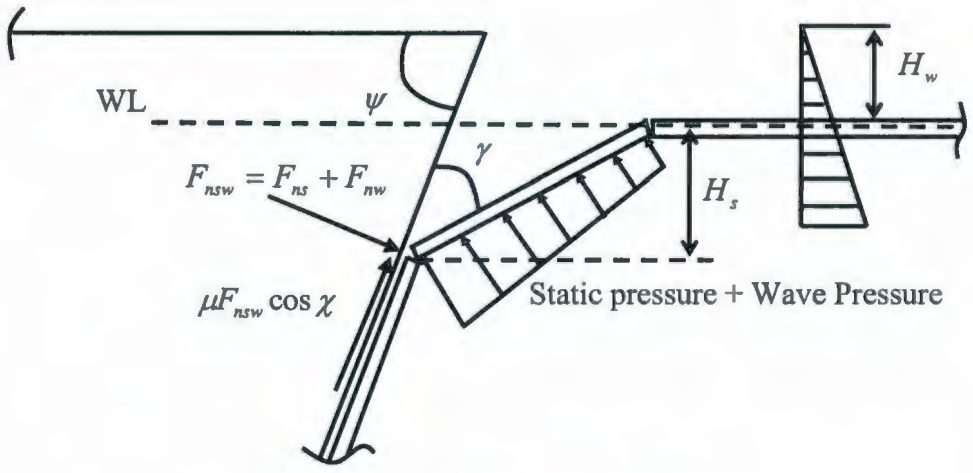

Figure 3.20 Viscous drag force

The height, H_w, can be added to H_s of the formula, 3-50, to calculate the force caused by wave height and water static pressure together.

The force normal to the hull surface for each ice cusp caused by bow wave and water static pressure on the turning ice floe can be calculated using equation 3-50.

$$F_{nsw} = \frac{A_{ice}\rho_w g(0.45 * H_s + H_w)}{[\cos\gamma - \mu\cos\chi\sin\gamma]} \tag{3-50}$$

where A_{ice} is the area of the ice piece.

3.3.6.3 Inertia Force due to Ice Piece Acceleration

3.3.6.3.1 Mass Force

After the rotating process of the ice cusps, they are pushed down along the hull surface by the laterally generated ice cusps as shown in Figure 3.23.

The ship turns in level ice normally with relatively low velocity and the broken ice piece is pushed down by the turning ice piece. It is reasonable to assume that the sliding speed along the hull is approximately equal to the ship's horizontal speed, V, as shown in Figure 3.21. In the figure, the velocities are all relative to the ship. The horizontal force equals the kinetic energy of the ice pieces divided by the

ship's travel distance, taking account of their added mass. The ice piece has an absolute vertical velocity:

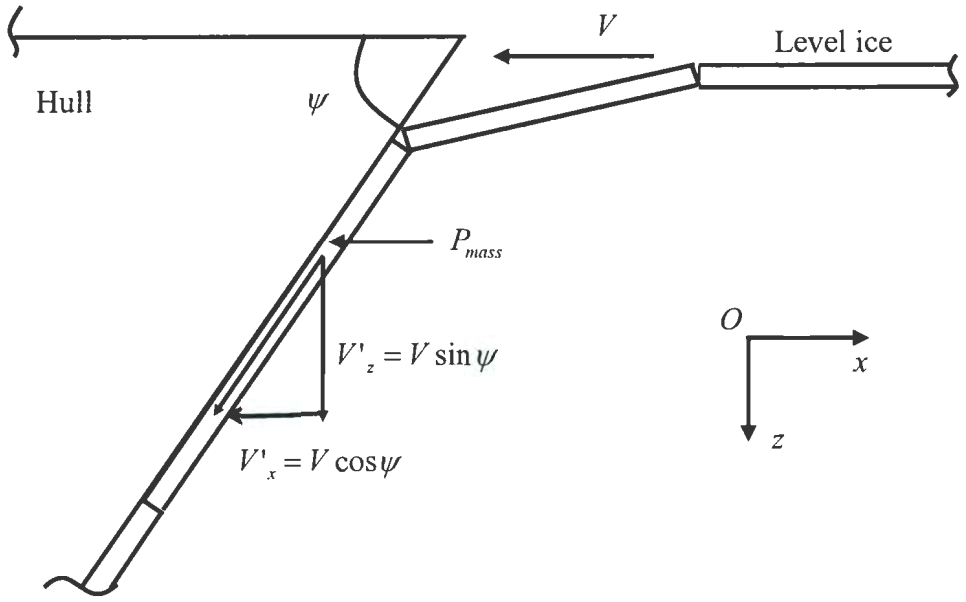

Figure 3.21 Sketch of ice pieces pushed down by the turning ice piece

$$V_z = V'_z = V\sin\psi \tag{3-51}$$

Where, V_z' is the vertical velocity of sliding ice pieces relative to the moving hull and the absolute horizontal velocity of ice piece is:

$$V_x = V - V'_x = V(1-\cos\psi) \tag{3-52}$$

Where, V_x' is the horizontal velocity of sliding ice pieces relative to the hull.

The kinetic energy, E_k, of the ice mass, M_{ice}, is

$$E_k = 0.5 \cdot (1 + C_{add\_mass}) M_{ice} (V_z^2 + V_x^2) = (1 + C_{add\_mass}) M_{ice} V^2 (1 - \cos\psi) \qquad (3\text{-}53)$$

The final ice mass force on unit width of the hull is equal to

$$P_{mass} = \frac{E_k}{0.5 * DW} \approx \frac{(1 + C_{add\_mass}) V^2 (1 - \cos\psi) * 0.5 \rho_{ice} DWh}{0.5 * DW} = (1 + C_{add\_mass}) \rho_{ice} h V^2 (1 - \cos\psi) \qquad (3\text{-}54)$$

Where, C_{add_mass} is the water added mass coefficient

Considering the ice frictional force, based on equation 3-54, the ice mass force on unit width of the hull is equal to

$$P_{mass} = (1 + C_{add\_mass}) \rho_i h V^2 (1 - \cos\psi)(1 + \mu \cot\psi) \qquad (3\text{-}55)$$

For the hull part with large sloping angles, the broken ice pieces are jammed around the waterline due to the frictional force. Then the ice pieces have the horizontal velocity approximately equal to the ship's horizontal speed, V. The ice mass kinetic energy is equal to

$$E_h = 0.5 * (1 + C_{add\_mass}) \rho_i DWhV^2 \tag{3-56}$$

3.3.6.3.2 Hydrodynamic Added Mass Coefficient

The added water mass coefficient is calculated using empirical formula (Blevins R., 1979). The ice piece can be regarded as thin plate as shown in Figure 3.22.

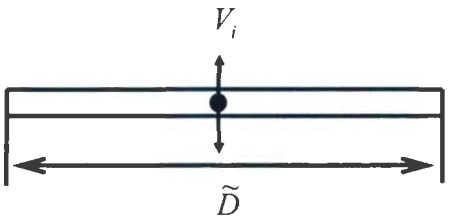

Figure 3.22 Sketch of plate for added mass calculation

The added mass per unit width, M_{T_add}, for the acceleration in the direction normal the plate can be estimated, as shown in Figure 3.22, using the following equation (Blevins, 1979):

$$M_{T\_add} = \rho_w \pi \frac{\tilde{D}'^2}{4} \tag{3-57}$$

Where $\tilde{D}'$ is the width of the projected plate normal to the velocity of the plate. The water added mass coefficient is calculated using the following equations for the ice pieces sliding on the hull as shown in Figure 3.23:

$$C_{add\_mass} = \frac{M_{T\_add}}{M_{ice}} = \frac{\rho_w \pi \frac{\tilde{D}'^2}{4}}{\rho_i \tilde{D} h} = \frac{\rho_w \tilde{D} \pi \sin^2(\psi + \psi')}{4 \rho_i h} \tag{3-58}$$

In the IHI model, $\tilde{D}$ is equal to the ice cusp depth, D.

Where, ψ' is the angle between the ice piece velocity and vertical direction as shown in Figure 3.23 and can be calculated using the following equation.

$$\psi' = \arctan\left(\frac{V_x}{V_z}\right) \tag{3-59}$$

Where, V_x and V_z are given in equation 3-52 and 3-51.

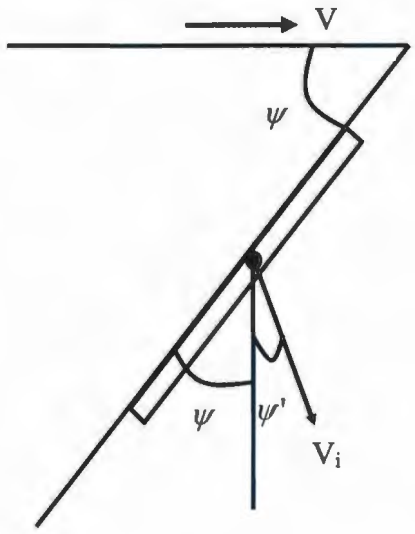

Figure 3.23 Sketch of ice piece sliding on the wet surface

3.3.6.4 Impact Force

After its rotation, the ice cusp slides along the wetted surface of the hull and is pushed downwards by other broken ice pieces. This sudden change of the rotational motion of ice cusp causes the impact force on the ship shell (Valanto 1987, 2001b). This impact can be calculated if the speed of the ship and the virtual mass of the ice floe are known. The angular velocity of ice cusp can be computed based on the geometry of the ice cusp and the hull velocity. If the moment of inertia of the rotating floe is known, the change in rotary energy can be calculated.

The actual position of the rotating axis is very difficult to be accurately determine considering that it is dependent on the actual ice piece size, viscous drag force, ventilation above the rotating ice floe, the static water pressure under the ice floe and the hull contacting force and frictional force. The accurate position of the rotation center, O, during the ice cusp rotary process, as shown in Figure 3.17 and 3.18, is dependent on the dynamic water-ice, ice-hull and ice-ice interaction. Considering the facts that the impact ice force is only one of many force components and in order to make the whole calculation short, a simplified axial position, which is at the end of the ice cusp, was adopted according to Enkvist (1972).

$$\frac{D_1}{D} \approx 1.0 \qquad (3\text{-}60)$$

Where D_1 is the length between the low edge of rotating ice floe and its rounded axis, oo', as shown in figure 3.17 and figure 3.18. D is the ice cusp depth.

The rotating energy of the ice floe can be calculated as

$$E_r = \frac{1}{2} J_i \omega_i^2 \tag{3-61}$$

Where J_i is the rotational moment of inertia of the floe around the axis, oo', as shown in Figure 3.17 and 3.18. ω_i is the angular velocity of rotating ice floe.

For the ice cusp defined in the model, its J_i can be calculated using the following equations:

$$J_i = \xi'' D^2 + 2\xi'' D * \Delta d + 1.2933 D^3 W \tag{3-62}$$

Where, Δd can be calculated using the following equation:

$$\Delta d = 0.6D - \frac{0.333\xi''^3 \sin^3 \xi - (\xi' - D)\xi''^2 [0.5\xi - 0.25\sin(2\xi)]}{\xi''} \tag{3-63}$$

ξ'' is equal to the following equation:

$$\xi''=\frac{\left(0.25W^2-D^2\right)^2\xi}{8D^2}-\frac{W\left(0.25W^2-3D^2\right)}{4D} \tag{3-64}$$

ξ and ξ' can be separately calculated as:

$$\xi=\arctan\frac{2D}{W} \tag{3-65}$$

$$\xi'=\frac{0.25W^2-D^2}{2D} \tag{3-66}$$

According to the geometrical relationship between the hull and the rotating ice cusp, the angular velocity of the rotating ice cusp can be calculated using the following equation,

$$\omega_i=\frac{V}{D(\sin\psi+\cos\psi/\tan\psi)} \tag{3-67}$$

The average ice force on a unit width along the waterline of the hull, P_{impact}, due to impact phenomena between rotating ice floe and hull during an icebreaking cycle can be calculated using energy method.

$$P_{impact} = \frac{E_r}{0.5DW} = \frac{(1-e^2)(1+C'_{add\_mass})J_i\omega_i^2}{D \cdot W} \tag{3-68}$$

where, e is the rebound coefficient, which is the ratio of the velocity of ice to the rebounding velocity of ice during the ice-hull impact and its value can be approximated as 0.1 based on the experimental investigation by Valanto (2001). C'_{add_mass} is the added mass coefficient caused by the hydrodynamic force on the rotating ice floe.

The motion of the ice floe during the turning process can be regarded as the combination of the above translational and rotary motions (see Figure 3.24).

The added mass per unit length for the rotary motion can be computed as (Blevins, 1979):

$$M_{R\_add} = \rho_w \pi \frac{\tilde{D}^4}{128} \tag{3-69}$$

The added mass per unit length for the translational motion, M_{T_add}, is calculated using equation 3-57.

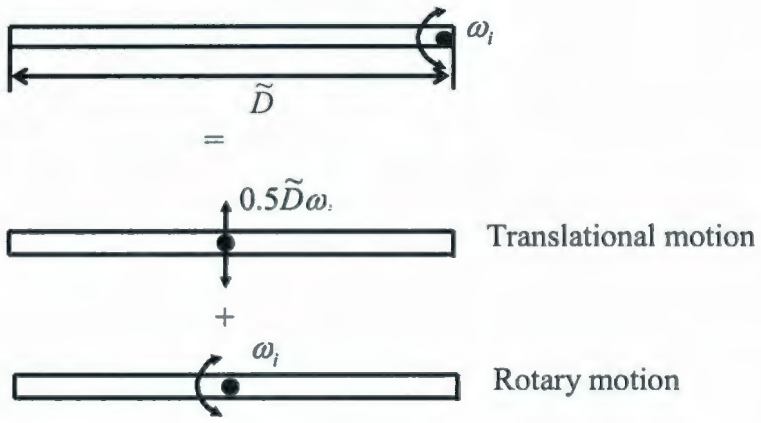

Figure 3.24 Decomposition of ice piece motion

Then, the normal force due to drag on the floe is calculated assuming that the floe is rotating around its rear edge. Then the added mass coefficient for the rotating motion of the plate around one edge can be calculated using the following the equation.

$$C'_{add\_mass} = \frac{M_{T\_add} + M_{R\_add}}{M_{ice}} = \frac{9\rho_w D^3 \pi}{128\rho_i h} \tag{3-70}$$

3.3.7 Buoyancy Force Component

The buoyancy component represents the lifting force by the submerged ice pieces due to the density difference between the ice and water. A flat-plate model is used to represent the underwater part of the hull for buoyancy force calculation. The

IHI model estimates the ice volume over each wet surface of the flat-plate model, as shown in Figure 3.25, based on ship motion in time domain.

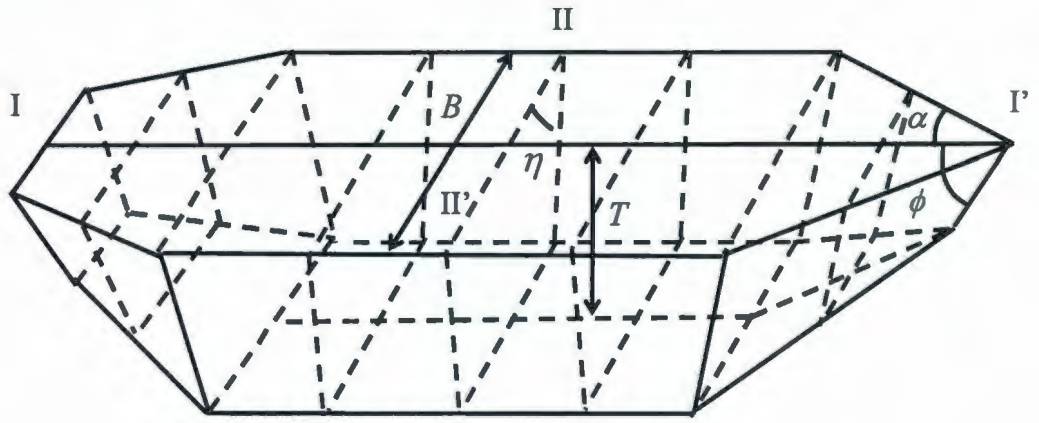

Figure 3.25 Sketch of a flat-plate model for buoyancy force calculation

Close observation during model tests has shown that the ice pieces broken by one side of the bow will slide to the bottom along the same side when the ship turns in ice. Since the amount of ice swept by one side of the bow is different from that of the other side, this difference in clearing ice from both sides of the bow contributes to the asymmetrical load leading to unbalanced sway force and yaw moment. In reference to Figure 3.26, S_1 and S_2 are the surface area of the bow on respective sides of the mid-longitudinal plane, AA'. The ice pieces generated by the L_1 side only slide on the S_1 surface and ice pieces by the L_2 side on the S_2 surface. Then, the amounts of ice on respective sides, S_1 and S_2, should satisfy the following equations (Lau et al., 2004).

$$\nabla_1 + \nabla_2 = \nabla \tag{3-71}$$

$$\frac{\nabla_1}{\nabla_2} = \frac{l_1}{l_2} \tag{3-72}$$

Where ∇ is the total ice volume on the bow; ∇_1 and ∇_2 the ice volumes on the respective sides, S_1 and S_2; Then l_1 and l_2 are the width of the covered area of the respective sides, S_1 and S_2. The cover ratios of the ice on the surfaces, S_1 and S_2, satisfy the following equations.

$$\xi_1 = \frac{l_1}{L_1} \tag{3-73}$$

$$\xi_2 = \frac{l_2}{L_2} \tag{3-74}$$

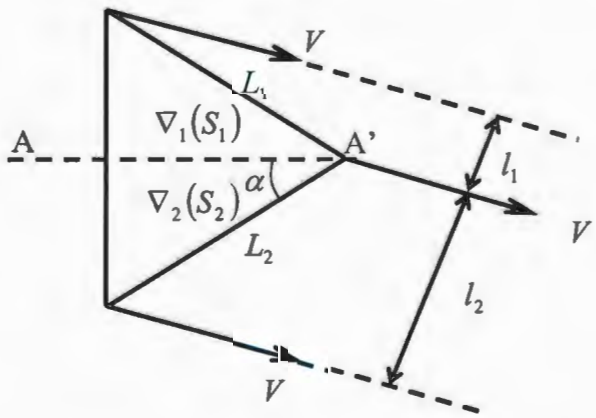

Figure 3.26 Sketch of broken ice swept by a wedge bow

Then the buoyancy force, F_{buoya}, on the submerged ice can be calculated by multiplying the projected area of the ice upon the hull, $A_{projected}$, and $\Delta\rho gh$.

$$F_{buoya} = \Delta\rho gh * A_{projected} \tag{3-75}$$

Where, $\Delta\rho$ is the density difference between the ice and water. h is the ice thickness.

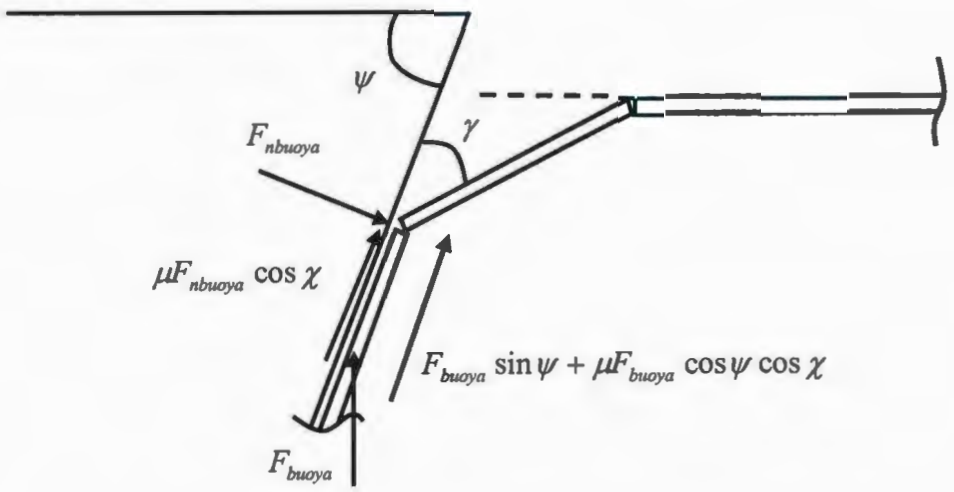

Figure 3.27 Turning and submerging of ice pieces

The motion of the turning ice floe is resisted by buoyancy force and the reaction frictional force from the submerged ice, as shown in Figure 3.27. The force normal to the hull due to the buoyancy force (Lindstrom, 1990),

$$F_{nbuoya} = \frac{\Delta\rho g h * A_{projected}(\sin\psi \sin\gamma + \mu\cos\psi\cos\chi\sin\gamma)}{\cos(\gamma) - \mu\cos(\chi)\sin(\gamma)} \tag{3-76}$$

The surge force, F_{xbuoya}, and sway force, F_{ybuoya}, can be calculated using the following derivations.

$$F_{xbuoya} = F_{nbuoya}(\sin\psi + \mu\cos\chi\cos\psi)\sin\alpha \tag{3-77}$$

$$F_{ybuoya} = F_{nbuoya}(\sin\psi + \mu\cos\chi\cos\psi)\cos\alpha \tag{3-78}$$

3.3.8 Average Force

The average force is estimated based on at least one completed ice breaking cycle. For one complete ice breaking cycle, the average force can be estimated by the integration of the force divided by one ice cusp depth from the hull directly contacting unbroken ice until the broken ice floe is turned parallel to the hull including the breaking force components and clearing force components. The average force on unit width along waterline of the hull can be acquired by the above total ice force over one complete ice breaking cycle divided by the width of each ice cusp. The average ice forces, breaking force and clearing force, on each segment can be obtained through integrating the average force densities on the ice-hull contacted area. The total average force is the linear sum of the buoyancy force

of the submerged ice, average breaking force and average clearing force. A scheme of the average force calculation in IHI model is given in Figure 3.28.

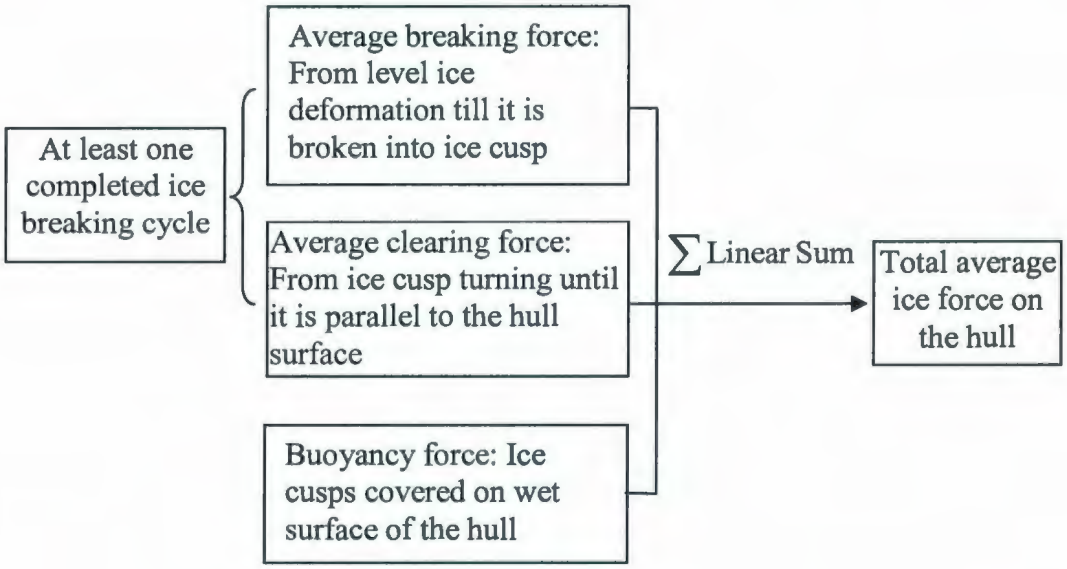

Figure 3.28 Average force calculation in IHI model

3.3.9 Global Force and Moment

The IHI model divides the hull's waterline into small discrete segments where ice contact is expected. The local breaking and clearing forces on each segment were computed separately. The corresponding yaw moments caused by the breaking and clearing forces on each segment were also calculated. The buoyancy force on each surface of the flat-plate model and resulting yaw moment were also calculated respectively. The global force and yaw moments on the whole hull can

be obtained through vectorially adding those forces and moments. A flow diagram of global force and yaw moment calculation in IHI model is given in Figure 3.30.

3.4 Implementation of IHI Model into Numerical Framework

The new ice-hull interaction model is developed for real-time simulation. It is expected to work as an internal module of a much larger numerical framework for ship-ice navigation simulation. This module performs ice force computation in time domain as a function of ice conditions, ship motions and ship geometries, as shown in Figure 3.29 and 1.1. At each time step, the IHI model estimates the ice-induced surge and sway force and the yaw moment on the hull due to the ship's planar motions (velocity and acceleration) in the horizontal plane. These ice forces are added to the loads imposed by other sources before computing the ship's motions via a motion solver.

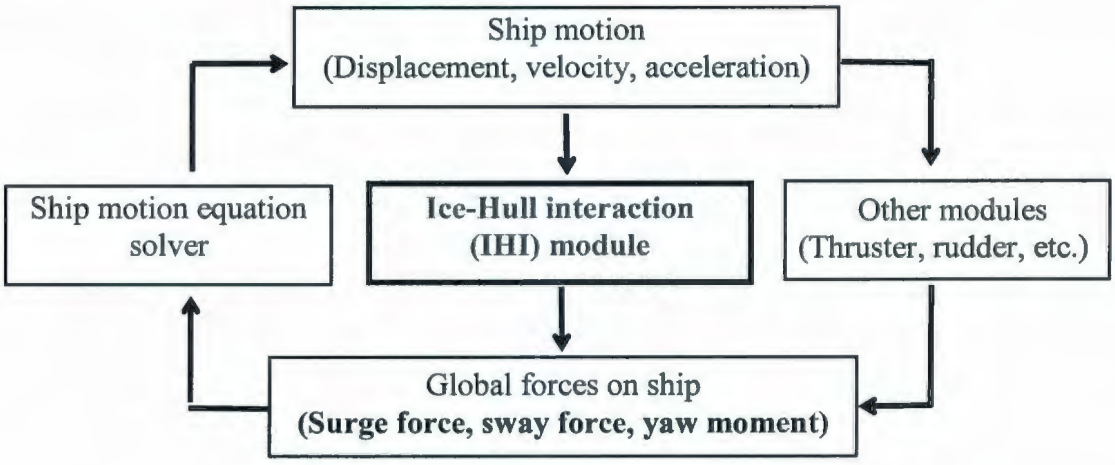

Figure 3.29 IHI model Implementation into the ship-ice simulator

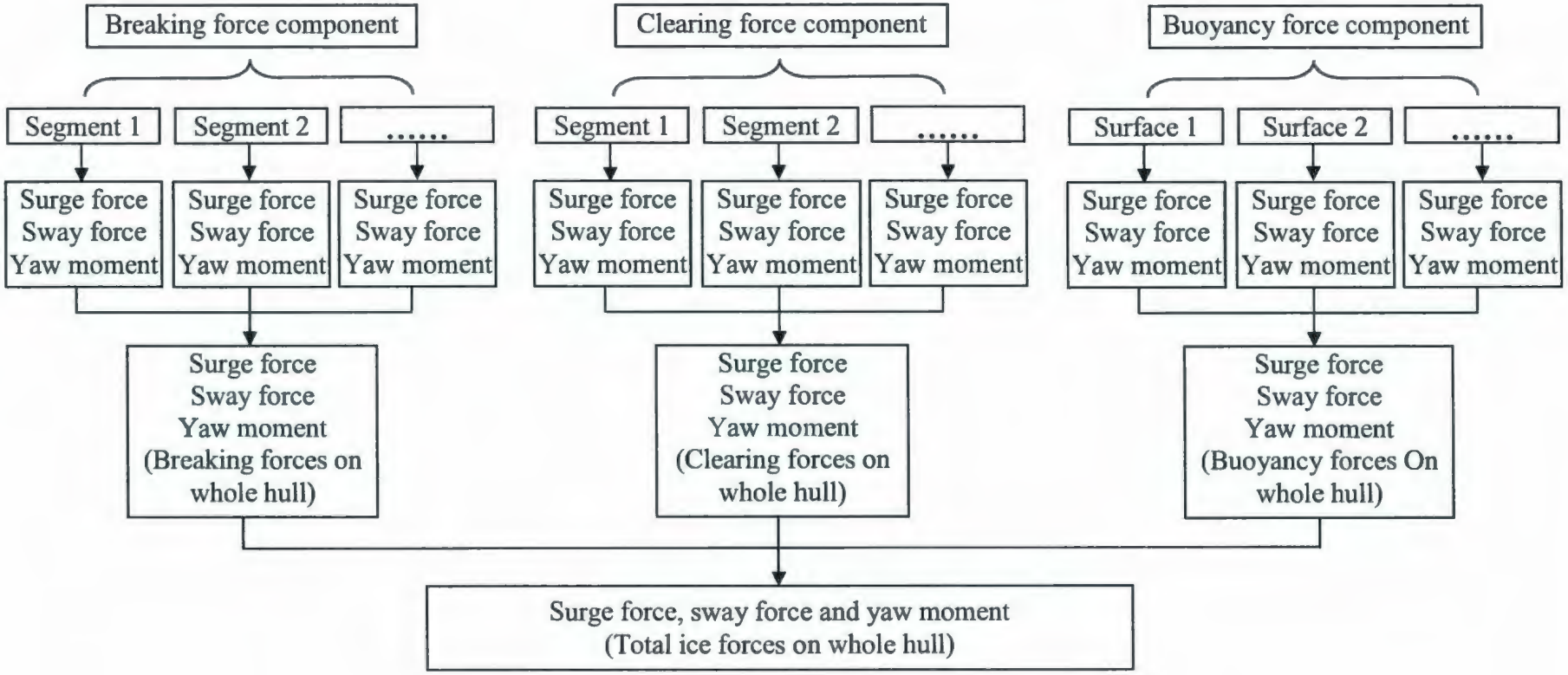

Figure 3.30 Global force and yaw moment calculation in IHI model

3.5 Extending IHI Model to Other Ice Conditions

The IHI model computes ice forces on the ship hull during the continuous icebreaking process. An analytical approach was used for model treatment in which other appropriate physical processes can be incorporated. This flexibility in model treatment allows extension of the model to other ice conditions, i.e. pack ice and rubble ice, by adopting corresponding ice-interaction models. For example, for the rubble ice condition, the crushing and shear failure of the rubble mass will be dominant, and the ice failure model should be modified accordingly. For pack ice condition, the breaking force due to ice failure may be ignored, and the clearing force and buoyancy forces may be calculated considering the ice cover density. By allowing six degree-of-freedom of the ship hull, and a better definition of the ice-hull contact geometry and the interaction forces due to this motion, the model can be extended to a more general 3-D ice load simulation.

3.6 Summary and Conclusions

This chapter documented the underlying theories of a new ice hull interaction (IHI) model designed for the ship-ice navigation real-time simulators. IHI model directly models the physical ice-hull interaction processes using analytical approach with numerical implementation, which makes the model numerically efficient. The adoption of fully derived mechanics formulae makes the model

more universal, applicable to different hull forms and other ice conditions. The whole hull is divided into small segments and the ice forces on each segment calculated separately. The contributions from breaking force, clearing force and buoyancy force are considered. The forces are calculated at each new increment of any prescribed motion, which makes the simulation responsive to arbitrary control inputs and hence arbitrary manoeuvres in ice.

Chapter 4 Numerical Implementation of IHI Model

This chapter presents the stand-alone numerical simulation software developed as part of this research. The software was written using MatLab language, which provides an independent numerical simulation platform for developing and benchmarking the desired IHI model.

4.1 Brief Descriptions of IHI Model Software

The IHI model is expected to be integrated into the numerical simulation framework of the Center for Marine Simulations (CMS) training simulator as an internal module as shown in Figure 1.1. A stand-alone numerical code using MatLab language was developed to provide an independent numerical simulation platform for developing and benchmarking the desired IHI model. The software simulates ice forces on the ship due to user-specified motions. The software allows direct inputs of ship geometries, ship prescribed motions, ice mechanical properties, initial ice edge that are required by the IHI model, and exports the computation for further processing, i.e., ice loads on the hull, ice-hull contact area, and channel configuration. The software retains flexibility and refinement spaces for future development of the IHI model. It also offers a user-friendly data exchange connection, which facilitates its implementation as a module in other ship navigation simulators like CMS training simulator.

The IHI model software is designed as a Visual Calculation Program (VCP). During the calculation process, the users can instantaneously watch the simulation process and check the simulation results, such as ship's motion, ice channel and calculated ice forces on the hull, surge force, sway force and yaw moment. It is important for the users to visualize the physical process of the ice-hull interaction and for the developer to refine the IHI model. It can also be regarded as a preliminary demonstration for the future application of IHI model in the CMS training simulator.

4.2 Structure of IHI Model Software

The IHI model software consists of a collection of 38 m-files (Matlab command file), i.e., Navigation.m, Param_input.m, Motion_ship.m, Hull_ice_model.m, Gener_chann.m, Ice_break_force.m, Ice_clear_force.m, Ice_buoya_force.m, Monit_calcu.m, Output_chann.m, Output_motio.m, Output_force.m, etc. The complete list of the created m-files for IHI model software and the running of the software are provided in Appendix A.

The present IHI software can simulate the prescribed ship maneuvers used in standard PMM ship model tests (Marineering Limited, 1997): i.e., static drift (resistance run and backing run), constant radius maneuver, pure yaw maneuver, pure sway maneuver, "Star" maneuver, arbitrary maneuver, etc. In the IHI

software, the ship motion matrix at each time-step is specified by the m-file, Motion_ship.m, and the ship motion is prescribed. A simple data monitoring the simulation tool was also interfaced with the main load module for monitoring during the simulation and the subsequent data processing. In IHI software suite, **Navigation.m** is the main simulation routine. The entire simulation using IHI model begins through running that file. The structure of this m-file is shown in Figure 4.1.

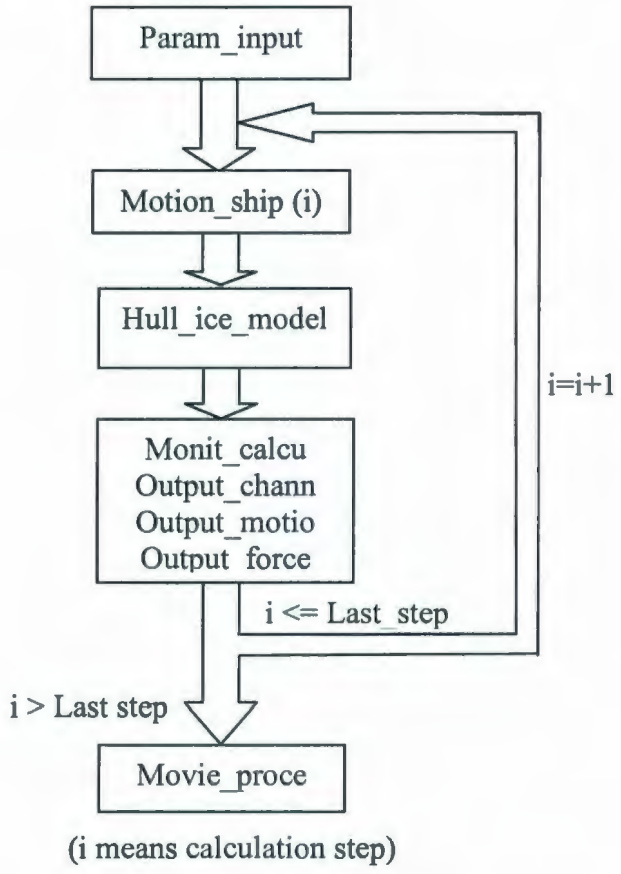

Figure 4. 1 Structure of Navigation.m and the main called m-files

The whole IHI code consists of three layers, **Parameters Input Layer (PIL), Core Calculation Layer (CCL)** and **Results Output Layer (ROL)**. Figure 4.2 shows the code structure for the IHI program and the associated main m-files.

The **PIL** receives the user-specified input to the IHI model, which consists of two main sub-routines, the Param_input.m and the Motion_ship.m. In this layer, the parameters controlling the simulations process and inputs needed by the IHI model calculation are provided.

The following input parameters for ship properties, ice mechanical properties, ship motions and control parameters are needed for each simulation run:

- **Ship geometries and dimensions**, i.e., Water line coordinates, frame angles, ship mass and its mass center, longitudinal length, beam width, draught, stem angle, entrance angle of waterline, and stern angle, etc.

- **Ice mechanical properties**, i.e., ice thickness, ice density, water density, gravity acceleration, ice elastic modulus, flexural bending strength, shear strength, compressive strength, Poisson ratio, and ice/hull frictional coefficients, etc.

- **Ship motions definition**, i.e., prescribed maneuver types, ship velocity, and ship acceleration, etc.

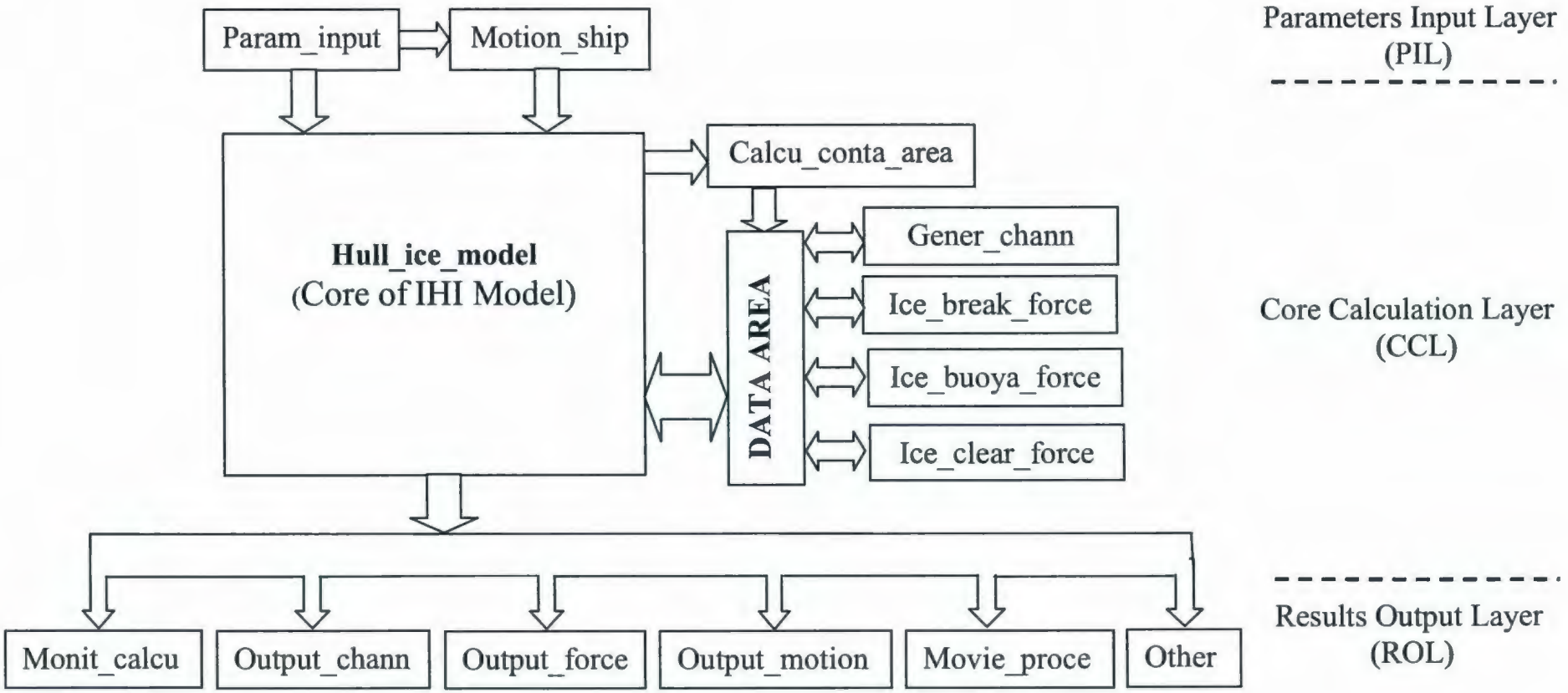

(Navigation.m is the simulation engine of the IHI model software and a simulation begins by running it)

Figure 4. 2 Software structure of IHI Model program with main m-files

- **Simulation control parameters**, i.e., simulation time, monitoring on/off control, monitoring parameters, channel saving on/off control, force saving on/off control, motion saving on/off control, movie generation on/off control, and channel width calculation on/off control, etc.

The **CCL** is the core part of IHI model code consisting of most routines in the software. It is the most complex part of the code. The **CCL** provided all calculation routines needed for the IHI model to be implemented into some other ship navigation numerical simulation frameworks as a force module.

This layer consists of the 24 routines, i.e., Hull_ice_model.m, Hull_ice_model.m, Gener_chann.m, Ice_break_force.m, Ice_clear_force.m, Ice_buoya_force.m, etc.

In **CCL** routine group, the m-file, Hull_ice_model.m is the main program. It provides a common interface to other **CCL** files, such as Calcu_conta_area.m, Gener_chann.m, Ice_break_force.m, Ice_buoya_force.m, Ice_clear_force.m, etc. This file also provides the interface to the **PIL** and **ROL** main routines. Its structure is shown in Figure 4.3.

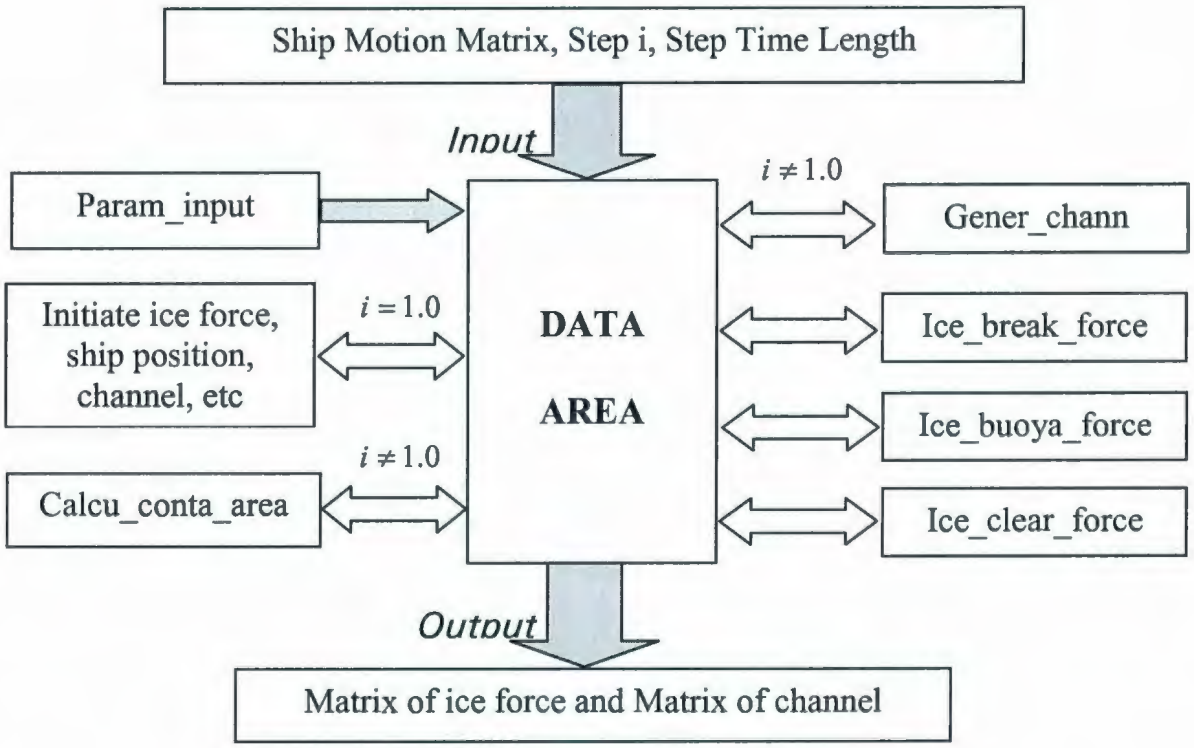

Figure 4. 3 Structure of Hull_ice_model.m and called m-files

The **ROL** generates and exports the corresponding simulation results, such as ice forces, channel, ship motion, etc. into some data files and simultaneously shows the corresponding data like ice force, simulation progress, ship motion and channel edge, etc. to monitor the simulation process. A DOS figure and a windows figure were created for providing on-line monitoring of the simulation as shown in Figure 4.4 and 4.5. Simulation outputs, i.e. simulation progress, the channel, ship motion, surge force on the hull, sway force on the hull, yaw moment on the hull, can be simultaneously displayed on the screen for monitoring. Several .dat files are created to store the calculation results at the same time. The 6 m-files are included in this layer, i.e., Output_motio.m, Output_chann.m, Output_force.m, etc.

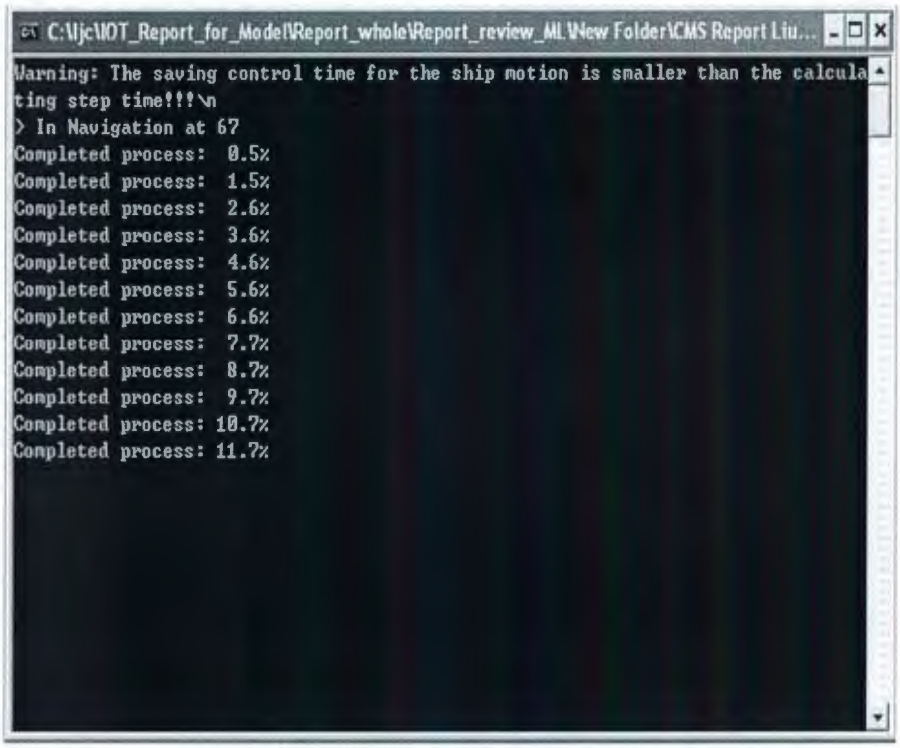

Figure 4. 4 DOS window on typical simulation run using IHI model software

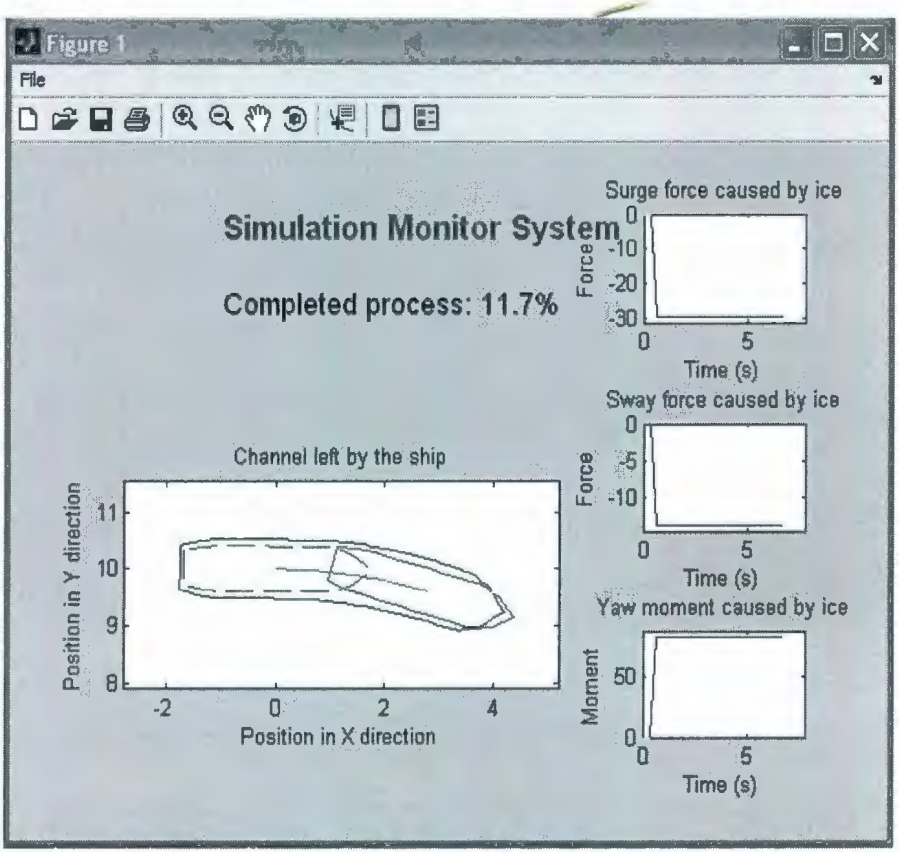

Figure 4. 5 Monitor figure in a typical simulation run using IHI model software

Chapter 5 Selection of Benchmarking Data Sets

Any developing mathematical model needs rigorous and detailed checks and benchmarks based on the corresponding experiments before it is accepted and applied in engineering design and operational planning. This benchmarking provides assessment of the accuracy of the current version of the IHI model and its software implementation. It also gives insights for further refinements of the model. The sufficient and reliable benchmark of the IHI model is also one key part for the whole developing process of the model. This chapter discusses the benchmark process of the IHI model using ship model tests.

As mentioned in Chapter 2, IOT has achieved good correlation between the model tests and full-scale trials (Spencer et al., 2001; Jones et al, 2006). Considering that the IHI model is used to calculate the ice force on the hull due to the ship's manoeuvres in ice in the captive modes, it is convenient and reasonable to select the data from some captive model tests, PMM ship model tests, as the reliable source for calibrating and benchmarking the IHI model

5.1 PMM Model Tests

Figure 5.1 shows the actual PMM on the shop floor. The PMM allows a model to move in exact, pre-programmed patterns while the global forces on the model and the motions of ice around the model can be measured and recorded. Typical PMM

model tests include resistance (advancing runs and backing runs), pure sway, pure yaw and constant radius manoeuvre that is essentialy an arc of a circle. By studying the forces on the model when the model is moving along the prescribed path, the movement of ice around the hull can be better understood. The test results obtained using the PMM can provide complete information on the hull force and moment derivatives.

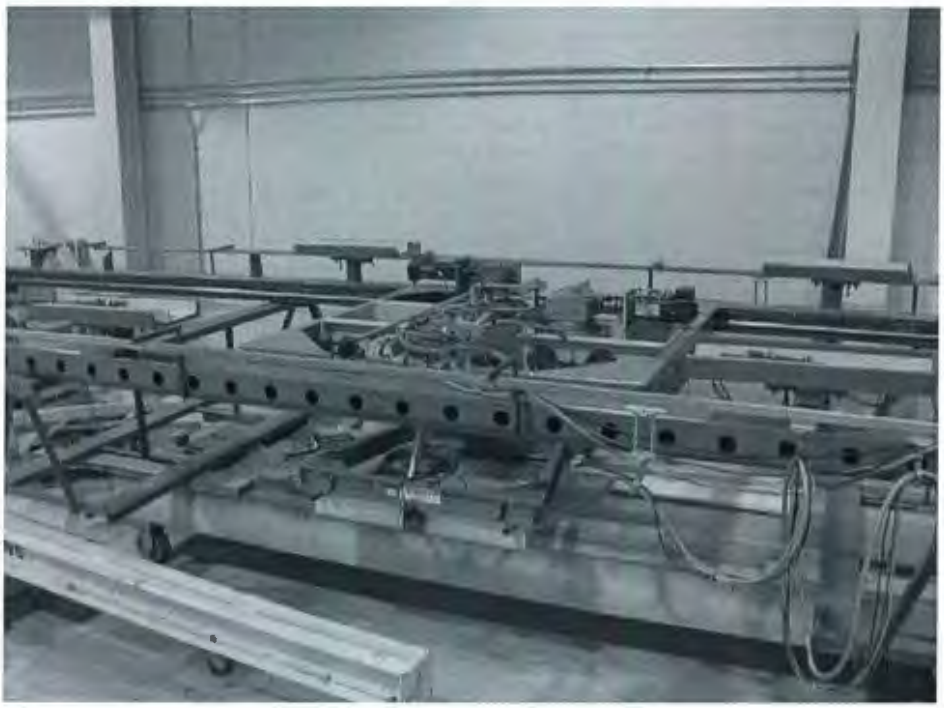

Figure 5.1 Actual Planar Motion Mechanism (PMM) on the floor (Lau, 2007)

The Institute for Ocean Technology, National Research Council of Canada (IOT/NRC) has a 90 m ice tank with a usable ice sheet 76 m in length (Figure 5.2).

It is the longest in the world and provides more data per test run than those from shorter tanks.

Figure 5.2 Scene of ice tank of NRC/IOT

(http://iot-ito.nrc-cnrc.gc.ca/facilities/it_e.html)

5.1.1 Ice Model

Physical modeling of ice-structure interaction is an important technique in determining ice loads and optimizing ice vessel designs. IOT adopts CD-EG/AD/S (Correct Density – Ethylene Glycol/Aliphatic Detergent/Sugar) ice to model sea ice (Spencer et al., 1990). With inclusions of air bubbles into the growing ice sheet, this model ice significantly improves scaling of ice density, elastic and

fracture properties. A process of warming the ice sheet after the freeze is used to correctly scale the model ice strength. This type of ice is far superior to urea model ice in all respects. The model ice properties routinely collected from every ice sheet include ice thickness, in-situ cantilever beam failure strength (flexural strength), characteristic length and consequently Elastic Modulus, shear and compressive strengths, and density. When it is needed, friction, in-situ compressive strength, in-situ shear strength, and fracture toughness can also be measured. The percentage concentrations of EG/AD/S for the present test series were 0.39/0.036/0.04. The standard ice density is about 0.85 Mg.m-3, in a solution of density 1.0025 Mg.m-3, corresponding to sea ice of density 0.9 Mg.m-3 in seawater (Spencer et al., 1990; Spencer, 1992).

Most typical ice test conditions, i.e., open water, level ice, pack ice, pre-sawn ice, rubble ice, etc., can be modeled at IOT with different ice mechanical parameters, i.e., ice thickness, ice density, ice cover ratio, friction force coefficients, flexural bending strength, shear strength and crushing strength (Spencer et al., 1990; Spencer, 1992, 1993).

5.1.2 Ship Maneuvers

Using the PMM apparatus, any motion in the horizontal plane, i.e., advancing, circling, pure yaw, pure sway, star manoeuvres etc., can be accurately controlled

and the global forces on the hull, surge force, sway force and yaw moment, can be measured and recorded.

The ice resistance in the advancing case and the yaw moment in ship manoeuvring case are the key factors that decide the limiting ice condition for ship navigation and ship manoeuvrability. Hence, at the starting stage of the model verification process, the surge force in ship model resistance tests and yaw moment in ship manoeuvring tests are selected for benchmarking the IHI model.

5.1.3 Ice Force Component Measurement in Tests

In the ice-hull interaction model, the total ice force on the hull is regarded as a linear sum of three ice force components: breaking ice, buoyancy force and clearing force. These force components can be extracted from the measured data in the PMM model tests, open water, level ice and pre-sawn ice.

Similar to the standard method for the conduct and analysis of ice resistance model tests in IOT, which details can be referred to Colbourne, Spencer, et al. (Colbourne, 1987; Spencer, 1992, 1993; Spencer, et al., 1992c, 1993) and Jones, et al. (2000, 2005), the force on the model in the level ice consists of the hydrodynamic force, ice breaking force, buoyancy force and clearing force. The force on the model in the pre-sawn ice (broken ice) tests consists of hydrodynamic

force, buoyancy force and clearing force. The hydrodynamic force on the model can be measured from open water model tests. In a pre-sawn model test at very low speed, the dynamic forces associated with ice piece rotation, ventilation, and acceleration are negligible and only buoyancy force and resulting frictional force are left. Therefore, the buoyancy force can be measured by the creeping velocity (low velocity as 0.02m/s) model tests in the pre-sawn tests by subtracting the hydrodynamic forces measured in open water tests. The clearing forces can be obtained through the results of the pre-sawn ice test results subtracting the buoyancy force and hydrodynamic force. The summary of the measured force composition in the model tests and ways to extrapolate the ice force components are given in Table 5.1.

Table 5.1 Force composition in model tests

Measured force	Model test	Hydrodynamic force	Breaking force	Buoyancy force	Clearing force
A	Level ice	+	+	+	+
B	Pre-sawn ice or Broken ice	+		+	+
C	Open water	+			

Extraction of ice force components

- Hydrodynamic force = C
- Breaking force = A – B
- Buoyancy force = B zero velocity
- Clearing force = B – B zero velocity-C
- B zero velocity can be obtained by model in pre-sawn ice or broken ice with creeping velocity.

It should be noted that the pre-sawn ice test was not conducted for maneuvering tests. The existing pre-sawn ice tests are all resistance tests.

5.2 Comparison between Measurements and Simulations

The three ice force components can be extracted from the model tests and the three ice force components in the ice-hull interaction model can be verified respectively.

The ice force component calculation sub-models, breaking component model, buoyancy component model and clearing component model, can be validated respectively in different ship's model tests. For example, the buoyancy force calculation sub-models and the clearing force calculation sub-model are validated using the data from model tests in pre-sawn ice. Then, the breaking force calculation sub-model is verified using data from the model tests in level ice

subtracting the calculated buoyancy force and clearing force provided by the validated buoyancy component sub-model and clearing component sub-model.

Because there are no existing pre-sawn ice tests for ship manoeuvring for IHI model benchmark, the IHI model predictions for pre-sawn ice conditions were compared with measurements in pack ice tests.

The specified manoeuvre in the PMM model tests can be simulated using the ice-hull interaction model software. The calculated ice forces were compared with the measured values in the tests. The channel geometric characteristics, the contact area between ice and hull, the ice crack shape, the ice pieces sliding on the wet surface of the hull and other phenomena were studied at the same time.

5.3 Benchmark of IHI Model Using PMM Model Tests

Two PMM test series at IOT with Terry Fox model and R-Class model were adopted for the benchmark of the IHI model in this thesis. Terry Fox icebreaker and R-class icebreaker represent two different but typical forms among today's icebreakers. The selected test series for two models are both captive tests and the measured experimental data from them can be conveniently applied to the benchmark of IHI model.

5.4 Free-running Model Tests and Full-scale Trials

Free-running tests can more closely model the ship's actual manoeuvres and directly evaluate the ship's manoeuvrability. If the ice loads on the hull corresponding to a certain manoeuvre can be measured or derived through some corresponding parameters like rudder angle, thrust, power etc. and ship motions like velocity, drift angle, turning radius, pivot point etc. can be controlled, measured and recorded, the free-running model tests can also be used to benchmark IHI model.

In this thesis, Izumiyama's free-running tests (Izumiyama K. et al., 2005), were adopted for benchmarking the IHI model through comparing the calculated ice force distributions on the hull and measured test data in qualitative form. The tests showed that although the model was self-propelled, the steady parts of the turning runs and resistance runs are sufficiently good to be used for comprise with IHI model simulation. The ice force distribution on the hull was directly measured using a series of sensor film sheets installed along the waterline of the model ship.

The above discussion is also valid for the full-scale trials.

It should be noted that the benchmarks of the IHI model using free-running model test or full-scale trial data greatly depends on the availability, completeness and

reliability of the experimental database. Benchmarking against the model tests in this thesis is presented in Chapters 6, 7 and 8, which includes Terry Fox test series, R-Class test series and NMRI test series.

Chapter 6 IHI Model Benchmark with Terry Fox Model Tests

In this chapter, the IHI model was benchmarked using the PMM Terry Fox model tests carried out at IOT (Derradji, 2004). The ice resistance force on the hull in the advancing runs and the yaw moments in the constant radius runs are compared between the test measurements and IHI model simulation results. The ice-hull contact and the channel width were also studied in order to understand the physical ice-hull interaction process and to check the same in the IHI model. The measured global ice forces on the hull from tests were discussed in order to show the theoretical base and capabilities of IHI model. The benchmarking provides assessment of the working processes of the IHI model and its potentials, accuracy and advantages in real-time ship-ice simulations. It also gives insights for future refinements.

6.1 Description of CCGS Terry Fox Icebreaker

CCGS Terry Fox is a Canadian Coast Guard heavy gulf icebreaker. The ship was originally named as "MV Terry Fox" before acquired by the Canadian Coast Guard in 1992. The CCGS Terry Fox was built by Burrard Yarrows Corporation in Vancouver in 1983 for Gulf Canada Resources and was originally designed to support hydrocarbon exploration activities in the Beaufort Sea. The ship was designed not only to escort tankers through ice but also to act as heavy-duty tug and supply vessels to support offshore oil rig platforms in a harsh environment.

She was classed as a "Heavy Gulf Icebreaker" by the Coast Guard and is now considered one of the most powerful icebreakers in the Coast Guard's inventory with an Arctic Class 4 icebreaking capability.

The hull is of double chine form and incorporates a semi-spoon shaped bow with air bubbler system, forward ice plough and raked transom stern. The simple hull geometry makes the 'Terry Fox' particularly suitable for mathematical modeling.

Table 6.1 lists the main particulars of CCGS Terry Fox Icebreaker. Figure 6.1 shows the ship's navigating in ice.

Table 6. 1 CCGS Terry Fox Icebreaker (Derradji et. al, 2004a)

Length Overall:	88.8 m
Breadth:	17.5 m
Draft:	8.2 m
Trim:	0.0 m
Buoyancy LCB:	35.2 m fwd
Displacement:	6895.8 m^3
Cruising Speed:	15.5 knots

Figure 6. 1CCGS Terry Fox navigating in ice

(http://www.ccg-gcc.gc.ca/vessels-navires/photos/terryfox.jpg)

6.2 Description of IOT "TERRY FOX" Model

IOT Terry Fox Model is a 1:21.8 scale model of the Canadian icebreaker, M.V. Terry Fox, outfitted with a rudder as shown from Figure 6.2. Series of resistance and manoeuvring tests in level ice and pre-swan ice using the model were carried out in IOT (Derradji et al., 2004). The rudder angle was kept zero in all ice tests. The Terry Fox Icebreaker water-line profile represented in the IHI Model are shown in Figure 6.3 and the corresponding geometries including waterline width, flare angle and side area are given in Table 6.2.

Figure 6.2 IOT Terry Fox model in its wooden cradle (Transverse direction view, Lau, 2007)

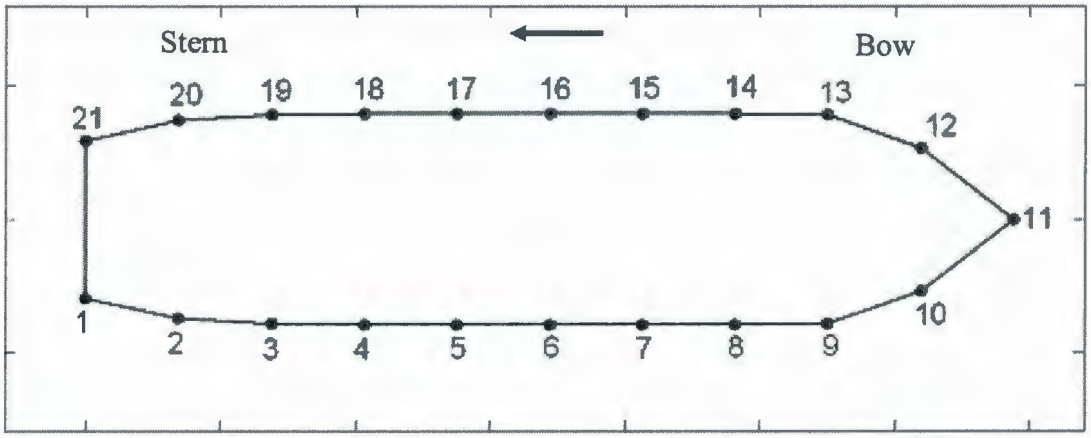

Figure 6.3 IOT Terry Fox model water line profile represented in IHI model

Table 6.2 Geometries[1] of IOT Terry Fox model represented in IHI model

Location[2] (m)	Half WL Width (m)	Flare angle (°)	Hull side area[3] (m^2)
3.440f	0.037	23.22	0.0705
3.096f	0.265	34.76	0.0705
2.752f	0.389	57.43	0.0883
2.408f	0.393	68.12	0.1003
2.064f	0.396	80.03	0.1248
1.720f	0.396	80.83	0.1253
1.376f	0.396	80.83	0.1254
1.032f	0.395	80.75	0.1297
0.688f	0.389	76.65	0.1236
0.344f	0.370	64.20	0.1041
0.000f	0.294	27.34	0.0969

Note:

[1] The Terry Fox model geometries were provided by NRC/IOT.

[2] The transverse plane was measured at interval forwards of the Aft Perpendicular.

[3] The equivalent area of the hull side surface under the waterline to the bottom at each section as shown in Figure 3.29.

Figure 6.4 PMM Terry Fox model test run in level ice (Derradji et al., 2004a)

Figure 6.5 PMM Terry Fox model test run in pre-sawn ice (Derradji et al., 2004a)

The test program consisted of resistance and constant circle manoeuvre conducted in level ice using a planar motion mechanism (PMM). The resistance test in the

pre-sawn ice condition was also carried out. The model speed ranged from 0.02 m/s to 0.6 m/s. The targeted ice thickness and flexural strength were 40 mm and 31.5 kPa, respectively. For details of the test series, please refer to the original reports (Derradji et al., 2004a, 2004b; Lau et al., 2007). Figure 6.4 and 6.5 respectively present typical scenes from PMM Terry Fox model test runs in level ice condition and in pre-sawn ice condition.

6.3 Uncertainty Analysis of Data Set

Experimental Uncertainty Analysis (EUA) is used to quantify the uncertainties in experiments. Through EUA, the agreement or disagreement between the measured results and their real values can be calculated. Institute for Ocean Technology of National Research Council (NRC/IOT) has carried out a series of research on applying EUA in analyzing the ship model ice tests (Derradji et al., 2002, 2004a, 2004b), which provided the basis to set up standards for uncertainty analysis in ice tank testing in the future.

Referring to the research work at IOT (Derradji et al., 2002, 2004a, 2004b; Lau et al., 2007), the application of EUA in the measured ice loads on the ship model, surge force, sway force and yaw moment, is introduced in this section.

In the experiments, the total uncertainty, U, is equal to the geometric sum of the bias uncertainty component, B, and the random uncertainty component, P (Coleman and Steele, 1998).

$$U = \pm\sqrt{\left(B^2 + P^2\right)} \tag{6-1}$$

Based on the analysis of experimental data, Derradji (2004a) concluded that, in ice tank experiments, the bias component, B, consisted of uncertainties in the calibrations of instrumentation and equipment like load cells, RVDT's (Rotary Variable Differential Transformers), yoyo potentiometers and DAS (Data Acquisition System). The random uncertainty component (also called precision component), P, consisted of uncertainties in environmental and human factors, which affects the repeatability of the test results. The random uncertainty sources included the changing test environment, initial test setup with small misalignments, human errors, etc.

According to the IOT model ice test results (Derradji et al., 2002, 2004a), the bias uncertainty component, B, is much smaller than the random uncertainty component, P, and can be neglected. Then, the total uncertainty can be simplified as equal to the random uncertainty component.

$$U = \pm P \tag{6-2}$$

According to uncertainty analysis of IOT model tests in ice, the time force history from one long ice test run can be divided into several segments and each segment is regarded as a statically independent test. It is suggested that each segment should be over 1.5 to 2.5 times the length of the ship model.

The first calculation step of EUA is to obtain mean force for each force segment. The second step is to calculate the mean of the means and the standard deviation of the means. The mean of the means and standard deviation of the means are needed to compute random uncertainties in the results of test run.

The Chauvenet's criterion was applied to identify the outliers that are discarded data points (Coleman and Steele, 1998).

$$Chauv = \left| \frac{F - Mean\_F}{STD\_F} \right| \tag{6-3}$$

Where, F is each mean force. $Mean\_F$ is the mean of the mean forces. STD_F is the standard deviations of force points.

The Chauv number for each data point should not exceed a certain prescribed value. The data points with the Chauv greater than the prescribed criterion were discarded, then the new mean of means and new standard deviation of means were calculated from the remaining data points. The random uncertainties in the mean forces can be calculated using the following equation:

$$U(F) = \frac{t*(STD\_F)}{\sqrt{N}} \tag{6-4}$$

Where t is a function of the degrees of freedom and the confidence limit, and N is the number of the remaining data points. For example, for a sample size N larger than 10 and a confidence limit of 95%, t is approximately equal to 2 (Coleman and Steele, 1998).

Random uncertainties are expressed in terms of uncertainty percentage (UP):

$$(UP(F)) = \frac{U(F)}{Mean\_F} * 100 \tag{6-5}$$

As the example, Table 6.3 and 6.4 list the calculated ice resistance data and uncertainties from the experiments. In the tables, the mean force is the average of all measured value within a time history force segment and the peak force is the

value with a non-exceedance probability of 99%. Figure 6.6 and 6.7 show the resistance force vs. ship velocity curve in level ice condition and peak resistance force vs. ship velocity curve and pre-sawn ice condition respectively.

Table 6. 3 Summary of level ice resistance forces in tests

Model Velocity (m/s)	Level Ice					
	Mean (N)	Stadv (N)	Uncertainty %	Peak (N)	Stadv (N)	Uncertainty %
0.1	27.88	1.70	3.3	67.07	7.14	4.3
0.2	34.08	2.33	2.6	123.17	16.89	10.7
0.4	46.47	1.09	1.7	264.10	23.42	13.8
0.6	52.07	2.62	3.5	384.26	45.85	8.5

Table 6. 4 Summary of pre-sawn ice resistance forces in tests

Model Velocity (m/s)	Pre-sawn Ice					
	Mean (N)	Stadv (N)	Uncertainty %	Peak (N)	Stadv (N)	Uncertainty %
0.1	2.08	0.35	5.8	17.80	1.46	5.8
0.2	11.22	0.54	3.0	31.26	0.75	7.1
0.4	13.40	0.26	1.4	51.42	2.04	4.1
0.6	27.77	0.55	1.1	85.685	12.51	11.2

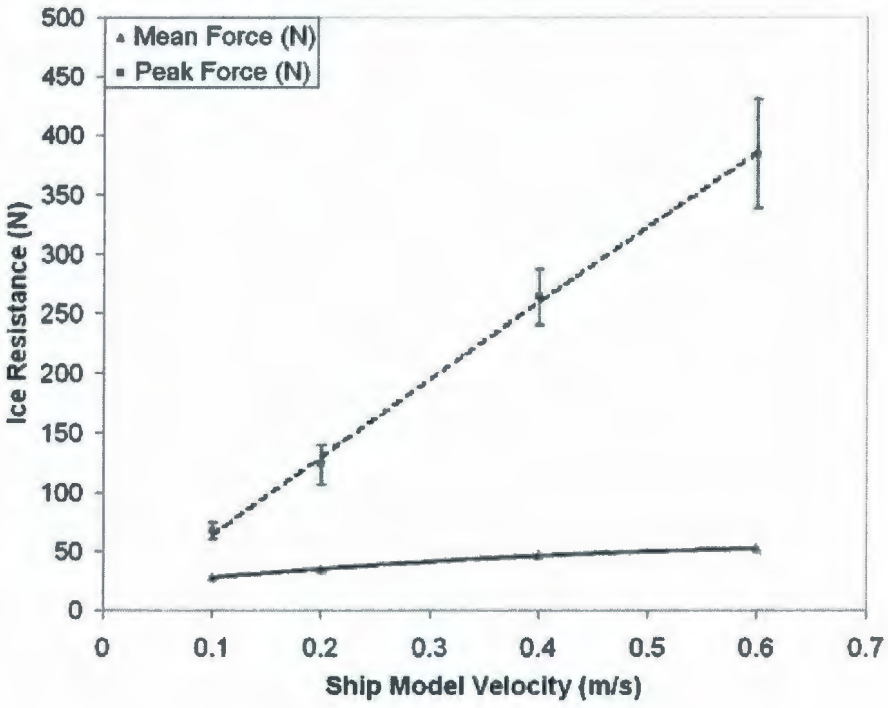

Figure 6. 6 Average ice resistance and peak resistance in level ice tests

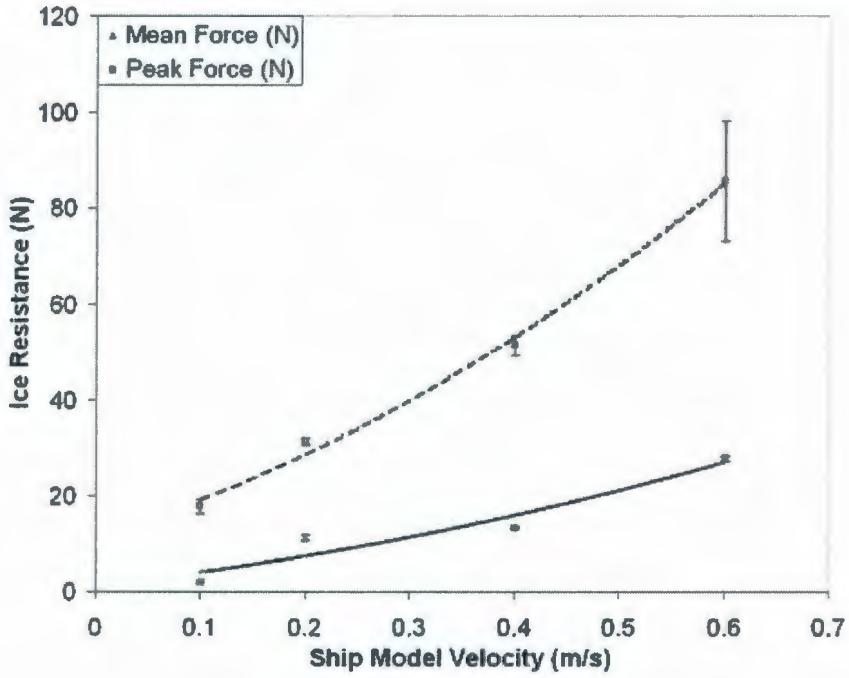

Figure 6. 7 Average ice resistance and peak ice resistance in pre-sawn ice tests

The natural ice resistance force on the ship hull is transient, irregular and with high frequency ice force components. Figure 6.7 and Figure 6.8 showed that the peak resistance value can be 3~8 times the average resistance in level ice tests or in pre-sawn ice tests. The peak resistance is also of much higher standard deviation than the average resistance in one specific ship-ice test run, the former is about 10~20 times of the later one. For average resistance, the ice force in level ice is of a little higher standard deviation than in pre-sawn ice.

Different from the ramming model of icebreaking, in which the momentary maximum force is the most important variable that determines the ship's ice breaking capacity in the continuous mode, the average ice breaking force within a time distance is of more interest because the kinetic energy of the ship should be large enough to overcome the momentary peak force exceeding the available thrust force and permit an integration of the force-distance function in the continuously ice breaking mode. The momentary maximum ice force on the hull is used for the hull structural strength, while the mean ice force is used in the ship navigation calculation. The IHI model estimates the ice forces needed for simulating the ship's steady manoeuvres in ice in the continuous mode. Hence, it neglects the high frequency ice force fluctuation and integrates ice force over a long time interval consisting of at least a few ice breaking cycles to arise at an equivalent local ice resistance. The mean ice force obtained from the experiments is adopted for benchmarking IHI model.

6.4 Resistance Run

A satisfactory simulation of the geometry of the broken channel is important, as the intact ice edge interacts with the ship hull leading to interaction loads. Figure 6.8 presents the channel left by Terry Fox model in 40 mm-31.5 kPa level ice sheet at a speed of 0.4 m/s. The blue color lines are added to the picture later in order to show clearly the average ice edges. Figure 6.9 shows the simulated channel edge of that test run using IHI model software. From Figures 6.8 and 6.9, we can see that the actual ice edge is irregular in the level ice breaking process. The IHI model calculates the average ice channel edge, based on which, the ice-hull contact area is calculated in order to calculate the ice forces.

Figure 6.10 shows the measured resistance (surge force) for Terry Fox model in 40 mm - 31.5 kPa level ice sheet at a speed of 0.4 m/s. Correspondingly, Figure 6.11 shows the resistance run simulated by IHI model for the same test condition.

From Figure 6.10, we can see that the actual ice forces on the hull are of high frequency ice force components. The IHI model neglects those high frequency force component and calculates the mean ice force on the hull as shown in Figure 6.11

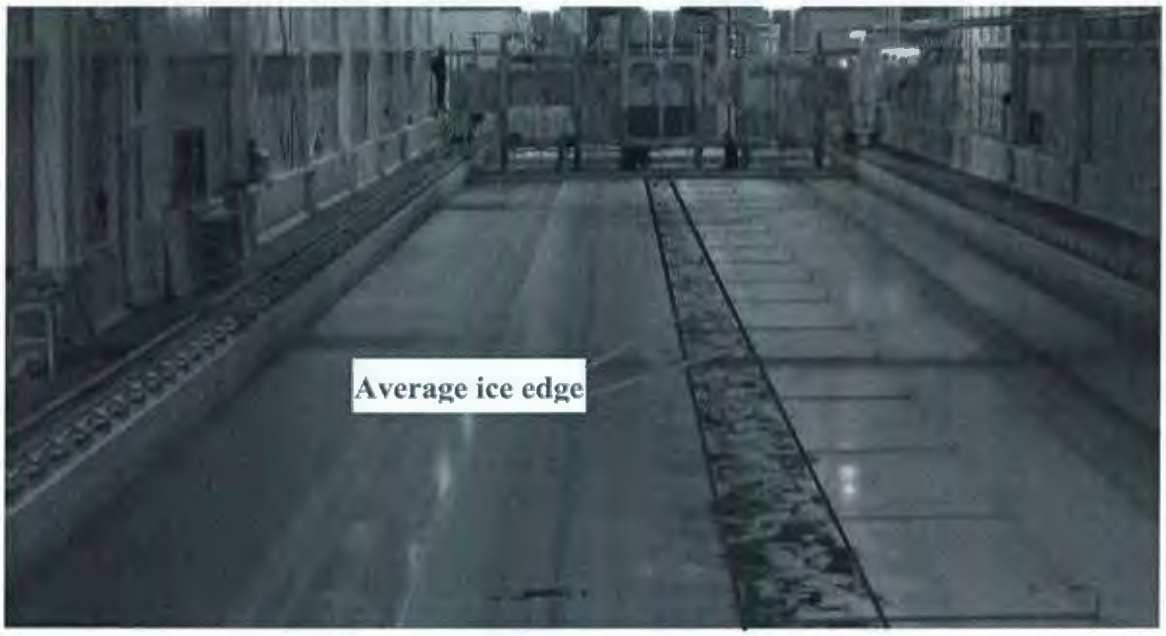

Figure 6.8 Channel left by Terry Fox model in resistance test run (Derradji et. al, 2004a)

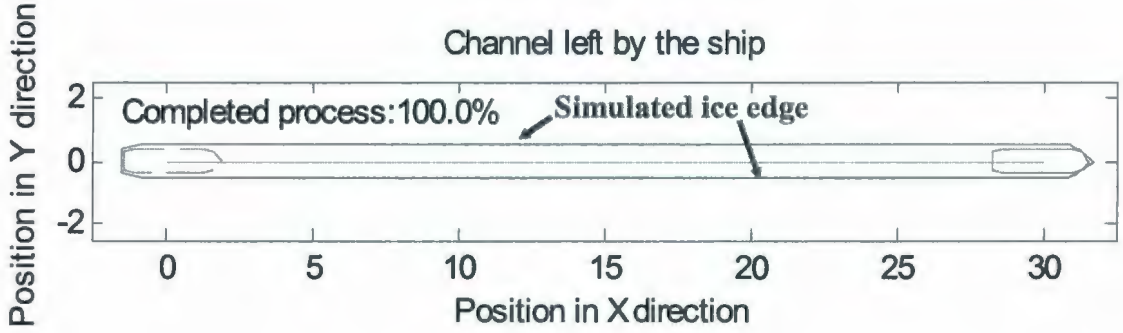

Figure 6.9 Tracked channel in IHI model program simulation for Terry Fox Icebreaker straight advancing run

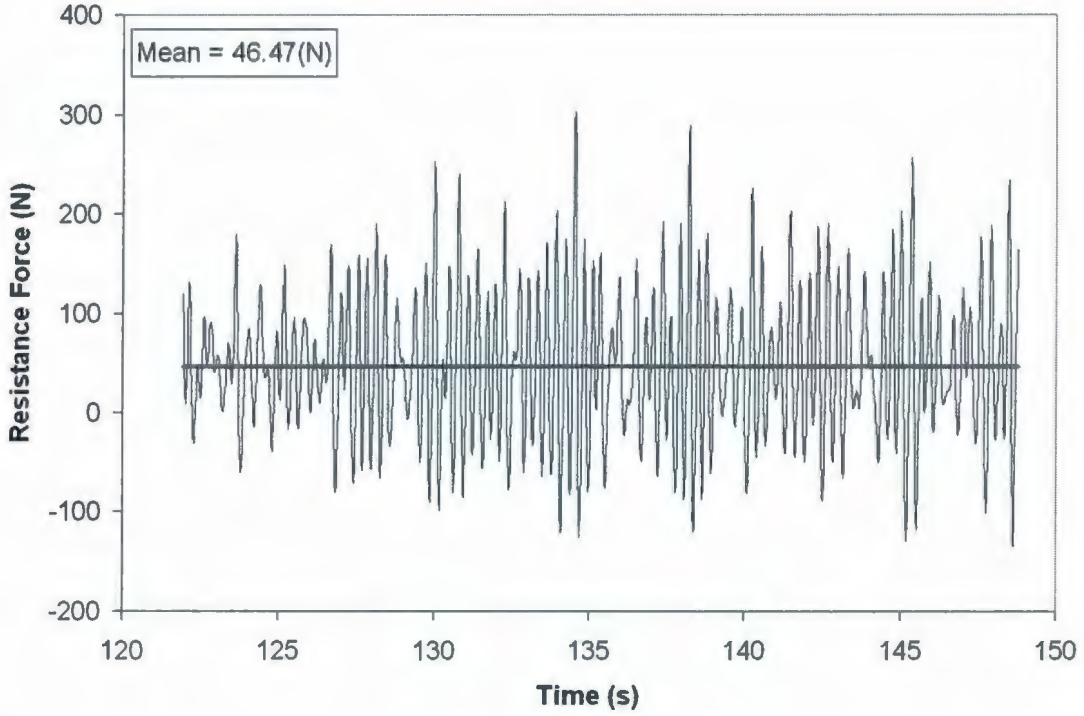

Figure 6.10 Measured ice resistance for Terry Fox model in 40 mm - 31.5 kPa level ice at a speed of 0.4 m/s (Derradji et al., 2004)

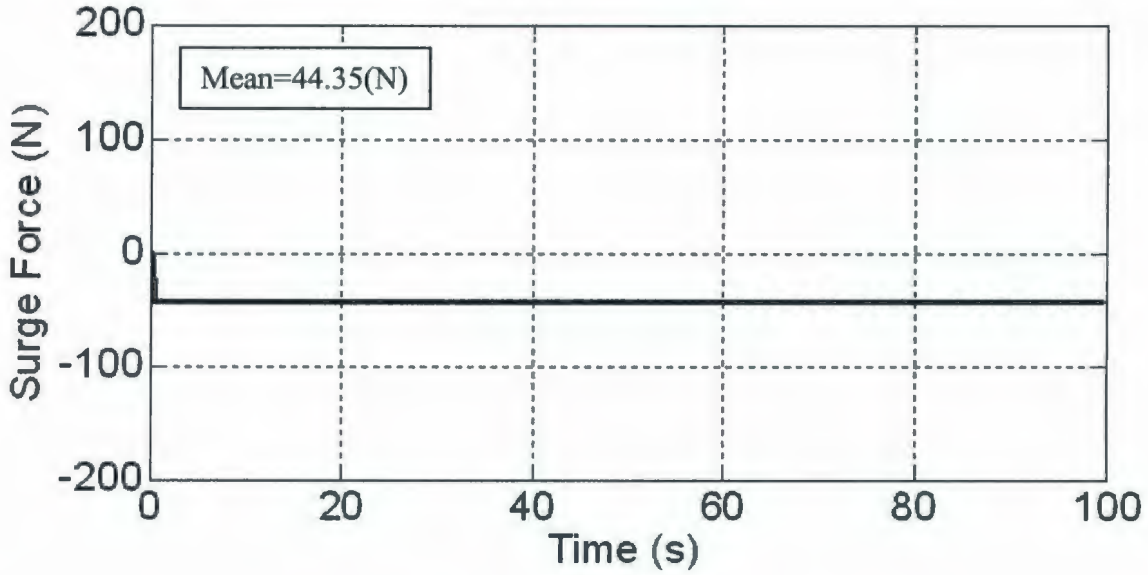

Figure 6.11 Calculated ice resistance from the IHI model for Terry Fox model in 40 mm - 31.5 kPa level ice at a speed of 0.4 m/s

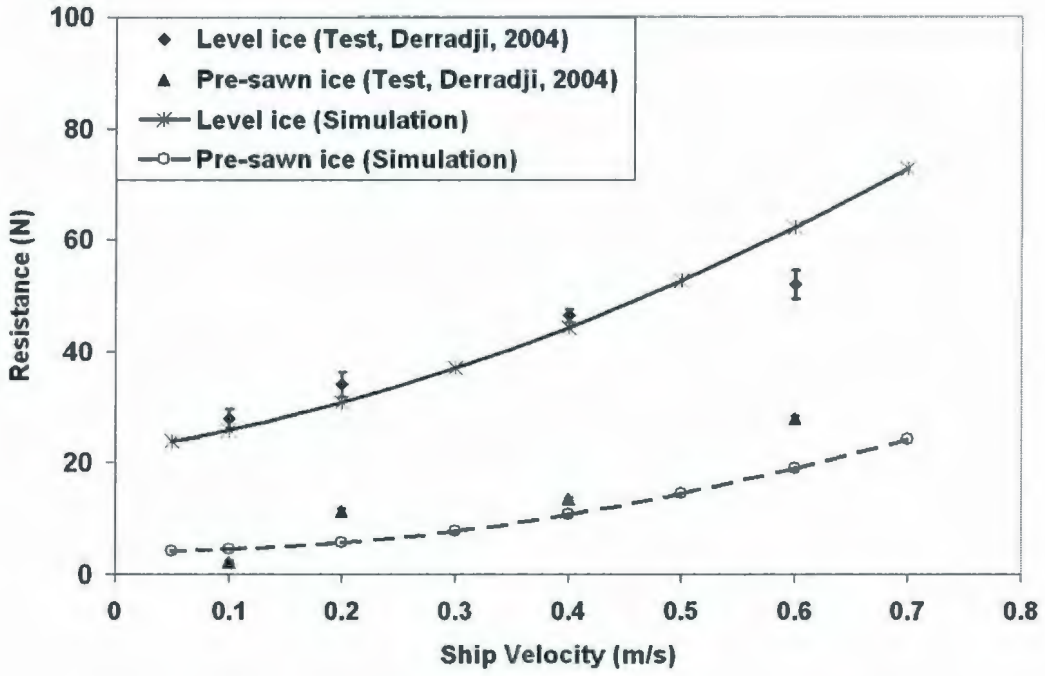

Figure 6.12 Comparison of measured and calculated ice resistances for Terry Fox model in 40 mm - 31.5 kPa ice at test speeds ranging from 0.1 to 0.6 m/s

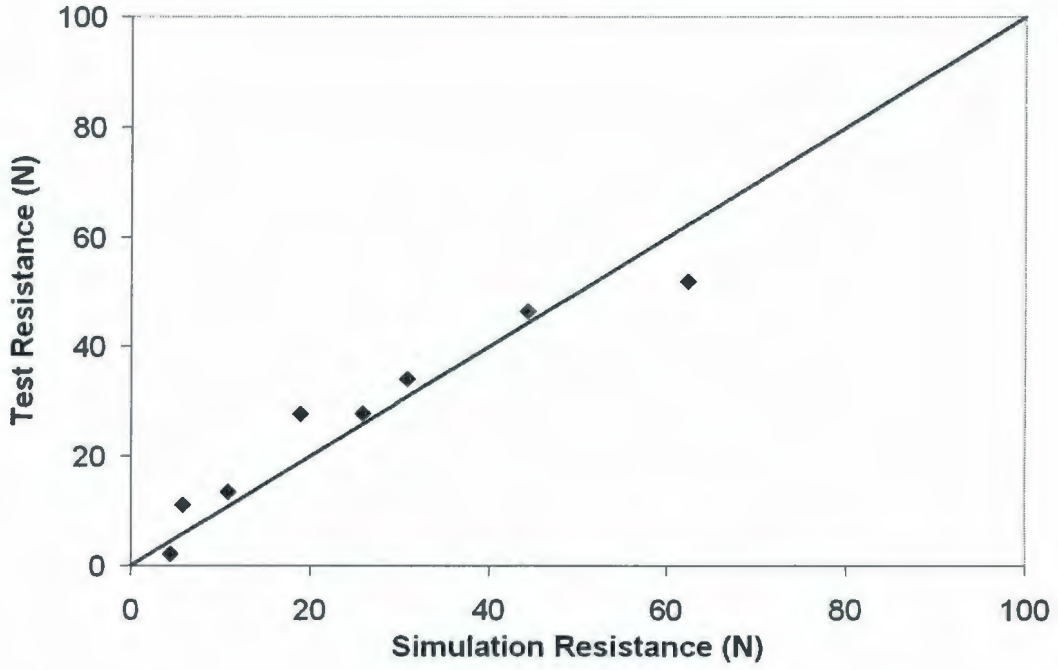

Figure 6.13 Comparison of measured and calculated ice resistances for Terry Fox Icebreaker in level ice and pre-sawn ice

Table 6.5 Comparison of measured and calculated ice resistances for Terry Fox model in level ice and pre-sawn ice

Model Velocity (m/s)	Level ice			Pre-sawn ice		
	Measrued Resistance (N)	Simulated Resistance (N)	Discrepancy (%)	Measured Resistance (N)	Simulated Resistance (N)	Discrepancy (%)
0.05	N/A	23.8	N/A	N/A	4.2	N/A
0.1	27.9	25.8	7.5	2.1	4.5	114
0.2	34.1	30.8	9.7	11.2	5.7	49.1
0.3	N/A	37.0	N/A	N/A	7.8	N/A
0.4	46.5	44.3	4.7	13.4	11	17.9
0.5	N/A	52.8	N/A	N/A	15	N/A
0.6	52.1	62.3	19.6	27.8	19	32.7
0.7	N/A	72.8	N/A	N/A	24	N/A

Figures 6.12 and 6.13 show comparisons of the calculated and measured ice resistances in level ice and pre-sawn ice for Terry Fox icebreaker in the 0.04 m-31.5 kPa ice at speeds ranging from 0.1 m/s to 0.6 m/s. Table 6.3 provides the data for the above comparison figures.

From the above comparisons, the following conclusions may be drawn: Most relative errors between predictions and measurements are within 20% of the

corresponding measurement. The trends of calculated data and measured data coincide well, which means that the calculated resistance fairly well matches the corresponding measurement. The relative errors are higher for the pre-sawn runs, which may be caused by the smaller reference forces in the pre-sawn runs and more obvious erratic effects due to pieces bumping into the hull.

The discrepancy may be caused by the following: In the simulation, the input values like ice thickness, ice density, failure strength, friction coefficients, etc, were adopted as the ideal targeted values. In fact, the measured data in tests has a spread scope around the targeted average value (Derradji et al., 2004). The random uncertainties in test runs affected the final comparison results. Except the force value at ship velocity, 0.6 m/s, which seems not to follow the data trend based on all measured data and the measurements for that run are possibly erratic, the calculated values are lower than measurements, which may be caused by the model neglecting the ice crushing at the stem, the secondary cracks on some big ice cusps and frictional forces during the ice sliding process on the underwater surface of the hull. The discrepancy may also be caused by the model idealization and simplifications of the problem treatment, i.e., the simple flat-plate representation of the model hull for buoyancy calculation; the idealized ice breaking process and clearing process, ice piece pattern, ice piece size, etc. The above discrepancy analysis is also applicable to other comparisons in this thesis.

It should also be noted that the theories of the model are derived based on low to medium ship speed. At high speed, the submersion process of ice pieces is very complicated and an independent resistance component may not exist (Kamarainen, 1994).

6.5 Constant Radius Run

The constant radius manoeuvre constitutes the most simple ice-hull interaction condition with the constant ship motion, interaction geometry, and yaw moment. This section provides the comparisons between Terry Fox Icebreaker constant radius manoeuvres and the corresponding PMM model test runs. The PMM Terry Fox model test data were taken from Lau (2007).

Figure 6.14 shows the measured yaw moment-time history for the run of Terry Fox model in 40 mm- 31.5 kPa level ice sheet with 10m radius and a tangential velocity of 0.4 m/s. Figure 6.15 correspondingly shows predicted yaw moment-time history for that run. From figures, 6.14 and 6.15, we can see that, similar to the ice resistance case, the IHI model also ignores the high frequency ice yaw moment components on the hull and calculates the average yaw moment.

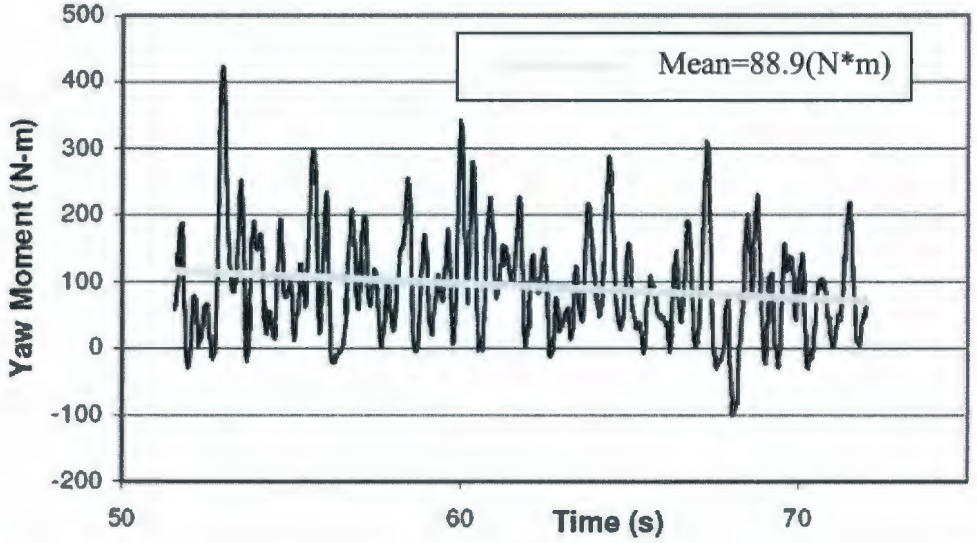

Figure 6.14 Ice yaw moment-time history measured for Terry Fox model 10 m radius runs with 0.4 m/s velocity in 40 mm - 31.5 kPa ice (Lau, 2007)

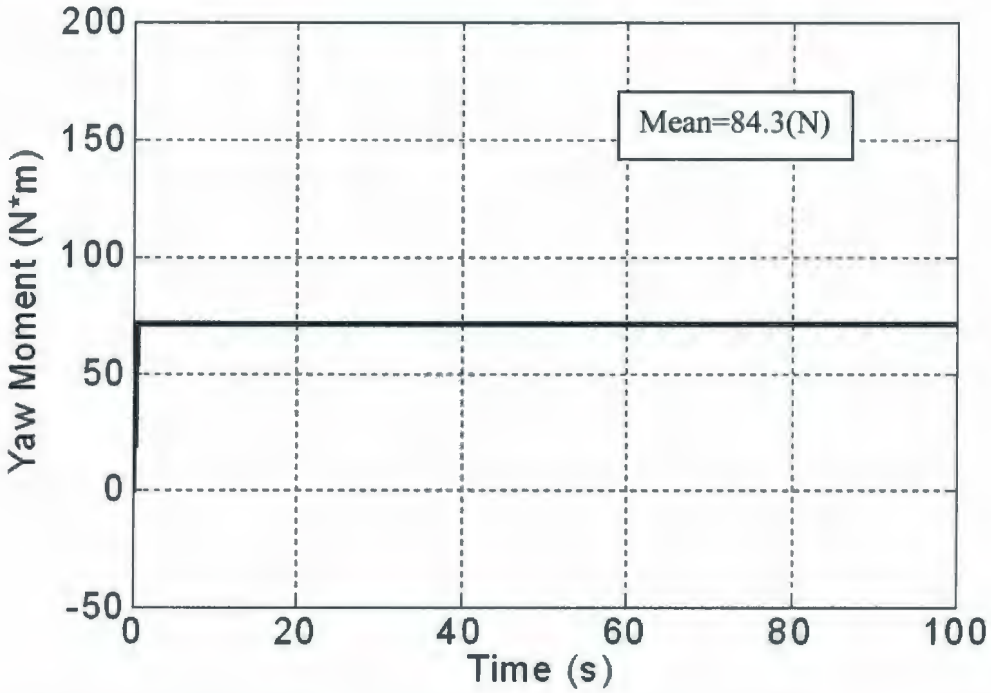

Figure 6.15 Ice yaw moment-time history simulated by IHI model for Terry Fox model 10 m radius runs with 0.4 m/s velocity in 40 mm - 31.5 kPa ice

Figure 6.16 shows the measurements and predictions of yaw moments for the Terry Fox model constant radius turns in a 0.04 m - 31.5 kPa ice sheet at 50 m radius and 10 m radius runs with ship velocity from 0.02 m/s to 0.6 m/s. Figure 6.17 shows the predicted and measured values for the same data set. Table 6.4 provides the data for the above comparison figures.

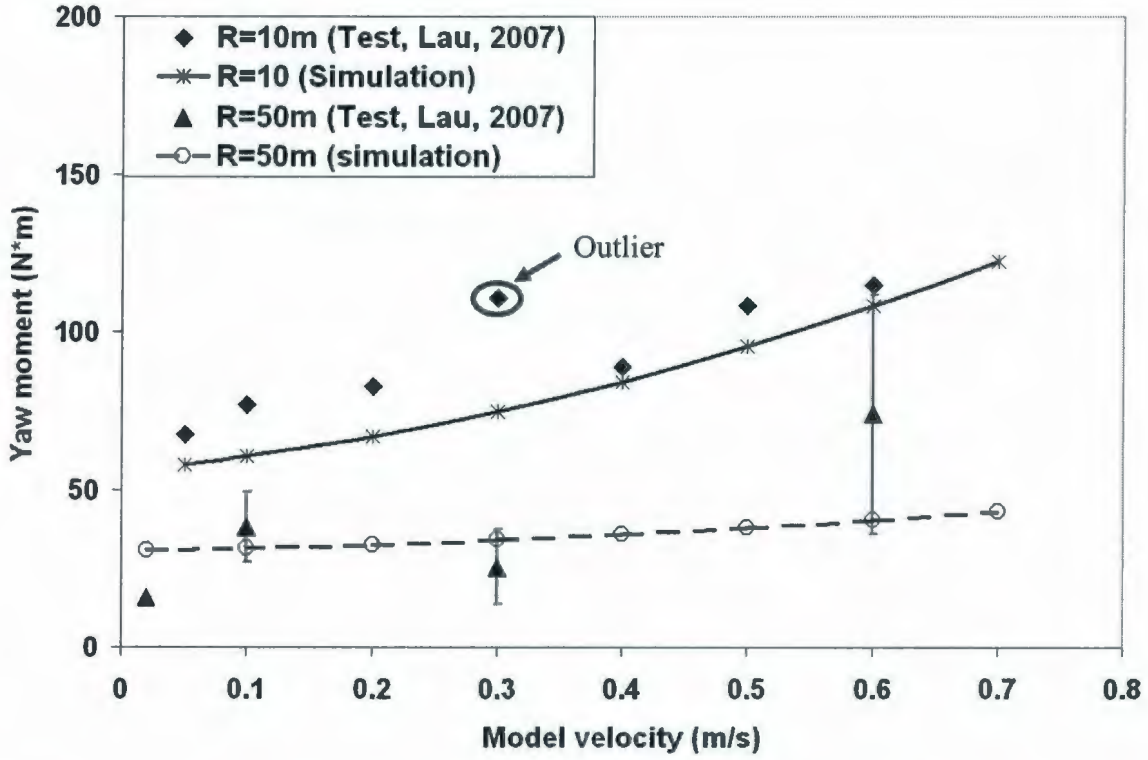

Figure 6.16 Comparison of measured and simulated ice yaw moments for Terry Fox model with 10 and 50 m radius turning in 40 mm - 31.5 kPa ice

Excluding the point at 0.3 m/s velocity, which is far away from the trend line of the measured data (Lau, 2006b), as shown in Figure 6.16, the relative errors of

prediction for 10 m turns were within 20% of the corresponding measurement; For the 50 m turns, the data spread is relatively large and only four test data points are available. The simulation results are within the spread of the measured data. Hence, the comparison showed that the IHI model predicted fairly well the yaw moment and the increasing trend of the data set.

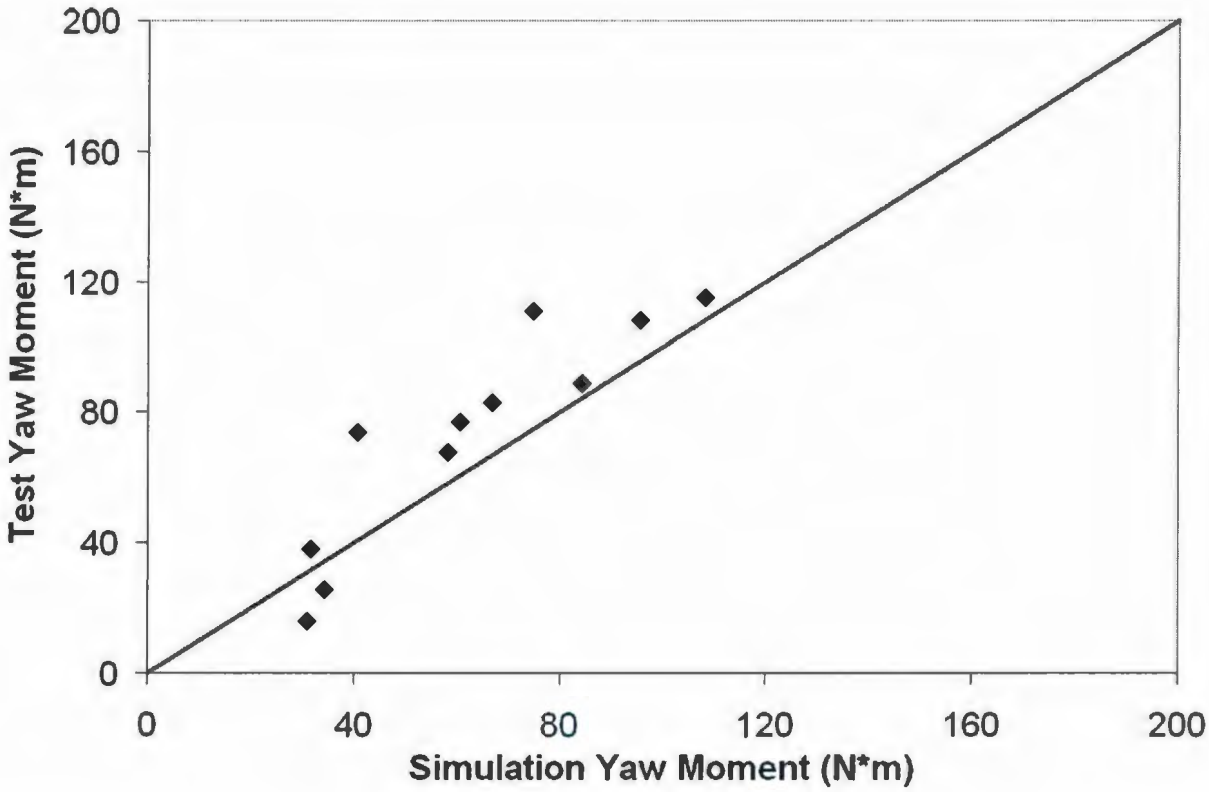

Figure 6.17 Comparison of measured and simulated ice yaw moments for Terry Fox model with 10 and 50 m radius turning in 40 mm - 31.5 kPa ice

Table 6.6 Comparison of measured and calculated ice yaw moments for Terry Fox model in constant radius runs

Model Velocity (m/s)	10 m Radius			50 m Radius		
	Measured Moment (N)	Simulated Moment (N)	Discrepancy (%)	Measured Moment (N)	Simulated Moment (N)	Discrepancy (%)
0.02	N/A	N/A	N/A	15.8	30.8	95.4
0.05	67.7	58.1	14.1	N/A	N/A	N/A
0.1	77.0	61.5	20	38.1	31.6	17.1
0.2	82.8	66.7	16.1	N/A	32.8	N/A
0.3	110.8	74.7	32.6	25.6	34.4	34.4
0.4	88.9	84.3	5.2	N/A	36.2	N/A
0.5	108.25	95.5	11.8	N/A	38.3	N/A
0.6	115.0	108.3	5.8	74.1	40.7	45.1
0.7	N/A	122.6	N/A	N/A	43.3	N/A

6.6 Channel Width

During ship navigation in level ice, the unbroken ice sheet is firstly broken due to flexural bending failure at the ice-hull contact area and the ice cusps are continuously generated with the ship's focused motions. Some of the cusps reach the hull bottom and leave the hull eventually and others may clear to the sides of

the ship. A channel is cleared behind the icebreaker. The channel's shapes and widths left by the ship in its constant radius turning runs are dependent on the ship's geometries, ship motions like velocity, drift angle, constant radius, etc. and ice properties. In essence, the ice properties and ship's velocities directly affect the size of ice pieces broken by the hull. The drift angle and constant radius directly affect the positions of the ice-hull contact and the shape of the ice edge left by the ship in its moving. The different channel width reflects different ice-hull contact condition that determines the ice force distribution along the hull surface and sensitively affects the global ice forces on the ship. Therefore, the channel left by the ship is also an important factor to check the accuracy of the IHI model and deserves comparison between model test results and simulation results.

Figure 6.18 shows a typical channel left by the model in a PMM constant radius run with Terry Fox model at 0.4 m/s tangential velocity and with 10 m radius. Figure 6.19 correspondingly shows the channel edges calculated by the IHI model for that test run.

The measured data for channel edge positions in the tests are discontinuous and affected by unavoidable human error. Therefore, the trend lines are used to fit the measurements to obtain the best match. Figure 6.20 compares the channel widths predicted by the IHI model to the corresponding measurement (Lau, 2007) as a function of turning radius. Table 6.5 provides the data used in Figure 6.22.

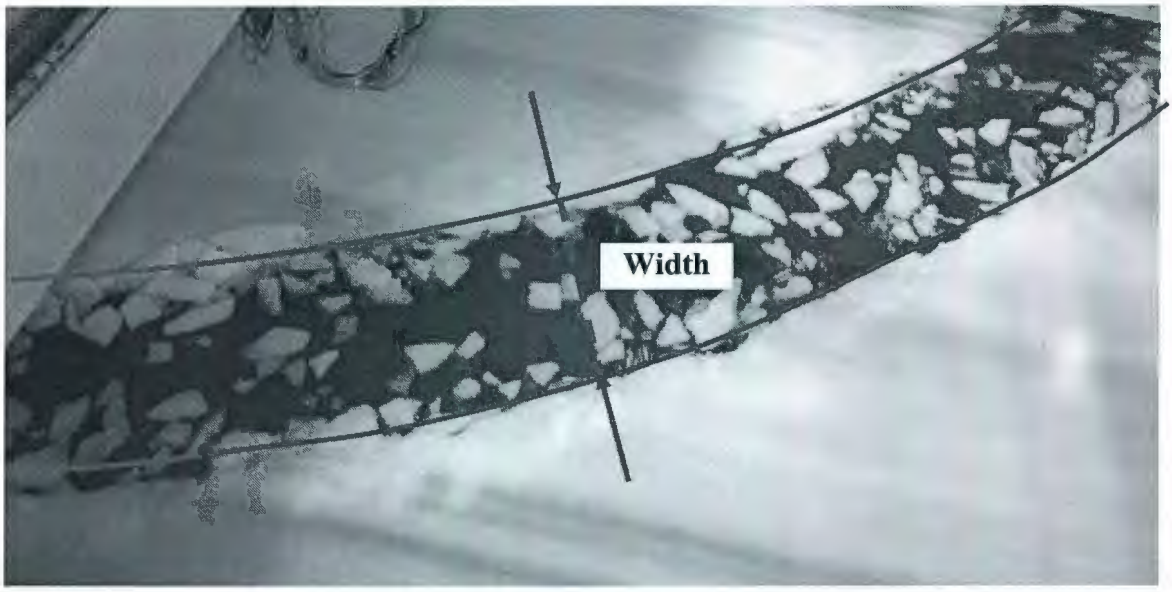

Figure 6.18 Channel left by Terry Fox model in constant radius test run

Figure 6.20 showed that the relative errors between measurements and predictions were both smaller than 10% for the 10 and 50 m radius runs. The discrepancy for10 m radius runs show a little larger than that for 50 m radius runs. The calculated channel widths for two runs were both within the spread of the measured data, which shows that the accuracy for predicting simulated channel edge was reasonable and acceptable.

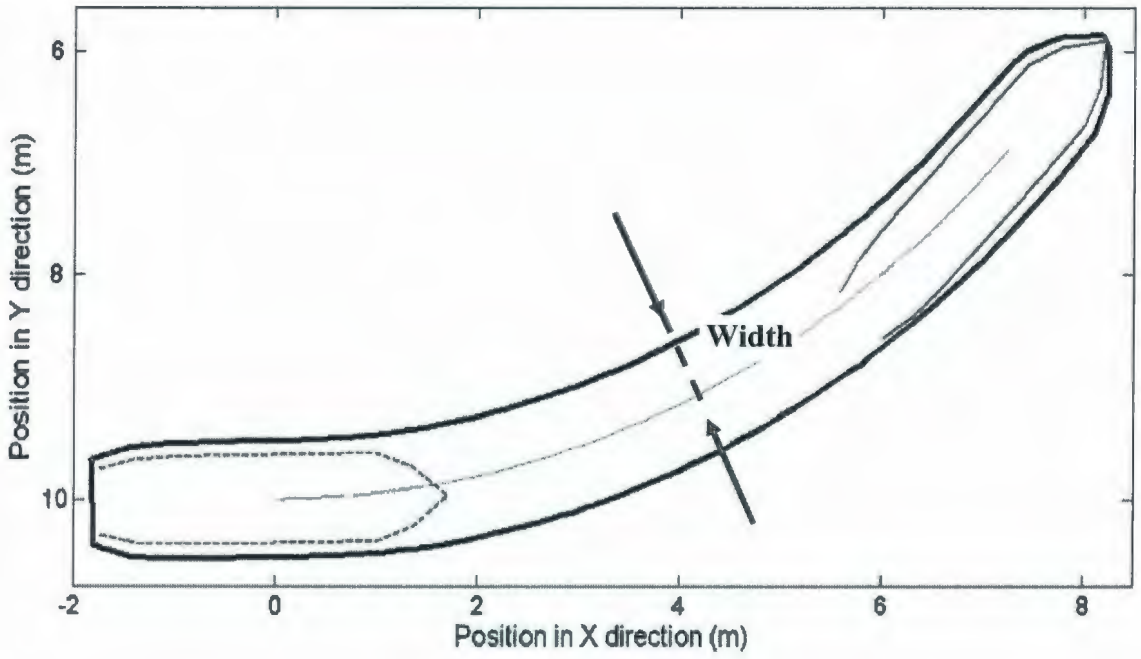

Figure 6.19 Sketch of the channel width in the ship's constant radius runs

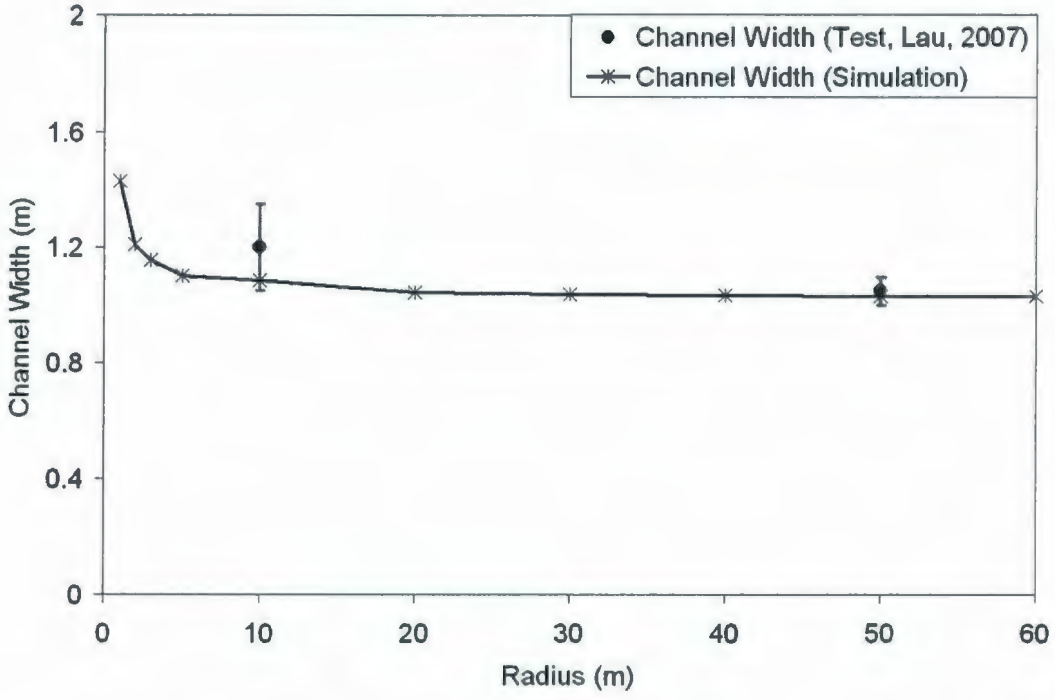

Figure 6.20 Simulated and measured channel widths as a function of the turning radius

Table 6.7 Comparison of measured and simulated channel widths for Terry Fox model test runs

Radius (m)	Measured Width (m)	Simulated Width (m)	Discrepancy (%)
1	N/A	1.43	N/A
2	N/A	1.21	N/A
3	N/A	1.16	N/A
5	N/A	1.10	N/A
10	1.2	1.086	9.5
20	N/A	1.046	N/A
30	N/A	1.039	N/A
40	N/A	1.034	N/A
50	1.05	1.033	1.6
60	N/A	1.030	N/A

The discrepancy between measurements and predictions can be explained as the following: The actual ice edge is irregular rather then smooth line as shown in Figures 6.4, 6.8 and 6.18. The measured data is average width of the ice edge. The measured data for channel edge positions in the model tests are discontinuous and subject to human errors. Especially, for the small radius runs, the running length is shorter. The measured points are also less. To that case, the human error affects

final results more. Also, actual control of the model's motion in ice is much more difficult than in open water. All of above factors affect the final scatter range of the measured data.

6.7 Summary and Conclusions

6.7.1 Summary

Resistance Runs

Terry Fox Icebreaker straight ahead runs in the 40 mm – 31.5 kPa ice at the speeds ranging from 0.1 to 0.6 m/s in level ice and pre-sawn ice were simulated using IHI model. Comparison between predicted resistances and measured resistances in tests showed that the relative errors between predictions and measurements were within 20% of the corresponding measurement.

Constant Radius Runs

Terry Fox Icebreaker constant radius manoeuvres in the 40 mm - 31.5 kPa level ice with 10 and 50 m radius and 0.02 to 0.6 m/s velocities were simulated using IHI model.

The relative errors of the prediction were within 20% of the corresponding measurement for 10 m radius runs. The predictions were within the spread range

of the measured data for 50 m radius runs. The calculated channel widths were within the spread range of the measured data.

6.7.2 Conclusions

This chapter presented the IHI model benchmark based on Terry Fox model test series, and verified the model's potentials, accuracy and advantages in simulating real-time ship manoeuvres in ice. The Terry Fox Icebreaker specific manoeuvres corresponding to the PMM test runs, resistance run and constant radius run, can be realistically simulated using the IHI model software. The comparison between model predictions to measurements includes ice-hull contact, channel and global ice forces.

The comparison between predictions and measurements showed that the IHI model predicted fairly well the ice forces on the hull, channel edges, ice-hull contacts and trends of the data set.

Chapter 7 IHI Model Benchmark with R-Class Model Tests

This Chapter presents the benchmark of the IHI model using IOT R-Class Icebreaker model test series. Among the R-Class model tests, the captive test data were selected for the model benchmark (Newbury and Williams, 1986a, 1986b; Colbourne, 1987a, 1987b; Williams et al., 1992, 1993; Newbury, 1992; Molyneux et al., 1998; Hoffmann, 1998, Shi, 2002). Besides the resistance runs and constant radius runs, sinusoidal test runs were also selected for comparison in order to showcase the IHI model's capability in simulating ship's arbitrary manoeuvres.

7.1 Description of CCG R-Class Icebreaker and IOT Model

Three R-Class icebreakers, CCGS Sir John Franklin, Pierre Radisson and Des Groseilliers, are operated by Canadian Coast Guard. Among them, R-Class icebreaker, Sir John Franklin, was built in 1979. It was originally used as an accommodations vessel by Canadian Shipping Company Canship at a nickel mine in Voisey's Bay, Labrador. The ship is presently crewed by the Canadian Coast Guard as one of its R-class icebreakers and renamed as Amundsen. Figure 7.1 shows the typical scene of the icebreaker, Sir John Franklin, navigating in ice.

The CCG R-Class Icebreakers have comparatively simple underwater hull forms, which have been a world-wide reference icebreaking hull form since they were

built in 1970's and have been extensively tested at many model ice basins around the world as the subject of the comparative ITTC study of model ice resistance (Spencer et al, 1992; Newbury, 1992). They have been tested at different scales in a variety of ice conditions in NRC/IOT and a comparatively complete database of its performance in ice tests has been built (Newbury and Williams, 1986a, 1986b; Colbourne, 1987a, 1987b, Williams et al., 1992, 1993; Newbury, 1992; Molyneux et al., 1998; Hoffmann, 1998); therefore, The IOT R-class model test sets were selected for benchmarking the IHI model.

Figure 7.1 CCG R-Class icebreaker, Sir John Franklin (Amundsen), navigates in ice

(http://www.innovationcanada.ca/19/images/north02.jpg)

The IOT R-Class model was built using the lines of CCG Sir John Franklin at the model scale, 1:20. The ship models were outfitted with twin propellers and a single centerline rudder. A series of PMM tests and towed resistance tests (Newbury, 1992, Hoffmann, 1998) were selected for benchmarking the IHI model. In the test runs, the model ship's speed was kept 0.6 m/s and the pivot point was always fixed at the centre mass of model ship.

Figure 7.2 and Figure 7.3 respectively give pictures of IOT R-Class Model from stern view and bow view. Table 7.1 lists the CCG R-Class Icebreaker's main dimensions. Figure 7.4 shows the IOT R-Class model waterline profile represented in IHI model. The geometries of the ship model represented in the IHI model are given in Table 7.2.

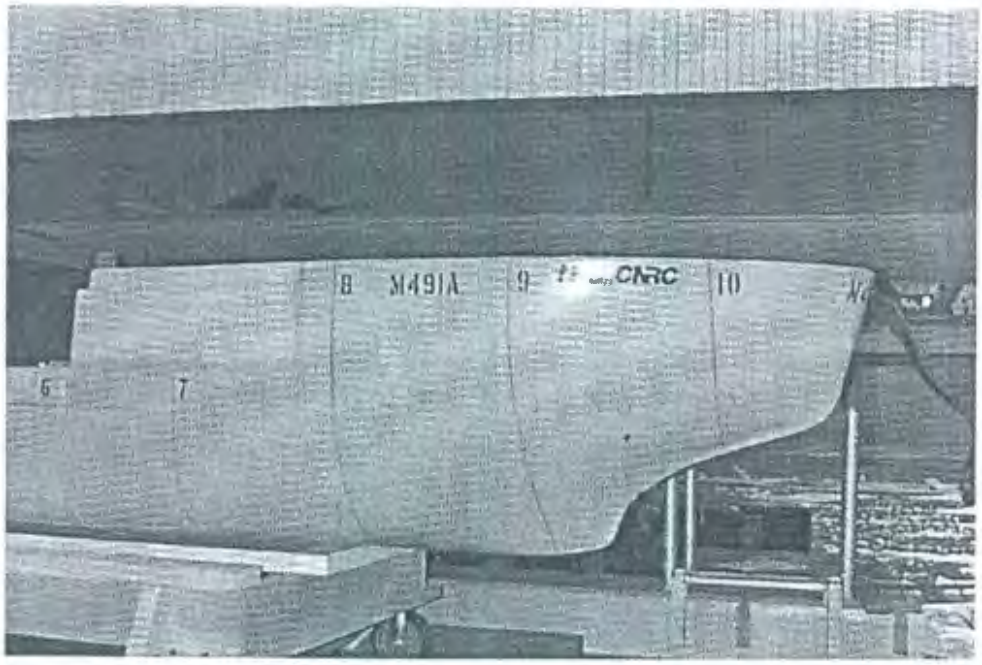

Figure 7.2 IOT R-Class icebreaker model (bow view, Molyneux et al., 1998)

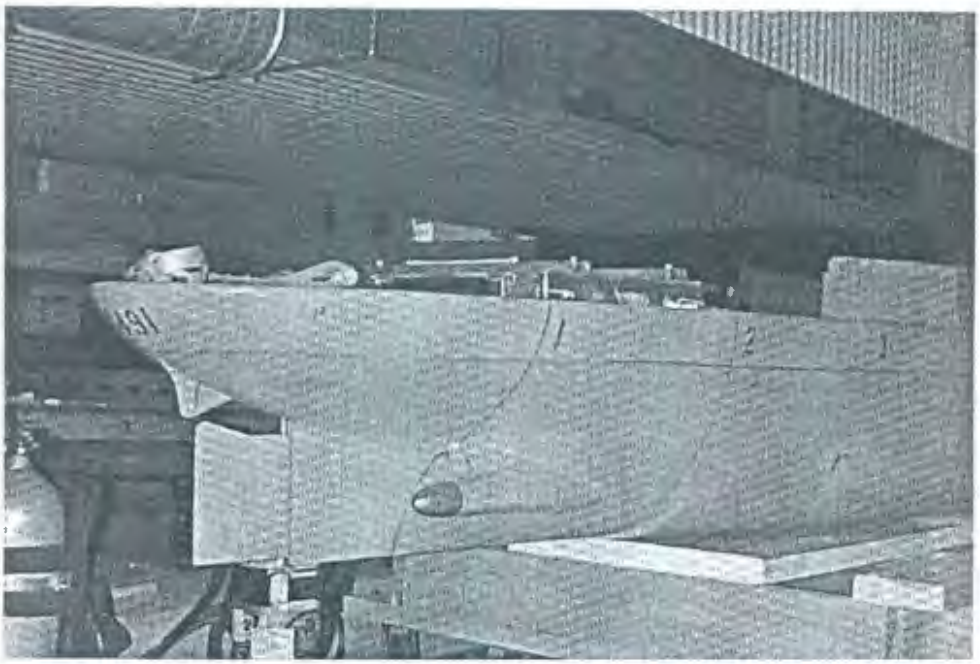

Figure 7.3 IOT R-Class icebreaker model (stern view, Molyneux et al., 1998)

Table 7.1 CCG R-class icebreaker

(Newbury, 1992; Hoffmann, 1998)

Length Overall:	96.52 m
Breadth:	19.5 m
Draft:	7.0 m
Trim:	0.48 m
Buoyancy Centre (LCB):	42.3 m fwd
Displacement:	7720 m^3
Cruising Speed:	2.68 m/s

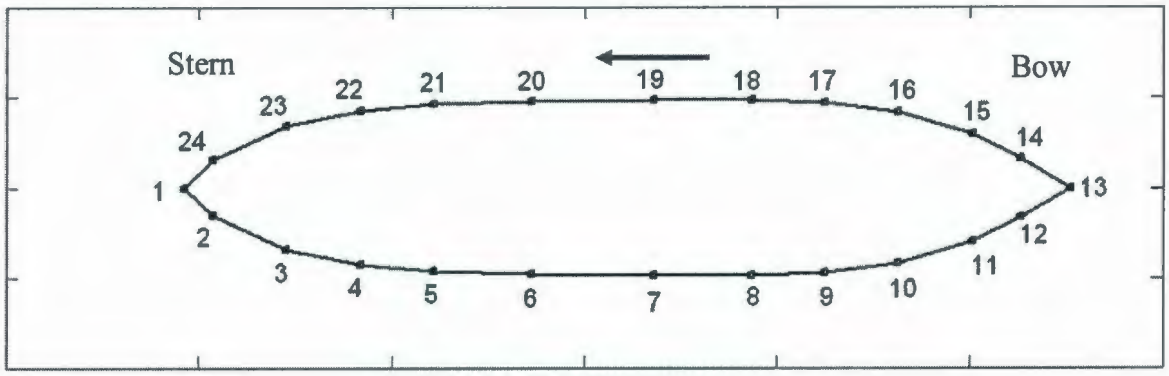

Figure 7.4 IOT R-Class model water line profile represented in IHI Model

Table 7.2 Geometries[1] of IOT R-Class model represented in IHI model

Location[2] (m)	Half WL Width (m)	Flare angle (°)	Hull side area[3] (m^2)
4.5257f	0.000	24.73	0.0404
4.2669f	0.1611	38.67	0.0404
4.0128f	0.294	52.56	0.0769
3.632f	0.417	50.25	0.1642
3.2504f	0.471	57.76	0.1537
2.8692f	0.483	68.33	0.1378
2.3609f	0.483	73.03	0.1710
1.7256f	0.478	73.78	0.2111
1.2173f	0.466	64.10	0.1747
0.8361f	0.426	53.20	0.1426
0.4549f	0.344	40.58	0.1234
0.0737f	0.154	28.11	0.0912
-0.0765f	0.0	35.99	0.0150

Note:
[1] The R-Class model geometries were provided by NRC/IOT.
[2] The transverse plane was measured at interval forwards of the aft perpendicular.
[3] The equivalent area of the hull side surface under the waterline till the bottom at each section as shown in Figure 3.29.

7.2 Resistance Run

7.2.1 Ice Resistance

The 1:20 scale R-Class model resistance test data were reported by Newbury (1992). The density of the model ice was 940 kg/m3. Five of the nine ice sheets had nominally identical properties of 35 mm thickness and 40 kPa flexural strength; two ice sheets were grown to 50 mm thickness with a target flexural strength of 40 kPa and the other two were 22.5 mm ice sheets which were tested at both 40 kPa and 20 kPa. A range of model velocities, from 0.15 to 0.90 m/s, was tested. The nominal ice/hull friction coefficient was 0.03. Besides the level ice resistance tests, pre-sawn ice resistance tests were also correspondingly performed for each level ice run with the same model speed and same ice thickness.

Figures 7.5, 7.6 and 7.7 show the comparisons between the calculated ice resistances and the corresponding measurements in R-Class model test runs with different ship velocities and different ice conditions. Tables 7.3, 7.4 and 7.5 respectively give the predicted and measured data.

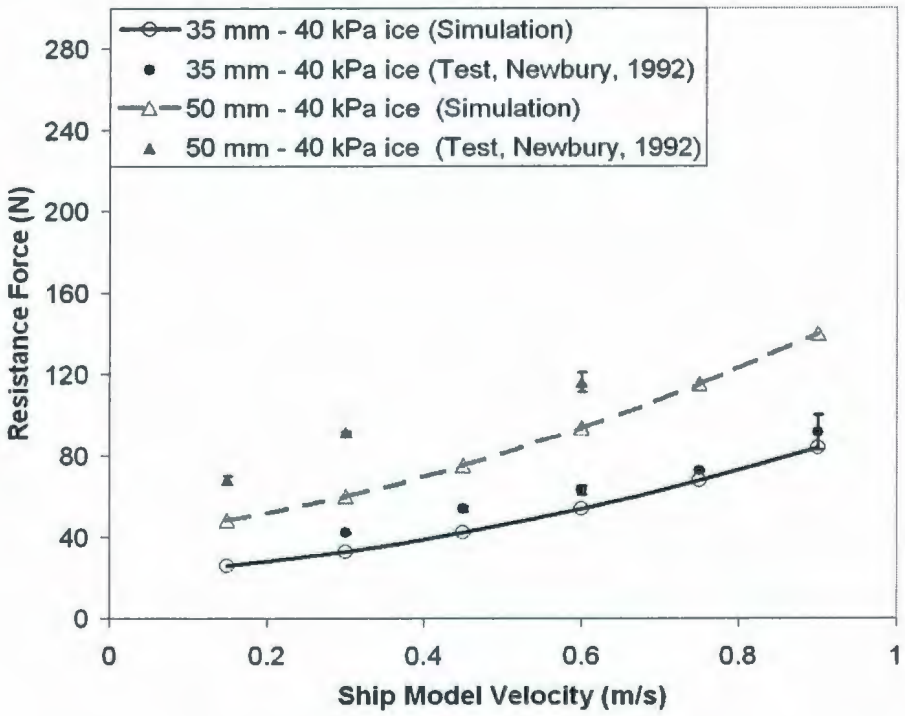

Figure 7.5 Comparison of measured and simulated ice resistances for R-Class model tests in 35 and 50 mm - 40 kPa level ice with speeds from 0.1 to 0.9 m/s

Table 7.3 Comparison of measured and calculated ice resistances for R-Class model test runs

Model Velocity (m/s)	35 mm – 40 kPa level ice			50 mm – 40 kPa level ice		
	Measured Resistance (N)	Simulated Resistance (N)	Discr. (%)	Measured Resistance (N)	Simulated Resistance (N)	Discr. (%)
0.15	N/A	25.9	N/A	68.1	48.5	27.9
0.3	42.2	32.8	22.2	91.5	60.0	34.3
0.45	54.2	42.3	22.0	N/A	75.2	N/A
0.6	63.1	54.0	14.4	116.2	93.7	19.4
0.75	72.5	67.9	6.3	N/A	115.3	N/A
0.9	91.8	83.9	8.6	N/A	140.0	N/A

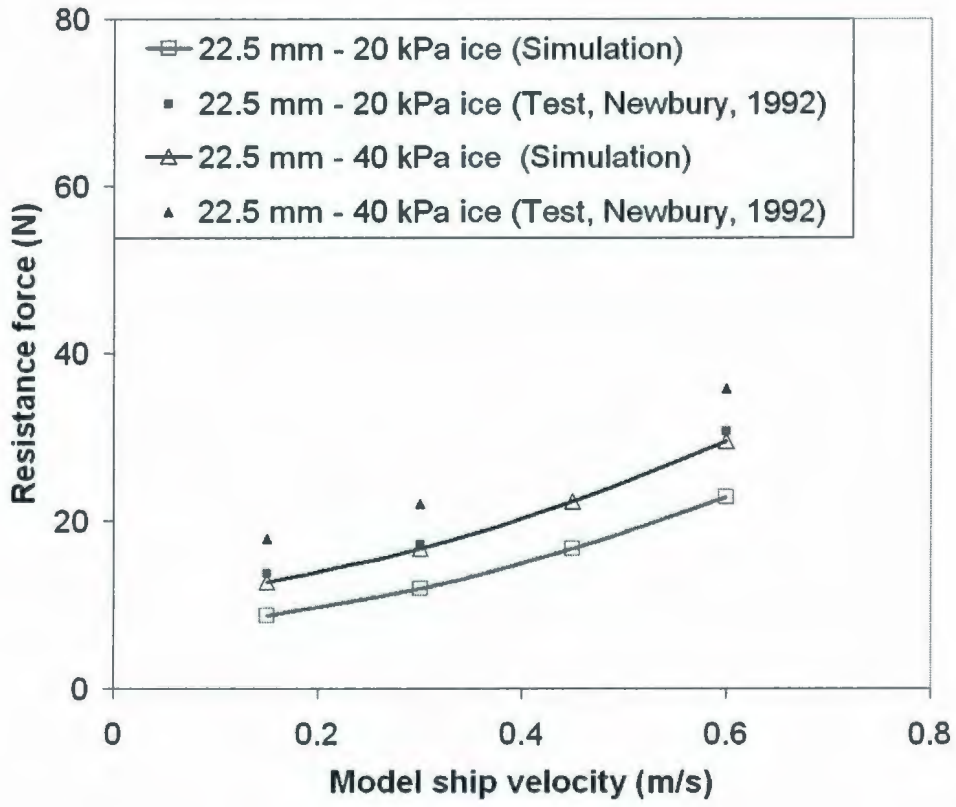

Figure 7.6 Comparison of measured and simulated ice resistances for R-Class model tests in 22.5 mm-20 and 40 kPa level ice with speeds from 0.1 to 0.6 m/s

Table 7.4 Comparison of measured and calculated ice resistances for R-Class model test runs

Model Velocity (m/s)	22.5 mm - 20 kPa level ice			22.5 mm - 40 kPa level ice		
	Measured Resistance (N)	Simulated Resistance (N)	Discr. (%)	Measured Resistance (N)	Simulated Resistance (N)	Discr. (%)
0.15	13.7	8.7	36.3	17.8	12.7	28.6
0.3	17.2	11.9	30.8	22.1	16.7	24.4
0.45	N/A	16.7	N/A	N/A	22.3	N/A
0.6	30.6	22.9	25.1	35.8	29.5	17.6

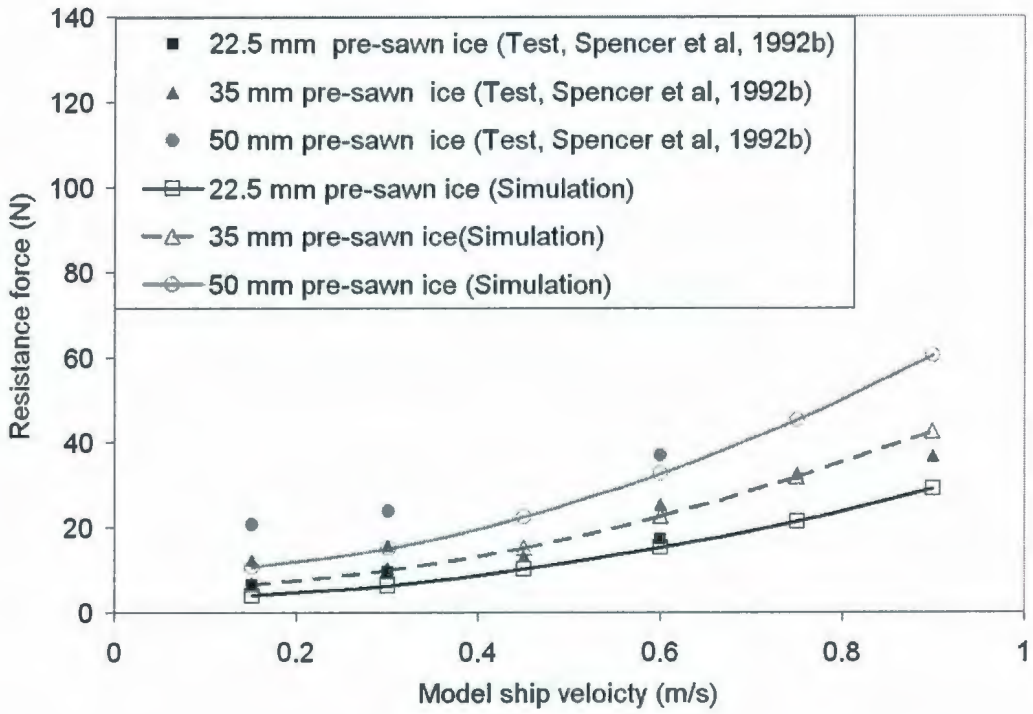

Figure 7.7 Comparisons of measured and simulated ice resistances for R-Class model tests in 20, 35 and 50 mm pre-sawn ice with speeds from 0.1 to 0.9 m/s

Table 7.5 Comparison of measured and simulated ice resistances for R-Class model test runs in pre-sawn ice

Model Veloc. (m/s)	22.5 mm pre-sawn ice			35 mm pre-sawn ice			50 mm pre-sawn ice		
	Meas. Resis. (N)	Simul. Resis. (N)	Discr. (%)	Measu. Resis. (N)	Simul. Resis. (N)	Discr. (%)	Measu. Resis. (N)	Simul. Resis. (N)	Discr. (%)
0.151	6.4	4.0	37.5	12.2	6.6	45.9	20.7	10.6	48.3
0.3	9.5	6.3	23.1	15.5	9.9	36.1	23.6	15.0	36.4
0.45	N/A	10.0	N/A	13.1	15.2	16.0	N/A	22.3	N/A
0.6	17.2	15.1	12.2	25.3	22.6	10.7	36.8	32.5	11.7
0.75	N/A	21.4	N/A	32.5	31.7	2.5	N/A	45.2	N/A
0.9	N/A	28.9	N/A	36.8	42.6	15.8	N/A	60.4	N/A

The comparison results showed that the discrepancies between test measurements and calculation results were within about 25% for most comparison points. The discrepancy became a little larger for those runs in the thicker ice sheet with higher flexural strength. The predictions are smaller than measurements, which may be caused to some extent by the ice jamming at hull shoulder.

7.2.2 Jamming at Hull Shoulder

Jones et al. (Jones et al, 1992, 1994, 2002a, 2002b) mentioned the phenomena of jamming at hull shoulder observed in their R-Class resistance tests. According to Jones et al.'s observation, the broken ice cusps rotate parallel to the hull and they become jammed between the hull and the intact ice sheet. This jamming occurs only in the vicinity of the shoulders where the flare angles can be steep, in excess of 80 degrees, and ice-hull friction can play a significant role in inducing jamming. Once the jamming happens, there is no net clearing force and failure occurs by means other than flexure, typically crushing. Also, the jamming process may lead to more secondary cracking of cusps, which results in smaller ice pieces and bigger breaking ice force. The result would be very high local loads and lead to the possibility of structural damage. The ice jamming at the shoulder has effects on resistance through ice-hull friction, which makes the ice resistance sensitive to the ice-hull friction coefficient (Jones et al, 1992, 1994, 2002a, 2002b).

In the following, a simplified calculation was carried out in order to qualitive study the jamming effects to the global ice force on the hull provided that the jamming has happened. The ice at R-Class model tests, 50 mm thickness, 20 kPa flexural strength and 83 kPa crushing strength, was selected. According to the observations from resistance tests and full-scale trials (Jones et al., 1992, 1994, 2002a, 2002b; Riska et al., 1987, 2001, 2006), only the crushing failure rather than bending failure will happen due to jamming and jamming only happens near the hull shoulder where the beam is near maximum as shown in Figure 7.8.

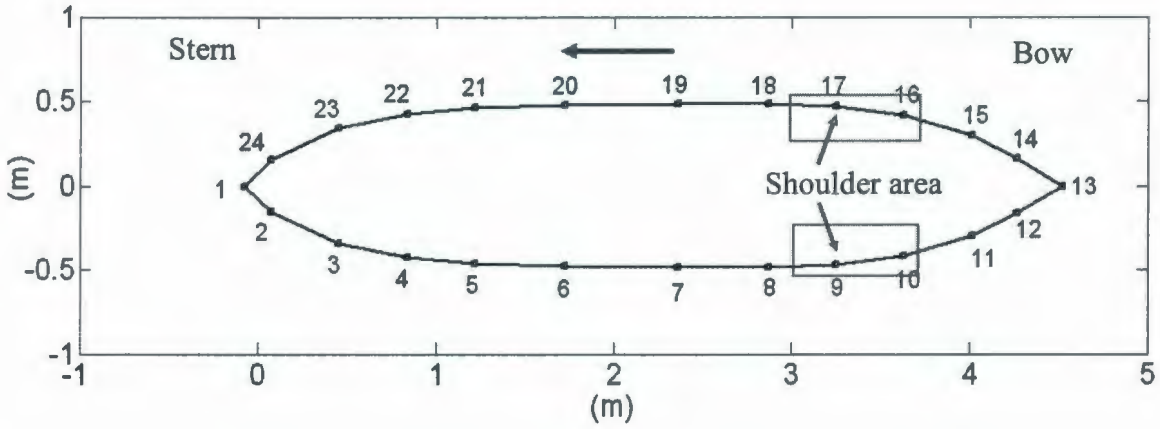

Figure 7.8 IOT R-Class model shoulder where jamming may occur

Considering the geometry of interaction between ice and hull surface as shown in Figure 3.11. Ice Cusp bending failure force is calculated using Kashtelyan's equation given in section 3.3.6.1. It is assumed that all the horizontal force causes

the crushing failure. Then the max crushing width of the ice cusp before the bending failure is approximately equal to:

$$W_{crush} = \frac{A_{crush}}{h} = \frac{F_H}{\sigma_c h} = \frac{0.518\sigma_f h}{\sigma_c}\tan\psi \qquad (7\text{-}6)$$

Where F_H is force component acting horizontally; ψ is sloping angle of the hull surface; h is the ice thickness; A_{crush} is the crushing area between the ice and the hull surface; σ_f is the flexural bending strength of ice; σ_c is the crushing strength of ice.

The ice cusp depth is about 0.2 times the characteristic length of the ice (Lau, et al., 2004) and for the 50 mm thick ice, the ice cusp depth is approximately 0.12 m and the corresponding ice cusp width is 0.38 m (Kotras, 1983). Using equations 7-6, it can be calculated that for 50 mm thick ice, the crushing width of the ice cusp is about 0.0063 m for the 45° sloping structure and 0.0356 m for the 80° sloping structure. Considering that the flare angle at the shoulder is in excess of 80 degrees, it is reasonable to select the crushing width, 0.0356 m, for the following calculation if it is assumed that only one ice cusp is jammed at each hull shoulder.

The ice pressure force affects the resistance through horizontal frictional force preventing the hull's surge motion. It can reasonably be expected that the jamming

phenomena simultaneously happen at both shoulders beside the longitudinal centre. Considering the water line at the shoulder there are nearly parallel to the surge direction, the ice-hull friction force caused by the jamming pressure completely contribute to the resistance.

$$R_{jam\,min\,g} \approx 2.0 * \mu * \sigma_c * h_i * W_{crush} \tag{7-7}$$

Where, $R_{jam\,min\,g}$ is the resistance force caused by ice crushing failure during the jamming; σ_c is the ice crushing strength; W_{crush} is the ice crushing width; μ is the ice-hull frictional coefficient.

For the 50 mm ice and 0.03 frictional coefficient, the resistance forces caused by the ice jamming is

$$R_{jam\,min\,g} = 2.0*0.03*0.083e6*0.05*0.036 = 8.96\ (N) \tag{7-10}$$

Figure 7.5 and Table 7.3 showed that 50 mm ice resistance is between 68 ~ 120 N. Then, the ice resistance is increased about between 7%~13% due to the ice jamming at the shoulder. The simulation results can be improved if the jamming is assumed. The jamming at the hull shoulder may cause an obvious resistance increase, which makes the ice resistance sensitive to the ice-hull frictional

coefficients. That was also coincident with observations in R-Class resistance tests by Jones, et al (1994, 2002).

The ice jamming is actually a very complicated dynamic interaction between the broken ice and the hull shoulder in the ship breaking ice process, which is dependent on the detailed geometrical lines of the hull shoulder, ship advancing velocity and ice properties like thickness, density, mechanical factors, etc. Laboratory investigations have shown that ice friction coefficient is higher where ice is crushed against the hull than where it is not (Williams, 1987; Williams, et al., 1987; Liukkonen, 1988; Gagnon, et al., 1989). The increase of ice-hull frictional coefficients also worsens the jamming situation in reverse.

The IHI model presented in this thesis doesn't accurately model the jamming phenomena. A multi-failure model considering the crushing failure, bending failure and shear failure was used to calculate the ice failure process during the ship breaking ice. This section only discussed qualitatively the jamming effects to ice resistance through some simplified calculations.

7.3 Constant Radius Run

In the manoeuvring tests (Williams, et al., 1996; Molyneux et al., 1998a, 1998b; Hoffmann, 1998)., the tangential velocity of the model ship was fixed at 0.6m/s and the targeted ice-hull frictional coefficient was equal to 0.06.

7.3.1 Comparison

Figure 7.9 and 7.10 respectively showed the calculated ice yaw moments in R-Class model constant radius manoeuvres and corresponding measurements in 30 and 50 mm thick level ice and broken ice. Table 7.6 and Table 7.7 listed the corresponding data presented in the above comparison figures.

The comparisons showed that the IHI model predictions are smaller than the measurements. The discrepancy between measurement and prediction is about within 25% in 30 mm and 50 mm broken ice. The big discrepancy exists for the level ice tests, especially for the large radius runs. That may be explained as the effects of the drift angles during the running, which is discussed in next section with more details.

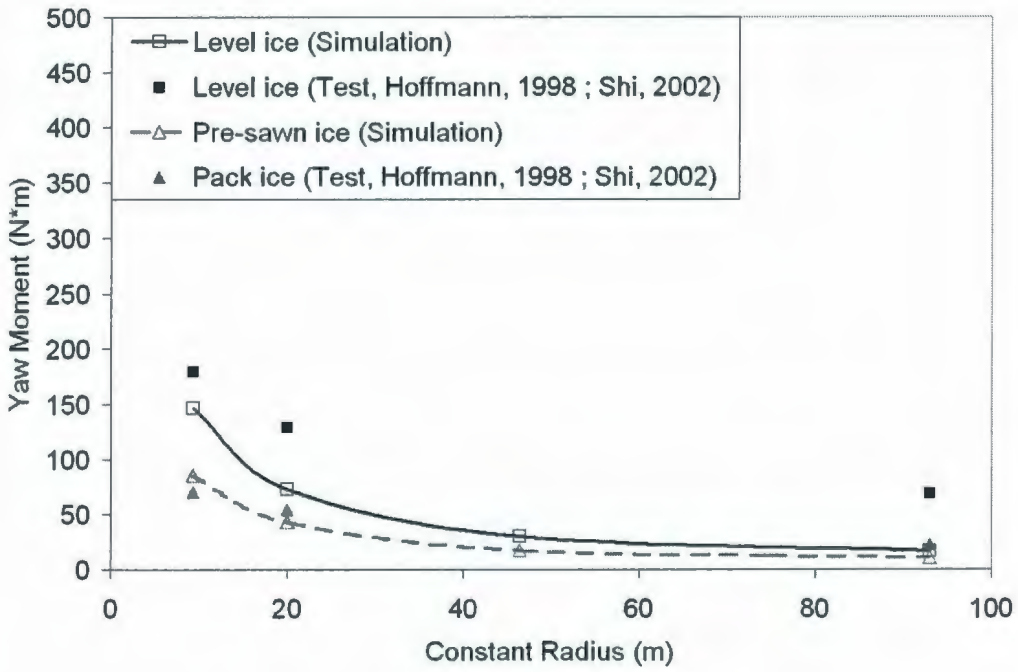

Figure 7.9 Comparison of measured and calculated ice yaw moments for R-Class model constant radius runs with 30 mm-20 kPa level ice and broken ice.

Table 7.6 Comparison of measured and calculated ice yaw moments for R-Class model constant radius runs

Model Velocity (m/s)	30 mm – 20 kPa level ice			30 mm broken ice		
	Measured Moment (N*m)	Simulated Moment (N*m)	Discr. (%)	Measured Moment (N*m)	Simulated Moment (N*m)	Discr. (%)
9.3	179.4	146.5	18.3	70.5	85.3	17.4
20	128.7	73.0	43.3	54.4	43.8	19.5
46.5	N/A	30.5	N/A	N/A	17.7	N/A
93	68.3	16.9	75.3	22.9	10.5	54.2

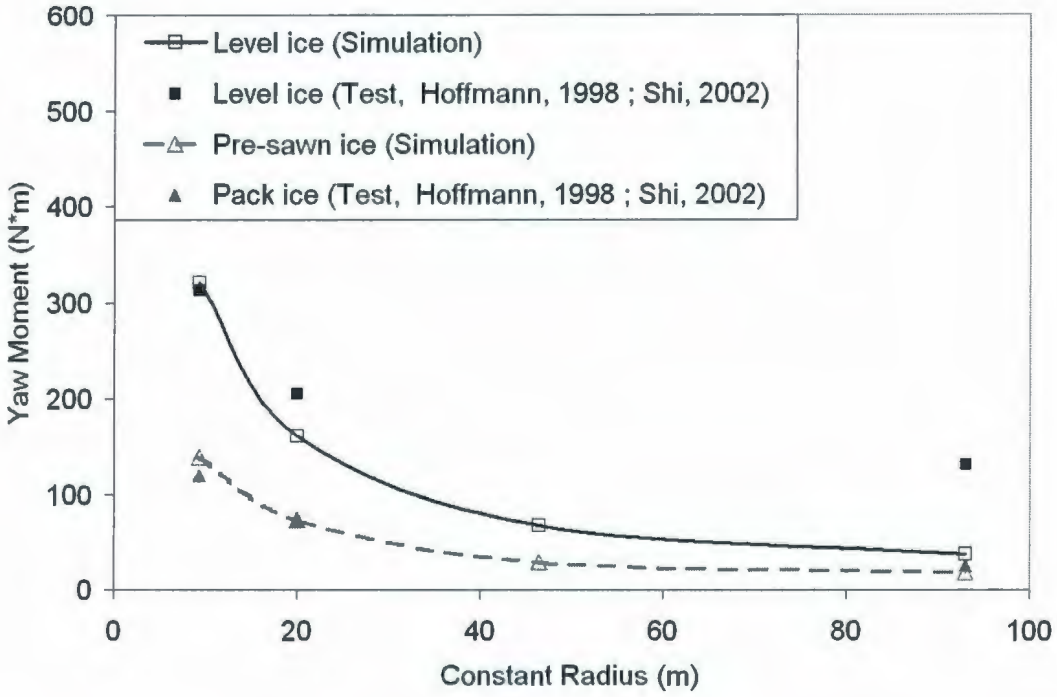

Figure 7.10 Comparison of measured and calculated ice yaw moments for R-Class model constant radius runs in 50 mm-20 kPa level ice and broken ice

Table 7.7 Comparison of the measured and calculated ice yaw moments for R-Class model constant radius runs

Model Velocity (m/s)	50 mm - 20 kPa level ice			50 mm broken ice		
	Measured Moment (N*m)	Simulated Moment (N*m)	Discr. (%)	Measured Moment (N*m)	Simulated Moment (N*m)	Discr. (%)
9.3	313.0	320.3	2.3	120.0	138.7	15.6
20	205.3	160.4	21.8	73.7	73.4	0.4
46.5	N/A	67.4	N/A	N/A	29.2	N/A
93	130.8	37.3	71.5	24.7	18.1	26.7

7.3.2 Drift Angle

Shi (2002) reported a drift angle, 5.6°, in the constant radius level ice runs although the programmed drift angle kept zero in the PMM tests.

Figure 7.11 shows comparisons between the predictions and measurements. Table 7.8 gives the data presented in the comparison figure. The comparison shows that the discrepancies between predictions and measurements are about within 15% in 30 mm ice tests and 35% in 50 mm ice tests.

The simulation results are bigger than test measurements after considering the drift angle. In fact, the drift angle, 5.6°, seems too big because the programmed drift angle is zero in the PMM tests. Such a big error is not usual in tests. That will be confirmed if it is possible in the future. If the more accurate experimental data are input into the IHI model, the discrepancy between test results and simulations will expectantly be further reduced.

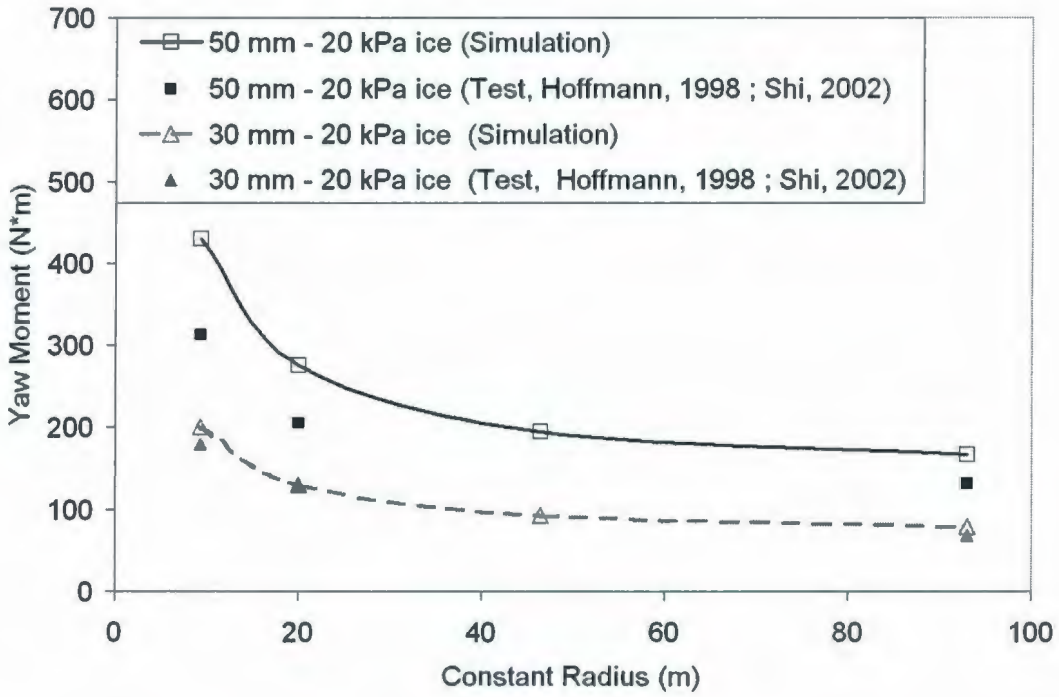

Figure 7.11 Comparison of measured and calculated ice yaw moments for R-Class model constant radius runs in 30 and 50 mm - 20 kPa level ice

Table 7.8 Comparison of measured and simulated ice yaw moments for R-Class model constant radius runs

Model Velocity (m/s)	30 mm - 20 kPa level ice			50 mm - 20 kPa level ice		
	Measured Moment (N*m)	Simulated Moment (N*m)	Discr. (%)	Measured Moment (N*m)	Simulated Moment (N*m)	Discr. (%)
9.3	179.4	200.6	11.8	313.0	430.8	37.6
20	128.7	130.6	1.5	205.3	276.0	34.4
46.5	N/A	92.4	N/A	N/A	194.8	N/A
93	68.3	79.0	15.6	130.8	165.9	26.8

7.4 Sinusoidal Runs

In the constant radius test, the model experiences a quasi-static yaw rate. Considering that the raw data measured in PMM model test includes the relatively low high frequency noise ice force component, the average yaw moment value in a sufficient long time with the constant ship motion and constant ice condition are usually adopted. While during the sinusoidal run, the yaw rate keeps changing in order to keep the centreline of the model always tangent to its path. Therefore, it is more practical and reasonable to compare the trend line of the test measurements and the line of the theoretical predictions. In the following comparison, the linear type of the trend line of the measured data is assumed considering that the yaw moment seems to be linear proportional to the small variations of the yaw rate with the constant ship velocity (Hoffmann, 1998).

7.4.1 Comparison

Figure 7.12 is the direct copy of the Figure 5-50 from Shi (2002), which shows the test results of R-Class model ship sinusoidal run of 0.6 m/s tangential velocity, 100 seconds period, 2.5 m amplitude in Y direction and zero drift angle in the 30 mm - 20 kPa flexural strength ice sheet. Obviously, the measured raw yaw moments are very scattered due to high frequency force components. And it is more practical to compare the trend line of the measured data to that of the predictions.

Figure 7.13, 7.14 and 7.15 respectively show the yaw moment comparison and sway force comparison between the simulation results and the measured results in the sinusoidal runs. We can see that the calculated yaw moment vs. yaw rate curves is roughly a straight line. The comparison also showed that the sloping angles of the measured curves and predicted curves agree fairly well.

Due to the hull geometrical symmetry of two sides of the longitudinal center, for zero yaw rate, the ship goes up straight and the ice yaw moment and ice sway force on the hull should be zero. Therefore, under the ideal condition, both the yaw moment vs. yaw rate curve and the sway force vs. yaw rate curve are through the origin of coordinates. The measured yaw moment vs. yaw rate curve and sway force vs. yaw rate curve both offset the origin point, as shown in Figure 7.13, 7.14 and 7.15, which may be explained as the effects from the existing drift angle during the running. Next section will give detailed discussion on it.

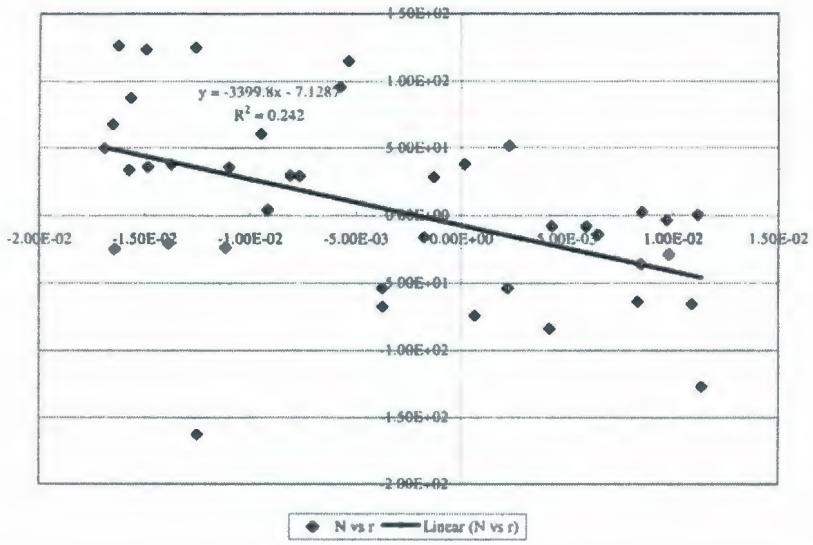

Figure 7.12 Regression test results of R-Class model sinusoidal run in 30 mm - 20 kPa level ice at a speed of 0.6 m/s (Shi, 2002). X-axis represents the yaw rate and Y-axis the yaw moment (Nm).

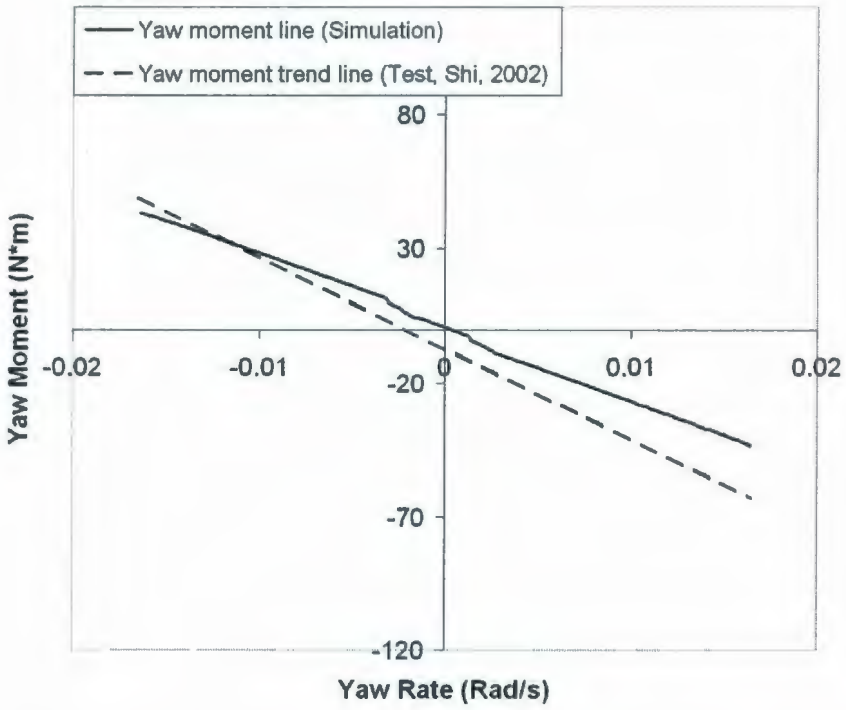

Figure 7.13 Comparison of measured and calculated ice yaw moments for R-Class model sinusoidal run in 30 mm - 20 kPa level ice

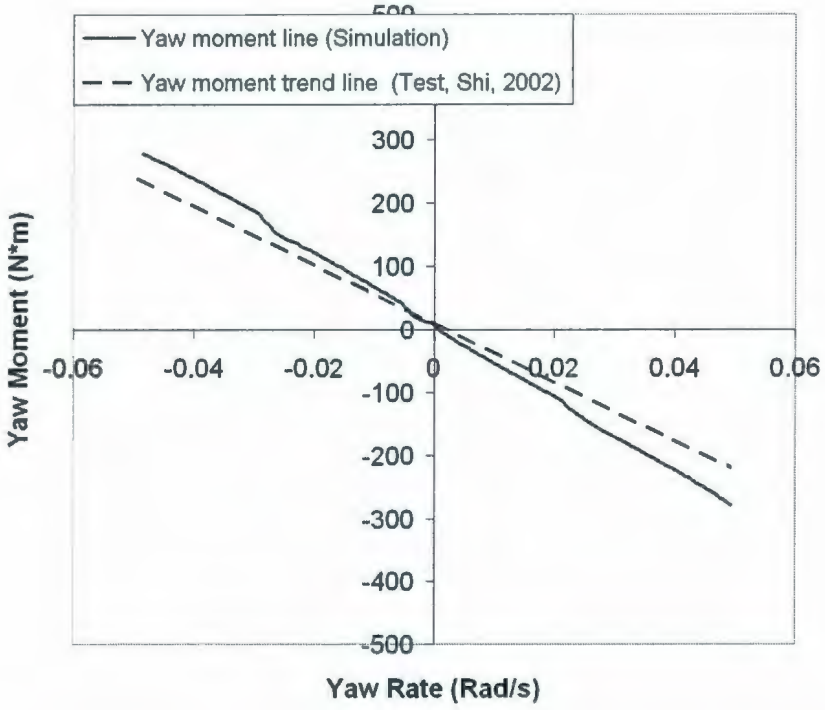

Figure 7.14 Comparison of calculated and measured ice yaw moments for R-Class Icebreaker sinusoidal run in 50 mm - 20 kPa level ice

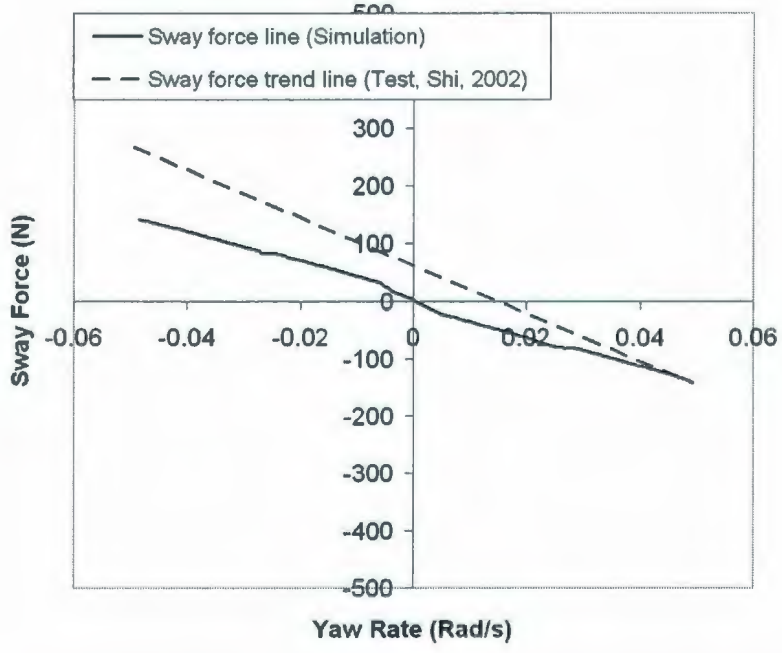

Figure 7.15 Comparison of measured and calculated sway forces for R-Class model sinusoidal run in 50 mm - 20 kPa level ice

7.4.2 Drift Angle

Shi (2002) reported a drift angle, 0.5°, during the sinusoidal runs. In the following simulations, a drift angle, 0.5°, was prescribed. Corresponding to Figure 7.13, 7.14 and 7.15, the comparisons between test results and predictions in 30 and 50 mm ice were presented in Figure 7.16, 7.17 and 7.18 respectively.

From the comparison figures, it can be seen that the calculated yaw moment vs. yaw rate curves and sway force vs. yaw rate curve all offset from the origin point of coordinates system when a drift angle is prescribed. The simulation results, the calculated yaw moments in 30 mm ice run and the calculated sway forces in 50 mm ice, are more coincident with the experimental data when the drift angle is considered during the running, while discrepancy between simulated curve and the measured line for the yaw moments in 50 mm ice run increases a little.

In fact it is much more difficult to maintain an exactly steady turning motion in ice than in open water. In the comparison, the straight type trend line is assumed and obtained based on the limited measured highly scattered data from tests as shown in Figure 7.16 and Figure 7.18. All above affected the final comparison results.

Therefore, although there are still some discrepancies, we can still say that the comparison between test data and IHI model simulation data theoretically verified

well a drift angle existing in the sinusoidal tests and its effects to the global ice force on the hull.

With accuracy improvements of ship model experiments and future refinements of IHI model, the discrepancy between measurement results and simulation results should be expectedly further reduced.

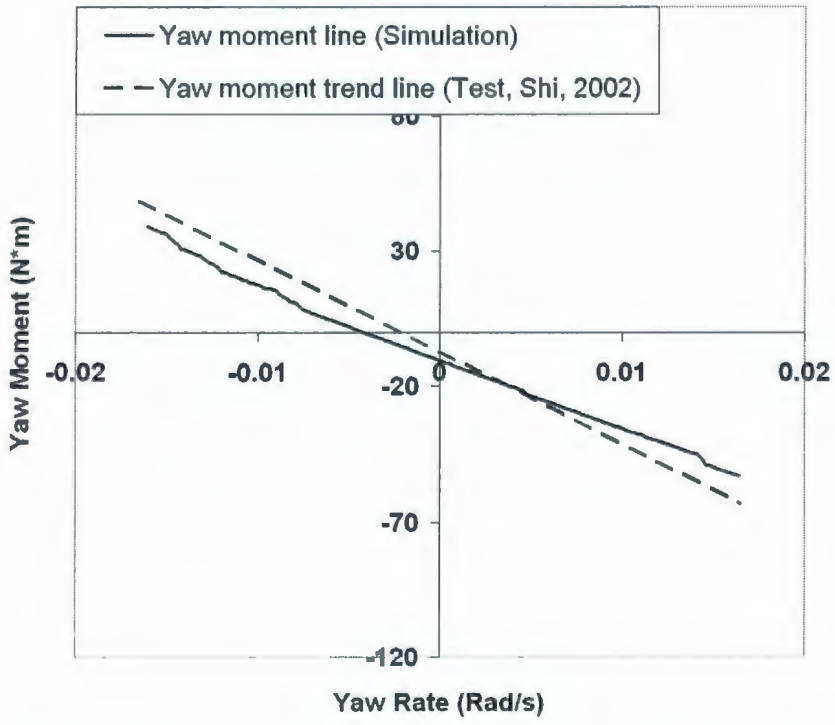

Figure 7.16 Comparison of measured and calculated ice yaw moments for R-Class model sinusoidal run in 30 mm - 20 kPa level ice considering a 0.5 deg drift angle

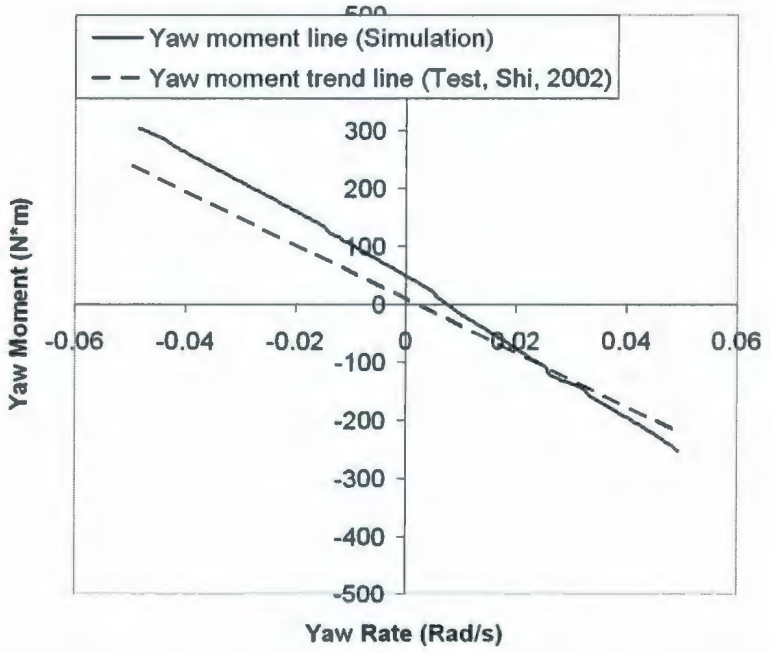

Figure 7.17 Comparison of measured and calculated ice yaw moments for R-class model sinusoidal run in 50 mm-20 kPa level ice considering a 0.5 deg drift angle

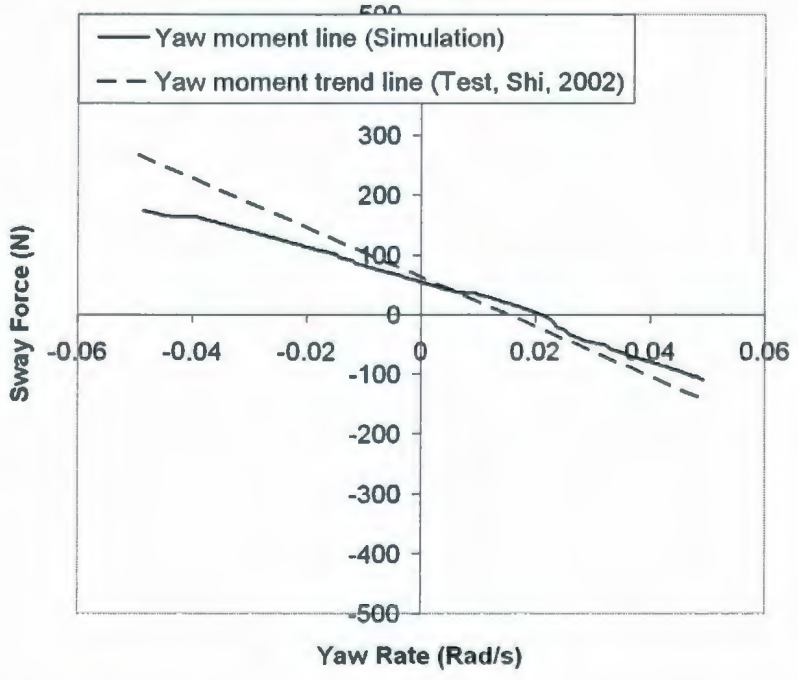

Figure 7.18 Comparison of measured and calculated ice sway forces for R-Class model sinusoidal run in 50 mm - 20 kPa level ice considering a 0.5 deg drift angle

The comparison showed that the IHI model successfully simulated the constant radius runs and sinusoidal tests with fairly good accuracy.

Comparing the benchmark results with considering drift angle and without drift angles in constant radius runs and sinusoidal runs, it can be found that the drift angle plays an important factor in influencing the global ice loads on the hull. Therefore, the drift angle of the model should be paid more attentions in the future PMM tests.

The small fluctuations of the IHI model simulated yaw moment vs. yaw rate curves and sway vs. yaw rate curves can be explained from the two sides:

On one side, in the IHI model, the whole R-class model hull is divided into 12 small sections as shown in Figure 7.7. The actual curved surface of each section is simplified as the flat-plate with the same sloping angle. Therefore, the continuous and smooth hull surface is represented discontinuously and rough to some extend in the model. During the sinusoidal runs, the ice-hull contact area and position kept changing. If the ice-hull contact moves into a new section at a certain moment, a sudden sloping angle change of the ice contacted hull surface may happen and a little ridge of the calculated ice force curve may result. The roughness of the calculation line can be weakened through increasing the number of sections in the IHI model.

On the other side, for the icebreakers like Terry Fox icebreaker, its water surface is naturally non-smooth as shown in Figure 6.3. Using the present test data acquisition approach, the straight type of trend line is assumed based on the measured data for the comparison, which can't accurately express the discontinuous changes of ice-hull contact and the hull frame angle. Therefore, a curve with some small roughness maybe more closely represents the actual average yaw moments on the ship.

7.5 Summary and Conclusions

7.5.1 Summary

Resistance Run

The comparisons showed that the discrepancies between calculated ice resistances and measurements are within about 25% for most comparison points. The effects to the global ice force by the ice jamming at the shoulder were discussed based on a simplified calculation provided the jamming already happens, which showed that jamming at the shoulder may increase ice resistance through ice-hull friction. The IHI model simulation results will be improved if the jamming can be accurately modeled.

Constant Radius Run

The big discrepancy exists for the constant radius runs in level ice especially for the large radius runs. The discrepancy for most cases are within 30%. The predictions are bigger than measurements, which maybe caused by the bigger drift angle, 5.6°, prescribed in the simulation than the test run. Because the programmed drift angle is zero in PMM tests, such a big drift angle is not usual and that needs confirmation if possible in the future. The drift angel effects to the yaw moments in constant radius runs are studied in Chapter 9.

Sinusoidal Run

The comparison showed that the measurements and predictions of the R-Class Icebreaker sinusoidal runs in 30 and 50 mm ices are both fairly coincident. It is theoretically confirmed that the measured ice yaw moment vs. yaw rate curve and sway force vs. yaw rate curve offsetting the origin point of the coordinates system can be explained as the drift angle effects during the running.

In the above simulations, the pivot point was always fixed at the mass centre of the ship. For the free-running trials, the corresponding rules may be a little different due to the changeable position of pivot point in the turning process.

7.5.2 Conclusions

This Chapter presented the verification of IHI model using CCG R-Class Icebreaker model tests carried out in NRC/IOT. Besides the resistance run and constant radius runs, the sinusoidal test runs of PMM R-Class model ship test series were also selected in order to showcase the IHI model's capability in simulating ship's arbitrary manoeuvres.

The comparison results verified that the developed IHI model fairly well predicts the CCGS R-class Icebreaker prescribed manoeuvres, straight going up run, constant radius run and sinusoidal runs, with good accuracy and universality. The benchmark also showed that the drift angle played an import role in influencing the global ice force on the hull and should be paid more attention in the future PMM tests.

Chapter 8 Comparison of Ice Force Distribution on Hull between IHI Model Preditions and Test Results

This chapter presented the more detailed comparison process for the IHI model on the ice force pressure distribution along the waterline of the hull using model tests. The model ship tests carried out in Japanese National Maritime Research Institute (NMRI) were introduced and adopted (Izumiyama et al, 1998, 1999, 2001, 2005; Kayo, 1993). The ice force distributions around the R-Class Icebreaker hull were calculated using IHI model and compared with qualitative NMRI test measurements. Two typical model ship test runs, straight-ahead runs and constant radius runs, were simulated and compared with measurements. The comparison on the ice force distribution acting on the hull further verified the accuracy, reasonability and feasibility of the IHI model. Some clues for further refining the IHI model may be expected.

8.1 Ice Force Distribution on Hull Test

The IHI model was built up based on a detailed mechanical analysis of the hull-ice interaction in level ice. In the model, the whole hull is divided into ten or more sections and the model calculates the average ice forces and moments on each section separately. Comparing the calculated ice force distribution on the hull with the test measurements is a more detailed benchmark for the model.

Izumiyama K. et al. (2005) presented one series of tests, in which the ice distributions around the hull waterline are measured and discussed in the model ship advancing runs and constant radius runs. In Izumiyama's tests, ice load acting on the model hull was measured using a pressure sensing system. The model was equipped with two podded thrusters and tested in a free-running performance. Turning tests as well as straight-going tests were performed. The paper presented the tests and preliminarily analyzed the ice force distributions in two cases: the turning runs and straight-going runs.

The model used for tests has a conventional icebreaking bow and a short parallel mid-body with 4.688 m length between perpendiculars, 0.875 m maximum waterline width and 0.25 m draft. The targeted thickness of the ice sheets in the tests include 30mm and 50mm and the targeted ice flexural strength is around 25 kPa. In Izumiyama's tests, for 7.5 rps, the model can attain a steady speed of about 0.25 m/s. To some extent, the ship model adopted in Izumiyama's test is similar to CCG R-Class icebreaker hull form. Therefore, it is reasonable to qualitatively compare the measurements from Izumiyama's tests with simulation results of R-Class Icebreaker in order to benchmark the IHI model.

A pressure measuring system I-SCAN was used to measure ice load on the model in Izumiyama's tests. The system consists of pressure sensing films with the 210 mm by 210 mm area for each one and a PC for collecting the measurement data as

shown in Figure 8.1 and 8.2. The sensor film consists of pressure-sensing spots in a grid arrangement of 44 by 44 and pressure measured at each spot was converted to a digit between 0 (no pressure) to 255 (maximum measurable pressure called a "Raw". A sum of Raws over the whole pressured sensing area is called a "Raw Sum". In this chapter "Raw Sum" is used to describe ice load on a film and qualitatively compared with the calculated line-pressure results along the waterline of R-Class hull using IHI model.

Figure 8.3 schematically showed the pressure sensor sheet positions on model along the waterline and the assigned corresponding numbers.

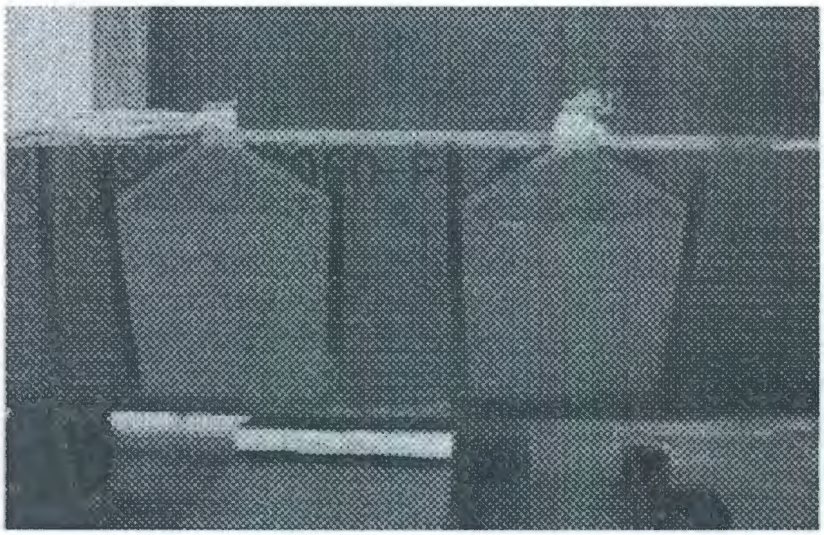

Figure 8.1 Sensor films in model ship (Izumiyama et al., 2005)

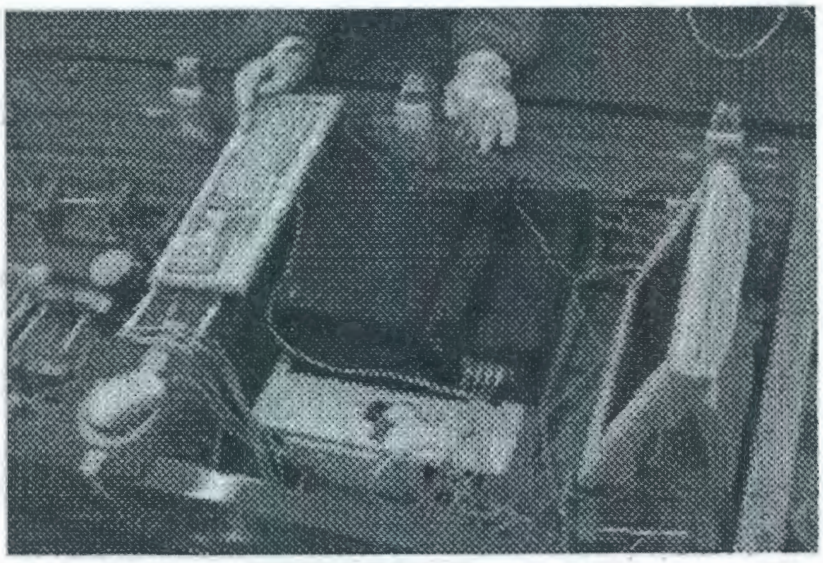

Figure 8.2 PCs for collecting data measured by pressure sensor films in model ship (Izumiyama et al., 2005)

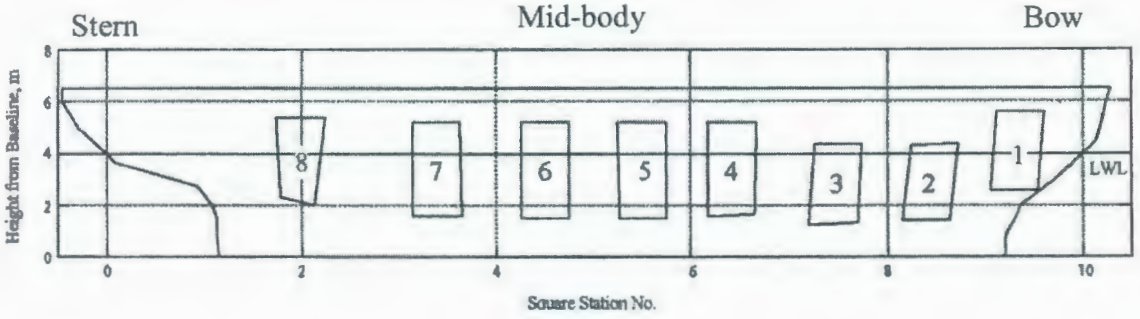

Figure 8.3 Pressure sensor sheet positions on model ship (Izumiyama et al., 2005)

8.2 Advancing Runs

In Izumiyama's tests (2005), three propeller rotation speeds, 6.6, 7.5 and 9.5, are tested for ship model's advancing tests, According to correlation of model speed

and propeller rotation speed presented in Izumiyama's paper (2005), the model's velocities in three cases were around 0.1, 0.3 and 0.5 m/s. Therefore, in the following IHI model simulations, the model's velocities are defined as 0.1, 0.3 and 0.5m/s respectively to represent 6.6rps, 7.5rps and 9.5rps runs. The ice has 30mm thickness and 25 kPa flexural strength as in tests.

Figure 8.4 shows average raw sum distribution in advancing tests measured in Izumiyama's tests. Figure 8.5 correspondingly shows the calculated average ice force distributions on one side of the R-Class icebreaker from the bow to the stern in its straight going up runs.

From Figure 8.4, it can be seen that the ice load mainly acts on the bow part of the hull. The Ice load level increases as the ship model speed increases. The calculated ice force distributions using IHI model shown in Figure 8.5 clearly reflects the same phenomena. It should be noted that the ship adopted in the simulation is R-Class icebreaker rather than the ship model in Izumiyama's tests. There some geometrical difference between those two hull forms. The measured ship model in tests has the shorter parallel mid-body than the R-class icebreaker hull adopted in simulation. Therefore, the maximum ice force distribution position measured in tests is a little far away the stem than the simulated ice force distribution on the R-class hull. In the future, if the same hull forms are adopted in the simulation and

tests, the coincidence between measurements and predictions will expectably be improved.

The above ice load distribution can be explained by ship-ice contact conditions during the running. Due to the inclined surface form at the bow of the R-class icebreaker, ice mainly fails in bending model at the bow when it contacts the unbroken level ice sheet in the straight going up run. Hence the width of the channel formed by the bow is slightly wider than the maximum waterline beam width of the R-Class Icebreaker and the hull's aft-body seldom directly contacts the unbroken ice.

From the test measurements, it was also observed that for the average ice load, the higher model speed gave the higher load (Izumiyama et al., 1999, 2005). Obviously, the IHI model simulation results theoretically confirmed it. The increase rates to ship speed of the three ice components, breaking force, clearing force and buoyancy force, are different, the obtained ice distribution curve are not actually parallel for different ship velocities.

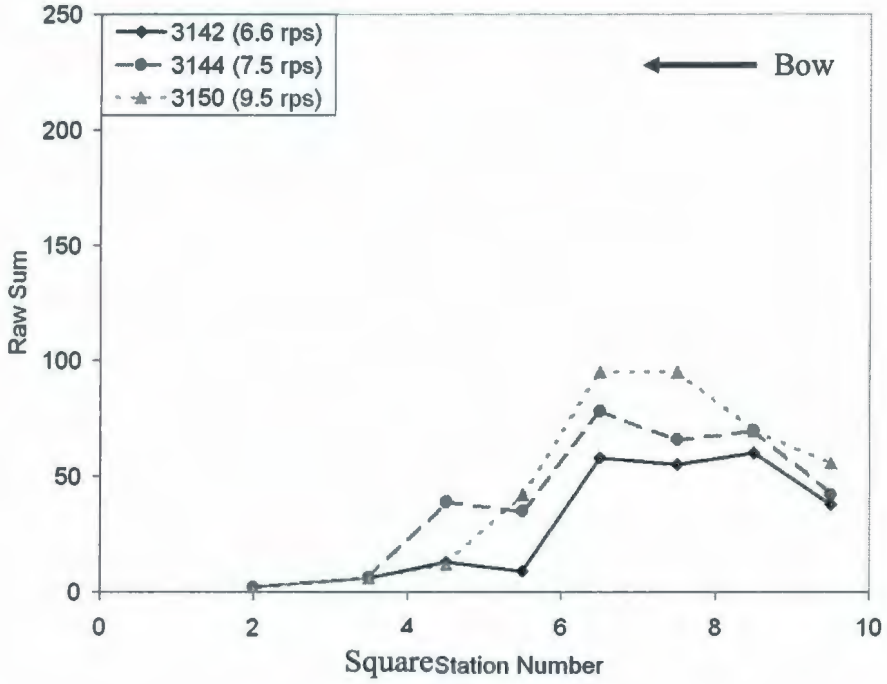

Figure 8.4 Average raw sum distributions in advancing tests (Izumiyama et al., 2005)

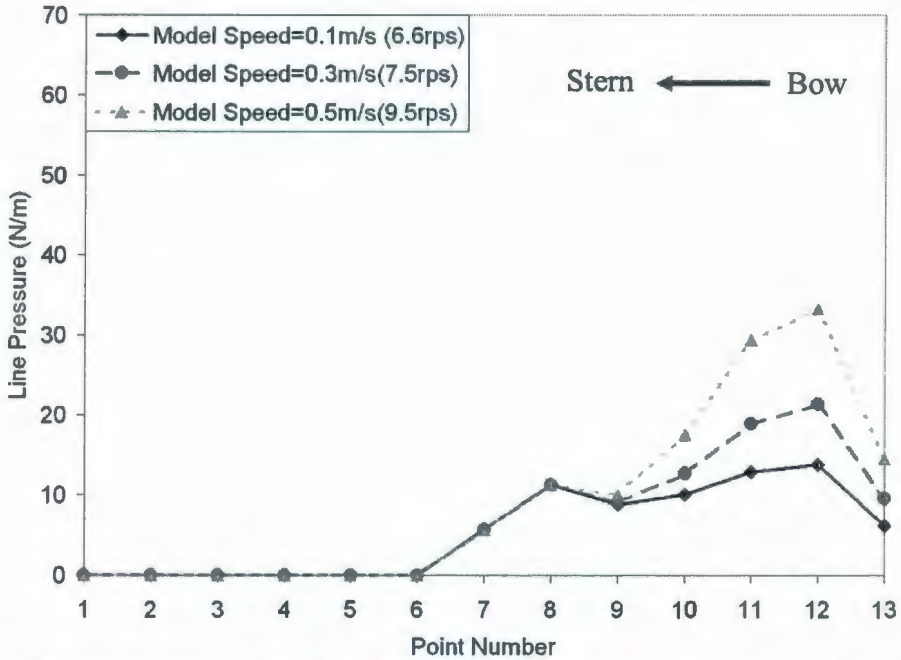

Figure 8.5 Ice pressure distributions in advance tests computed by the IHI model for R-Class model in 30 mm-25 kPa ice sheet at the speeds of 0.1, 0.3 and 0.5 m/s

8.3 Constant Radius Run

Although the Izumiyama's turning tests are free running ones, its results of the steady part of the turning running is sufficiently good (Izumiyama et al., 2005). In the turning runs, the propeller rotation speed keeps 7.5rps and according to correlation of model speed and propeller rotation speed presented in Izumiyama's paper (2005), the model ship's velocity is around 0.25 m/s. From the model track given in the paper, the radius for the steady turning part is around 20 m.

The turning tests presented in Izumiyam's paper includes two runs: Test No. 3146 and Test No. 3147. In test No. 3146, the pod angle is -20° and the propeller rotation speed is 7.5 rps. The sensor sheets are located at the out side hull of the turning model ship. In test No. 3147, the whole test run was divided into two phases: the pod turned –30° at the first phase and +30° at the second phase. The whole run showed a S-shaped turn. Obviously, the sensor sheets were at the outside hull of the turned model ship at the first phase and at inside hull at the second phase. So that, at the first half part, the ice force distribution on the outside of the hull of the turning the mode ship was measured and at the second half part, the ice force distribution on the inside of the hull was measured. Also, the model's tangential velocity was regarded as 0.25 m/s.

For comparisons between simulations and tests, the ice condition in the simulation was defined as 30 mm thick and 25 kPa flexural strength. The ship model's tangential velocity ware prescribed as 0.25 m/s and the turning radius 20 m.

In the free-running tests and full-scale trials in ice, the negative drift angle that can be observed during the turning process to make the bow head inside (Lindstrom, 1990, Izumiyama, 2005). In the Izumiyama's tests, the transverse component of propeller thrust pressed the aft-body against the ice edge at the outside of the hull. Considering that the pod angle in No. 3147 is bigger than that in No. 3146 and the drift angle in test 3147 should also be bigger than that in No. 3146, in the corresponding IHI model simulations, a $-1.0°$ drift angel was applied to the 30 m constant radius run and a $-5.0°$ drift angle was applied to the 20 m constant radius run to represent the Test No. 3146 and Test No. 3147 respectively. This is consistent with a larger rudder angle and larger drift angle for the smaller turning radius during the free-running tests (Lindstrom, 1990). The pivot point is always fixed at the mass centre of the R-Class Icebreaker.

Figure 8.6 showed the measured test data. In the figure, No. 3146 curve represents the measured average raw sum distribution on outside of the hull in the 3146 test run. No. 3147_out curve represents the measured raw sum distribution on outside of the hull and No. 3147_in represents the raw sum distribution on inside in 3147

run. The average raw sum distribution in the straight going run, Test No. 3144, was also presented in order to given a comparison with the turning case.

Figure 8.7 showed the calculated ice pressure distribution on the R-Class Icebreaker hull in the IHI model simulations. In the figure, the ice force distribution in the straight going run with the ship velocity, 0.3 m/s, is also presented. Figures 8.9 ~ 8.13 show the calculated average ice pressure distribution for R-Class Icebreaker 10 m radius turning with 0.25 m/s tangential velocity in 30 mm - 25 kPa ice with drift angles -5.0°, -1.0°, 0.0°, 1.0° and 5.0° respectively. In order to understand the ice force distribution on the hull due to different drift angles, the turning cases with zero and positive drift angles are also simulated.

From tests results and the simulations, Figures 8.7 and 8.8, it can be observed that with the drift angle increasing, the higher ice loading occurs in the aft-body in the outside of the turn (represented by the red ice distribution curves in two figures), while the inside hull receives very low load represented by the blue ice distribution curve in Figure 8.7 and the green ice distribution curve in Figure 8.8. The coincidence between tests and simulation in ice force distributions also gives support to the IHI model.

Figure 8.8 shows that the ice load distributions on the bow are almost same between turning and straight-going tests. The slightly lower average values for

turning tests may be caused by the lower ship speed, 0.25 m/s, in turning case and ship speed, 0.3 m/s, in the advancing case. The ice force load distribution on the aft-body in the turning case is much bigger than that in the advancing cases. The above phenomena are coincident with the Izumiyama's test results as shown in Figure 8.7.

The IHI model simulation results and test results both show that ice load distributions in the straight-going and turning models are different. Ice load is predominantly in the bow area in the straight-going run. In the turning model, the average ice load distribution shows considerably high loads on outside of the aft-body and bow part and very low on inside of the aft-body in turning runs, as shown in Test No. 3147 curves of Figures 8.7 and 8.8. This difference of ice load can be explained by difference in ship-ice contact. In the advancing runs, the aft-body will not directly contact unbroken ice due to the wide channel created at the bow. In the turning runs, the aft-body may directly contact the ice edge in the outside of the turn.

The comparison and discussion on the ice force distributions on the hull in the R-Class Icebreaker's straight going up run and turning runs showed very good qualitative correlation between the simulation results and model test results. That provided evidence of the reasonability and correctness of the developing IHI model.

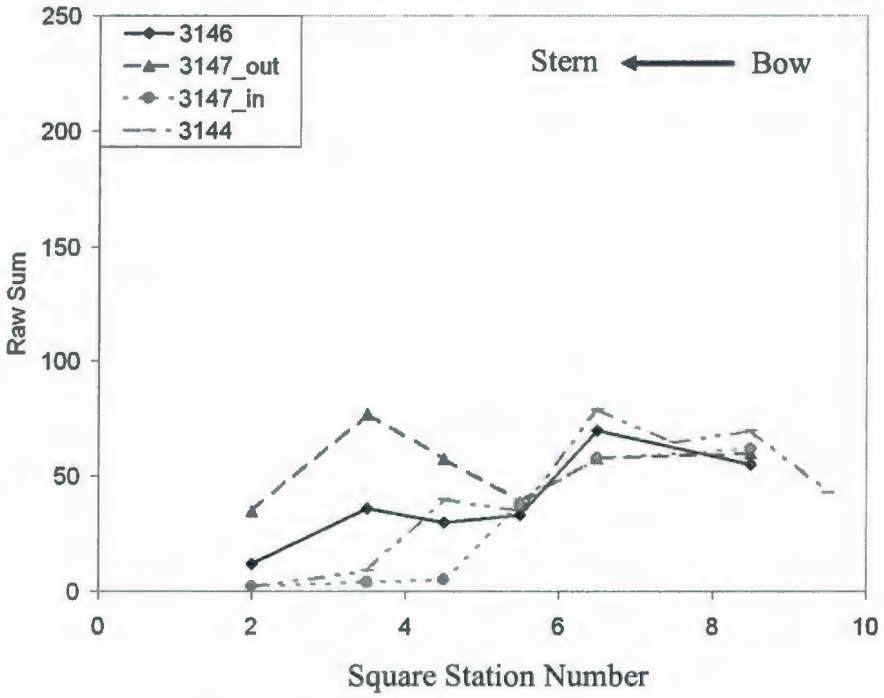

Figure 8.6 Average raw sum distribution in turning tests (Izumiyama et al., 2005)

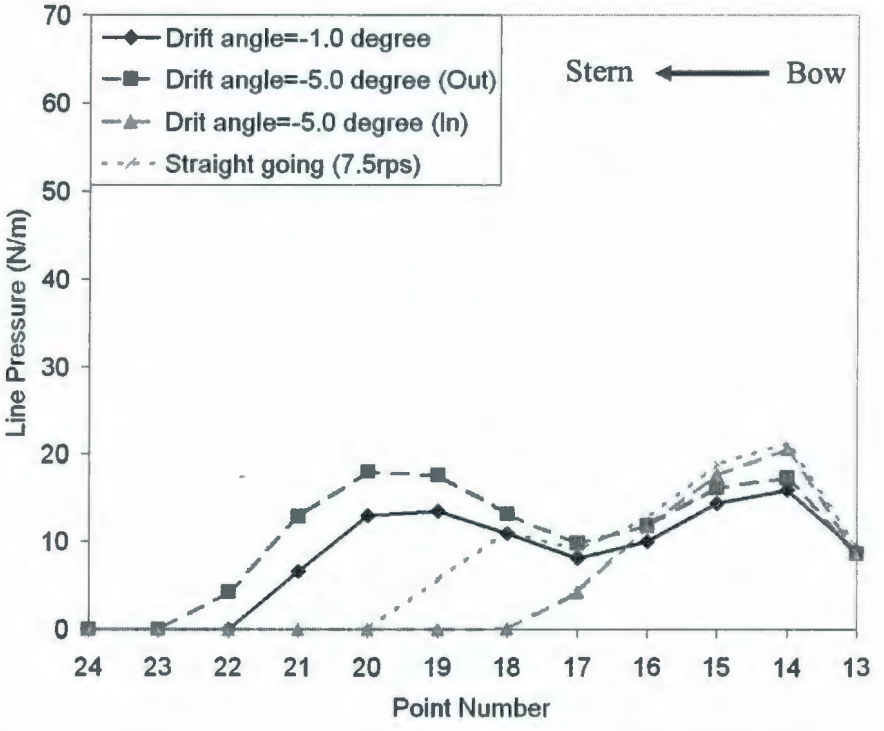

Figure 8.7 Ice pressure distribution in turning tests computed by IHI model for R-Class model in 30 mm - 25 kPa ice with 0.25 m/s tangential velocity

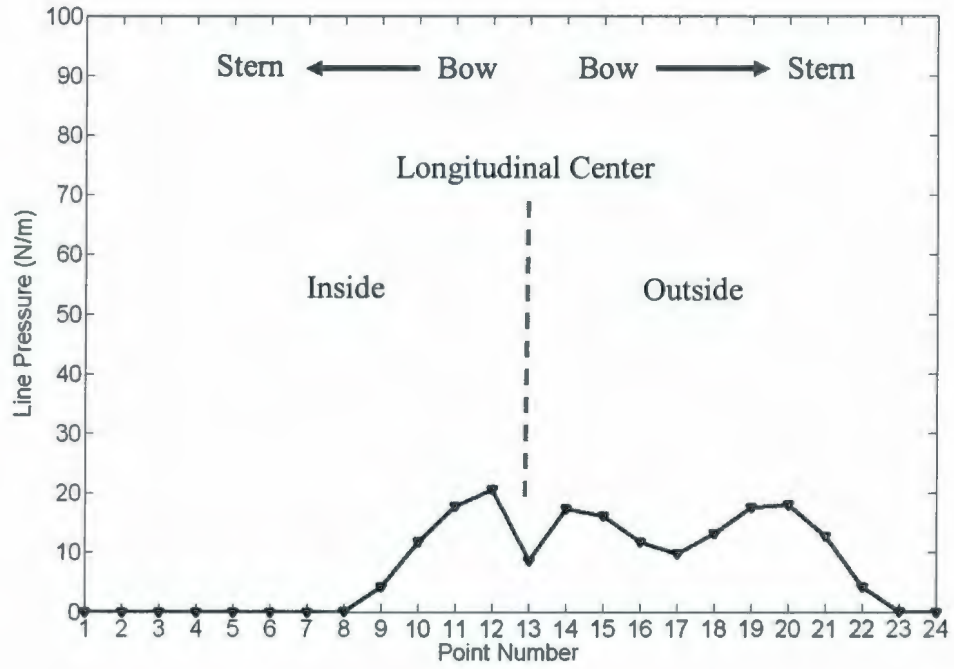

Figure 8.8 Ice pressure distribution for R-Class model 20 m radius turning with 0.25 m/s tangential velocity in 30 mm - 25 kPa ice (Drift angle = -5.0°)

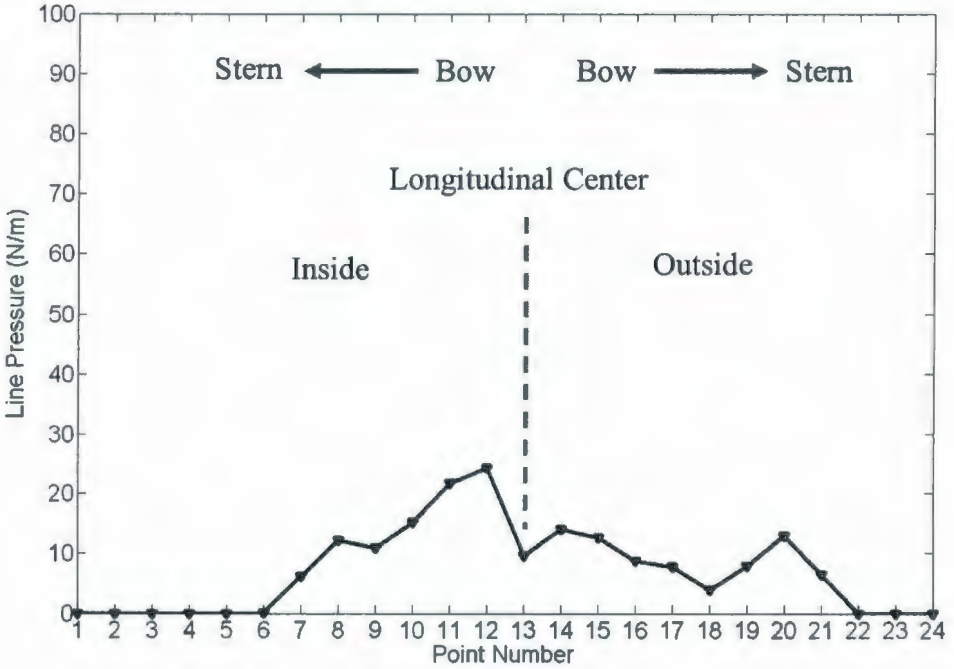

Figure 8.9 Ice pressure distribution for R-Class model 20 m radius turning with 0.25 m/s tangential velocity in 30 mm - 25 kPa ice (Drift angle =-1.0°)

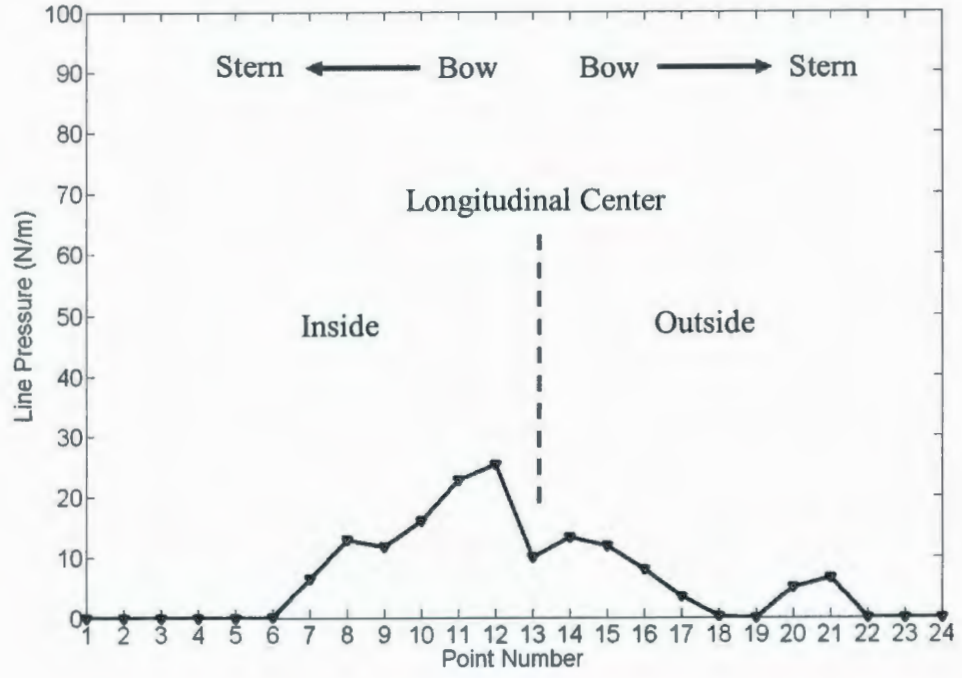

Figure 8.10 Ice pressure distribution for R-Class model 20 m radius turning with 0.25 m/s tangential velocity in 30 mm - 25 kPa ice (Drift angle =0.0°)

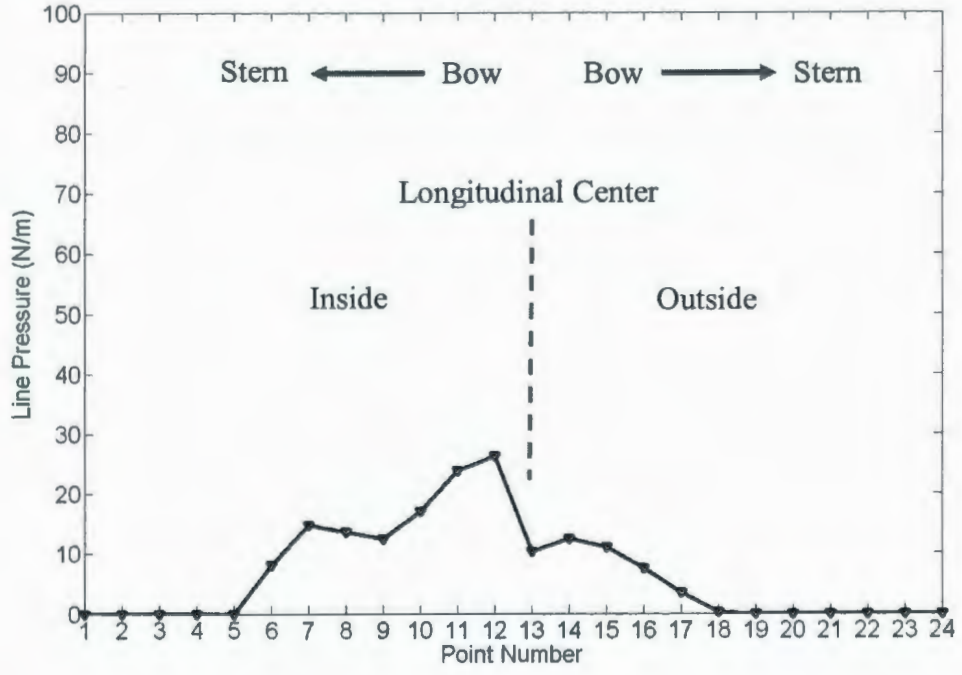

Figure 8.11 Ice pressure distribution for R-Class model 20 m radius turning with 0.25 m/s tangential velocity in 30 mm - 25 kPa ice (Drift angle =1°)

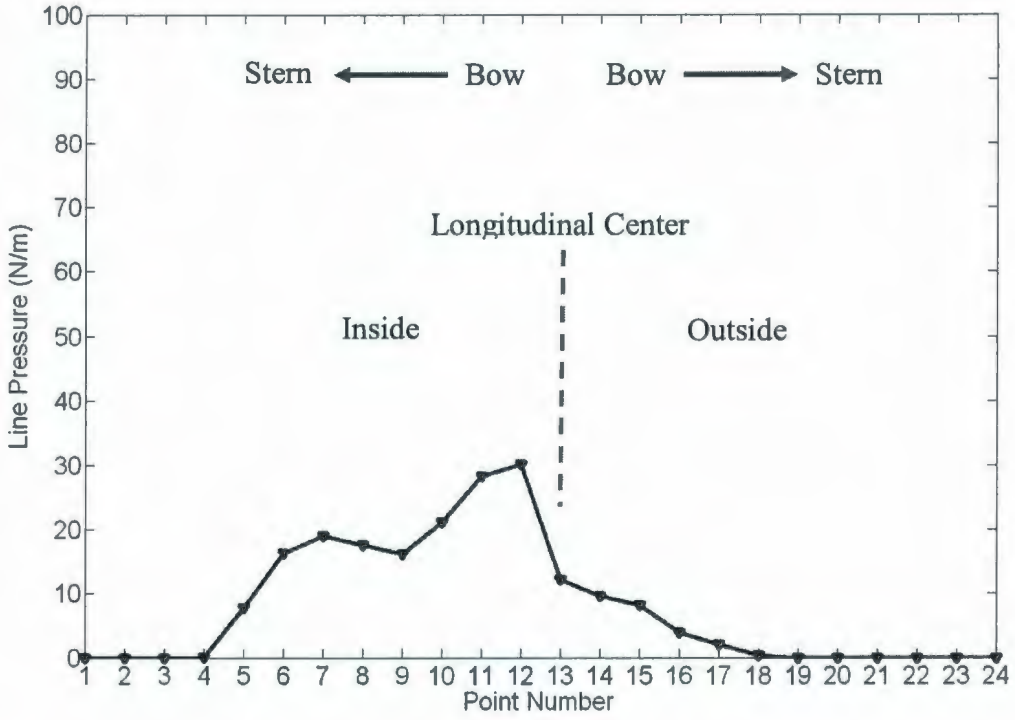

Figure 8.12 Ice pressure distribution for R-Class model 20 m radius turning with 0.25 m/s tangential velocity in 30 mm - 25 kPa ice (Drift angle =5.0°)

8.4 Turning Radius Effects

In previous sections, the drift angel and ship velocity effects on the ice force distribution were studied. This section focuses on the turning radius effects on the ice force distribution on the hull and more R-Class model ship turning runs with different radii were simulated using the IHI model.

Figure 8.13~Figure 8.19 show the ice pressure distribution for R-Class model ship in constant radius runs with different radii, 5 m, 10 m, 30 m, 40 m, 50 m and 100 m, and straight going up runs, in 30 mm - 25 kPa ice. In the simulations, the ship's

tangential velocities were always predefined as 0.25 m/s and the drift angle keeps zero. The pivot point was fixed at the mass centre of the ship.

On the small radius runs, the highest ice pressure distributes on the inside of the hull and the stern of the outside also has relative high ice pressure. The mid-body of the hull only has low ice pressure distribution as shown in Figure 8.14. With the increase of the turning radius, the fore body of the outside of the hull experiences higher ice pressure as shown in Figures 8.15 and 8.16, while the stern part eventually doesn't have ice pressure on it as shown in Figure 8.17. More high ice pressure distribution is located at the bow of the hull around the longitudinal centre, and the inside bow part experiences higher pressure than outside bow part. That difference decreases with the continuous increase of the turning radius as shown in Figure 8.18. It can be expected, if the turning radius is infinity, then the ice pressure distribution on the two sides of longitudinal center of the hull will be same. At that case, the ship runs become the straight going runs. The ice force distribution will be similar as shown in Figure 8.19.

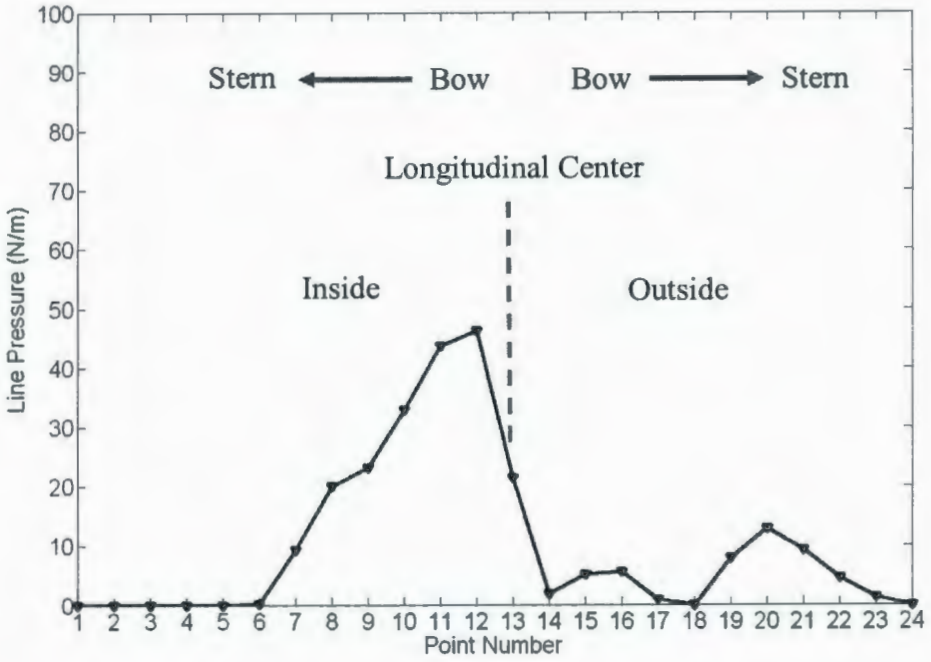

Figure 8.13 Ice pressure distribution for R-Class model 5 m radius turning with 0.25 m/s tangential velocity in 30 mm - 25 kPa ice (Drift angle =0.0°)

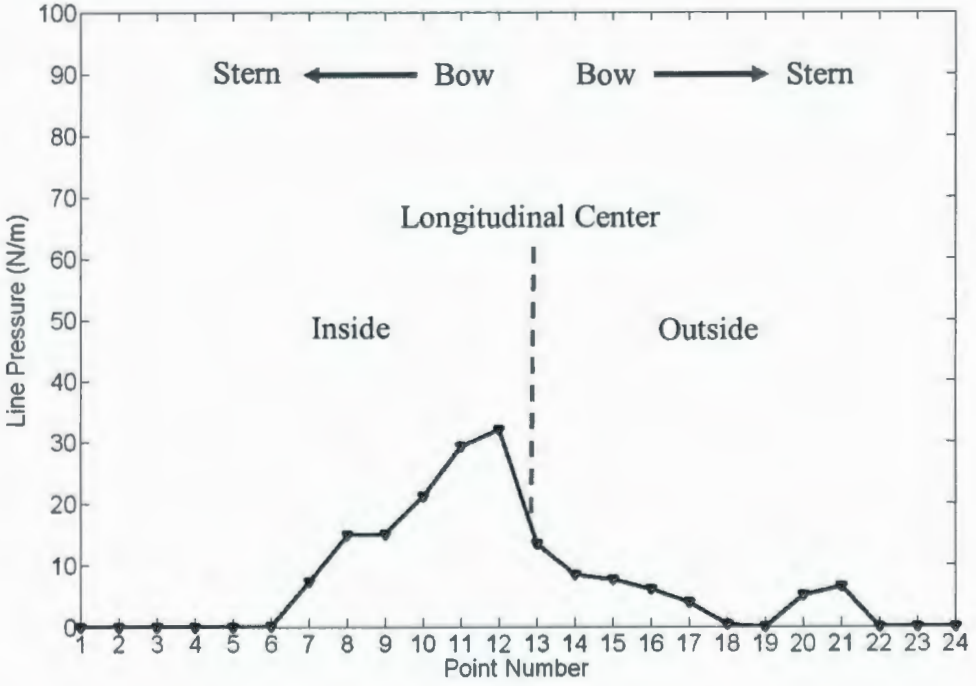

Figure 8.14 Ice pressure distribution for R-Class model 10 m radius turning with 0.25 m/s tangential velocity in 30 mm - 25 kPa ice (Drift angle =0.0°)

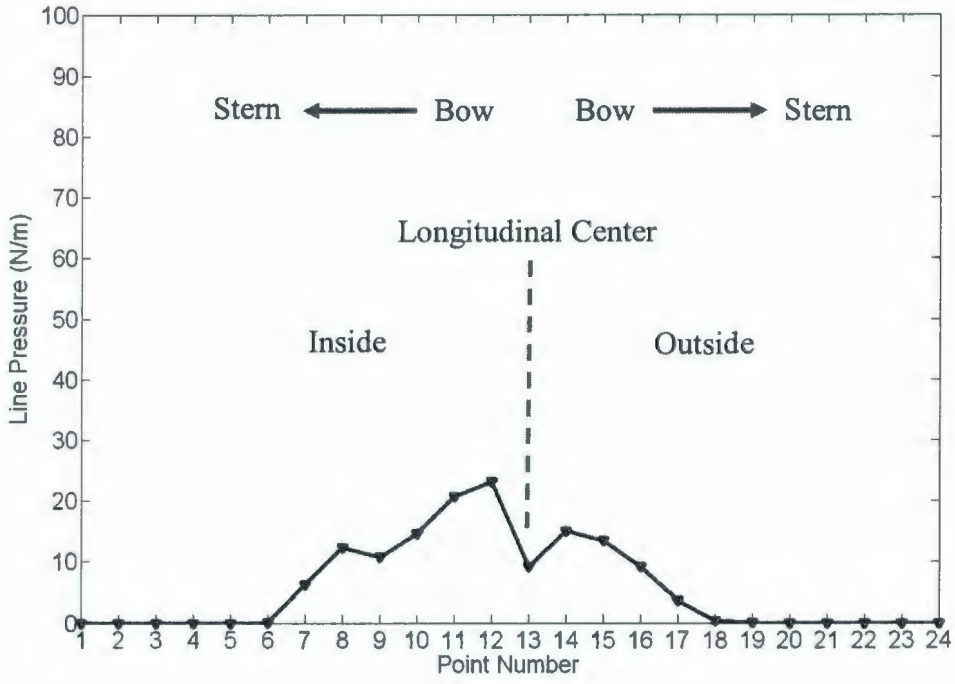

Figure 8.15 Ice pressure distribution for R-Class model 30 m radius turning with 0.25 m/s tangential velocity in 30 mm - 25 kPa ice (Drift angle =0.0°)

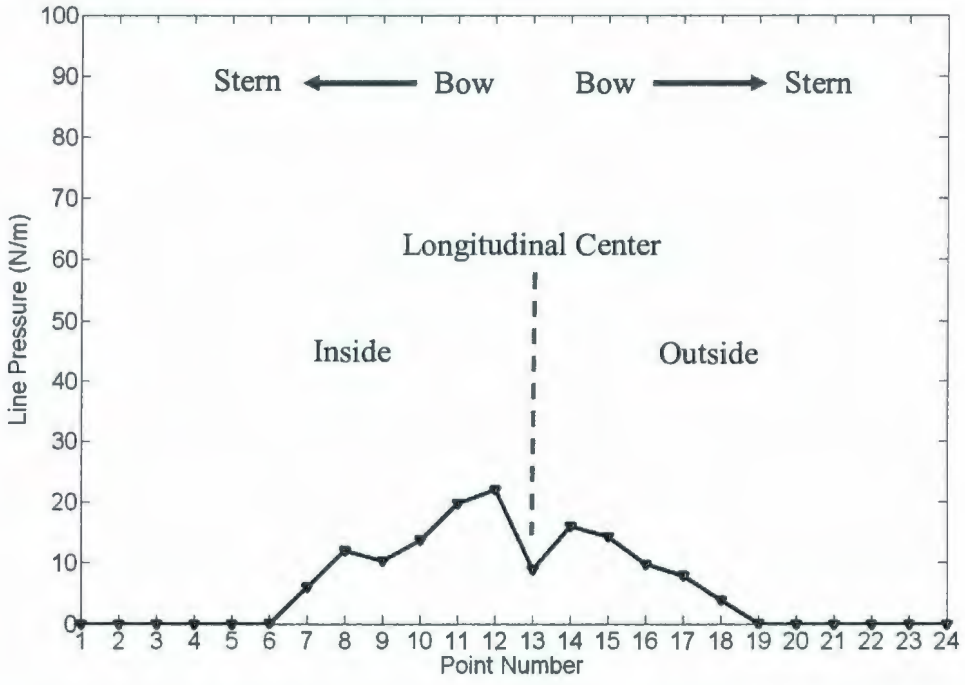

Figure 8.16 Ice pressure distribution for R-Class model 40 m radius turning with 0.25 m/s tangential velocity in 30 mm - 25 kPa ice (Drift angle =0.0°)

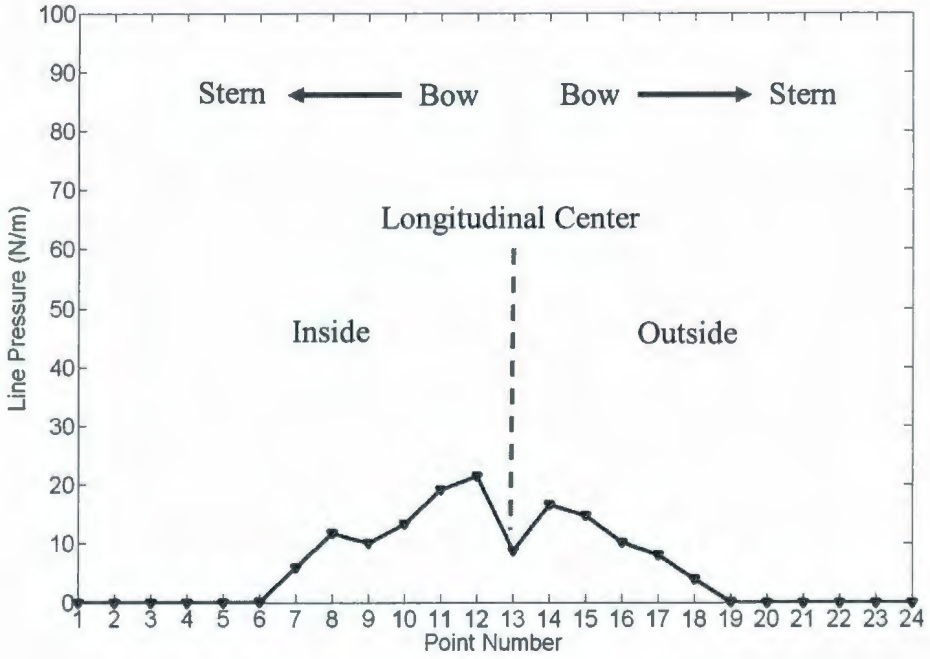

Figure 8.17 Ice pressure distribution for R-Class model 50 m radius turning with 0.25 m/s tangential velocity in 30 mm - 25 kPa ice (Drift angle =0.0°)

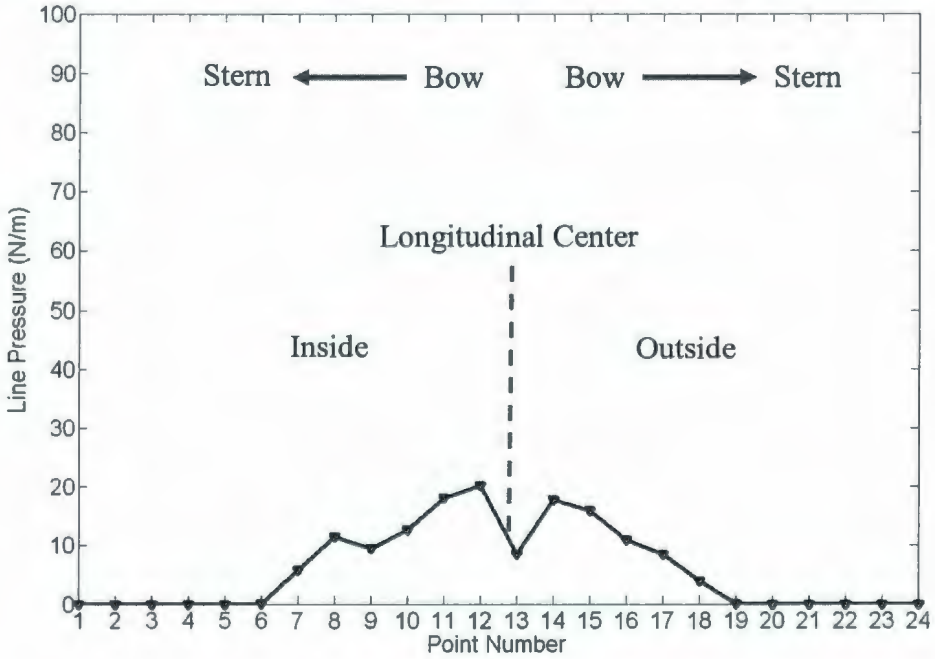

Figure 8.18 Ice pressure distribution for R-Class model 100 m radius turning with 0.25 m/s tangential velocity in 30 mm - 25 kPa ice (Drift angle =0.0°)

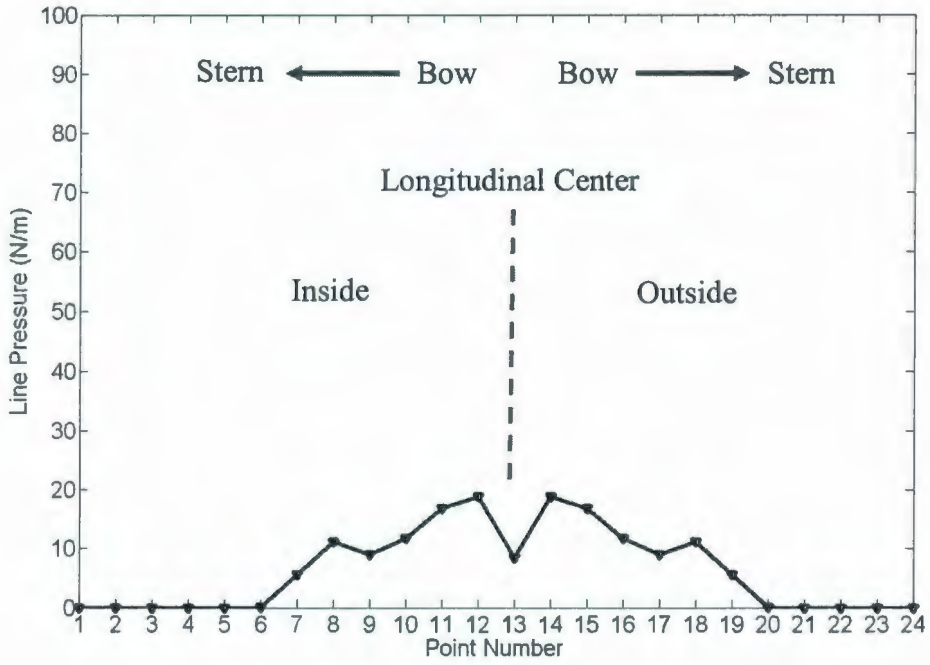

Figure 8.19 Ice pressure distribution for R-Class model in resistance runs with 0.25 m/s velocity in 30 mm - 25 kPa ice (Drift angle =0.0°)

8.5 Summary and Conclusions

8.5.1 Summary

Resistance Run

In the resistance runs, both IHI model simulations and Izumiyama's tests coincidently showed that the high average value distribution located in the bow area and low load acting on the aft-body. Ice load level at the bow increased as the ship speed increased.

Constant Radius Run

In the IHI model simulations, the constant radius runs with –1.0° drift angel and the run with –5.0° drift angle represented the Izumiyama's Test No. 3146 and No. 3147 (Izumiyama et al., 2005) respectively considering that Izumiyama's tests were free-running tests and the drift angles observed during the running. The simulation results and test results coincidently showed that in the turning run, the big ice load acts on the outside of aft-body while very low ice load at the inside. The difference of ice load distribution between advancing run and turning run could be explained by the difference of the ship-ice contact. In the advancing runs, the aft-body of the model doesn't directly contact the ice edge due to the wide channel created at the bow. In the turning model, the outside of the aft-body may also directly contact the ice edge.

Turning Radius Effects

In the constant radius runs with the small radius runs and zero drift angles, the most high ice pressure distributes on the inside of the hull and the stern of the outside also has relative high ice pressure and the mid-body of the hull only had low ice pressure distribution. With the increase of the turning radius, the fore body of the outside of the hull experienced higher ice pressure, while the stern part eventually didn't have ice pressure on it. More high ice pressure distribution was located at the bow of the hull around the longitudinal centre, and the inside bow part experienced higher pressure than the outside bow part. That difference

decreased with the increase of the turning radius until diminishing at the straight going up run.

8.5.2 Conclusions

This Chapter presented the IHI model verification process using NMRI tests carried out by Izumiyama et al (1998, 1999, 2001, 2005). The ice force distributions along the hull waterline during the ship advancing runs and constant radius runs in level ice were studied based on the IHI model simulations and the NMRI tests.

The comparison results between test measurements and simulations showed very good coincident in qualitative and the same mechanical phenomena were observed in tests and simulations, which provides evidence of the correctness and accuracy of the IHI model. The research in this chapter also shows the potentials for detailed calibrations and further refinements of IHI model if the additional experimental data on ice force distributions on the hull are available in the future.

Chapter 9 Parametric Analysis of IHI Model

9.1 Introduction

This chapter presented a parametrical check and analysis of the IHI model. The content in this chapter concentrated on the effects on ice forces on the hull from the ship motions, drift angles, turning radius and ship velocity, from the ice properties, ice thickness, ice strengths and ice-hull interaction frictions and from the ship geometries, waterline length to waterline beam ratio. The ice failure modes, flexural failure, crushing failure and shear failure, for different ice conditions and structural flare angels were studied during the process of the hull breaking the level ice based on the multi-model ice failure model adopted in IHI model. Through the detailed parametrical analysis of the IHI model, the accuracy and reasonability of the developed model was further verified. Based on gained understanding the ice-hull interaction, the insights for further refining IHI model were obtained. Terry Fox Icebreaker was selected for the simulations presented in this chapter.

9.2 Ice Mechanical Properties

9.2.1 Ice Failure Mode

In IHI model, a multi-failure model, considering bending failure, shear failure and crushing failure, was adopted to represent the ice failures along the hull waterline during the ship navigating in level ice. The parametric checks of the multi-failure model were provided in this section.

9.2.1.1 Bending Failure with Initial Crushing Failure

Using IHI model, the hull's critical flare angle, at which the horizontal force due to flexural bending failure is equal to the maximum crushing force endured by each ice cusp, was calculated for different ice-hull frictional coefficients, the ship velocities and ice thickness. Correspondingly, the hull's critical flare angles, at which the ice cusp is blocked due the ice-hull frictional forces, were also calculated.

Figure 9.1 shows the flare angles under the different model ship velocities and different ice-hull frictional coefficients in the 35 mm – 31.5 kPa ice. Figure 9.2 shows the flare angles under different ice-hull frictional coefficients and 0.3 m/s model ship velocity in the 31.5 kPa ice with different ice thickness.

The calculation results showed that the flare angles are all in excess of 80 degrees. The higher ice-hull friction, higher ship velocity and thicker ice means the smaller critical flare angles that caused jamming phenomena more easily happen. That can be explained as: with increase of the hull breaking ice velocity, the ice cusp size decreases and the maximum crushing force for each cusp also decreases. Therefore, the critical flare angle, at which the flexural bending failure caused horizontal forces is equal to the maximum crushing force endured by each ice cusp, certainly decreases; the ice flexural bending failure is proportional to the ice thickness square and the crushing force is linearly proportional to the ice thickness. Therefore, with increase of the ice thickness, the critical flare angle also decreases; the ice-hull frictional force prevents the broken ice to be pushed down and balances some part of the vertical force acting on the ice. With increase of the ice-hull frictional coefficient, more part of the force to bend the level was balanced and it is more difficult to cause a bending failure, which means the case that only crushing failure happens more easily. Therefore, the critical flare angles, at which only the crushing failure happens without the bending failure, decreases for the increasing ice-hull frictional coefficient.

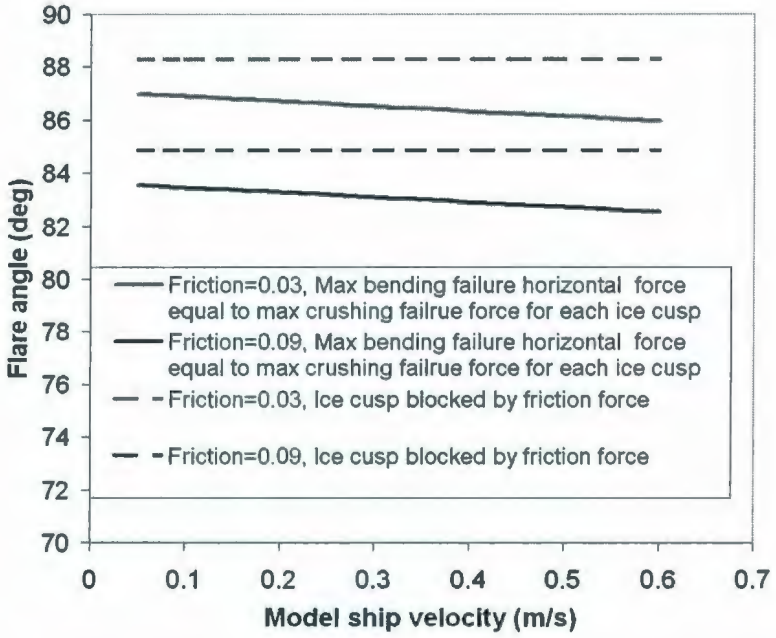

Figure 9.1 The minimum flare angles at which the ice cusp is blocked due to frictional force or maximum bending failure horizontal force equal to maximum crushing failure force for each cusp in the 35 mm – 31.5 kPa ice

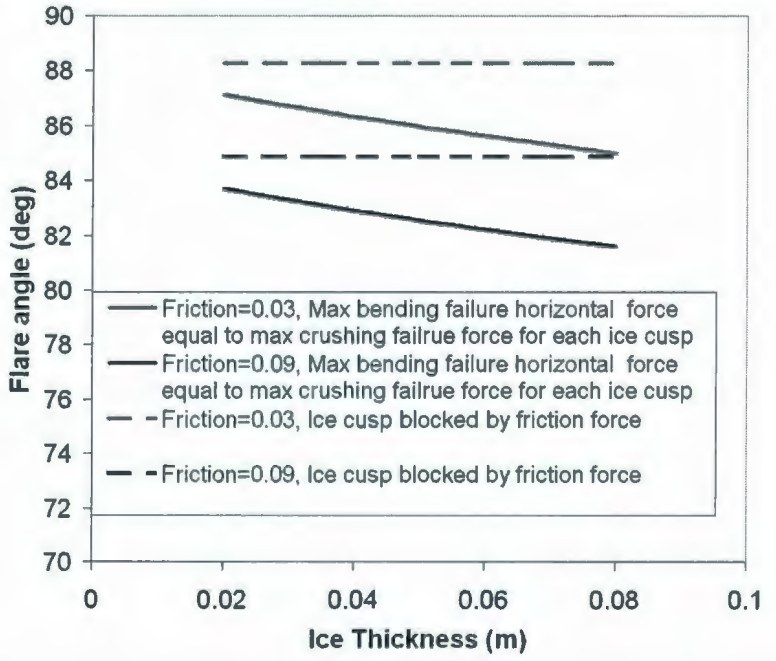

Figure 9.2 The minimum flare angles at which the ice cusp is blocked due to frictional force or maximum bending failure horizontal force equal to maximum crushing failure force for each cusp at 0.3 m/s model velocity and in 31.5 kPa ice

9.2.1.2 Shearing Failure with Initial Crushing Failure

Figure 9.3 shows the calculated critical flare angles, at which the ice shear failure happens before the bending failure, for two kinds of ice. For each case, the strength ratios between crushing failure strength, bending failure strength and shear failure strength are same. The calculation results showed that with increase of the ice thickness, the critical flare angle decreases. For the ice with the same ratio of ice strengths, the calculated critical flare angles also keep same, which can be explained the ice failure at the failure mode with the minimum ice failure force and the same ratio of ice strength means the flexural bending failure force and shear failure force increase or decrease at the same ratio.

Figure 9.4 shows the critical flare angles for the ice with 31.5 kPa flexural strength, 130 kPa crushing strength and different shear strengths. The calculation results show the smaller critical flare angle for the weaker shear strength ice and the shear failure more easily happens before the bending failure.

Figure 9.5 presents the ice that may only exist in theories, which shear strength is very weak compared the flexural bending strength and crushing failure strength. For the natural ice accounted by ship, its strength ratio between crushing strength, flexural bending strength and shear strength only changes within a certain range.

The calculation results showed that besides the shear mode I, on which the crushing surface completely penetrates through the whole ice profile, and the shear failure mode II as shown in Figure 3.16, on which the crushing surface doesn't penetrate through the whole ice profile as shown in Figure 3.16, may happen for the structures with the different flare angles. When the flare angle of the hull is above angle curve of the shear mode I or between upper bound angle curve of the shear mode II and lower bound angle curve of the shear mode II, the shear failure happens before the bending failure.

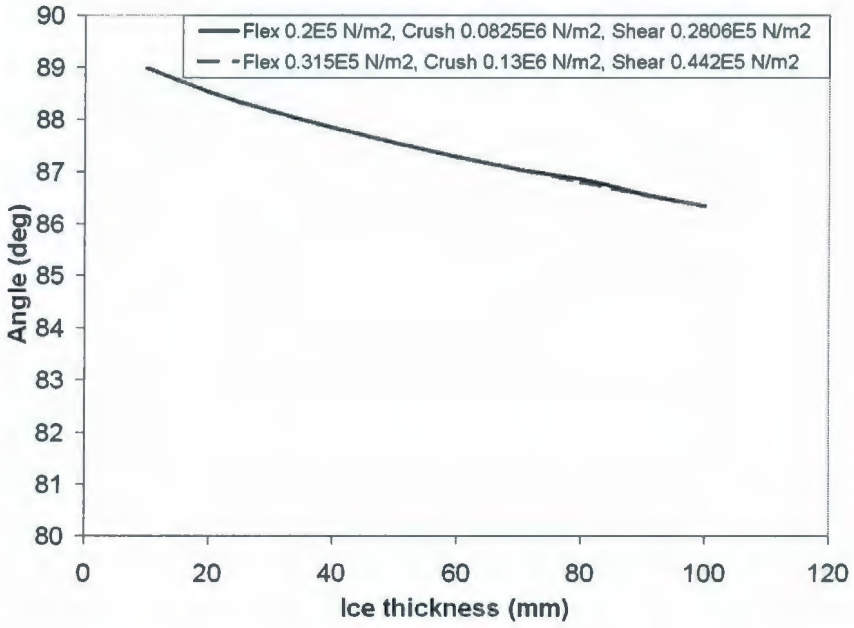

Figure 9.3 Flare angles at which ice is broken by shear failure before bending failure in R-Class model test ice, 20 kPa flexural, 82.5 kPa crushing and 28.1 kPa shearing strength, and Terry Fox model test ice, 31.5 kPa flexural, 130 kPa crushing and 44.2 kPa shearing strength

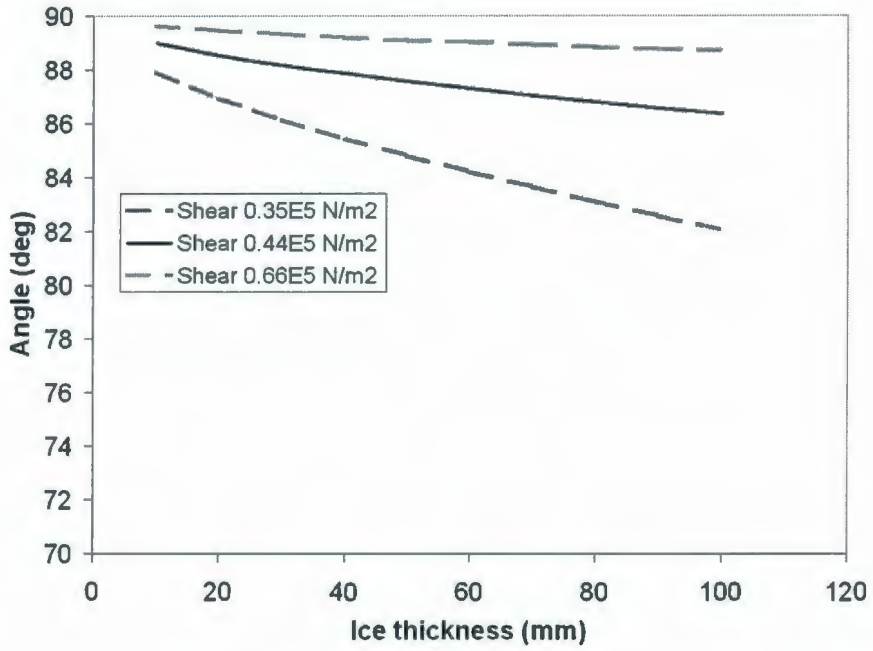

Figure 9.4 Flare angles at which ice is broken by shear failure before bending failure for the ice with different shear, 31.5 kPa flexural and 130 kPa crushing strength

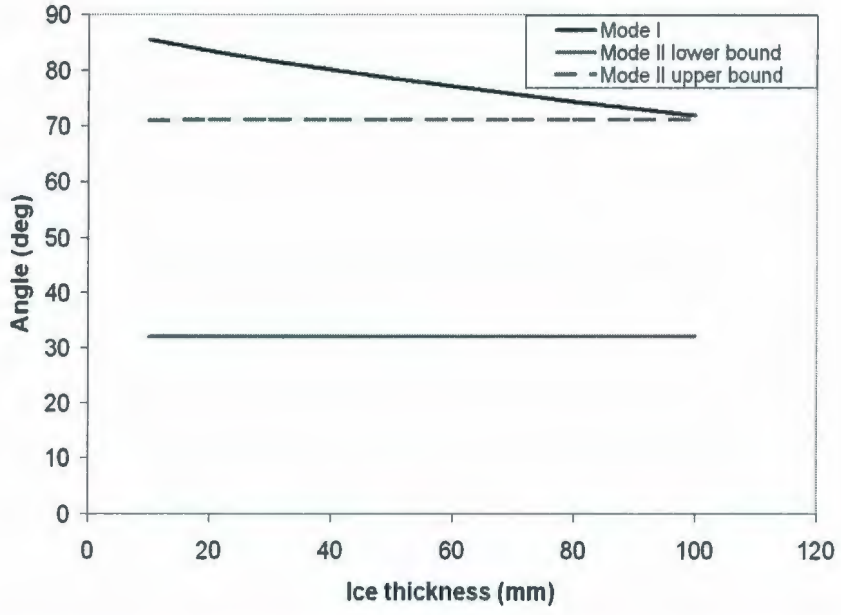

Figure 9.5 Flare angles at which ice is broken by shear failure before bending failure for the ice with 31.5 kPa flexural, 130 kPa crush and 22.1 kPa shear strength

*9.2.2*Ice Mechanical Strength

Based on the IHI model simulations, the effects from ice mechanical strengths, crushing strength, bending strength and shear strength, are studied in this section.

Figure 9.6 and 9.7 respectively show Terry Fox model ice resistance force vs. ice flexural strength curve in resistance runs and yaw moment vs. ice flexural strength curve in its 10 m constant radius runs with the model velocity, 0.3 m/s, and in 35 mm thick level ice and pre-sawn ice. In the figures, the ice crushing strength changes with the flexural strength at the same ratio as the 31.5 kPa flexural and 130 kPa crushing strength ice

Figure 9.6 and 9.7 show that the pre-sawn ice loads on the hull is independent to the ice strength. The ice load in level ice increases with the ice strength increases due to the increase of the ice breaking force component. With increase of the crushing strength and constant bending strength, the global ice force decreases a little, because the amount of initial crushing before flexural failure also decreases.

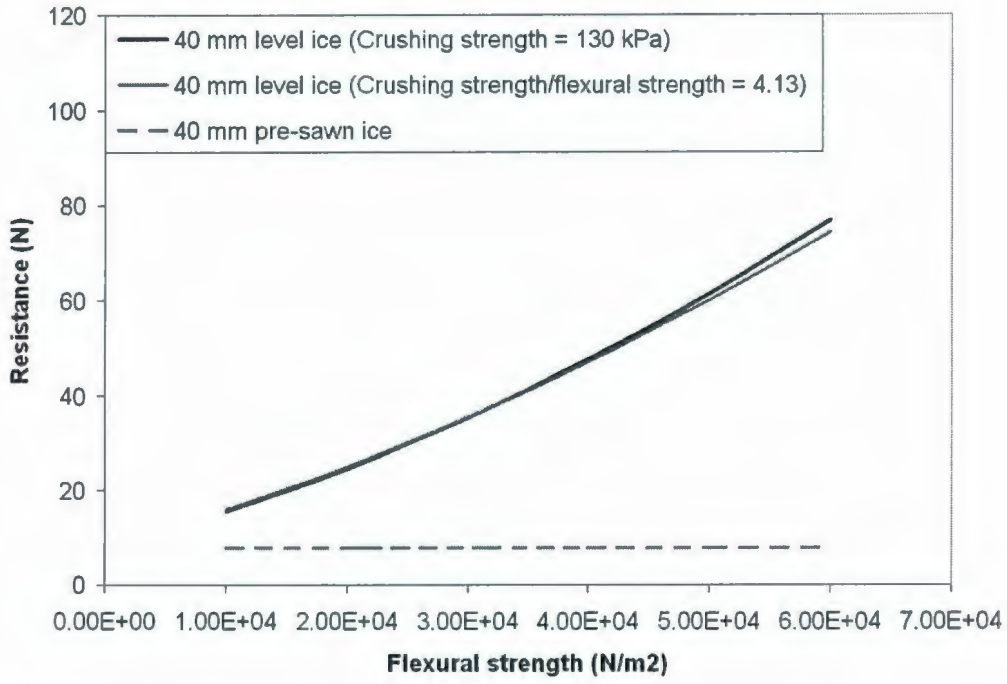

Figure 9.6 Terry Fox model ice resistance vs. ice flexural strength with 0.3 m/s model velocity and in 40 mm thick ice

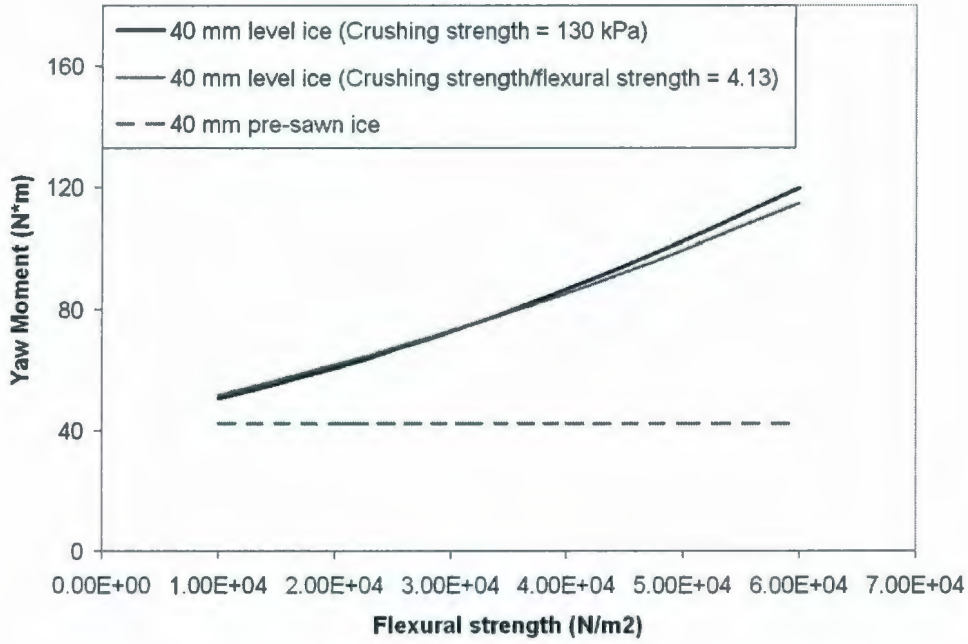

Figure 9.7 Terry Fox model ice yaw moment vs. ice flexural strength in the 10 m constant radius turning with 0.3 m/s model velocity and in 40 mm thick ice

*9.2.3*Ice Thickness

Figures 9.8 and 9.9 respectively show Terry Fox Icebreaker resistance vs. ice thickness curve in the resistance runs and yaw moment vs. ice thickness curve with 0.3 m/s model velocity and in 40 mm thick level ice and pre-sawn ice.

The figures showed that the pre-sawn ice force increases nearly linearly with the increase of the ice thickness. That can be basically explained that in the pre-sawn ice condition, no ice breaking forces are generated and the buoyancy force and clearing force are directly dependent to the amount of the ice that is submerged by the hull and covering on the water surface of the hull in unit time. And the increase of ice thickness approximately linearly increases that ice amount. Besides the ice force components in pre-sawn ice, buoyancy force and clearing force, the breaking ice force is also included in the ice force in level ice condition. As we know, the breaking force increases with nearly square of the ice thickness. Increasing the ice mechanical strength directly increases the minimum ice load to fail the ice and generate the ice cusp in each ice breaking cycle and finally causes the average force on the hull.

Figure 9.8 and 9.9 also showed the same mechanical phenomena for ice forces on the hull: The ice force increases more in level ice than that in the pre-sawn ice

while increasing the ice thickness. The hardened ice strength more quickens that ice force increase due to ice thickness process.

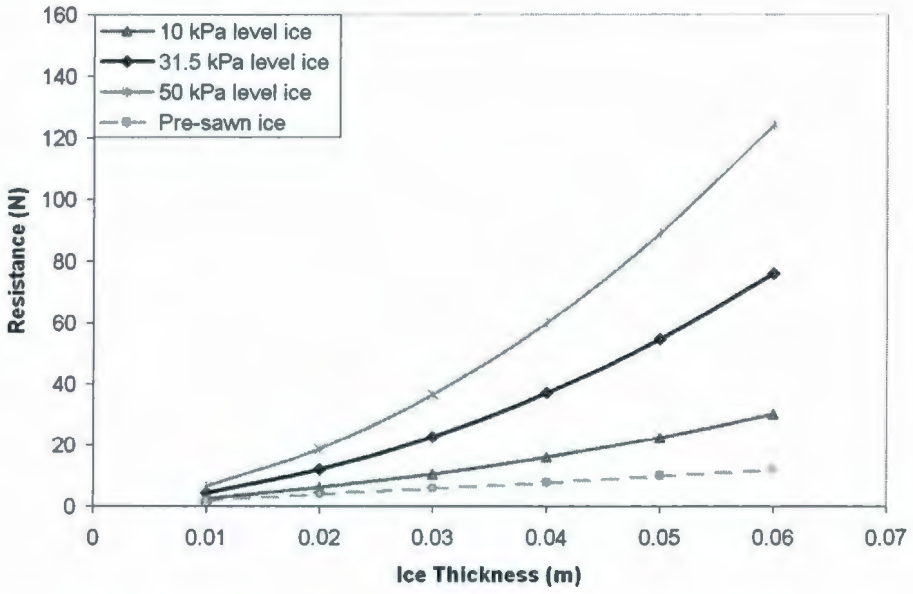

Figure 9.8 Terry Fox model ice resistance vs. ice thickness in advancing runs with 0.3 m/s ship velocity

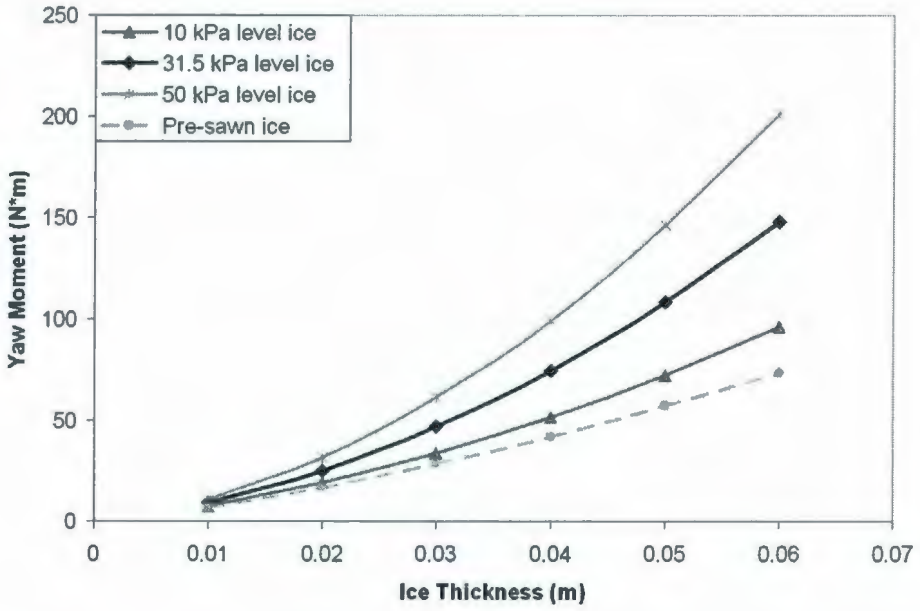

Figure 9.9 Terry Fox model ice yaw moment vs. ice thickness in 10 m constant radius runs with 0.3 m/s tangential velocity

*9.2.4*Ice-hull friction

In the IHI model, the dynamic frictional forces between hull and the ice sheets are considered and their effects to the final global forces on the hull are calculated. In this section, some discussion on that friction effects is given based on the IHI model simulations of Terry Fox model straight going and constant radius turning in level ice sheet.

According to the model tests and full-scale experiments, the ice-hull friction coefficient is usually between 0.01 and 0.2 (Williams M. et al., 1987, Spencer D, et al., 2002, Jones J., 2005). Therefore, the ice resistances in straight-up runs and yaw moments in 10 m constant radius runs for Terry Fox Icebreaker with 0.3 m/s tangential velocity in 40 mm – 31.5 kPa ice are simulated using the IHI model with the frictional coefficient from 0.0 to 0.2. Figure 9.10 shows the simulation results. Besides in the level ice, the ice forces on the hull in the pre-sawn ice are also provided in the figure.

From Figure 9.10, we can see that for Terry Fox Icebreaker with 0.3 m/s tangential velocity in the 40 mm thick and 31.5 kPa ice, the effect of the friction coefficient from 0.0 to 0.1, the total ice yaw moment in 10 m constant radius runs and 50 m constant radius runs increased the global ice loads on the hull about 10%. The

friction coefficient from 0.1 to 0.2 also increases the total ice force about within 15%.

Based on the adopted idealization and simplification of present IHI model, the friction coefficients between 0.0 and 0.2 didn't show significant effects on the global ice yaw moments on the hull. The comparison shows that the frictional force calculation in present IHI model is reasonable and the simulation results are also consistent with the conclusions from the studies by Molyneux et al., in which they pointed out that "the experimental results showed that there would be a considerable improvement in resistance due to the reduced friction coefficient. This improvement in resistance is not translated into an improvement in manoeuvrability" (Molyneux et al., 1998).

It should be noted that the present IHI model doesn't accurately model the ice jamming at the shoulder. As discussed in previous section 7.22, the ice jamming at the hull shoulder may affect the ice resistance through the ice-hull frictions. Therefore, the present model may to some extent underestimate the ice-hull friction effects, especially to ice resistance. The future refined IHI model will address that problem through considering ice jamming.

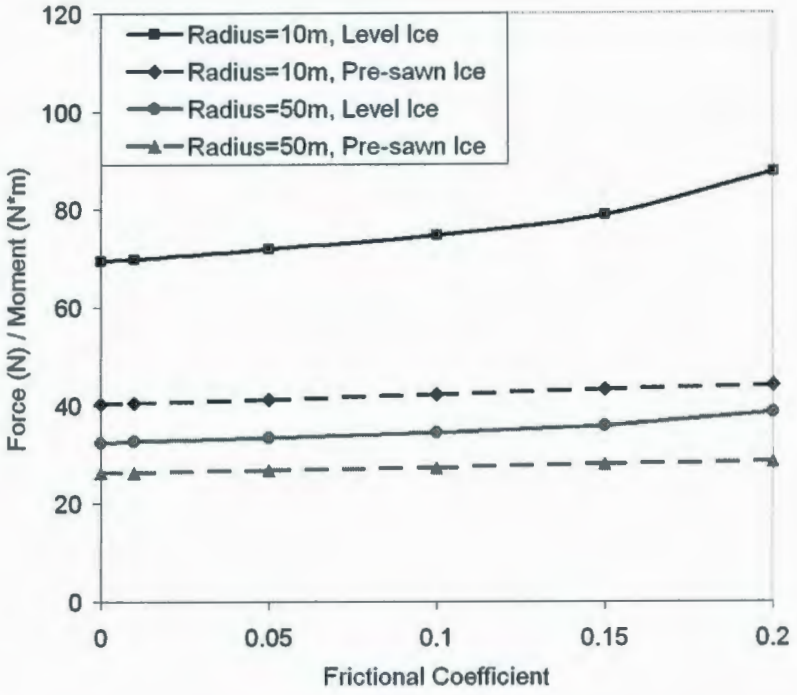

Figure 9.10 Ice Yaw moments in 10 and 50 m constant radius runs for Terry Fox Model with 0.3 m/s tangential velocity in the 40 mm – 31.5 kPa ice

9.3 Ship Motions

9.3.1 Drift Angle and Turning Radius

9.3.1.1 Effects on Ice-Hull Contact

The ice-hull contact area and position directly determines the ice force distribution along the waterline. The global ice forces on the hull are equal to the vectorial integrations of ice force distribution. Therefore, the ice-hull contact condition sensitively affects the global ice loads on the hull. In the simulations presented in angle remains zero. The pivot point is fixed at the mass centre of the ship.

Figures 9.11, 9.12 and 9.13 present the IHI model simulations of Terry Fox Icebreaker in the constant radius runs with 5, 10 and 50 m in the 40 mm - 31.5 kPa level ice respectively. The simulations show that the stern and aft-hull also directly contacts the unbroken ice in 5 m turn while only the bow part directly does so in the 10 and 50 m turns.

During the ship manoeuvring process, the steady turning motion with zero drift angle is an idealized specific manoeuvre that is only realized in some captive model tests like PMM model ship tests. The drift angles are inevitable in the free running tests and full-scale trials. The drift angle during the ship turning also directly affects the ice-hull contact condition and global ice forces on the hull. Therefore, that is worthwhile to examine the effects of the drift angle during the ship navigation. Figure 9.14, 9.15 and 9.16 respectively show the simulations of Terry Fox Icebreaker in the 10 m constant radius runs with -3°, -10° and 10° drift angles in the 40 mm – 31.5 kPa level ice.

Figure 9.12 shows the ship contacts the intact ice edge only at the bow when turning with a zero drift angle and 10 m radius. When the ship turns with a -3.0 deg drift angle, the ship also contacts the intact ice edge at the stern as shown in figure 9.14. It should be mentioned that, the contact between stern and the intact ice edge is intermittent in nature due to the straight waterline and curve ice edge.

When the ship turns with a -10° drift angle, the entire outside of the hull directly contacts the intact ice edge including the bow, mid-body and the stern as shown in Figure 9.5. When the ship turns with a 10° drift angle, the entire inside of the hull direct contact the intact ice edge as shown in Figure 9.16.

Obviously, the drift angle influences the ice-hull contact area and location that determine the ice force distribution on the hull; therefore, the drift angle plays an important role in determining the global ice loads on the hull.

It should be noted that, among the above manoeuvres, the manoeuvres with drift angle +10° and 0° in the ship constant radius runs are the idealized ship motions and only realized in theories or in some captive model ship tests like PMM model tests. In the free-running tests and full-scale ship trials, such a ship steady motion case is unrealistic under the condition of ship propeller thrust and rudder moment. The detailed discussion on it will be given in the following section.

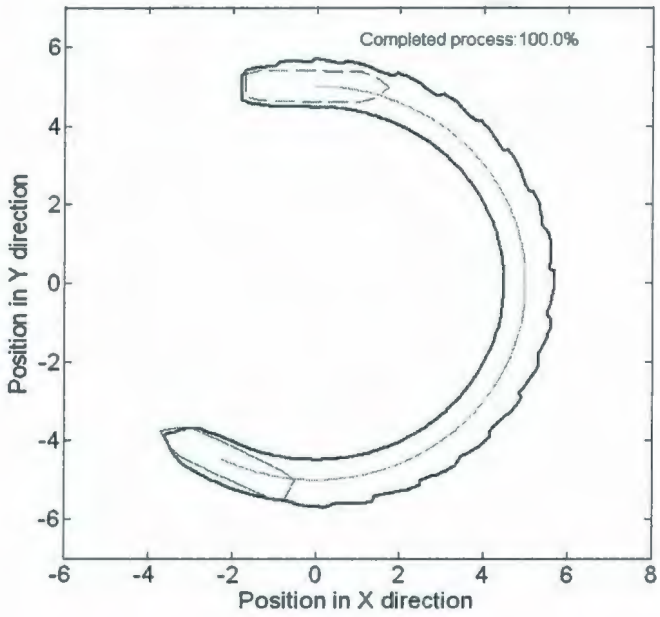

Figure 9.11 Terry Fox model 5 m radius turning with 0.3 m/s tangential velocity and zero drift angle

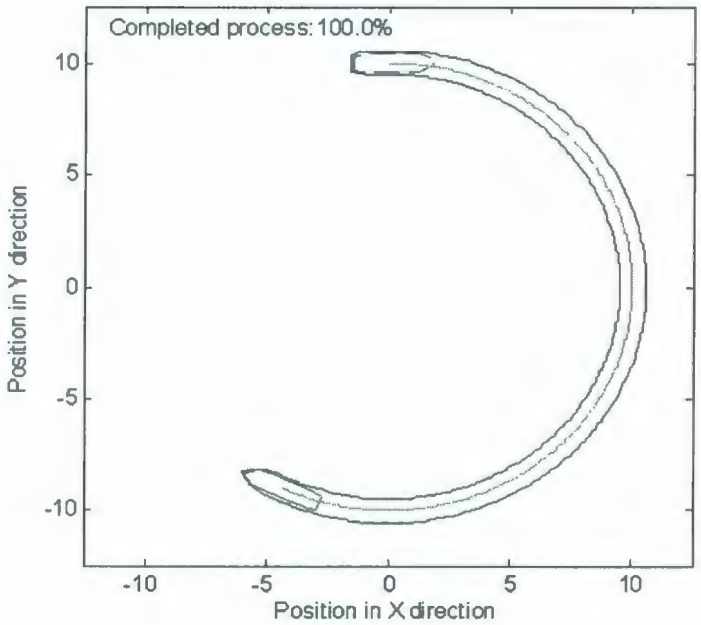

Figure 9.12 Terry Fox model 10 m radius turning with 0.3 m/s tangential velocity and zero drift angle

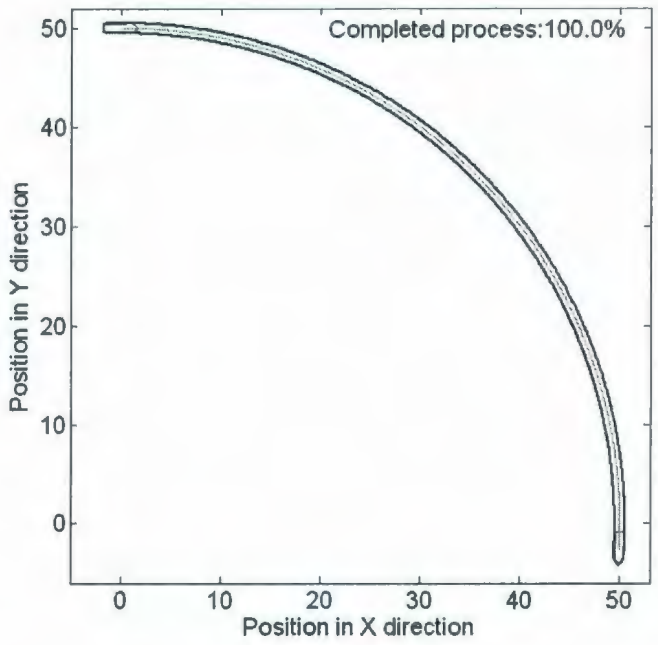

Figure 9.13 Terry Fox model 50 m radius turning with 0.3 m/s tangential velocity and zero drift angle

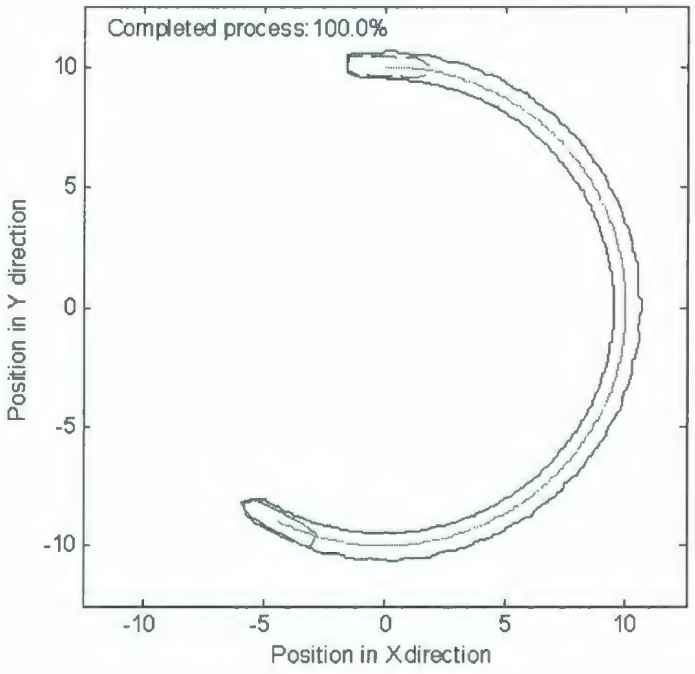

Figure 9.14 Terry Fox model 10 m radius turning with 0.3 m/s tangential velocity and –3.0° drift angle

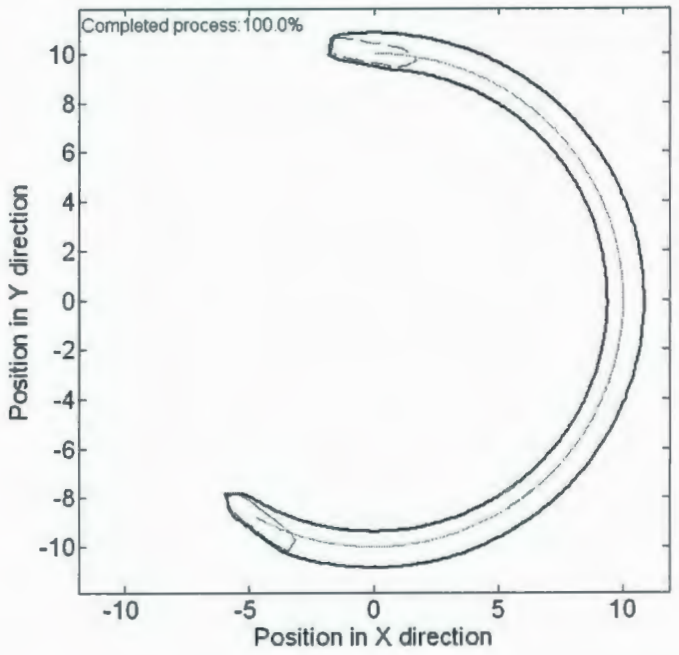

Figure 9.15 Terry Fox model 10 m radius turning with 0.3 m/s tangential velocity and –10° drift angle

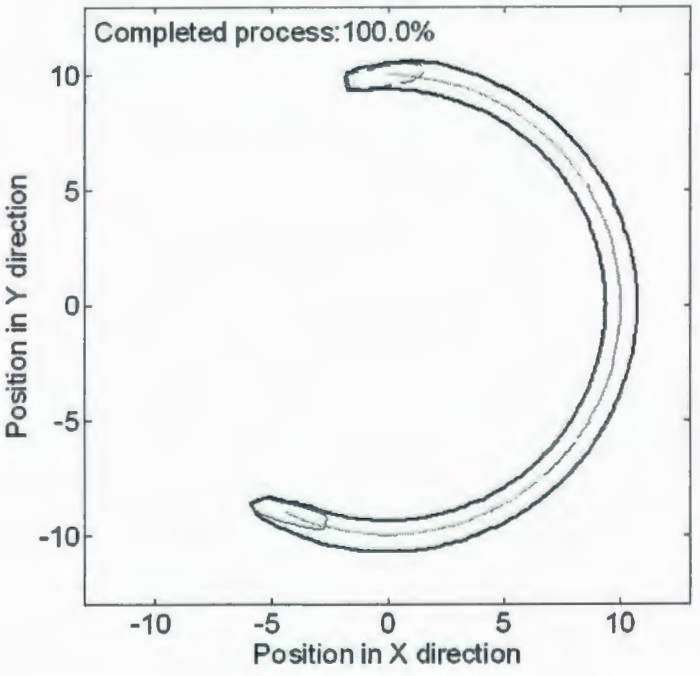

Figure 9.16 Terry Fox model 10 m radius turning with 0.3 m/s tangential velocity and +10° drift angle

9.3.1.2 Effects on Channel Width

Following the above discussion of Section 9.3.1.1, the drift angle directly affecting the ice-hull contact during the ship turning process, this section focuses on the channel width left by the ship for the different drift angles and turning radius runs, which is of important value for the icebreaker escort.

Figure 9.17 shows the channel widths vs. drift angles for Terry Fox Icebreaker 5, 10 and 50 m radius turning runs and straight going up run in the 40 mm - 31.5 kPa level ice. The ship's tangential velocity is prescribed as 0.3 m/s and the pivot point is fixed at the mass centre of the ship.

From simulation results, it can be seen that, in general, the channel width vs. drift angle curve shows a "V" shape. Obviously, for the straight going up run, the channel width vs. drift angle shows a standard "V" shape with the top end at the Y-axis. The curve for 50 m radius run is nearly superposition. With the decrease of the turning radius, the shape of "V" is more obviously affected by the stern's contacting ice condition at the different drift angles.

The simulation results show that, for constant radius turns, the drift angle that causes the smallest channel width (Tip end point) may be nonzero as shown in figure 9.17.

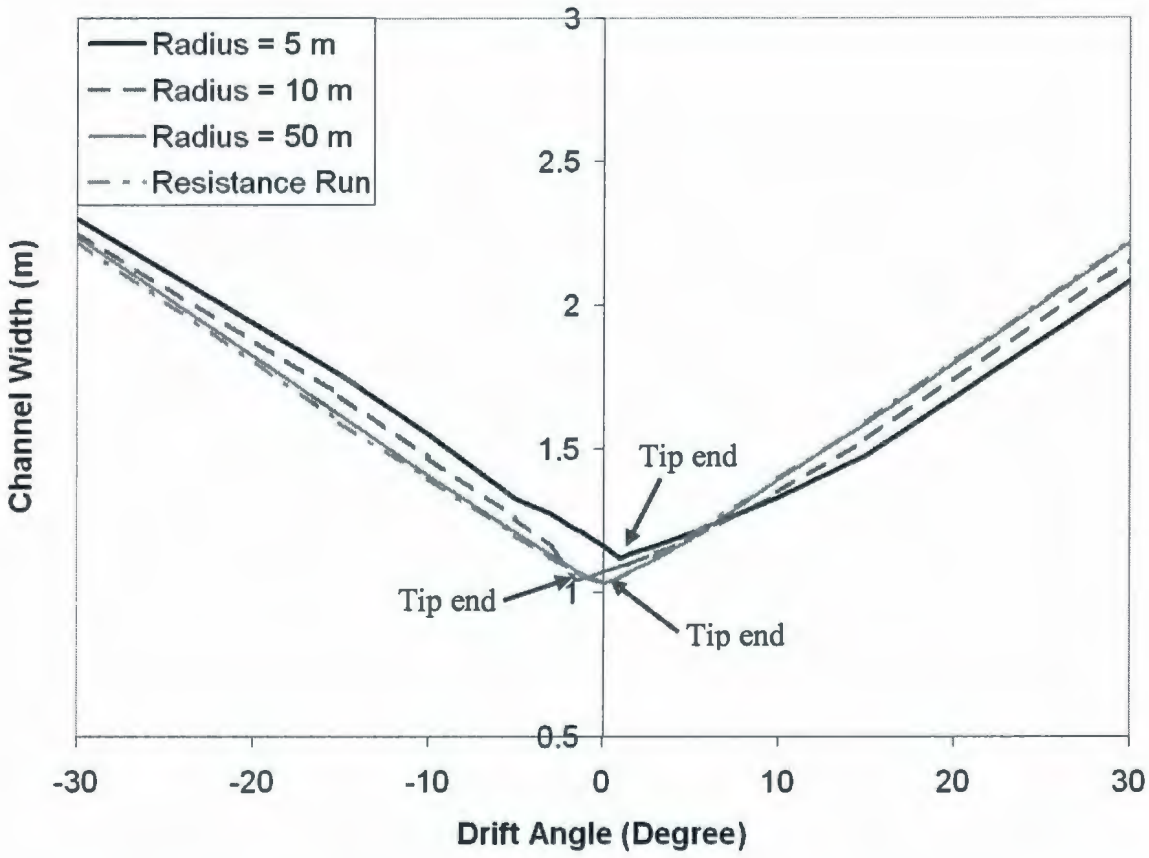

Figure 9.17 The channel width vs. drift angle for Terry Fox model 5, 10 and 50 m radius runs and resistance run with 0.3 m/s tangential velocity

The drift angles associated with the smallest channel widths (Tip end point in figure 9.17) for different turning radii were calculated and re-plotted in Figure 9.18. The two parts of the curve in Figure 9.18 indicate two different breaking processes dependent of ship geometry and the ice properties. In Part I, the stern always breaks the ice with negative drift angle. In Part II, the drift angle decreases with the increase of turning radius when the stern contacts the unbroken ice. Minimum channel width corresponds nearly to zero drift angle for a large radius

indicating that even a very small drift angle will cause the stern to break the ice when a ship turns with a large radius.

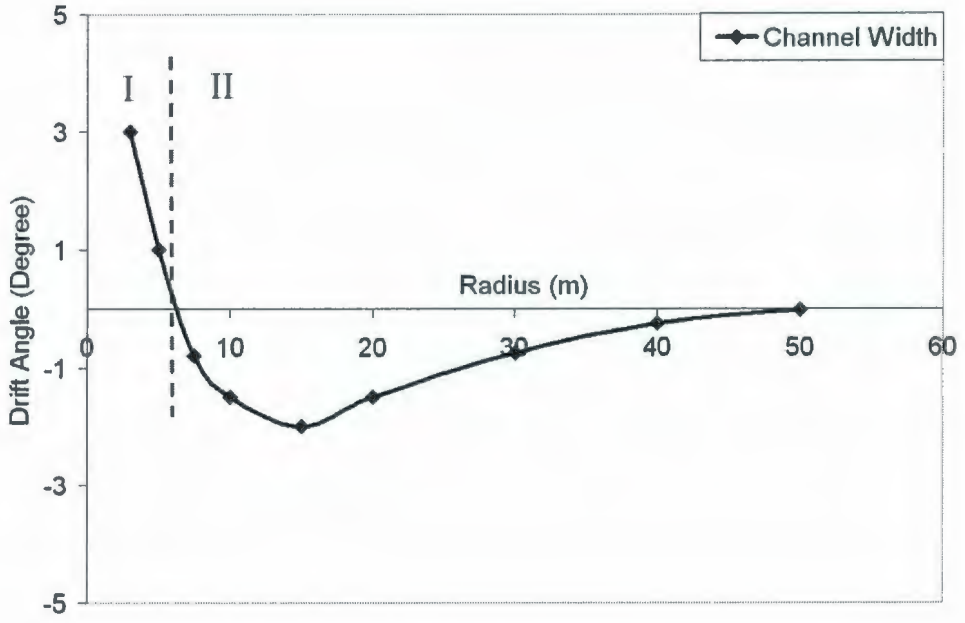

Figure 9.18 Drift angles causing the narrowest channel widths in different radius runs

9.3.1.3 Effects to Ice Forces

As analyzed in Section 9.1.1 and 9.1.2, the drift angle and turning radius directly affects the ice hull interaction area, which determines the ice force distribution around waterline and finally determines the global ice forces on the hull. Therefore, it is worthwhile to examine the effect of the drift angle and radius to the

ice loads on the hull, which are the direct factors to affects the ship's manoeuvrability in ice.

Figure 9.19 and figure 9.20 respectively show the IHI model calculated yaw moments and sway forces during Terry Fox Icebreaker 10 m radius runs with 0.3 m/s tangential velocity, different drift angles from –30 deg to 30 deg and in 40 mm - 31.5 kPa ice. As comparison, the ice forces in the pre-sawn ice are also presented in the figures.

From the figure 9.19, it seems that smallest yaw moment point (zero yaw moment) is at the drift angle, 10°. In fact, that ship motion case is only for theoretical analysis, because in reality the sway force is more than 400 N at the 20° drift angle, as shown in Figure 9.20, which is beyond the ship's turning ability under the rudder moment and propeller thrust.

Figure 9.21 shows the ice force distribution along the waterline of the hull in –3.5°, 0.0° and 20°. As mentioned in chapter 3, the yaw moment and forces are calculated in the moving coordinates, which origin point is always fixed at the mass centre of the hull. In the 20° drift angle run, the higher ice force distribution moves to the inside of the turning ship around the hull mass centre, which sensitively increases the sway force while the yaw moment contrarily decreases compared to the zero drift angle run.

In fact, the increase of the drift angle means that more of the hull side including the stern will directly contact the unbroken ice and this changes the ice distribution on the whole hull. For the free-running ship, its turning pivot point may leave the gravity centre further and the assumption that the pivot point fixed at the ship mass centre will be inappropriate.

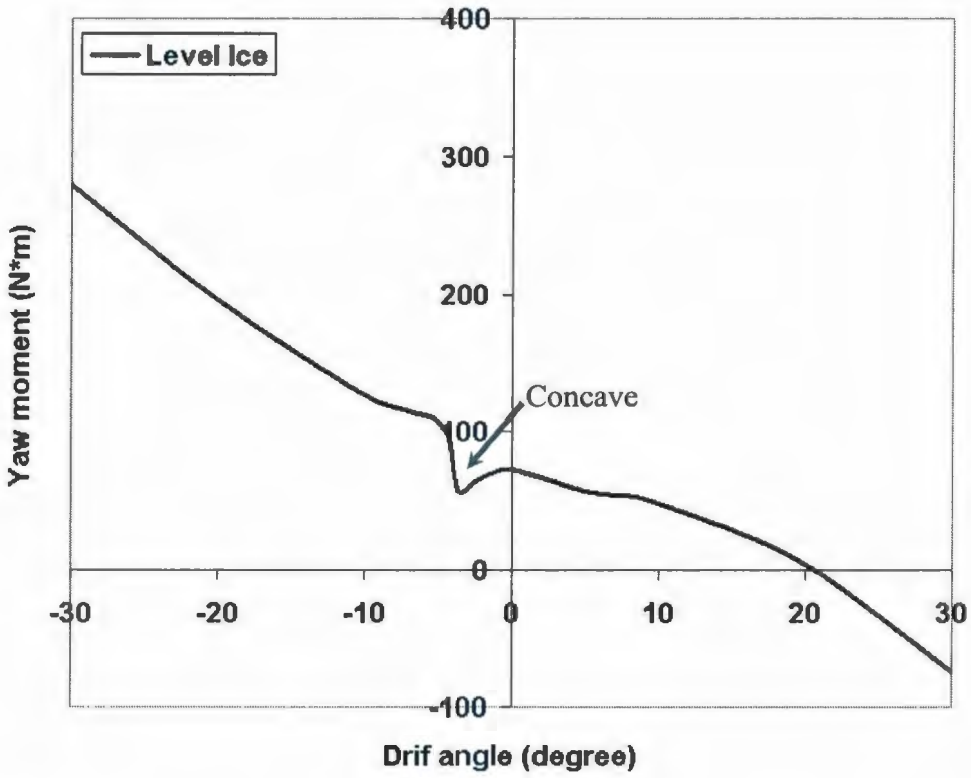

Figure 9.19 Yaw moment vs. drift angle for Terry Fox Icebreaker 10 m radius turning with 0.3 m/s tangential velocity in 40 mm - 31.5 kPa ice

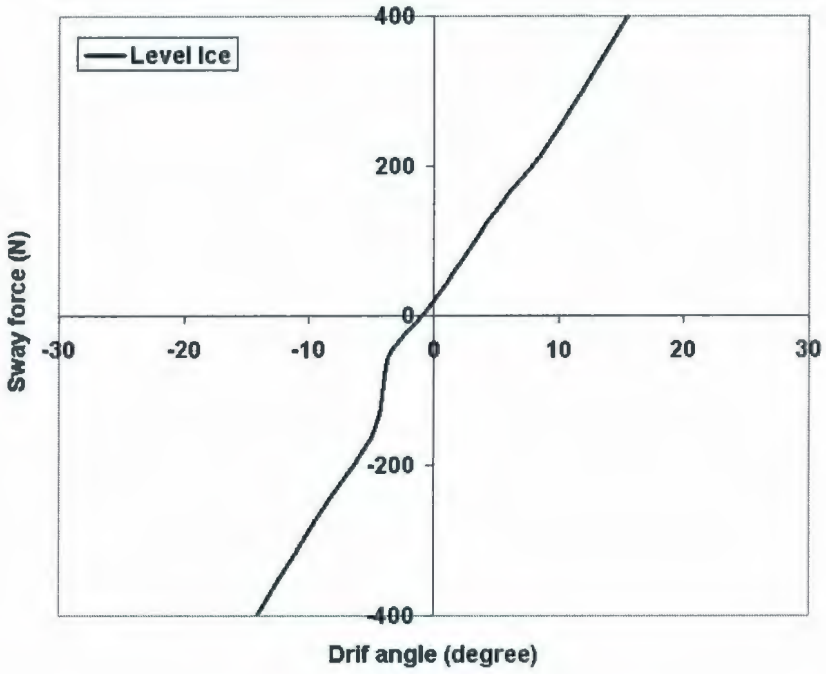

Figure 9.20 Sway force vs. drift angle for Terry Fox model 10 m radius turning with 0.3 m/s tangential velocity in 40 mm – 31.5 kPa ice

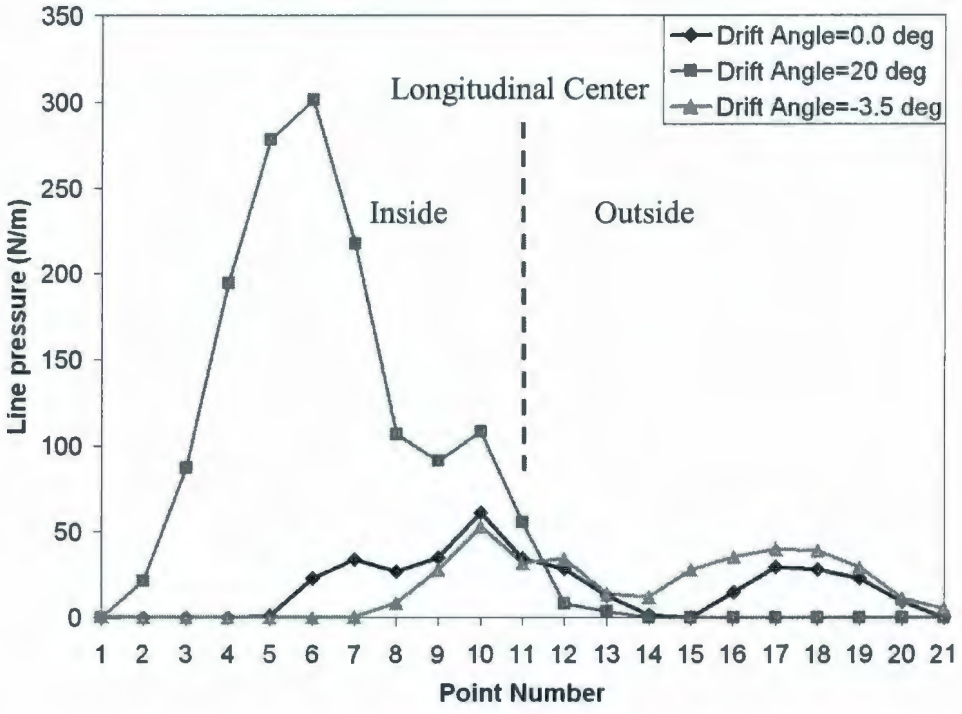

Figure 9.21 Ice pressure distribution for Terry Fox model 10 m radius turning with 0.3 m/s tangential velocity in 40 mm - 31.5 kPa ice

Figure 9.22 shows yaw moment vs. drift angle curves in the turning runs with the constant radius, 5, 10, 20 and 50 m, and the straight going run. Figure 9.23 shows the corresponding sway force vs. drift angle curves.

From the simulation results, it can be seen that the yaw moment increases with the increase of the drift angle. In the straight going run and large radius manoeuvres, the curves are nearly linear. The yaw moment increases with decrease of the radius in the constant radius runs. For the 5 and 10 m radius turns, the yaw moment vs. drift angle curves show the obvious fluctuations around the zero drift angle areas, which is caused by the stern's beginning to directly contact the unbroken ice sheet. For the large radius turning runs and straight going run, a small drift angle will cause the aft-body of the hull to directly contact the ice, which obscures the drift angle trend. The corresponding sway force vs. drift angle curves in figure 9.23 also shows the similar phenomena as in Figure 9.24. The analysis of those phenomena is the same as the discussion for the yaw moment.

Obviously, the ice-hull contact is the direct factor to determine the final global ice forces on the ship. That also shows the IHI model's accuracy and reasonability in the ice force calculation for ship's any manoeuvres in ice: Calculating the ice forces on the hull based on the ice-hull contact area.

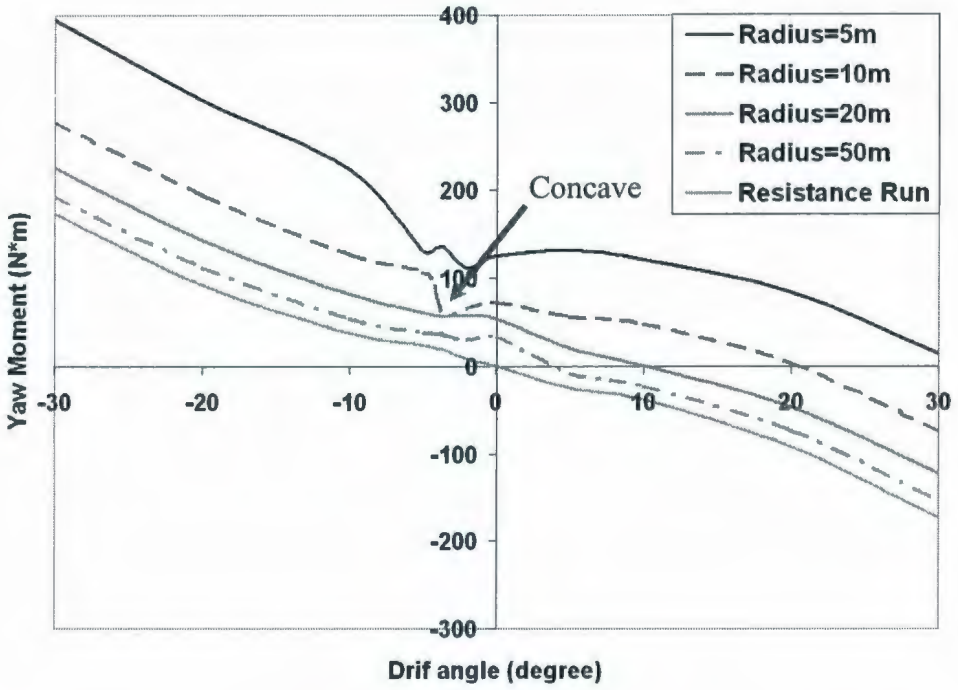

Figure 9.22 Yaw moment vs. drift angle for Terry Fox model different radius turning with 0.3 m/s tangential velocity in 40 mm - 31.5 kPa ice

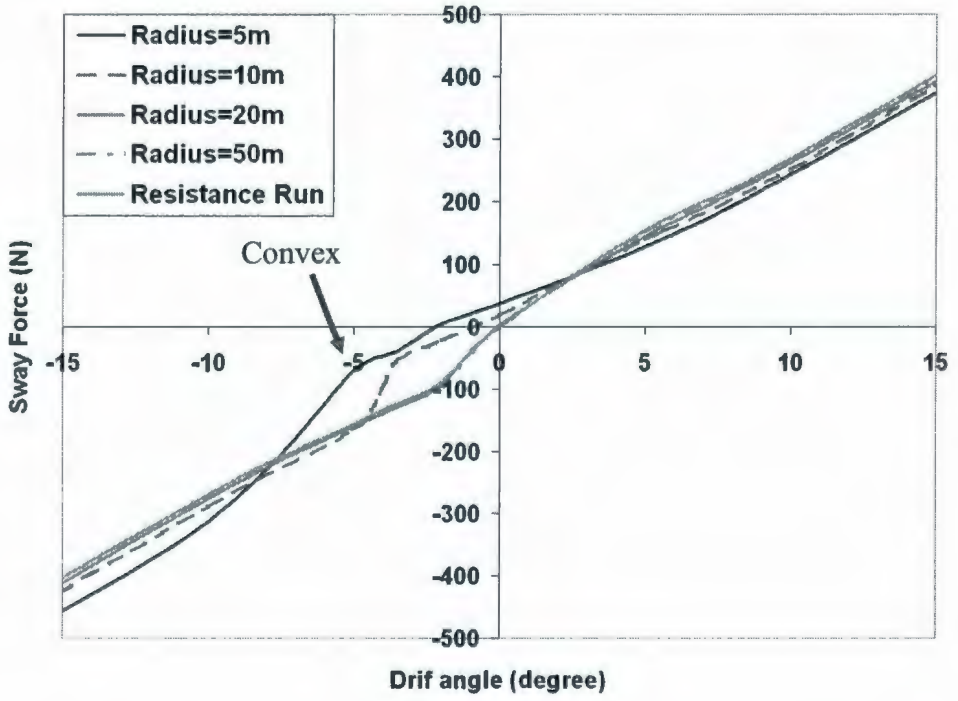

Figure 9.23 Sway force vs. drift angle for Terry Fox model different radius turning with 0.3 m/s tangential velocity in 40 mm - 31.5 kPa ice

Edwards (Edwards R., et al., 1976) studied the block coefficient and ice thickness effects to the ship turning ability based on the model test results. The actual full-scale ship's manoeuvres are found very complicated and the pivot point is changed between 0.1 and 0.4 of the ship's length from the bow due to the different ship mass distribution, ship geometries, ice conditions and external forces exerted by the stern rudder and propeller etc (Edwards et al., 1976; Kendrick et al, 1984; Rupp, et al. 1993; Pierce et al., 1987). It is easy to expect that the position of the pivot point is also a major factor affecting the turning circle capability of a ship and the relationship between the ice yaw moment and ship drift angle is also different for the different pivot point position. The detailed studies and mathematical simulation of the ship free-running manoeuvres are beyond the current research scope of this thesis and, therefore, the discussion is not presented here.

9.3.2 Ship Velocity

This section studied the relationship between yaw moment and ship's tangential velocity in constant radius runs. In chapter 6, IHI model benchmark using IOT Terry Fox model test series, several Terry Fox model constant radius runs, 10 and 50 m radius and tangential velocities from 0.05 m/s to 0.6 m/s, have been simulated and compared with the tests as shown in figure 6.20 and 6.21. Here, more Terry Fox icebreaker turning runs in level ice were simulated using IHI

model software. Figure 9.24 presents the yaw moment vs. ship velocity curves with several constant radius, 5, 10, 20, 50 and 100 m.

The simulation results figures show that the ice yaw moment increases with the increase of the ship's tangential velocity during its turning process. The sloping angles of yaw moment vs. ship velocity curves for different turning radius are different. The smaller turning radius means steeper sloping yaw moment vs. ship velocity curves, which can be basically understood as that the smaller turning radius results in more hull parts directly breaking level ice and bigger global ice force on the hull. If the increase of the force pressure on the hull due to the same ship tangential velocity increase are assumed the same for the ship's constant radius manoeuvres, the absolute increase of the global ice yaw moment in small radius turning runs is obviously bigger than that in bigger radius turning runs.

It should be noted that the pivot point is fixed at the mass centre of the ship and the drift angle is prescribed at zero in the simulations. It can be expected that in reality the pivot point's location is nearer the bow, and the stern is in more direct with contact the unbroken ice during the turning process. The direct contact will result in increase of ice yaw moment on the hull during the constant radius turning runs.

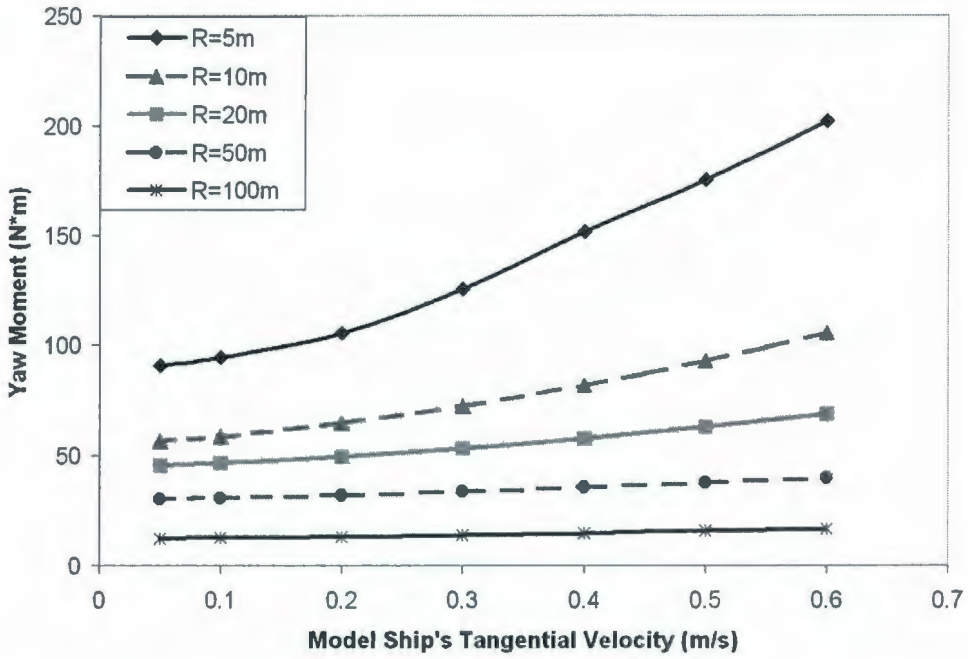

Figure 9.24 Terry Fox model yaw moment vs. ship's velocity in the constant radius runs with 0.3 m/s model velocity and 40 mm thick ice

9.3.3 Yaw Rate

In this section, the relationship between the ice yaw moment and the yaw rate is studied. For the constant radius runs, the yaw rate is equal to the ratio of the tangential velocity and turning radius. In the following, Terry Fox model constant radius runs in 30 mm - 20 kPa ice with different turning radius and tangential velocities were simulated using IHI model software. In the simulations, the drift angle was always prescribed as zero and the pivot point was fixed at the mass centre of the ship.

Figure 9.25 shows the yaw moment vs. radius curve with constant tangential velocities. Figure 9.26 shows the yaw moment vs. yaw rate curve and figure 9.27 shows the yaw moment vs. reciprocal of radius curve.

From figure 9.25, it can be seen that for the same turning radius, the global ice yaw moment increases with the increase of ship tangential velocity. It can be basically explained as: with the increasing of ship velocity, the ice load density on the unit area of the hull also increases. The global ice force is equal to the vectorially integration of the ice load distribution and its value certainly increases with the ice load distribution's increase.

Figure 9.26 shows that, for the constant ship tangential velocity, the yaw moment approximately linearly increases with the raw rate in the ship turning cases and for different ship tangential velocity, the sloping angle of the line is different as shown in figure 9.26. That is coincident with the assumptions for analyzing the PMM ship test data by Hoffmann K. (1998) and Shi Y. (2002). If for the yaw moment vs. the reciprocal of radius curves, the differences among the sloping rates of the three curves are more obvious as shown in figure 9.27.

In the above simulations, the pivot point was always fixed at the mass center of the model ship. In the actual full-scale trials, that point can be changeable and the corresponding rules may also be modified to some extent.

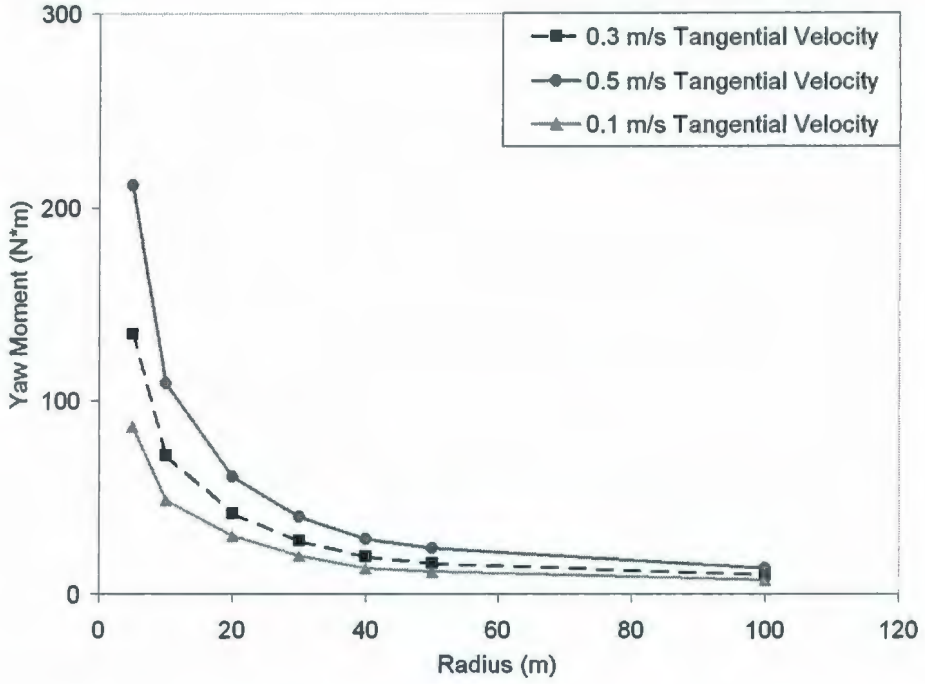

Figure 9.25 Yaw moment for Terry Fox model in constant radius runs with different radius and velocities in 40 mm - 31.5 kPa ice (Drift angle =0.0°)

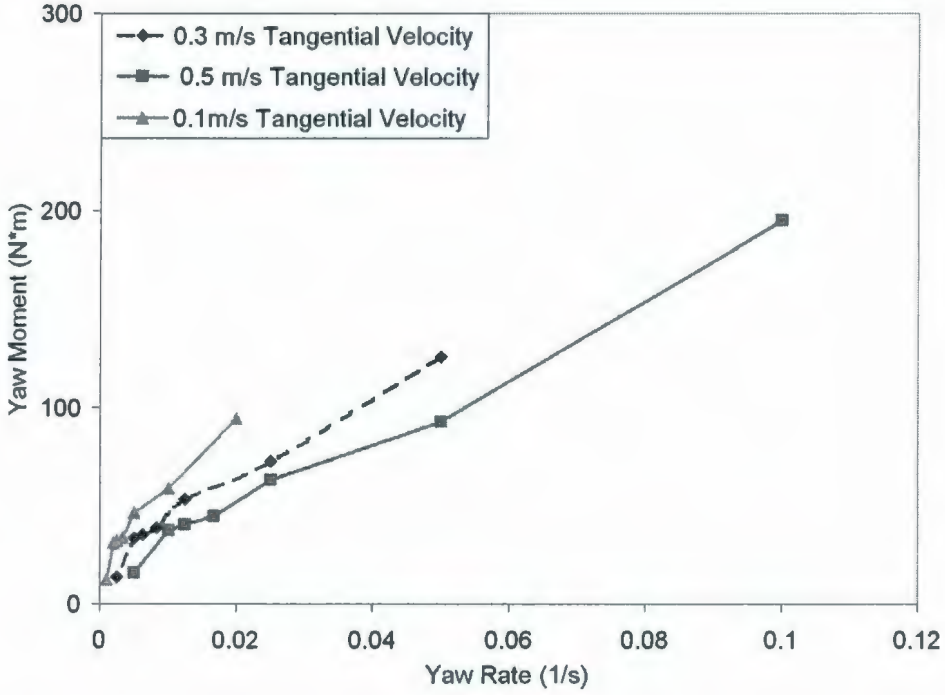

Figure 9.26 Yaw moment for Terry Fox model ship in constant radius runs with different radius and velocities in 40 mm - 31.5 kPa ice (Drift angle =0.0°)

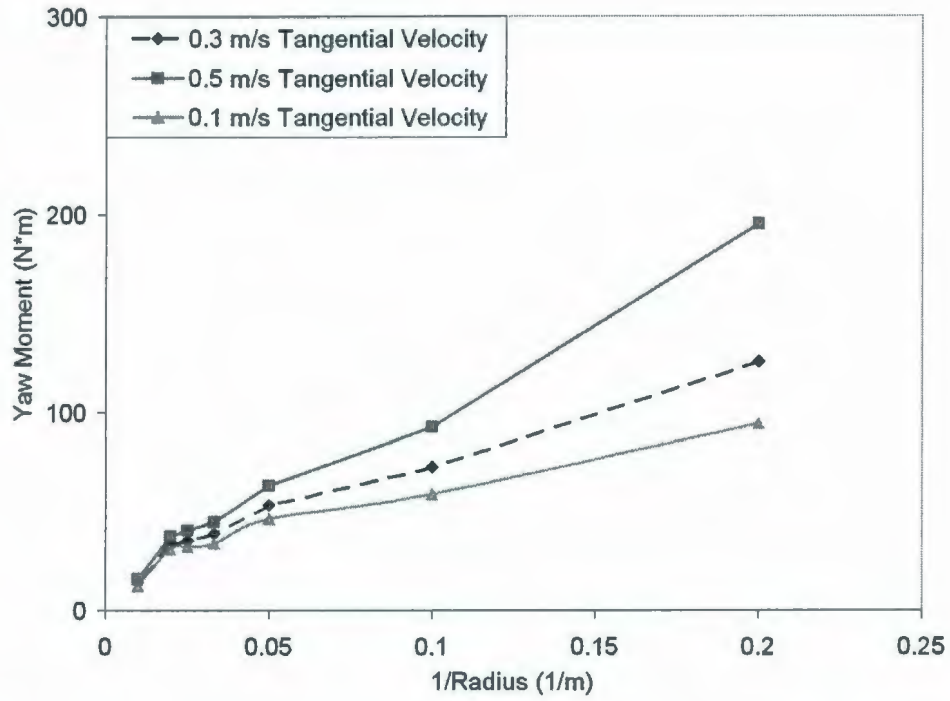

Figure 9.27 Yaw moment for Terry Fox model ship in constant radius runs with different radius and velocities in 40 mm -31.5 kPa ice (Drift angle =0.0)

9.4 Hull Geometries

The IHI model is originally designed to be able to simulate the navigations of the different hull forms, but the model can also provide the guidance for designing the hull. The results of hull geometrical effects on ice forces based on the simulations and experiments also provide the model credibility and clues for refining IHI model.

In this section, the effects from the waterline length to waterline beam ratio to the ship manoeuvrability are considered based on IHI model simulations. Several new

hull forms with different waterline length to waterline beam ratios (L/B) are generated through lengthening or shortening the parallel mid-body of the hull and adopting Terry Fox icebreaker bow and stern as shown in figure 9.28. Here, the hull with the L/B ratios, 2.5, 3.5, 4.3438 (Terry Fox icebreaker), 5.5, 6.5 and 7.5, are selected for the discussion. The ice condition was defined as 0.872 m thickness, 687 kPa flexural strength, 2834 kPa crushing strength and 964 kPa shear strength.

Figures from 9.29 to 9.31 show the snapshots of the simulation of the ship with different waterline length to waterline beam ratios, L/B=2.5, 3.44 and 7.5, in 218 m radius turning runs using IHI model program respectively.

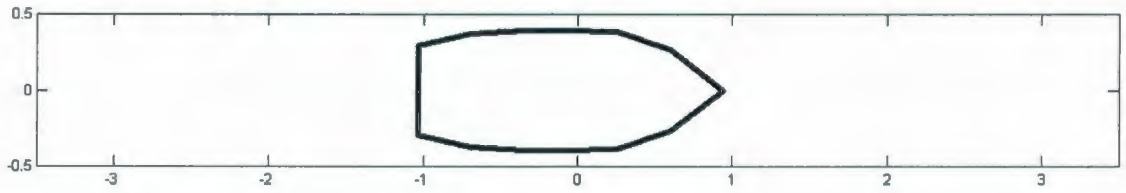

L/B=2.5

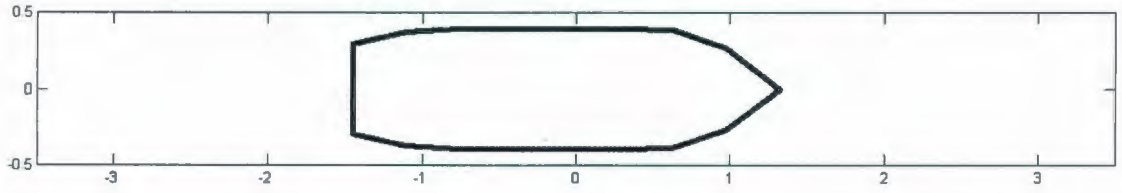

L/B=3.5

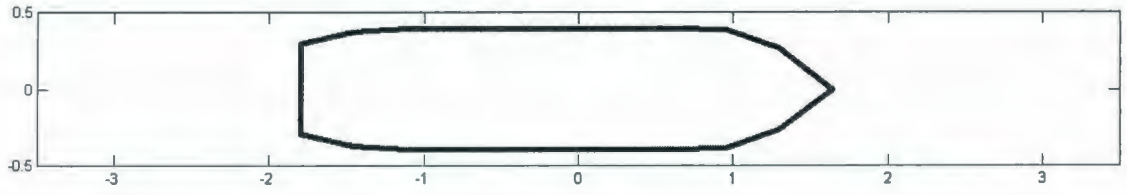

L/B=4.3438 (Terry Fox ship)

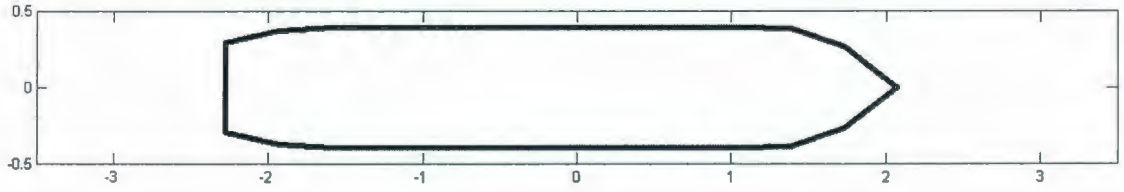

L/B=5.5

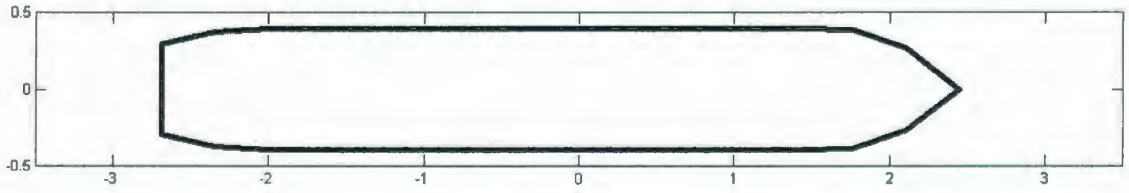

L/B=6.5

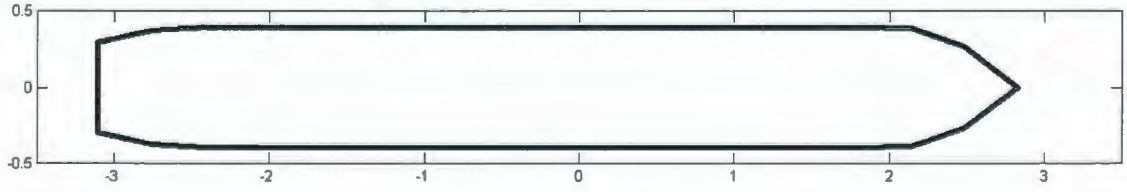

L/B=7.5

Figure 9.28 Waterline profiles for the hull with different length-beam ratio and same Terry Fox icebreaker bow and stern

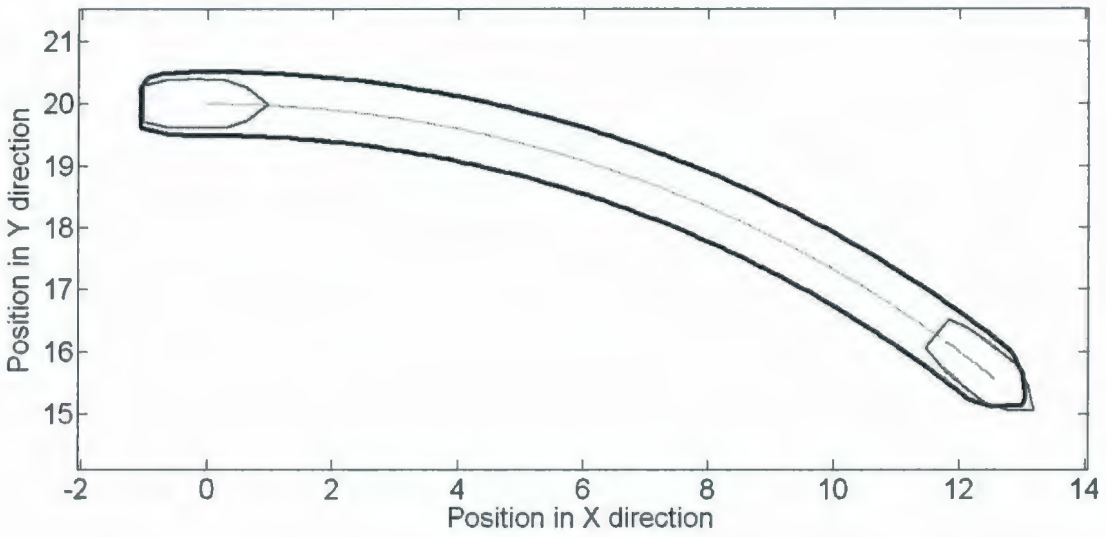

Figure 9.29 Snapshot of IHI model simulation for the ship with small waterline length to waterline beam ratio, L/B=2.5, in 20 m radius turning run

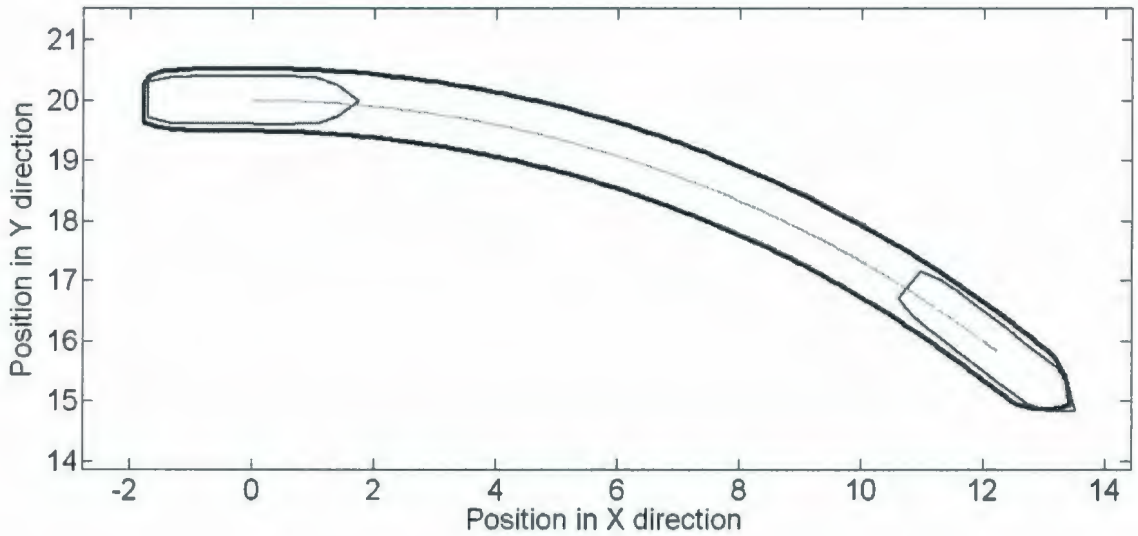

Figure 9.30 Snapshot of IHI model simulation for the ship with waterline length to waterline beam ratio, L/B=4.344, in 20 m radius turning run

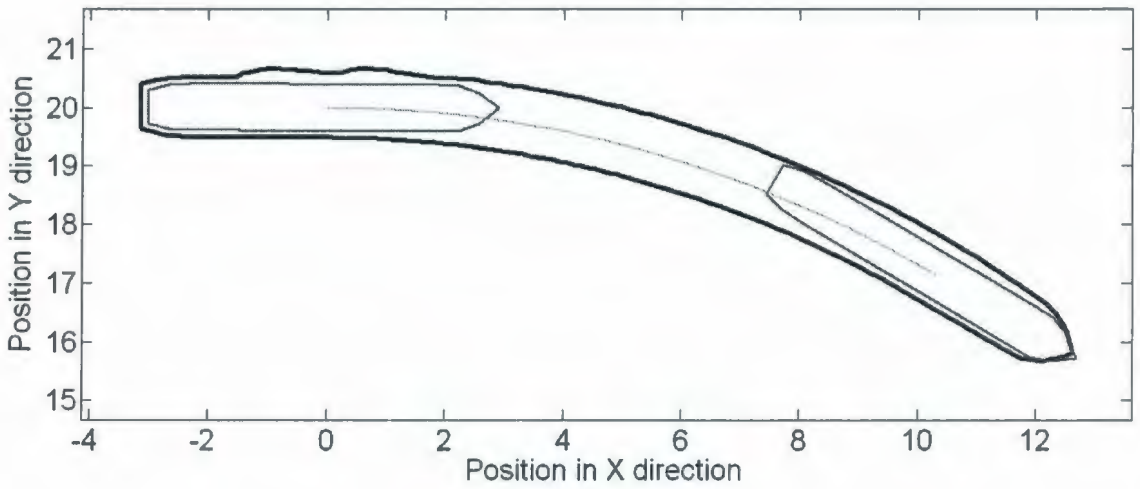

Figure 9.31 Snapshot of IHI model simulation for the ship with big waterline length to waterline beam ratio, L/B=7.5, in 20 m radius turning run

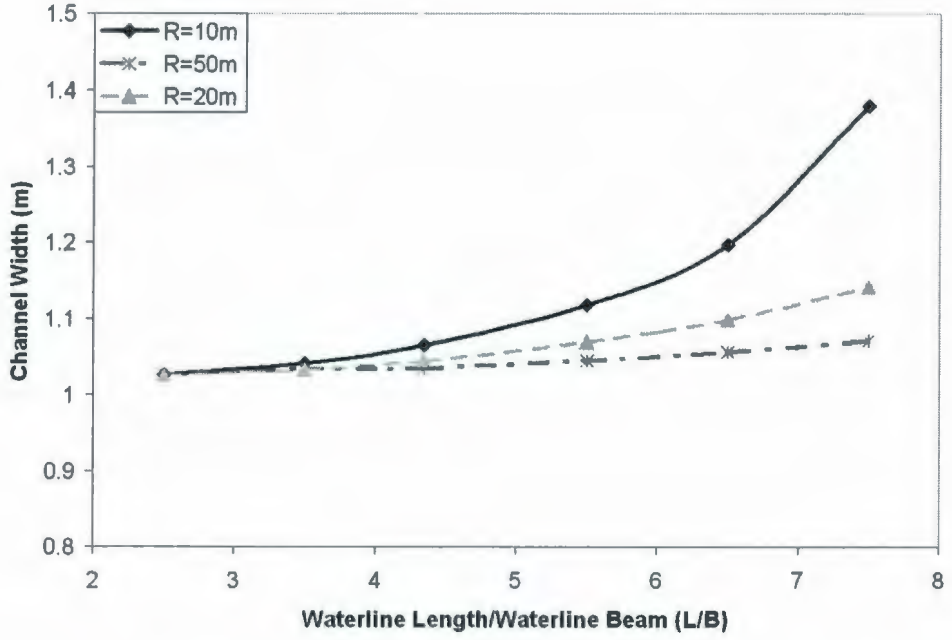

Figure 9.32 The channel width vs. waterline length to waterline beam ratios (L/B) for the hulls with Terry Fox ship bow and stern in the level ice

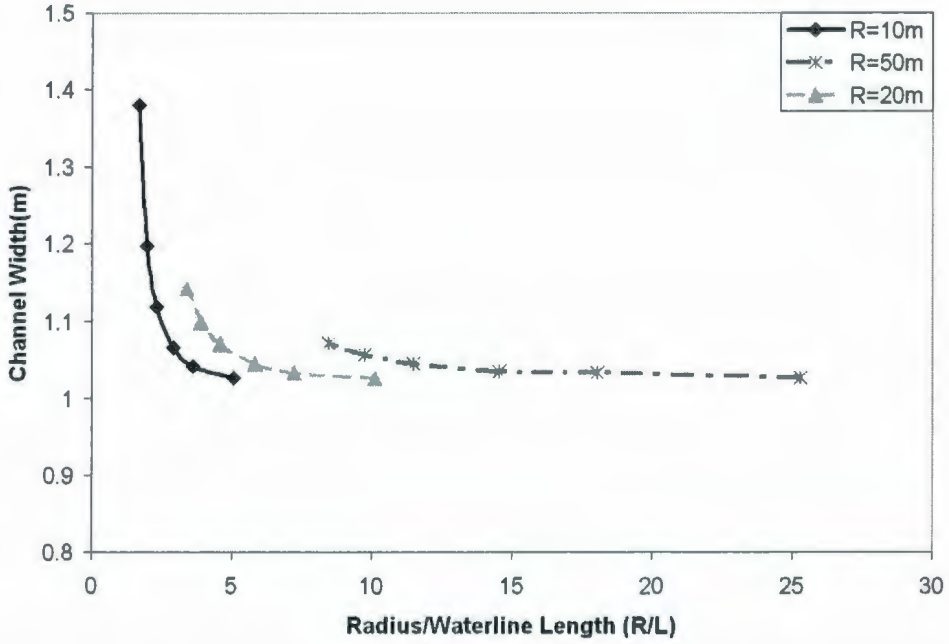

Figure 9.33 The channel width vs. constant radius to waterline length ratio (R/L) for the hulls with Terry Fox ship bow and stern in the level ice

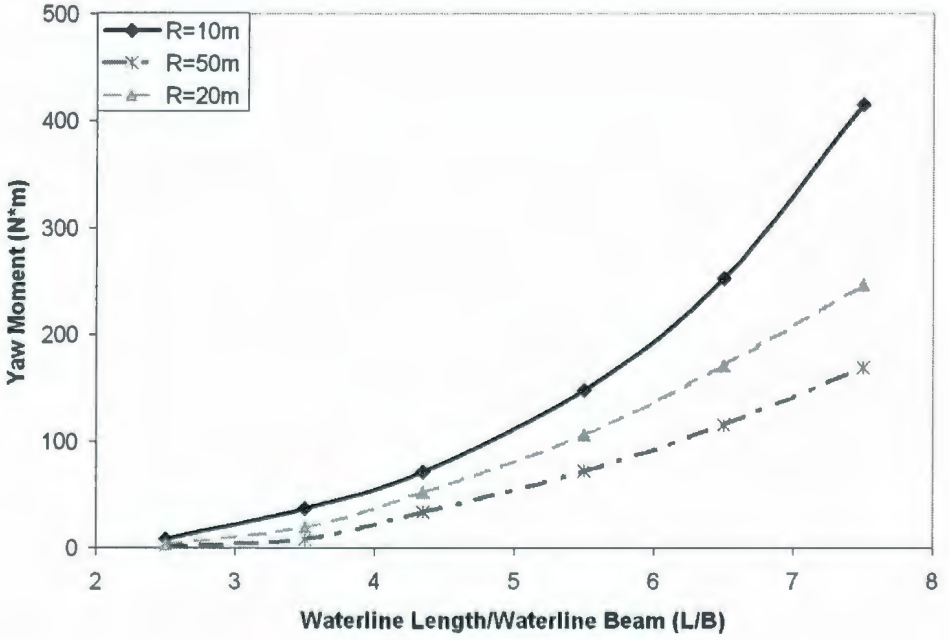

Figure 9.34 The yaw moment vs. waterline length to waterline beam ratios (L/B) for the hulls with Terry Fox ship bow and stern in the level ice

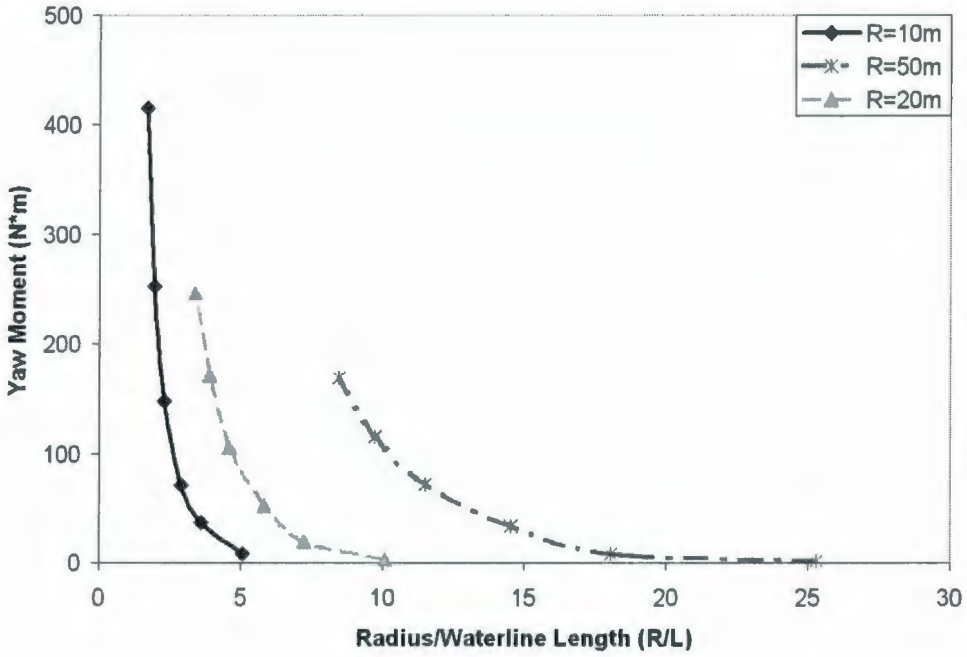

Figure 9.35 The yaw moment vs. constant radius to waterline length ratio (R/L) for the hulls with Terry Fox ship bow and stern in the level ice

Figure 9.32 shows the curves of channel width vs. waterline length ratio (L/B) of the hulls with Terry Fox bow and stern in level ice at different constant radius runs. Figure 9.33 presents the curves of channel width vs. constant radius to waterline length ratio (R/L). The simulation result figures show that the width of the hull left channel increases with increase of the waterline length to waterline beam ratio (L/B) in the fixed constant radius runs. The channel width decreases with increase of the turning radius to waterline length ratio (R/L) for the same turning radius runs.

Figure 9.34 shows curves of the yaw moment vs. waterline length ratio (L/B) of the hulls with same Terry Fox bow and stern in level ice at different constant radius runs. Figure 9.35 correspondingly presents the curves of the yaw moment vs. constant radius to waterline length ratio (R/L).

With increase of the waterline length to waterline beam ratio (L/B), the yaw moment required for the same constant radius turning increases as shown in figure 9.34. On the other hand, for the same yaw moment, the bigger the waterline length to waterline beam ratio (L/B), the larger is the turning radius. The turning radius to waterline length ratio (R/L) increases with increase of the turning radius for the constant yaw moment as shown in figure 9.35. The snapshots of the IHI model simulation show that the stern may more possibly directly contact the unbroken level ice for the hull with the bigger waterline length to waterline beam ratio (L/B). It should be mentioned that, besides the waterline length to waterline beam ratio (L/B), the position of the pivot point with the corresponding drift angles during the turning process is the key factors to determine whether the stern directly contacts the unbroken level ice. It can be expected that the pivot point's location is nearer the bow, the stern more possible directly contacts the unbroken ice during the turning process. In the IHI model simulations for this section, the pivot point was always fixed at the mass center of the ship and the drift angle prescribed at zero.

It should be noted that the above conclusions can not be simply extended to the free running ship conditions for the purpose of determining the relationship of the ship turning radius and rudder angle. The ice yaw moments caused by the same rudder angle and pod-propeller angle on the hulls with different waterline length to waterline beam ratios (L/B) will be different. The pivot point position can be changeable in the process of the free-running ship manoeuvring.

9.5 Summary and Conclusions

9.5.1 Summary

9.5.1.1 Ice Mechanical Properties

Ice Failure Mode

The parametric checks of the multi-failure model were provided. The calculation results showed that the flare angles at which at which the horizontal force due to flexural failure is equal to the maximum crushing force endured by each ice cusp, and the flare angles at which the ice shear failure happens before the bending failure or the ice cusp is blocked due to ice-hull friction force, are all in excess of 80 degree. The higher ice-hull friction, higher ship velocity and thicker ice means smaller critical flare angles and that means that jamming phenomena more readily happens. For all ice with the same ice strength ratios, the calculated flare angle at which shear failure happens before the bending failure, is also same.

Ice Mechanical Strength

The effects from ice mechanical strengths, crushing strength, bending strength and shear strength on the global forces on the hull were studied. With increase of the crushing strength, the global ice force decreases a little, because the amount of initial crushing ice also decreases for a given bending strength.

Ice Thickness

It can be found that the pre-sawn ice force increases nearly linearly with the increase of the ice thickness, which can be basically explained as increasing ice thickness linearly increases the amount of ice submerged and covering on the wet surface of the hull. Compared to the pre-sawn ice condition, the ice force increase in level ice due to the ice force thickness increase is more due to the included the breaking ice components than the buoyancy force components and clearing force component. The higher ice strength accelerates that ice force increase due to ice thickness dependence.

Ice-Hull Friction

Based on the adopted idealization and simplification of present IHI model, the friction coefficients between 0.0 and 0.1 didn't show significant effects on the global ice yaw moments on the hull during the ship turning process, which is coincident with observations from the former ice model ship experiments. The ice-hull friction effect to global ice force, especially to ice resistance, may be

underestimated to some extent because the ice jamming at the shoulder can't be accurately modeled using present IHI model.

9.5.1.2 Ship Motions

Drift Angle and Radius Effects on Ice-Hull Contact

The IHI model simulation results proved that the drift angle and turning radius directly influences the ice-hull contact area and location that determine the ice force distribution on the hull and finally determine the global ice forces on the hull.

Drift Angle and Radius Effects on Channel Width

In general, the channel width vs. drift angle curve shows a "V" shape for the constant radius runs. The channel width vs. drift angle curve for the straight going up run shows a standard "V" shape with the top end at the Y axis. When a ship turns with a small radius, the stern always breaks the ice with negative drift angle, while a large turning radius run, a very small drift angle will cause the stern to break the ice.

Drift Angle and Radius Effects on Ice Forces

From the simulation results, it can be seen that the yaw moment increases with the increase of the drift angle in the constant radius runs. In the straight going run and

large radius manoeuvres, the curves are nearly linear. For the constant drift angles, the yaw moments decrease with the increase of the turning radius. In the runs with small radius runs or big drift angles, the stern may will also directly break the ice and contribute to the global ice forces. In the runs with the big drift angles, the high ice force distribution moves to the inside of the hull and near the pivot point of hull, causing the sway force to quickly increase while the yaw moment changes little and even decreases. For the free-running ship, the pivot point of the ship running may be further from the gravity centre if the small radius or big drift angles exist and the assumption that the pivot point fixed at the ship mass centre will be inappropriate.

Tangential Velocities and Yaw Rates on Ice forces

The tangential velocities and Yaw Rate effects on global ice forces on the hull in the constant radius runs were studied. The simulation results showed that the ice yaw moment increases with the increase of the ship's tangential velocity if the radius keeps constant. The sloping angle of yaw moment vs. ship velocity curves at different radius runs are different. The smaller turning radius runs show steeper slope of yaw moment vs. ship velocity curves. For the constant ship tangential velocity, the yaw moment coarsely linearly increases with the increase of the raw rate. For the different ship tangential velocities, the sloping angles of the yaw moment vs. yaw rate curves are different. The runs with big velocity show the steeper sloping yaw moment vs. yaw rate curves.

9.5.1.3 Hull Geometries

A preliminary study on the effects from the waterline length to waterline beam ratio to the ship manoeuvrability was carried out. The simulation results showed that with increase of the waterline length to waterline beam ratio, the channel width left by the hull and the yaw moment required for the same constant radius turning both increase. The yaw moment and channel with decreases with the increase of the turning radius to waterline length ratio for the same turning radius runs. In the calculations, the pivot point was always fixed at the mass centre located with the same forward to afterward ratio of hull length.

9.5.2 Conclusions

The parametric analysis in this chapter provided a detailed check of the IHI model. The model's accessibility and accuracy in real-time simulating the ship's manoeuvres in ice were further verified. The parametric analysis also showed that the present IHI model worked correctly and as it was designed.

Chapter 10 Specific Maneuver Simulations Using IHI Model

10.1 Introduction

In this chapter, several specific ship manoeuvres were simulated using IHI model and discussed in order to showcase the IHI model's capability and accuracy in simulating the ship's arbitrary manoeuvres. The simulated maneuvers included backing maneuver run, pure yaw maneuver, pure sway maneuver, "Star" maneuver run and arbitrary maneuver run. The global ice forces on the hull and ice edge, ice-hull contacts were studied and discussed, which showed the IHI model's accuracy and universality in real-time simulating the ship's arbitrary maneuvers in ice. Some general conclusions on ship's maneuverability in ice were comprehensively drawn, which was of great values for future research on ship operating in ice and future mathematical modeling ship navigating in ice. The curves of ice loads in the ship prescribed maneuvers were also the important evidences for the model's accuracy through comparing the ship-ice experimental data. The clues for further refining IHI model were also gained.

Terry Fox Icebreaker was selected for all the simulations presented in this chapter.

10.2 Backing Maneuver

Modern icebreakers have rotating azimuth thrusters for better manoeuvrability (Akinturk et al, 2003, 2004a, 2004b; Soininen, 1998; Wang et al, 2004; Riska et al., 2005). Due to the 360-degree free rotation of the azimuth propulsion, excellent steering performance of ship is realized in harbour and some very shallow passages. Together with powerful propulsion, it is possible for the ship to perform the backing navigation in ice.

Based on Terry Fox Icebreaker geometries, one simplified and idealized bare stern breaking ice process was modeled without considering effects from the propellers, rudder or other appendages. Figure 10.1 shows the simulated scene of Terry Fox model backing in a 40 mm - 31.5 kPa level ice with -0.3 m/s velocity and zero drift angle. Figure 10.2 shows the calculated ice resistance force time history during the backing process.

The simulation results verified that the IHI model could work well in this specific run, backing navigation. Hower, it should be noted that the IHI model only considers the hull breaking ice process. The effects from the rudder, propeller or other stern appendages are neglected in the research for this thesis. Modeling the stern breaking ice including all those effects still needs more work in the future.

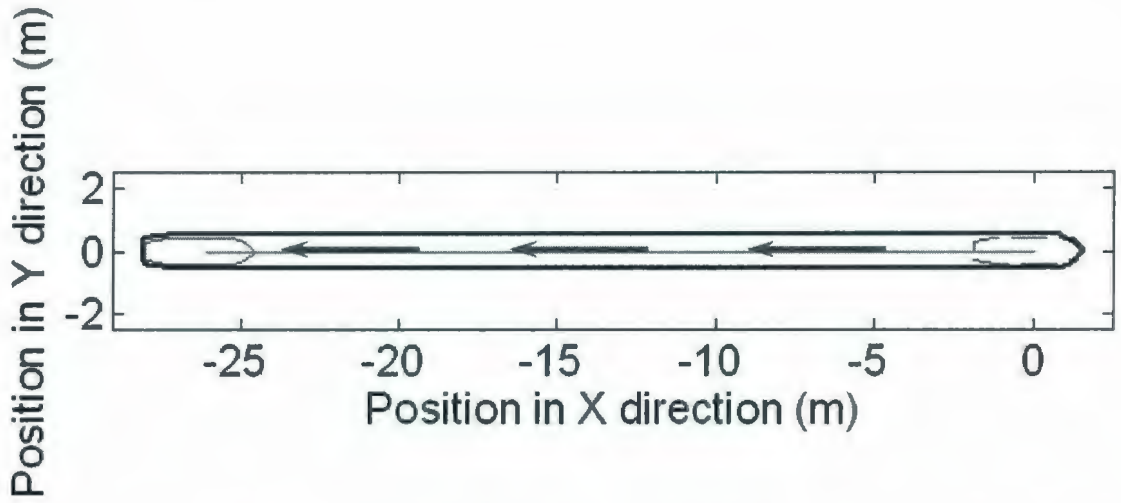

Figure 10.1 Simulation of Terry Fox model backing run with 0.3 m/s backing velocity and zero drift angle in 40 mm – 31.5 kPa ice

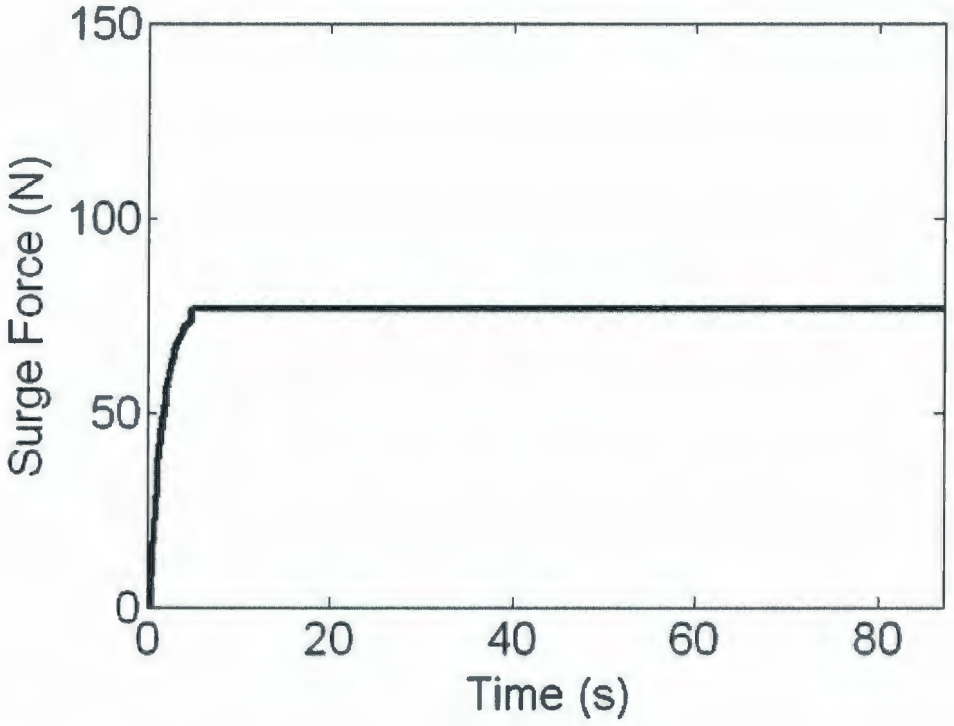

Figure 10.2 Ice resistance force in Terry Fox model backing run with 0.3 m/s backing velocity and zero drift angle in 40 mm - 31.5 kPa ice

10.3 Pure Yaw Maneuver and Pure Sway Maneuver

Two typical ship manoeuvres in PMM model test, pure yaw run and pure sway run, (Marinering Limited, 1997; Spencer D., 1998) for the Terry Fox model in level ice were simulated and discussed in this section. In the two runs, the Terry Fox model kept 0.6 m/s tangential velocity, 200 seconds period, 2.5 m amplitude in Y direction and zero drift angle.

Figures 10.3 and 10.4 show the simulated channel geometry in pure yaw run and pure sway run respectively. The channel widths in the two manoeuvres are plotted against model ship locations as shown in Figure 10.5. The simulations show that channel width changes in a big range and nearly one side of the hull from bow to stern directly contacted the unbroken ice in the pure sway run, while the channel width nearly keeps constant and only the bow directly contacts the unbroken ice in the pure yaw run.

Figures 10.6 and 10.7 respectively show the yaw moment-time history predictions for the two manoeuvres. Figures 10.8 and 10.9 respectively show the sway force-time history predictions.

The yaw moment curves for the two manoeuvres both roughly show a more or less sinusoidal shape, but the force levels are different and the ice yaw moment on the

hull in the pure yaw run is much smaller. The ship motions corresponding to the maximum value and minimum value of the yaw moment curves in two runs are different, which means that causes of the yaw moment on the hull in two runs are different. The sway force during the pure yaw run is much smaller than pure sway run. The above phenomena can be explained from the ice-hull contacts during the runs: In pure yaw run, only the bow contacts the ice edge while most of one side of the hull from the bow to stern contacts the ice edge in the pure sway run. Compared to the pure sway run, the ice hull contact area change is more complicated in the pure yaw run. The changing part of ice-hull contact is close the ship mass centre during the running which makes it affects the sway force more obviously than the yaw moment as shown in Figure 10.6 and Figure 10.8.

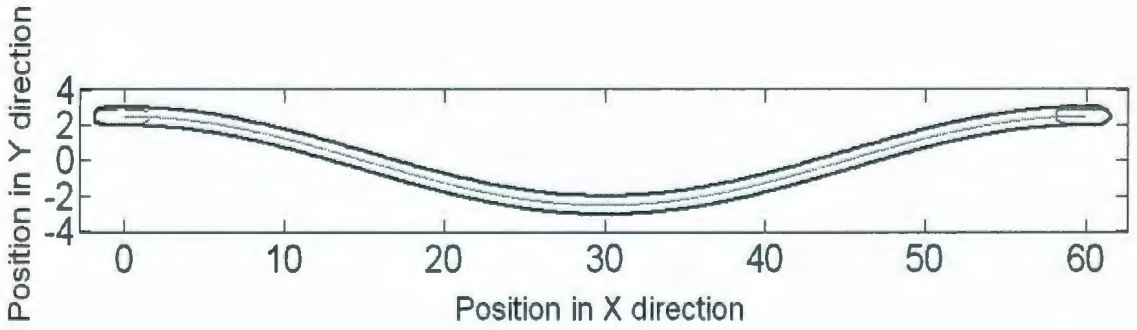

Figure 10.3 Channel in pure yaw run with 0.3 m/s velocity, 200 seconds period, 2.5 m amplitude in Y direction and zero drift angle in 40 mm – 31.5 kPa ice

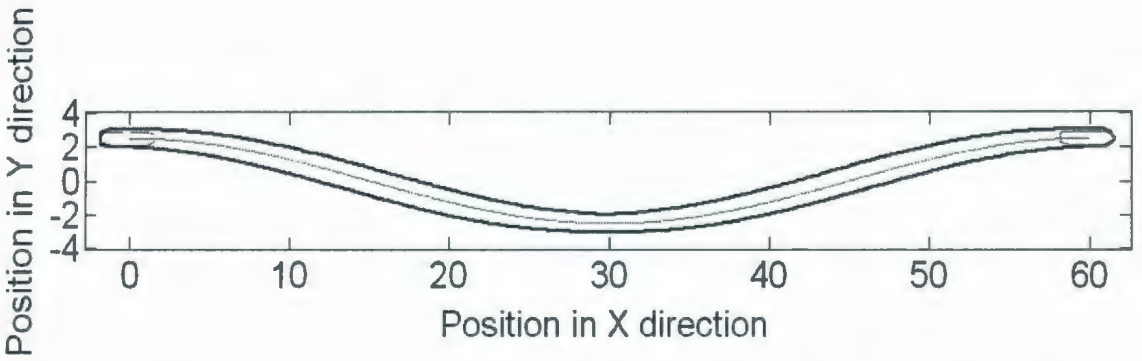

Figure 10.4 Channel in pure sway run with 0.3 m/s velocity, 200 seconds period, 2.5 m amplitude in Y direction and zero drift angle in 40 mm - 31.5 kPa ice

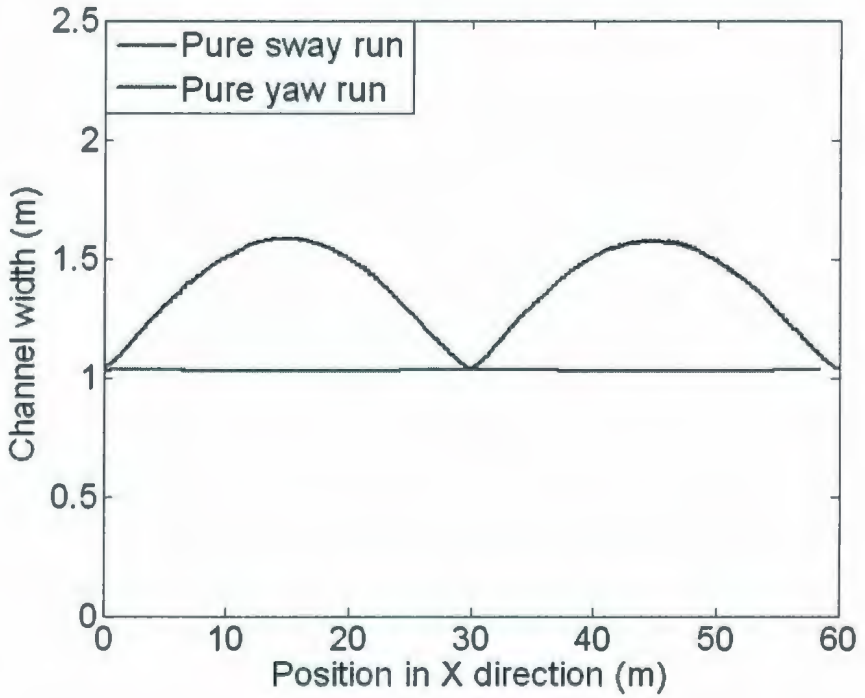

Figure 10.5 Channel widths in pure sway and pure yaw runs with 0.3 m/s velocity, 200 seconds period, 2.5 m amplitude in Y direction and zero drift angle

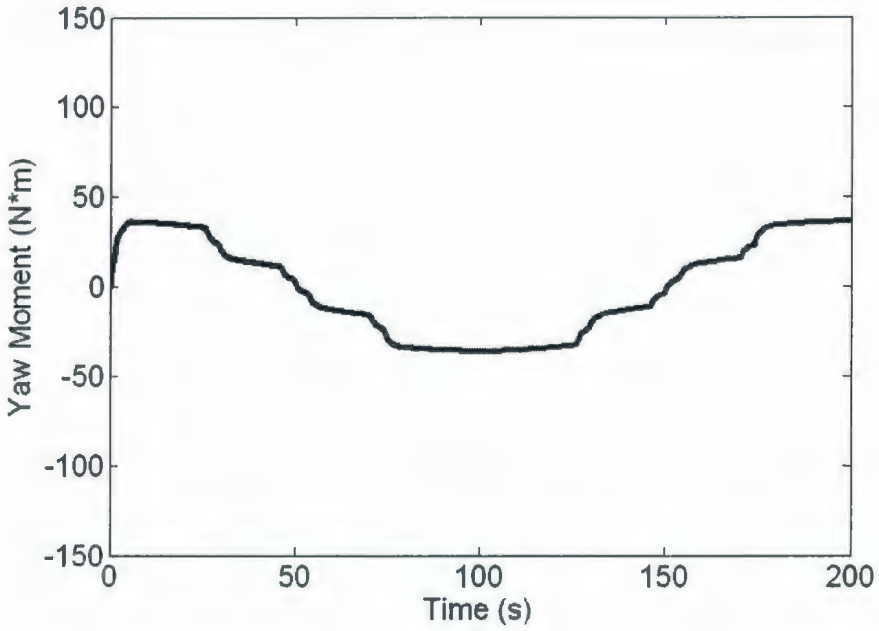

Figure 10.6 Yaw moment in pure yaw run with 0.3 m/s velocity, 200 seconds period, 2.5 m amplitude in Y direction and zero drift angle in 40 mm - 31.5 kPa ice

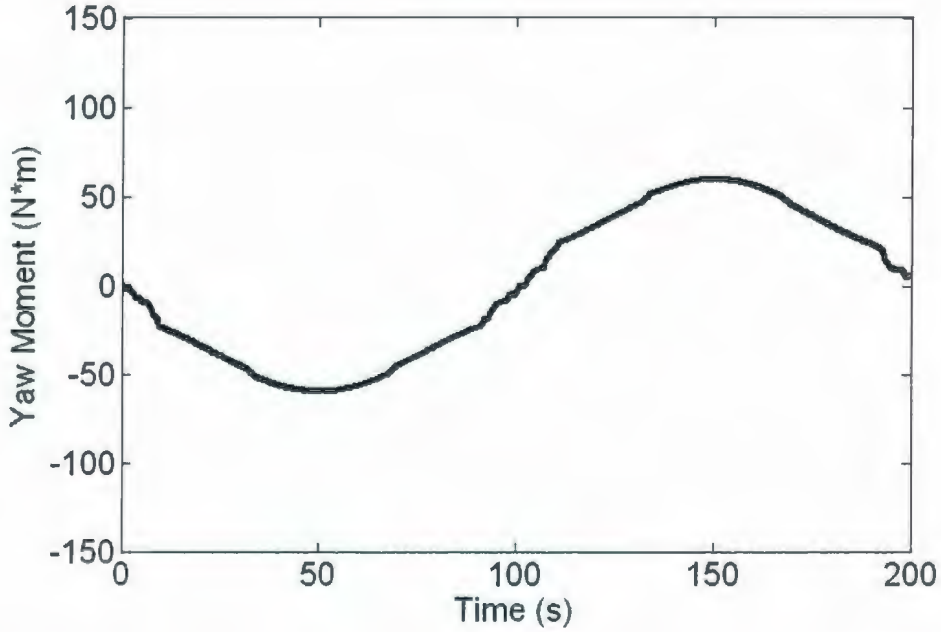

Figure 10.7 Yaw moment in pure sway run with 0.3 m/s velocity, 200 seconds period, 2.5m amplitude in Y direction and zero drift angle in 40 mm - 31.5 kPa ice

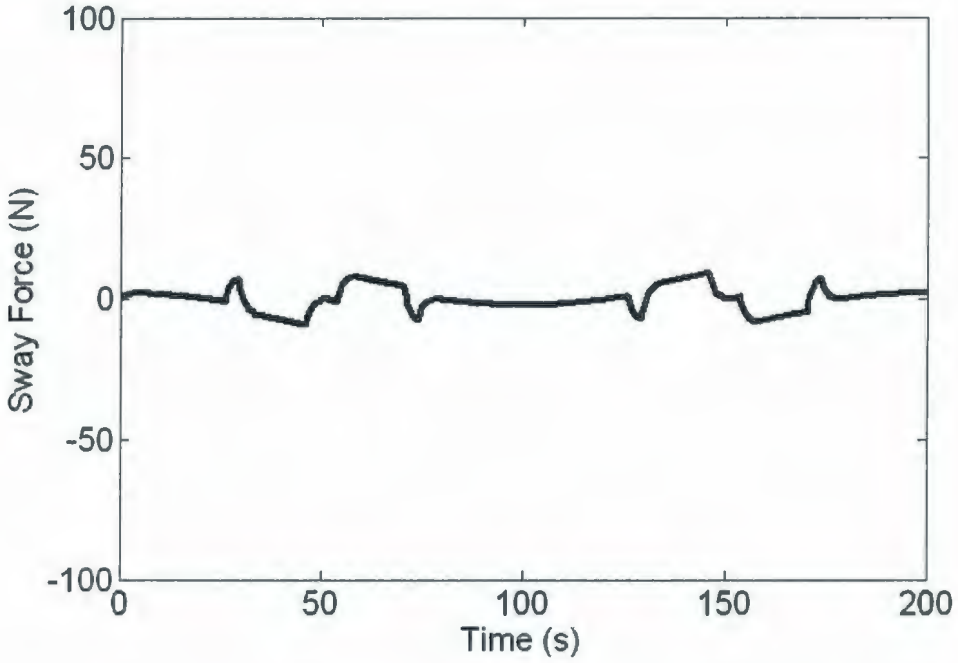

Figure 10.8 Sway force in pure yaw run with 0.3 m/s velocity, 200 seconds period, 2.5 m amplitude in Y direction and zero drift angle in 40 mm – 31.5 kPa ice

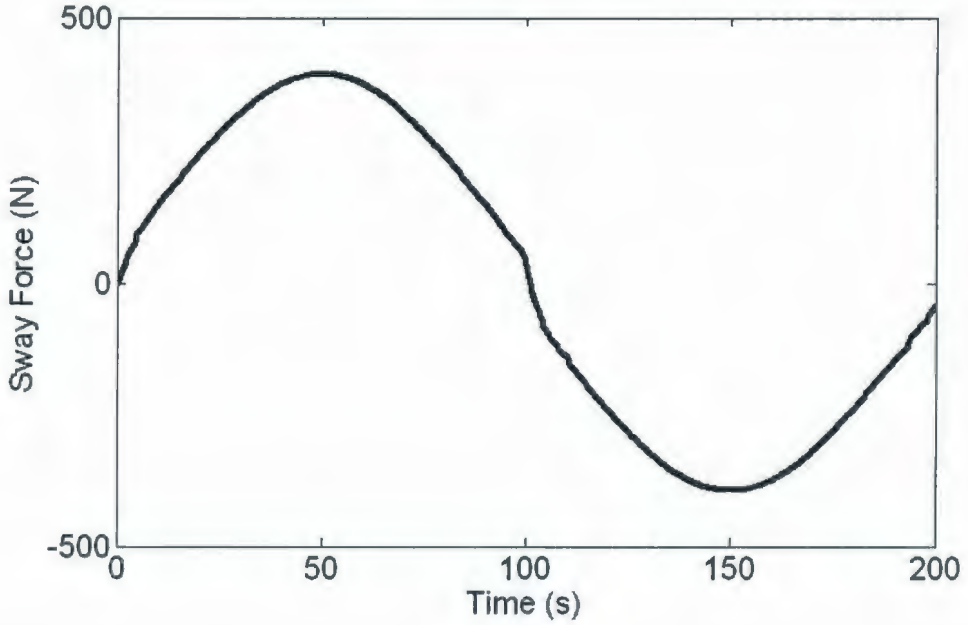

Figure 10.9 Sway force in pure sway run with 0.3 m/s velocity, 200 seconds period, 2.5 m amplitude in Y direction and zero drift angle in 40 mm - 31.5 kPa ice

10.4 "Star" Maneuver

The standard "Star" manoeuvre is an unsteady manoeuvre commonly carried out by icebreakers to achieve a partial change in course or a complete and rapid reversal of heading. During the manoeuvring process, the rudder's angle keeps changing and the ship's track shows the shape like a "Star". One idealized "Star" manoeuvre was simulated using IHI model, in which, the whole manoeuvre track consists of three same constant radius arcs tangentially connected with each other. The ship was prescribed with constant drift angle and constant tangential velocities. Two "Star" manoeuvres, "star" manoeuvre with 5 m radius arcs and "star" manoeuvre with 30 m radius arcs, were simulated.

Figure 10.10, 10.11 and 10.12 show the snapshots during the small "Star" manoeuvre simulation. Figure 10.13 correspondingly shows the yaw moment time history calculated in IHI model simulation. Figure 10.14 shows the snapshots during the big "Star" manoeuvre simulation. Figure 10.15 correspondingly shows the simulated yaw moment time history and sway force time history.

In the small star maneuvering, the former channel left by the hull affects the late ice-hull contact, which results the ice-hull contact and the global ice forces on the hull changing as shown in Figure 10.13, while within each arc of big star maneuver, the ice-hull contact and the global ice forces on the hull keep constant

and the whole maneuver like a combination of three independent constant radius runs as shown in figure 10.15. In small star manoeuvres, the ship finishes a rapid heading reversal within a small area, while a big area for the ship reversing direction is needed in big star manoeuvres. The "Star" manoeuvre will lose its values and maybe a simple "U" manoeuvre is more practical if an enough wide passage exists for the ship's navigation. The yaw moment in small "star" manoeuvres are bigger than in big star manoeuvres due to the stern's contacting ice, which may exceed the ship turning ability. Obviously, there is a balance point between the required navigation area and ship's turning ability. The mathematical simulation using IHI model in advance may provide a theoretical guidance for the ship operator. The simulation in this section proved the IHI model's accuracy in simulating this idealized "star" maneuver.

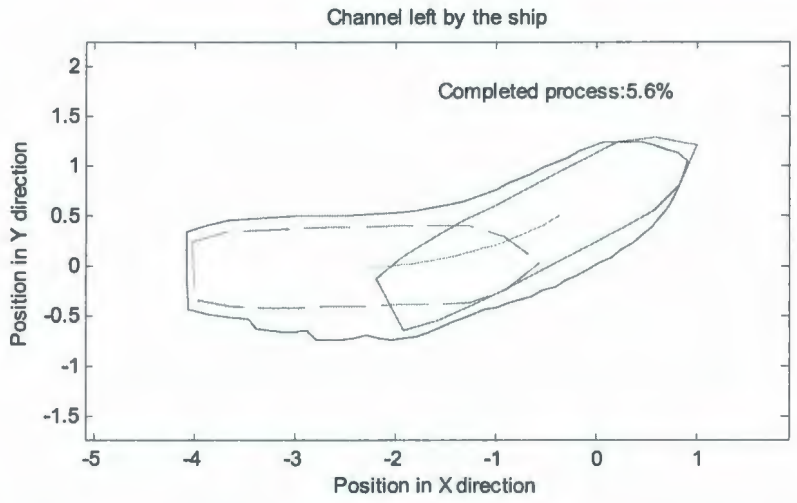

Figure 10.10 Snapshot of the prescribed "Star" manoeuvre with 5 m radius arcs of Terry Fox model run using IHI model software

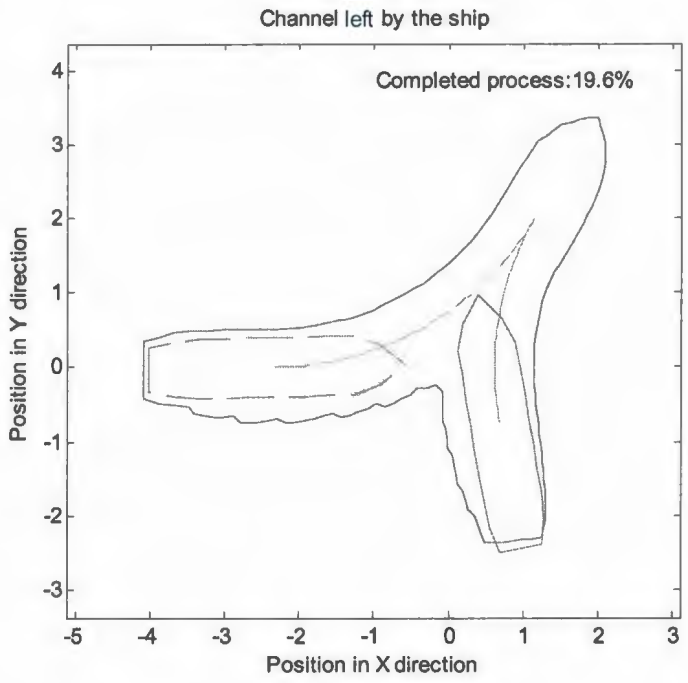

Figure 10.11 Snapshot of the prescribed "Star" manoeuvre with 5 m radius arcs of Terry Fox model run using IHI model software

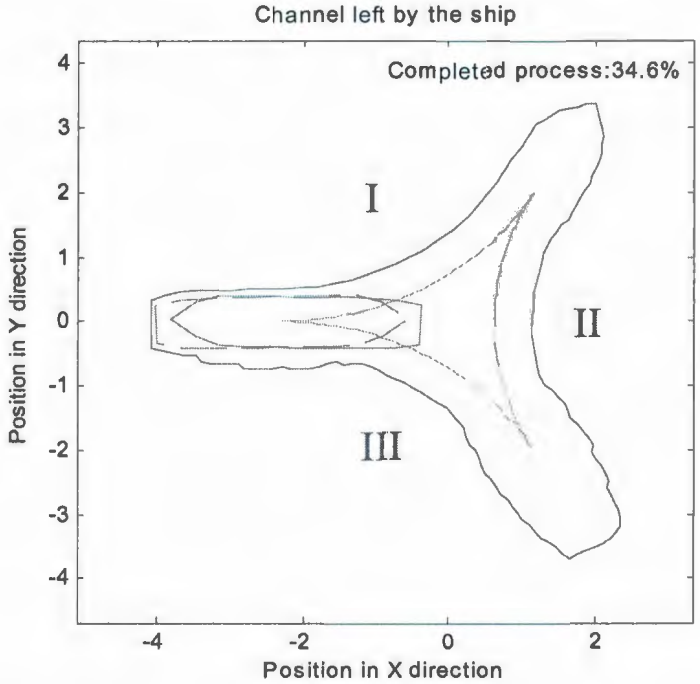

Figure 10.12 Snapshot of the prescribed "Star" manoeuvre with 5 m radius arcs of Terry Fox model run using IHI model software

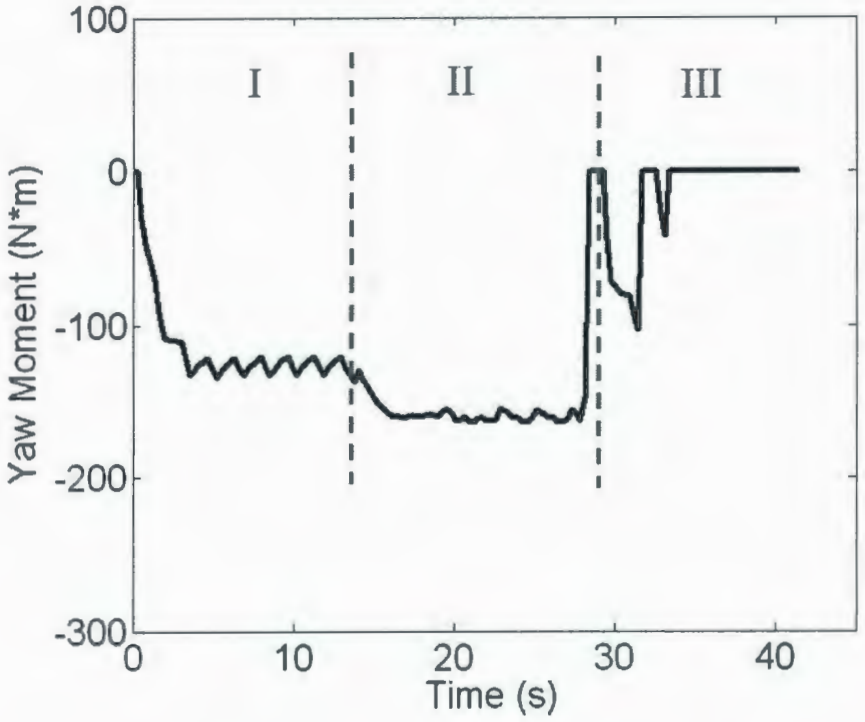

Figure 10.13 Yaw moment in the "Star" manoeuvre with 5 m radius arcs of Terry Fox model with 0.3 m/s velocity in 40 mm - 31.5 kPa ice

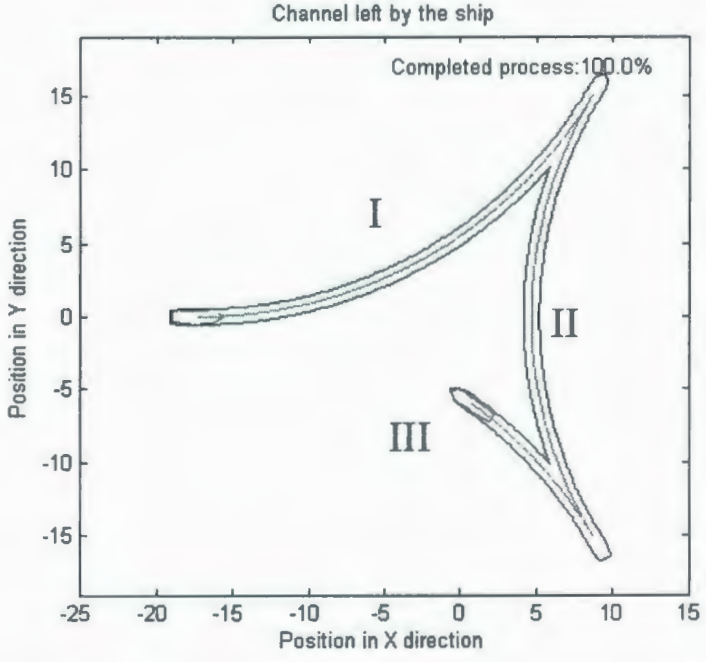

Figure 10.14 Snapshot of the prescribed "Star" manoeuvre with 30 m radius arcs of Terry Fox model with 0.3 m/s velocity in 40 mm - 31.5 kPa ice

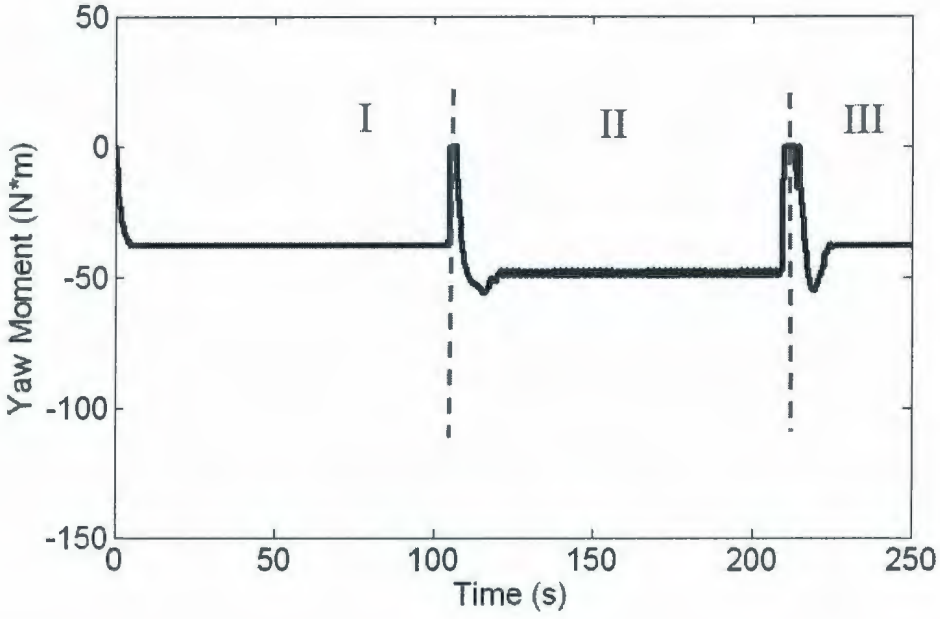

Figure 10.15 Yaw moment in "Star" manoeuvre with 30 m radius arcs of Terry Fox model with 0.3 m/s velocity in 40 mm – 31.5 kPa ice

10.5 Arbitrary Maneuver

The IHI model is designed to simulate the ship's any manoeuvres in ice. In this section, an arbitrary manoeuvre was simulated using the IHI model to show the model's ability to simulate arbitrary manoeuvres as shown by a series of snapshots (Figures 10.16 ~ 10.25). The simulated yaw moment, sway force and surge force time histories were respectively shown in Figure 10.26, 10.27 and 10.28. In the simulation, the ship motion was prescribed. This simulation shows such a complex manoeuvre can be easily simulated in a numerical framework. On the other hand,

in such complicated manoeuvres, obviously, it is impossible to represent it using a simple analytical formula.

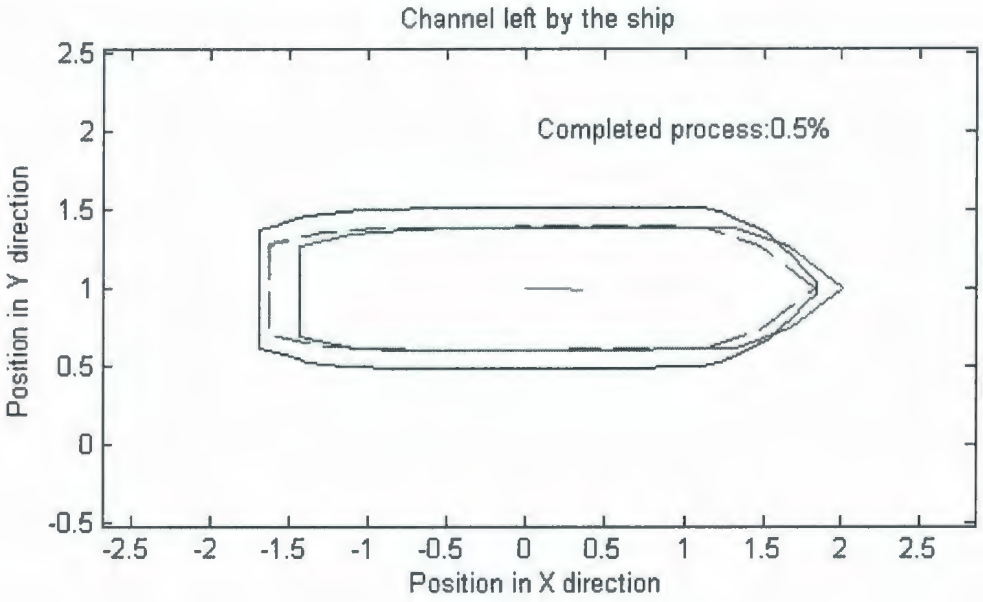

Figure 10.16 Snapshot of the simulation of Terry Fox model prescribed arbitrary manoeuvre using IHI model software

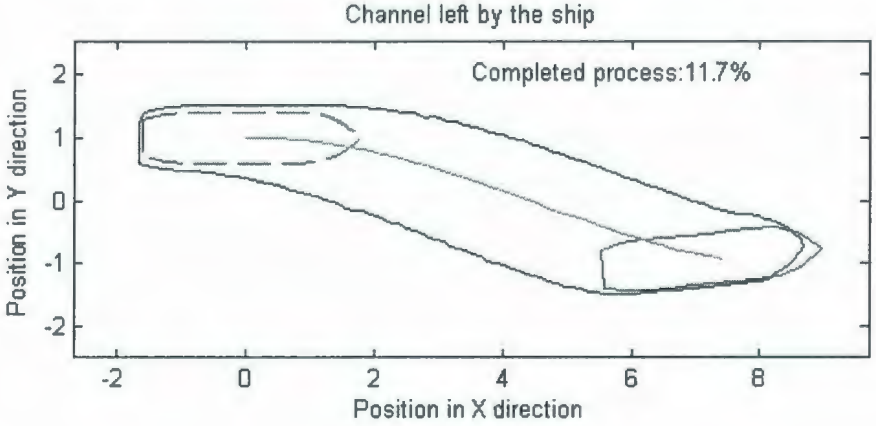

Figure 10.17 Snapshot of the simulation of Terry Fox model prescribed arbitrary manoeuvre using IHI model software

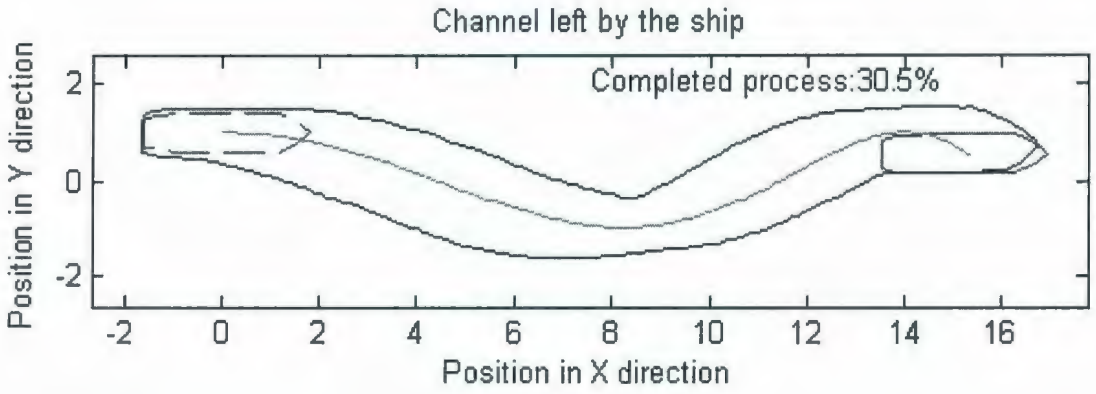

Figure 10.18 Snapshot of the simulation of Terry Fox model prescribed arbitrary manoeuvre using IHI model software

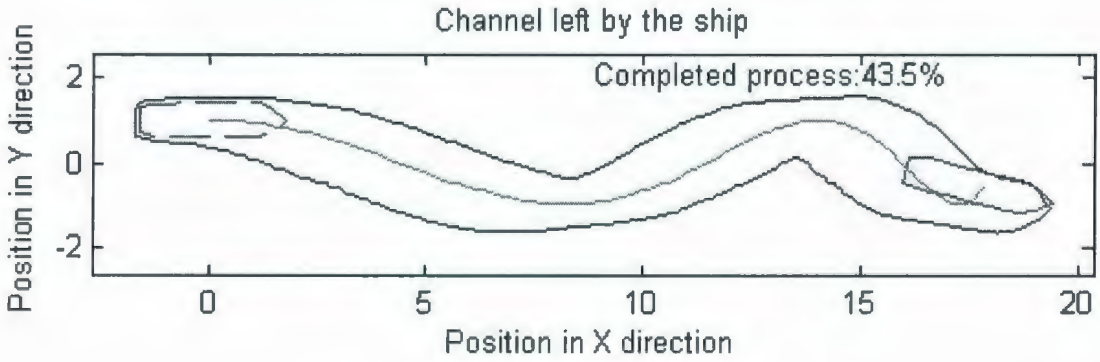

Figure 10.19 Snapshot of the simulation of Terry Fox model prescribed arbitrary manoeuvre using IHI model software

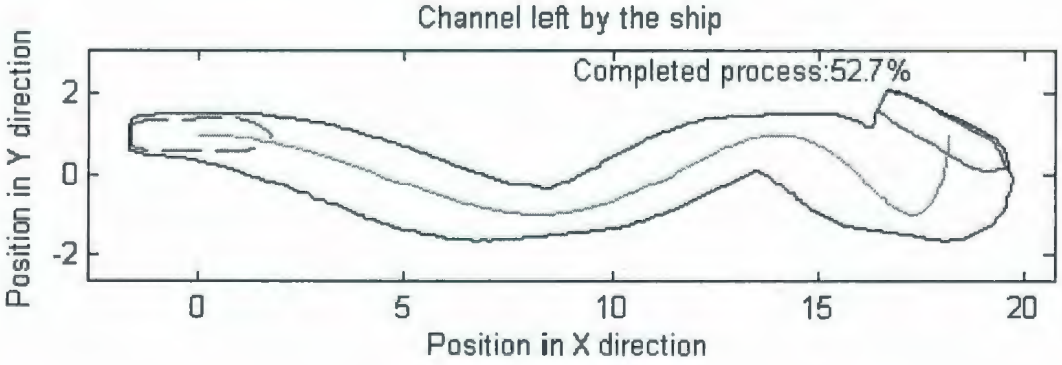

Figure 10.20 Snapshot of the simulation of Terry Fox model prescribed arbitrary manoeuvre using IHI model software

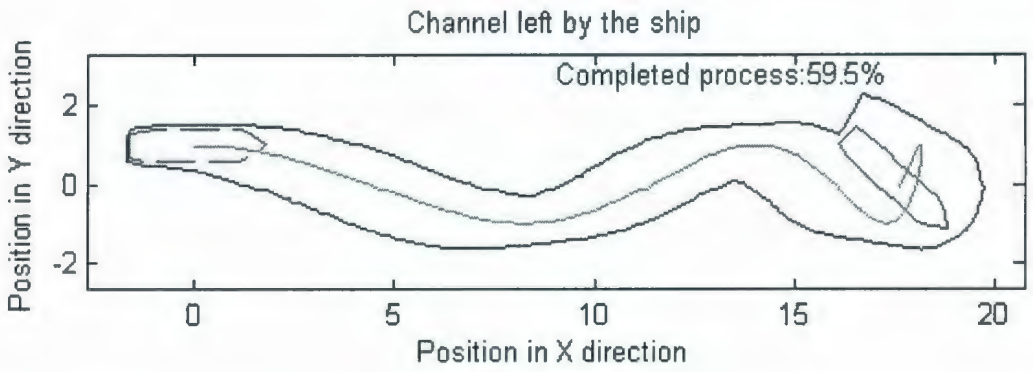

Figure 10.21 Snapshot of the simulation of Terry Fox model prescribed arbitrary manoeuvre using IHI model software

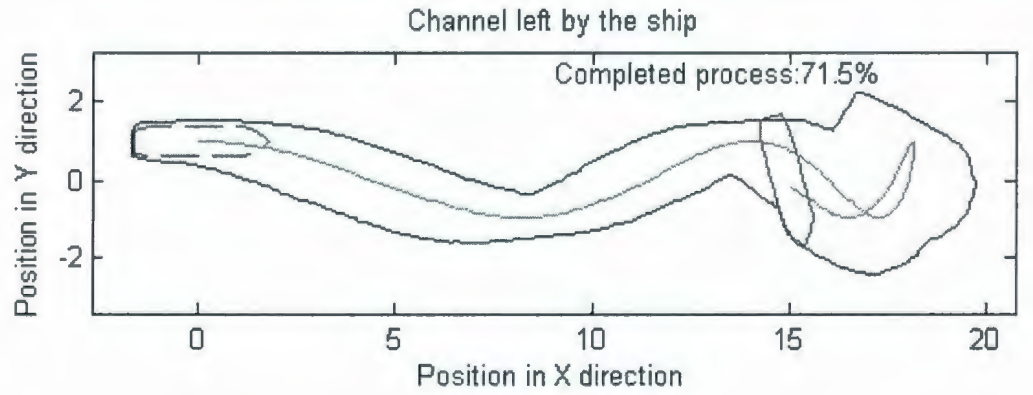

Figure 10.22 Snapshot of the simulation of Terry Fox model prescribed arbitrary manoeuvre using IHI model software

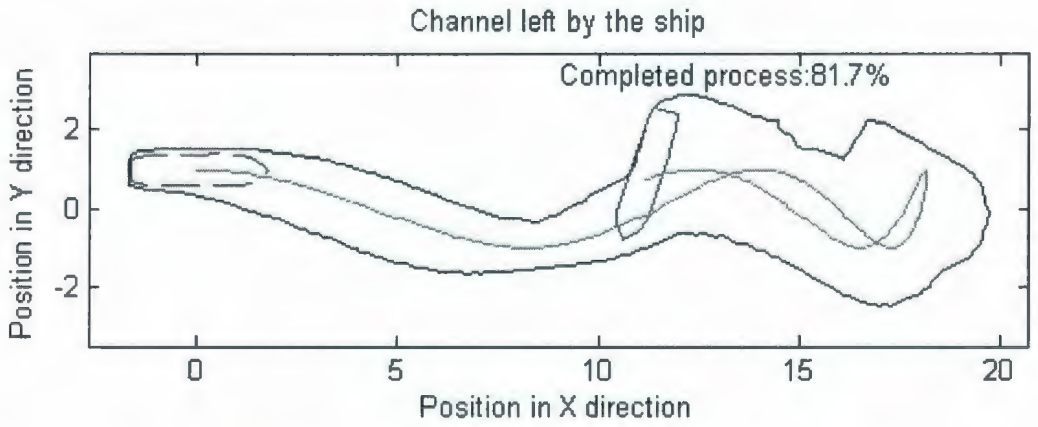

Figure 10.23 Snapshot of the simulation of Terry Fox model prescribed arbitrary manoeuvre using IHI model software

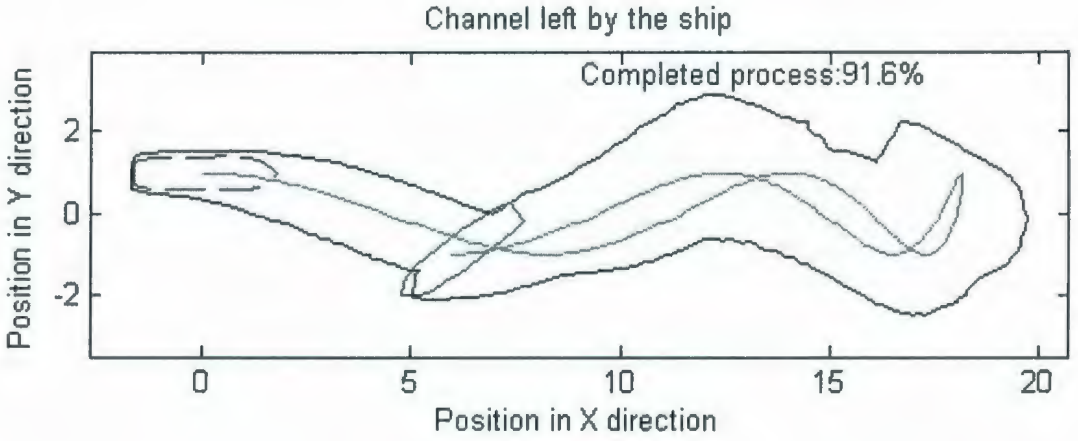

Figure 10.24 Snapshot of the simulation of Terry Fox model prescribed arbitrary manoeuvre using IHI model software

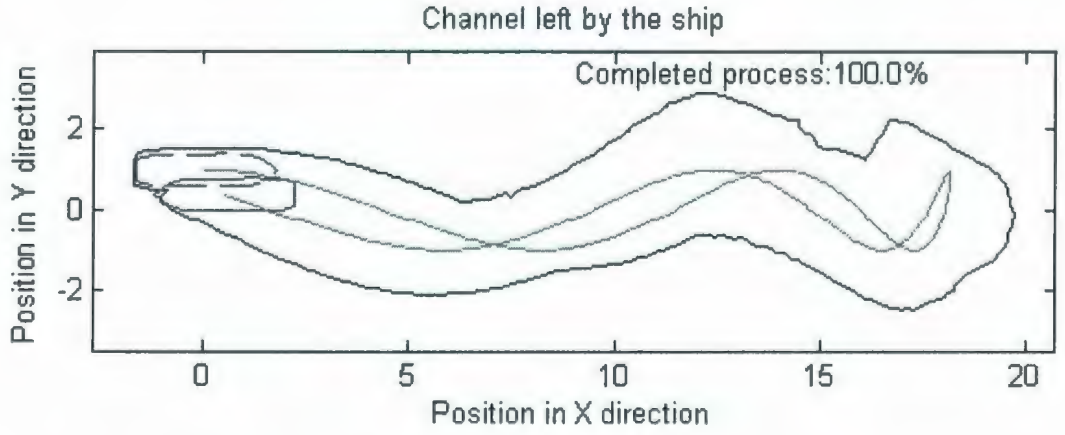

Figure 10.25 Snapshot of the simulation of Terry Fox model prescribed arbitrary manoeuvre using IHI model software

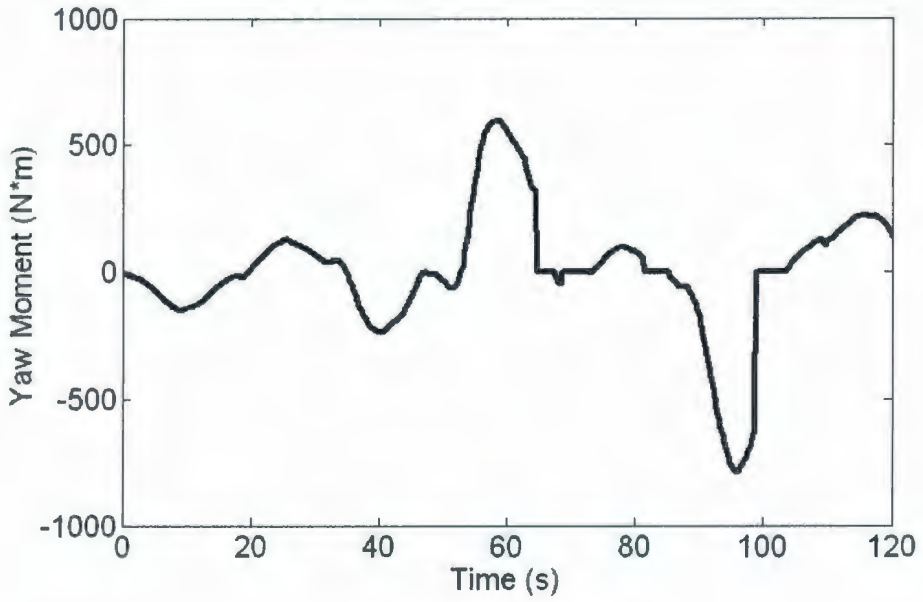

Figure 10.26 Yaw moment in the prescribed arbitrary manoeuvre of Terry Fox model in 40 mm – 31.5 kPa ice

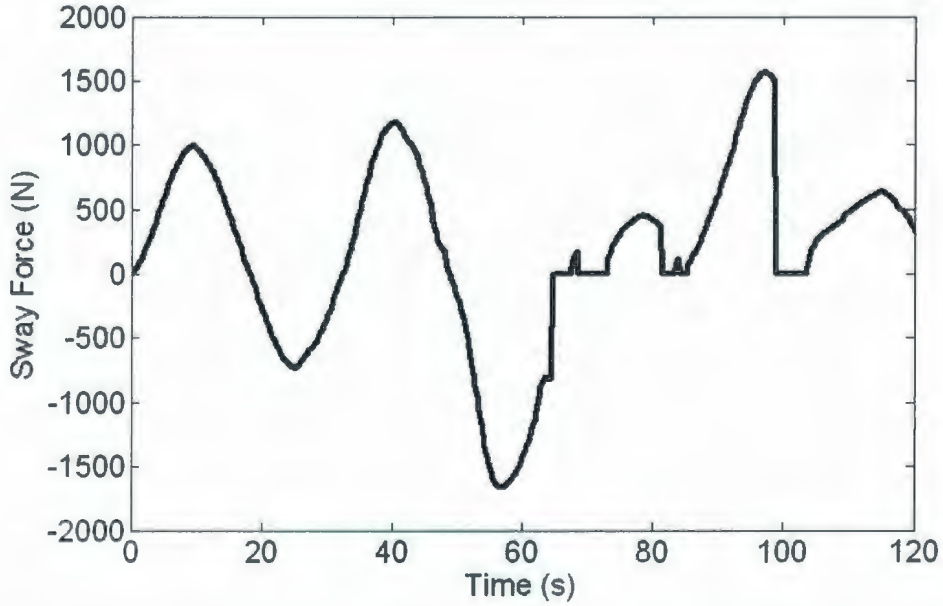

Figure 10.27 Sway Force in the prescribed arbitrary manoeuvre of Terry Fox model in 40 mm – 31.5 kPa ice

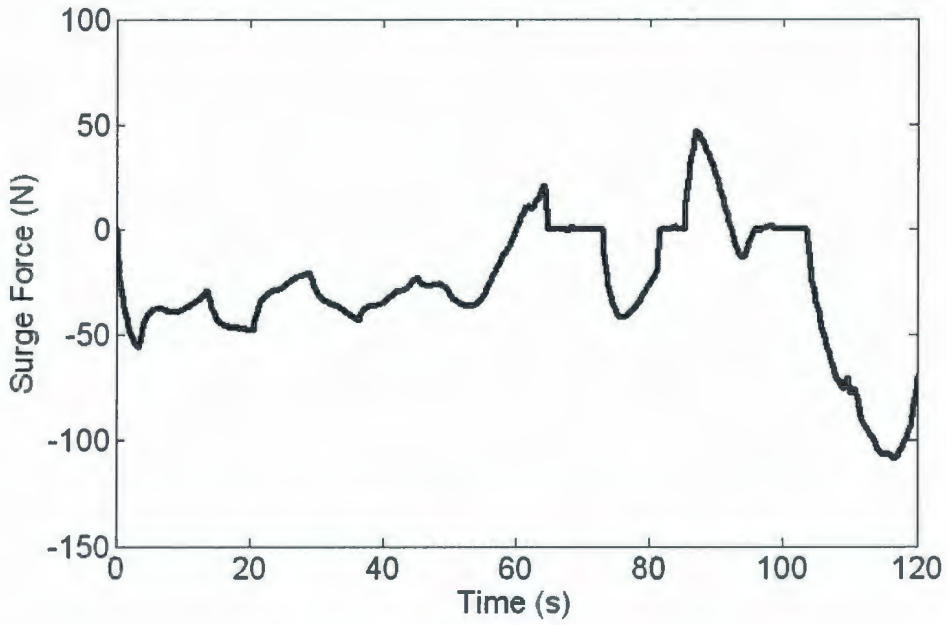

Figure 10.28 Surge Force in the arbitrary manoeuvre of Terry Fox Model in 40 mm – 31.5 kPa ice

The above simulation examples proved that IHI model could comparatively well model the physical process of ship-ice interaction: During the ship manoeuvring in level ice, not only does the bow directly contact the unbroken level ice, the aft-hull may also directly break ice. The ice-hull contact area directly affects the ice force distribution on the hull, which determines the final global forces on the whole ship for its manoeuvring motions. The IHI model firstly calculate the ice-hull contact area based on the ship motion and current ice edge, then the ice caused loads on the hull are calculated using some corresponding ice-structure interaction mechanic theories. The complicated manoeuvre is impossible to be modeled by a simple analytical formula. The IHI model fairly well solves that problem.

It should be noted that the ship motions were prescribed and the pivot point of the ship was always fixed at its mass centre in the above simulations. For the free-running ship manoeuvres, the pivot point is changeable and may possibly move farther away from the ship's mass centre during the manoeuvring, which results that some modifications may be needed when applying the conclusions provided in this chapter in the real ship navigations. The mathematical modeling of the free-running ship navigation in ice is beyond the present research scope in this thesis and is not discussed in details here.

The movies for the all above simulations are provided on a CD attached to this thesis as the Appendix B.

10.6 Summary and Conclusions

10.6.1 Summary

Backing Manoeuvre

One simplified and idealized bare stern of Terry Fox icebreaker breaking ice process was simulated using IHI model without considering effects from the propellers, rudder or other appendages. The successful simulation showed the IHI model could work well in the specific manoeuvre, backing manoeuvre.

Pure Yaw Manoeuvre and Pure Sway Manoeuvre

Two typical prescribed manoeuvres in PMM model tests, pure yaw run and pure sway run, for the Terry Fox Icebreaker were simulated. In the pure yaw run, the channel width nearly keeps constant, while the channel width varies cyclically with the large amplitude in pure sway run. The simulated yaw moment curves for the two manoeuvres both roughly show a more or less sinusoidal shape, but the force levels are different and the force causes are also different: In pure yaw run, only the bow directly contacts the ice edge, while in the pure sway run, most of one side of the hull from the bow to the stern directly contacts the ice edge and the icebreaking at stern contributes to additional yaw moment on the hull. The sway force during the pure yaw run is much smaller than that in the pure sway run.

"Star" Manoeuvre

Two prescribed "Star" manoeuvres, "Star" manoeuvre with small radius arcs and "Star" manoeuvre with big radius arcs, were simulated using IHI model software. In the small star manoeuvres, the former channel left by the hull affects the late ice-hull contact and the global ice forces on the hull kept changing. In the big manoeuvre, within each arc of big star manoeuvre, the global forces on the hull kept constant and the whole manoeuvre looks like a combination of three independent constant radius runs. The yaw moment in small star manoeuvre is bigger than big star manoeuvre. There is a balance point between the required ship manoeuvring area and the ship's turning ability. The mathematical simulation

using IHI model can provide a theoretical guidance for the ship operator. The simulation also shows the model's potentials to implemented into a ship navigation training simulator to simulate an actual "Star" manoeuvres.

Arbitrary Manoeuvre

A prescribed arbitrary manoeuvre was simulated using IHI model to show the model's ability to simulate arbitrary manoeuvres. The simulation examples prove that IHI model can comparatively well model the physical process of ship breaking ice. A very complicated manoeuvre is impossible to be represented by a simple analytical formula. The developed IHI model satisfactorily solves that problem through calculating the ice-hull contact area based on the ship motion and current ice edge in time domain and tracking the ship motion in a housing keep method.

10.6.2 Conclusions

Through simulating several typical model ship manoeuvres using IHI model software, the IHI model was further checked and the model's accuracy and universality in real-time simulating the ship's any manoeuvres in ice were verified. Some general conclusions on ship's manoeuvrability in ice were drawn, which is of great values for steering the ship in ice and mathematically modeling ship-ice interaction. Several curves of ice loads in the ship prescribed manoeuvres were

provided, which are also the important evidences for the model's accuracy through comparing the experimental data. Some clues for future more refinements on IHI model were obtained.

It was proved that the IHI model can satisfy the requirements of some real-time ship navigation simulators like the CMS training simulator: the model favourably predicts the global ice forces on the hull during ship's arbitrary manoeuvres required by the simulator with good numerical efficiency and universality.

Chapter 11 Summary and Recommendations

This thesis provided a new physically based mathematical ice-hull force distribution model as the key ice component of the real-time ship navigation in ice simulator, which is also a basic and necessary step towards the final target of the IOT's whole research: a general model that can reliably simulate the ship's any manoeuvres in any ice conditions.

The technical contributions to mathematically modeling ship manoeuvring in ice in this doctoral research were listed as the following.

11.1 Contributions

1. The requirements of ice-hull interaction model applied in navigation simulators, training simulators or auto pilot systems were firstly summarized as **Simulation Accuracy**, **Numerical Efficiency** and **Universality**, which provides standards for evaluating the existing mathematical models and guidance for developing new mathematical models.

2. It was the first time to give a comprehensive literature review on mathematically modeling ship manoeuvres in ice, especially in level ice. The

existing typical mathematical models on ship navigation in ice were comprehensively summarized and critically studied.

3. A new mathematical ice-hull interaction (IHI) model that can be applied in real-time simulations of the ship's arbitrary manoeuvres in ice is developed. Using analytical approach with numerical implementation, the model directly mathematically models the physical ice-hull interaction process with good numerically efficiency. In the model, the forces are calculated at each new increment of any prescribed motion based on the ice-hull contact area, which makes the model to own the capacity to respond to arbitrary control inputs and hence arbitrary manoeuvres in ice.

4. The hull-ice contact area was calculated based on the ship motion and ice edge in the time domain and the channel was tracked using a simple house keeping method, based on which the ice forces on the hull are calculated. A multi-failure ice model considering bending failure, shear failure and crushing failure was adopted to calculate the ice failures along the waterline of the hull from the bow to the stern in quantitatively for the first time. Both viscous and inertial effects are incorporated into the clearing force. It is the first time to use mechanics theories to calculate the ice clearing loads in the ship turning case, which is feasible because of the extensive experimental data, both numerical and visual, that is available for validation at IOT.

5. A stand-alone 'i' numerical simulation software using MatLab language was developed which provided an independent numerical simulation platform for developing and benchmarking the desired IHI model. It simulated ice forces on the ship due to user-specified motions. The captive PMM model test runs can be realistically simulated using the software. The software is of high flexibility and friendly data exchange interface, which makes it easy to code the refined IHI model or implement the IHI model into other ship navigation simulators.

6. The benchmark of the IHI model was carried out based on two PMM test series, Terry Fox Model and R-Class Model, carried out in IOT. The Izumiyama's tests were adopted to check the ice load distribution on the hull. It is the first time to adopt such an extensive set of experimental data for the mathematical model's validation with so many details, which enables the separate force components validations and parametric validation for the mathematical model.

7. The ship-ice interaction was investigated through parametric analysis and specific manoeuvre simulations based on the developed IHI model, which also serves as the verification of the IHI model's accuracy and universality. The effects to the ice force distribution and global ices on the hull from the ship motions, ice properties and ship geometries were studied based on IHI model simulations and experiments. Also, the ice failure modes considering breaking

failure, shear failure and crushing failure during the hull breaking the level ice are studied using the multi-model ice failure model adopted in IHI model. Several prescribed typical ship manoeuvres like backing manoeuvre, "Star" manoeuvre, pure yaw manoeuvre, pure sway manoeuvre, and arbitrary manoeuvres were simulated and studied using IHI model. Such a detailed parametric analysis on ice-hull interaction has not previously been conducted. Some general conclusions and comprehensive views on the ship manoeuvring in ice were drawn, which was of high value for the operators in steering ship in ice. Some typical curves of ice loads due to ship's motions, ice properties and hull geometries were obtained, which can also be regarded as the important evidences for the IHI model's correction and accuracy.

11.2 Summary and Conclusions

1. The requirements for mathematical modeling ice-hull interaction applied in training simulators, navigation simulators or auto pilot systems can be summarized as: **Simulation accuracy**: the model should be able to correctly 'feel' the ship's response; **Numerical efficiency**: the model should be able to estimate the ice-force on the hull within the short time; **Universality**: an ideal model should be able to simulate the ship's any maneuvers in ice.

2. A literature review on modeling ship manoeuvres in ice, especially in level ice, was made in order to provide the research basis for modeling ice-hull interaction for the real-time simulations: Lewis' model, Spencer's model, Milano's model, Kotras et al's model and Lindqvist's model are for ice resistance only. Lindstrom's model considered only the bending failure of the ice. Canmar's model is restricted to constant radius turns. Menon's time domain model and Williams and Waclawek's model are both limited in accuracy and universality. The high hardware requirements and long calculation time present a large challenge for applying FEM model and DEM model in real-time simulations. It was shown that none of the existing models can completely satisfy the requirements of real-time ship navigation in ice simulations.

3. A new mathematical ice-hull interaction (IHI) model applied in real-time simulations of the ship's arbitrary manoeuvres in ice was developed: The model adopted the analytical approach with numerical implementation. It was built on a detailed mechanics analysis of the ice-hull interaction and considered the breaking, buoyancy and clearing force components using the relevant theories. The model firstly calculates the hull-ice contact area based on the ship motion and current ice edge at each calculation step, based on which the ice forces on the hull are calculated. A multi-failure ice model was adopted to model the ice failure process along the waterline of the hull from the bow to

the stern. A flat-plate model was used for the buoyancy force calculation and the volume of ice covering the wet surface of the model was calculated in time domain. Both viscous and inertial effects were incorporated into the clearing force computation. The whole hull is divided into several small segments. The ice forces on each segment are theoretically calculated separately and vectorially added together to get the global force on the whole hull. The adoption of the analytical approach yields a short calculation time, which makes the model very suitable for real-time simulations. Since the forces are calculated at each new increment of any prescribed motion, the resulting simulation has the capacity to respond to arbitrary controlled inputs and hence arbitrary manoeuvres. The IHI model records the broken channel created by the ship in the prevailing arbitrary ship manoeuvres.

4. The IHI model in this thesis was coded as a stand-alone "i" simulation software using MatLab. The IHI model software is designed as a Visual Calculation Program (**VCP**). During the calculation process, the users can instantaneously watch the simulation process and check the simulation results, such as ship's motion, ice channel and calculated ice forces on the hull, surge force, sway force and yaw moment. The current version of the IHI software can simulate the prescribed ship maneuvers used in standard PMM ship model tests: i.e., advancing or backing runs, constant radius turning, pure yaw, pure sway, "Star" manoeuvres, arbitrary manoeuvres, etc.

5. The IHI model was benchmarked using the IOT PMM Terry Fox model test series. The resistance runs including level ice and pre-sawn ice conditions and constant radius runs, 10 m and 50 m radius, were selected and compared with IHI model simulations. The validity of the IHI model was assessed through comparing its predictions to measurements from the model tests including ice-hull contact, channel width, and global ice loads on the hull. The comparison results showed the IHI model fairly well predicted the Terry Fox model tests.

6. IHI model was benchmarked using IOT PMM R-Class model test series. Besides the resistance tests and constant radius tests, two sinusoidal test runs, in 30 mm and 50 mm thick ice sheet, were also selected for the benchmark in order to showcase the IHI model's capability in simulating ship's arbitrary manoeuvres. Besides the level ice and pre-sawn ice, the turning runs in broken ice were also included. Comparing the test results and simulation results showed that the IHI model fairly satisfactorily predicted the R-Class Icebreaker test runs. The jamming at the shoulder and drift angle effects to global ice forces are studied: The jamming at shoulder may result an increase of ice resistance through ice-hull friction; The drift angle effectively affects the global ice forces on the hull, which should be paid more attention during the tests.

7. The tests by Izumiyama et al. (1998, 1999, 2001, 2005) were adopted for benchmark the ice force distributions on the hull calculated by IHI model. Two type of runs, straight going up run and turning runs, were selected for the benchmark. The simulations and tests showed coincident in qualitative: In the resistance runs, the high ice load distribution acting on the bow area and low load acting on the aft-body. The ice load level increases as the model speed increases. In the turning runs, the big ice load occurs in the aft-body in the outside of the turn. With the drift angle increase, the higher ice load acts on the outside of the aft-body during the turning runs. The above phenomena can be explained by ship-ice contact: The aft-body doesn't directly contact the ice edge due to a wider channel created by the bow in the resistance runs while the aft-body may directly contact the ice edge during the turning runs.

8. Investigation on ice-hull interaction was carried out based on the IHI model simulations and the experiments, which also serves as the verification of accuracy and universality of the IHI model. The whole content consists of two parts, parametric analysis and specific manoeuvre simulations.

Parametric Analysis: Some general conclusions and comprehensive views on the ship manoeuvring in ice were obtained: It was theoretical confirmed that the critical flare angles that shear failure happens before the bending failure were all in excess of 80 degrees for most ice. Compared to the pre-sawn ice

condition, the ice force increase in level ice due to the ice force thickness increase is more due to the included the breaking ice components besides the buoyancy force components and clearing force component. The ice-hull friction force didn't cause a large ice yaw moment during the ship turning process. In general, the channel width vs. drift angle curve shows a "V" shape for the constant radius runs. With smaller turning radius, the shape of "V" is more obviously affected by the stern's breaking the ice sheet. When a ship turns with a small radius the stern always breaks the ice with negative drift angle, while a large turning radius run, a very small drift angle will cause the stern to break the ice. The ice yaw moment increases with the increase of the ship's tangential velocity during its turning process. The smaller turning radius runs own steeper sloping yaw moment vs. ship velocity curves. For the turning runs with constant ship tangential velocity, the yaw moment approximately linearly increases with the raw rate in the ship turning cases. With increase of the waterline length to waterline beam ratio, the channel width left by the hull and the yaw moment required for the same constant radius turning both increase. The yaw moment and channel with decreases with the increase of the turning radius to waterline length ratio for the same turning radius runs.

Specific Manoeuvre Simulations: One simplified and idealized Terry Fox Icebreaker stern breaking ice was successfully simulated using IHI model. Two typical manoeuvres in PMM model tests, pure yaw run and pure sway run,

were simulated and compared: In the pure yaw run, the channel width nearly keeps constant, while the channel width varies cyclically with the large amplitude in pure sway run. Compared to the pure sway force, the ice yaw moment on the hull in the pure yaw run is much smaller. In pure yaw run, only the bow contacts the ice edge and the aft-body of the hull may also do so only at some abrupt turning part. In the pure sway run, most of one side of the hull contacts the ice edge and the icebreaking at stern contributes to additional yaw moment on the hull. The actual "Star" manoeuvres were approximately represented using three connected arcs of the constant radius turning and simulated using IHI model software. The prescribed arbitrary manoeuvre was simulated using the IHI model to show the model's ability to simulate arbitrary manoeuvres. The simulations showed the IHI model correctly "feels" the ship's manoeuvres with different ice-hull contacts.

11.3 Recommendations

Simplifications in the problem treatment were made to make the problem solvable analytically, however, these simplifications led to errors in the IHI model predictions. Further refinements of the current model are needed to improve the model's accuracy. The IHI model integrated many existing research achievements on ice-hull interaction mechanics. During that integration process, some errors are inevitably created. Those errors can be checked out and eliminated based on the

more detailed benchmark and calibration using additional experimental data, which also provides the clues for further refinements of the IHI model.

11.3.1 Refinement of IHI Model

The refinements of IHI model may include paying more attention on the details of ice-hull interaction physical process, ship geometries and ship motions and adopting more advanced theories may be adopted to more detailed and reliably model the physical process of ice hull interaction.

- The complete sliding process for all ice cusps captured and calculated considering more details.
- Ice jamming around the hull shoulder. More physical details of the ice failure process when the ice acting on the vertical surface or the surfaces with large sloping angles.
- The coupling effects between those force components which are assumed independent at present model, especially for the ship with high velocity.
- Interaction between curve surface and ice.
- The challenges of modelling pack ice, rubble ice and also snow cover would have to be addressed for the future refinements of IHI model.
- Besides the ship's motion in horizontal plane, the ship's motions in vertical plane, heave, pitch and roll, especially under the thick ice condition.

- The effects from hull appendages, rudders, propellers, etc. to the ice forces on the hull.

11.3.2 Benchmark of IHI Model

The refined IHI model should be benchmarked and calibrated with more details based on more model ship tests and full-scale trials:

- Besides the ice force data, more experimental data with the details of ice-hull interaction, channel, ice failure process and sliding process.
- The Captive model tests on the ice force distribution on the hull depending on PMM system in IOT.
- More experimental data from the specific ship maneuvers.
- Benchmark of IHI model depending on the data from the free-running tests.
- Benchmarking the IHI model using the data from the full-scale trials.

Publications

1 **Liu Jiancheng,** Lau, M, and Williams F.M., 2008, "Numerical Implementation and Benchmark of Ice-Hull Interaction Model for Ship Manoeuvring Simulations", **Proceedings of the 19th IAHR International Symposium on Ice**, Vancouver, B.C., Canada, pp215~226.

2 **Liu Jiancheng,** Lau, M, and Williams F.M., 2007, "Mathematical Modeling of Ice-Hull Interaction for Real Time Simulation of Ship Manoeuvring in Level Ice", **Institute for Ocean Technology (IOT) Report: LM-2007-06**.

3 **Liu Jiancheng**, Lau, M, and Williams F.M., 2007, "Software of IHI Model for Simulating Ship Manoeuvring in Level Ice", **Institute for Ocean Technology (IOT) Report: LM-2007-07.**

4 **Liu Jiancheng**, Lau M., Williams F.M., 2006, Mathematical Modeling of Ice-Hull Interaction for Ship Maneuvering in Ice Simulations, **Proceedings of the 7th International Conference and Exhibition on Performance of Ships and Structures in Ice,** Banff, Alberta, Canada (Icetech06_126_R0, CD).

5 Lau M., **Liu Jiancheng**, Derradji A., Williams F.M., 2004, Preliminary Results of Ship Maneuvering in Ice Experiments Using a Planar Motion Mechanism, **Proceedings of the 17th International IAHR Symposium on Ice, Saint Petersburg, Russia,** pp479-487.

6 **Liu Jiancheng**, Gu Yongning, Wang Zili, Ma Yande, Liu Wenmin, 2001, Fatigue assessment of FPSO. **Ocean Engineering,** Vol. 119(12), pp 50~55.

7 **Liu Jiancheng,** Li Runpei, Gu Yongning, Zhang Jianbo, 2000, Feasibility Study on Simply Equipped Single Point Mooring System. **Journal of Shanghai Jiao Tong University,** Vol 134(1), pp132~136.

8 **Liu Jiancheng**, Gu Yongning. 2000, A Study on Stress Concentration at Hatch Corner for Ship with Large Openings. **Ship Engineering,** No. 6, pp6~12.

9 **Liu Jiancheng**, Gu Yongning, 2000, A decoupling and reverse method of multi-point ice-force measurement from the response of the platform. **Ocean Engineering,** Vol. 118(12), pp7~12.

10 **Liu Jiancheng**, Gu Yongning, 2000, Stress Concentration at Hatch Corner for Ship with Large Opening and the Engineering Solutions, **Proceedings of 1st National Conference on Naval Architecture and Ocean Engineering,** Shanghai Jiao Tong University, P.R. China, August, pp300~308.

Reference

Abkowitz, M., and Liu, G. (1988). Measurement of Ship Resistance, Powering, and Maneuvering Coefficients from Simple Trials during a Regular Voyage, *Transactions of SNAME*, Vol96, pp. 97-128.

Aboulazm, A. (1989). Ship Resistance in Ice Floe Covered Water (Pack ice). *PhD Thesis*, Faculty of Engineering and Applied Science, Memorial University of Newfoundland, St. John's, Canada.

Aboulazm, A., and Muggeridge, D.B. (1989). Analytical Investigation of Ship Resistance in Broken or Pack Ice. *Proceedings of 18th International Conference on Offshore Mechanics and Arctic Engineering (OMAE'89)*, New York, Vol. IV, pp. 359-363.

Akinturk, A., Jones, S., Moores, C., and Bell, J. (2003). Measuring ice loading on podded propellers system. *Proceedings of the 22nd International Conference Offshore Mechanics and Arctic Engineering*, Cancun, Mexico (CD-no page numbers).

Akinturk, A., Jones, S., Duffy, D., and Rowell, B. (2004a). Ice Loads on azimuthing podded propulsors. *Proceedings of the 23rd International Conference*

on Offshore Mechanics and Arctic Engineering (OMAE'04), New York (CD-no page numbers).

Akinturk, A., Jones, S., Duffy, D., and Rowell, B. (2004b). Measuring Podded Propulsor Performance in Ice. *Proceedings of the 1st International Conference on Technological Advances in Podded Propulsion*, School of Marine Science and Technology, University of Newcastle Upon Tyne, UK, pp. 187-198.

Akexander, I.B., Sergey, V.K., and Shankar, U.B. (1997). Application of an Empirical-Statistical Model of Ship Motion in Ice to New Types of Icebreakers and Ships. *Proceedings of the 16th International Conference on Offshore Mechanics and Arctic Engineering/14th International Conference on Port and Ocean Engineering under Arctic Conditions (Joint OMAE/POAC Conference)*, Vol. IV, pp. 43-49.

Arunachalam, V., and Muggeridge, D.B. (1993). Ice Pressure on Vertical and Sloping Structures through Dimensional Analysis and Similarity Theory. *Cold Regions Science and Technology*, Vol. 21, pp. 231-245.

Black, L. (1958). Relative Strength of Plates on Elastic Foundation. *Transactions of the E.I.C*, Vol. 2, pp. 129-131.

Blevins, R. (1979). Formulas for Natural Frequency and Mode Shape. *Copyright by Van Nostrand Reinhold Company*, Inc., New York, USA.

Bjerkelund, C. (1986). Level Ice Physical Properties in support of the M.V. ARCTIC Performance Trials in Baffin Bay and Admiralty Inlet. Norland Science and Engineering Ltd., *TDC Report 6671.*

Bruneau, S. (1996). Development of a First-Year Ridge Load Model. *PhD Dissertation*, Faculty of Engineering and Applied Science, Memorial University of Newfoundland, St. John's, Canada.

Cammaert, A., and Muggeridge, D. (1988). Ice Interaction with Offshore Structures. Van Nostrand Reinhold, New York, USA.

Carter, D. (1983). Ship resistance to continuous motion in level ice. *Transport Canada Repo*rt, TP-3679E.

Colbourne, B. (1987a). A Three Components Method of Analyzing Icebreaking Resistance. *Institute for Ocean Technology (IOT) Report*: IR-1989-07.

Colbourne, B. (1987b). Test in Ice of a 1:8 Scale Model of the CCG R-Class Hull. *Institute for Ocean Technology (IOT) Report: TR-AVR-07.*

Colbourne, B., and Lever, J. (1992). Development of a Component-Based Scaling System for Ship-Ice Model Tests. *Journal of Ship Research*, Vol. 36, No. 1, pp. 77-87.

Coleman, H.W. and Steele, W.G. (1998). Experimentation and Uncertainty Analysis for Engineers. 2nd edition, John Wiley & Sons publications, New York.

Cowpes, B. (1991). Resistance and propulsive performance trials of the MV Terry Fox and MV Ikaluk in level ice. *Report by Fleet Technology Limited*, prepared for the Transportation Development Centre, Policy and Coordination Group, Transport Canada.

Crago, W.A., Dix, P.J., and German, J.G. (1971). Model icebreaking experiments and their correlation with full-scale data. *Trans. RINA*, Vol. 113, pp. 83-108.

Croasdale, K. (1980). Ice Forces on Fixed, Rigid Structures. *Cold Regions Research and Engineering Laboratory Special Report*, No. 80-26.

Croasdale, K., Cammaert, A., and Metge, M. (1994). A Method for the Calculation of Sheet Ice Loads on Sloping Structures. *Proceedings of the 12th IAHR Symposium on Ice*, Trondheim, Norway, pp. 874-885.

Daley, C. (1984). Baffin – A Dynamic Ship-Ice Interaction Model. *Paper No.F, Ice Tech-84 Symposium*, Calgary, May, pp. F1-F8.

Daley, C. (1991). Ice Edge Contact - A Brittle Failure Process Model. *Acta Polytechnica Scandinavica*, Mechanical Engineering Series No. 100, Helsinki 1991, published by the Finnish Academy of Technology.

Daley, C., and Riska, K. (1990). Review of Ship-Ice Interaction Mechanics. *Report from Finnish-Canadian Joint Research Project No. 5, 'Ship Interaction with Actual Ice Conditions'*, Faculty of Mechanical Engineering, Helsinki University of Technology, Espoo, Finland.

Daley, C., Riska, K., and Smith, G. (1997). Ice forces and ship response during ramming and shoulder collisions: phase III: harmonization of polar ship rules. *Report of Memorial University of Newfoundland Ocean Engineering Research Centre,* LR-ICE-97001.

Daley, C., Tuhkuri, J., and Riska, K. (1998). The Role of Discrete Failure in Local Ice Loads. *Cold Regions Science and Technology,* Vol., 27, Issue 3, pp. 197-211.

Daley, C. (1999) Energy Based Ice Collision Forces. *Proceedings of 15th International Conference on Port and Ocean Engineering under Arctic Conditions (POAC'99),* Vol. 2, pp. 674-686.

Dempsey, J. (2000). Research Trends in Ice Mechanics. *International Journal of Solid and Structures,* Vol 37, pp. 131-153.

Derradji-Aount, A. (2003). Multi-surface Failure Criterion for Saline Ice in the Brittle Regime. *Cold Regions Science and Technology*, Vol. 36, pp. 47-70.

Derradji-Aount, A. (2004), A Method for Calculations of Uncertainty in Ice Tank Ship Resistance Testing, Proceedings of the 19th International Symposium on Sea Ice, Mombetsu, Japan, pp196~206

Derradji-Aount, A. (2005). Explicit FEA and Constitutive Modeling of Damage and Fracture in Polycrystalline Ice – Simulations of Ice Loads on Structures. *Proceedings of the 18th International Conference On Port and Ocean Engineering and Under Arctic Conditions (POAC'05),* Vol. 1, pp. 225-238.

Derradji-Aount, A., Moorses, C., and Stuckless, S. (2002). Terry Fox Resistance Test, The ITTC Experimental Uncertainty Analysis Initiative. *Institute for Ocean Technology (NRC/IOT) Report,* TR-2002-01.

Derradji-Aount, A., and Thiel, A. (2004a). Terry Fox Resistance Tests – Phase III (PMM) Testing ITTC Experimental Uncertainty Analysis Initiative. *Institute for Ocean Technology (NRC/IOT) Report,* TR-2004-05.

Derradji-Aount, A., Izumiyama, K., Yamaguchi, H., and Wilkman, G. (2004b). Experimental Uncertainty Analysis for Ice Tank Ship Resistance Experiments Using a Model for a Canadian Icebreaker Terry Fox. *Oceanic Engineering International,* Vol. 8, No. 2, pp. 49-68.

Edwards, R., Lewis, J., Wheaton, J., and Coburn, J. (1972). Full Scale and Mode Tests of a Great Lakes Icebreaker. *Transactions of the Society of Naval Architects and Marine Engineers (SNAME),* Vol. 80: pp. 203-231.

Edwards, R., Major, R., and Kim, J. (1976). Influence of Major Characteristics of Icebreaker Hull on Their Powering Requirements and Maneuverability in Ice. *Transactions of the Society of Naval Architects and Marine Engineers (SNAME),* Vol. 84: pp. 364-407.

Enkvist, E. (1972). On the Ice Resistance Encountered by Ships Operating in the Continuous Mode of Icebreaking. *The Swedish Academy of Engineering Science in Finland,* Report No. 24.

Enkvist, E. (1979). The ship-ice interaction. *Proceedings of the 5th International Conference on Port and Ocean Engineering under Arctic Conditions (POAC),* Vol.2, pp. 977-1002.

Envist, E., and Makinen, S. (1984). A Fine Grain Model Ice. *Proceedings of IAHR International Symposiums on Ice,* Hamburg, Germany, Vol. II, pp. 217-227.

Ettema, R., Sharifi, M.B., Geogakakos, K.P., and Stern, F. (1991). Chaos in continuous-model icebreaking. *Cold Regions Science and Technology,* Elsevier Science Publishers B. V., Amsterdam, pp. 131-144.

Fuglem, M., and Jordaan, I., (1999). Estimation of maximum bow force for arctic vessels. *Proceedings of IAHR Symposium on Ice,* Potsdam, New York, 1998, Ice in Surface Waters, Ed. H.T. Shen, Balkema, 2:947-955

Gagnon, R., and Molgaard, J. (1989). Crushing friction experiments on freshwater ice. *Proceedings IUTAM Symposium on Ice-Structure Interaction,* St. John's, Canada, pp. 405-421.

Goldstein, R.V., and Osipenko, N.M. (1989). Fracture Mechanics in Modeling of Icebreaking Capability of Ships. *10th International Conference on Port and Ocean Engineering under Arctic Conditions (POAC'89)*, Lulea, Sweden, pp. 33-43.

Hamza, H., and Shih, L.Y. (1989). Numerical Modeling of Pack Ice Interaction with Ships. *Institute for Ocean Technology (IOT) Report,* LR-1989-01.

Heinonen, J. (1999). Simulating Ridge keel Failure by Finite Element Method. *Proceedings of the 15th International Conference (POAC'99),* Vol. 1, Helsinki, pp. 956-963.

Heinonen, J. (2004). Constitutive Modeling of Ice Rubble in First-Year Ridge Keel. *Disseration for degree of Doctor of Technology*, Helsinki University of Technology, Espoo, Finland.

Hetenyi, M. (1974). Beams on Elastic Foundation, Theory with Application in the Fields of Civil and Mechancial Engineering. *University of Michigan Press and Simultaneously in Rexdale,* Canada, by John Wiley and Sons Canada.

Hoffmann, K. (1998). Ship Manoeuvring in Ice with the Planar Motion Mechanism R-Class Testing. *Institute for Ocean Technology (NRC/IOT) Report,* LM-1998-19.

Hopkins, M.A. (1994). On the Ridging of Intact Lead Ice. *Journal of Geophysical Research,* Vol. 99, 16351-16360.

Hopkins, M.A. (1998). Four Stages of Pressure Ridging. *Journal of Geophysical Research.* 103(C10): 21883-21891.

Hopkins, M.A., Daly, S.F., and Lever, J.H. (1996). Three-dimensional Simulation of River Ice Jams. *Proceedings of 8th International Specialty Conference Cold Regions Engineering,* Charlottesville, pp. 582-593.

Izumiyama, K., Wako, D., and Uto, S. (1998). Ice Force Distribution on a Flat Indentor. *Ice in Surface Waters,* Shen (ed.), Vol 2, Balkenma, Rotterdam, ISBN 90 54109718, pp. 917-922.

Izumiyama, K., Wako, D., and Uto, S. (1999). Ice Force Distribution Around a Ship Hull. *Proceedings of the 15th International Conference on Port and Ocean Engineering under Arctic Conditions (POAC'99),* Vol 2, pp. 707-716.

Izumiyama, K., Wako, D., and Uto, S. (2001). Ice Pressure Acting Over a Model Ship Hull. *Proceedings of the 16th International Confernece on Port and Ocean Engineering under Arctic Conditions (POAC'01),* Vol. 2, pp. 793-802.

Izumiyama, K., Wako, D., Shimoda, H., and Uto, S. (2005). Ice Load Measurement on a Model Ship Hull. *Proceedings of the 18th International Confernece on Port and Ocean Engineering under Arctic Conditions (POAC'05),* Potsdam, USA, Vol. 2, pp. 635-646.

Jansson, J-E. (1956a). Ice-breakers and their design. *Pt.I. European Shipbuilding*, No. 5, pp. 112-128.

Jansson, J-E. (1956b). Ice-breakers and their design. *Pt.II. European Shipbuilding,* No. 6, pp. 143-151.

Jebaraj, C., Swamidas, A.S.J., and Jones, S.J. (1988). Dynamic of Ship Ice Interaction. *Institute for Ocean Technology (IOT) Report*, LM-AVR-28.

Jebaraj, C., Swamidas, A.S.J., and Shih L.Y. (1989). Numerical Modeling of Ship Ice Interaction. *Institute for Ocean Technology (IOT) Report*, IR-1989-02.

Johnston, M., Timco, G.W., Frederking, R., and Miles, M. (2007). Measuring Global Impact Forces on the CCGS Terry Fox with an Inertial Measurement System called MOTAN. *Cold Regions Science and Technology* (Article in Press).

Jones, J. (1987). Ice Tank Test Procedure at the Institute for Marine Dynamics. *Institute for Ocean Technology (NRC/IOT) Report*, LM-AVR-20.

Jones, J. (1989). A review of ship performance in level ice. *Proceedings of 18th International Conference on Offshore Mechanics and Arctic Engineering (OMAE'89)*, New York, Vol. IV, pp. 325-342.

Jones, J. (2004). Ships in Ice – A Review. *25th Symposium on Naval Hydrodynamics,* St. John's, Canada, Vol (2), pp. 1-18.

Jones, J. (2005). Resistance and Propulsion Model Test of USCGC Healy (Model 546) in Ice. *Institute for Ocean Technology (NRC/IOT) Report*, LM-2005-02.

Jones, J., and Murdey, D. (2000). Resistance in Ice. *Institute for Ocean Technology Standard Test Method Report*, 42-8595-2/TM7, Institute for Marine Dynamics, St. John's, Newfoundland, Canada.

Jones, J., and Moores, C. (2002). Resistance Tests in Ice with the USCGC Healy. *Proceedings of the 16th IAHR International Symposiums on Ice,* Dunedin, New Zealand, pp. 410-415.

Jones, J., Spencer, D., and McKenna, R. (1994). Icebreaking Performance from Model Scale Tests. *International Conference and Exhibition on Performance of Ships and Structures in Ice (ICETECH'94),* pp. H-1-H19.

Jones, J., and Lau, M. (2006). Propulsion and Manoeuvring Model Tests of the USCGC Healy in Ice and Correlation with Full-Scale. *International Conference and Exhibition on Performance of Ships and Structures in Ice (ICETECH'06),* Banff, Canada (CD).

Jordaan, I. (1987). Probabilistic Analysis of Environmental Data for Design of Fixed and Mobile Arctic Offshore Structures, Reliability and Risk Analysis in Civil Engineering. *Proceedings of the 5th International Conference on Application of Statistics and Probability in Soil and Structural Engineering (ICASP),* Vol. 2., Vancouver, BC, pp. 1130-1137.

Jordaan, I. (2001). Ice Mechanics of Ice-Structure Interaction. *Engineering Fracture Mechanics,* Vol. 68, pp. 1923-1960.

Jordaan, I., and McKenna, R. (1991). Processes of deformation and fracture of ice in compression. *Proceedings IUTAM-IAHR Symposium on Ice-Structure Interaction,* St. John's, Canada, pp. 283-309

Jordaan, I., Fuglem, M., and Matskevitch, D. (1996). Pressure-area relationships and the calculation of global ice forces. *Proceedings of 13th IAHR Symposium on Ice,* Beijing, China, Vol. 1, pp. 166-175.

Kamarainen, J. (1994). On the Speed Dependence of the Ice Submerging Resistance in Level Ice. *Proceedings of the 11th International Offshore and Polar Engineering Conference under Arctic Conditions (POAC'94),* Japan, pp. 578-583.

Kashtelyan, V. (1960). Priblizhennoye Opredelenive Usiliy, Razrushyayushchikh Ledyanoy Pokrov (An Approximate Determination of Forces which Breaks up a Floating Ice Plate). *Problemy Arktiki I Antarktiki*, Yyp. 5, pp. 31-37.

Kashtelyan, V., Poznjak, I., and Ryvlin, A. (1968). Ice Resistance to Motion of a Ship. *Translation, Sudostroenie, Leningrad,* Translation by Marine Computer Application Corp.

Kayo, Y. (1993). Measurement of Ice Distribution on an Icebreaker Bow Model Composed by Load Panels. *10th International Conference on Port and Ocean Engineering under Arctic Conditions (POAC'93),* pp. 329-337.

Kendrick, A., Dadachanji, N., and Quart, B. (1984). M.V. ARCTIC – Maneuvering Performance in Ice. *Final Report.* Transport Canada. TP 5684E.

Kerr, A. (1975). The bearing capacity of floating ice plates subjected to static or quasi-static loads: a critical survey. *U.S. Army Cold Regions Research and Engineering Laboratory*, Hanover, N.H., Research Report 333.

Kerr, A. (1976). The Bearing Capacity of Floating Ice Plates Subjected to Static or Quasi-Static Loads. *Journal of Glaciology*, Vol. 17, No. 76, pp. 229-268.

Kerr, A. (1996). Bearing Capacity of Floating Ice Covers Subjected to Static Moving and Oscillatory Loads. *Applied Mechanics Reviews*, Vol 49, No. 11, pp. 463-476.

Kerr, A., and Haynes, F. (1988). On the determination of the average Young's modulus for a floating ice cover. *Cold Regions Science and Technology*, Vol. 15, pp. 39-43.

Kerr, A., and Palmer, W. (1972). The Deformations and Stresses in Floating Ice Plates. *Acta Mechanica*, Vol. 15, pp. 57-72.

Kivimaa, S. (1992). Full-Scale Trials on Hull Resistance and Bow Ice Load in Level Ice on Board the Cutter M.S. Uisko. *Third International Conference on Ice*

Technology, Cambridge, MA, USA, Advances in Ice Technology, Computational Mechanics Publications, Boston, pp. 169-180.

Kivimass, S. (1993). Long-Term Ice Load Measurement with an Ice Load Panel on Board the Cutter M.S. Uisko. *Proceedings of the 12th Int. Conference on Port and Ocean Engineering under Arctic Conditions (POAC'93)*, Vol.1, pp. 338~347.

Kotras, T., Baird, A., and Naegle, J. (1983). Predicting ship performance in level ice. *Trans. SNAME (Society of Naval Architects and Marine Engineers)*, Annual Meeting, Vol.91, New York, pp.329-349.

Kujala, P. (1994a). On the Statistics of Ice Loads on Ship Hull in the Baltic. *Dissertation for the degree of Doctor of Technology*, Mechanical Engineering Series No. 116, Helsinki University of Technology, Espoo, Finland.

Kujala, P. (1994b). Ship-Ice Contact and Design Ice Loads. *International Conference and Exhibition on Performance of Ships and Structures in Ice (Icetech'94)*, pp. A1-A19.

Kujala, P. (1996). Semi-empirical Evaluation of Long Term Ice Loads on a Ship Hull. *Marine Structures*. Vol. 9. pp. 849-871.

Lau, M. (2001). A Three Dimensional Discrete Element Simulation of Ice Sheet Impacting a 60 ° Conical Structure. *Proceedings of the 16th International Conference on Port and Ocean Engineering under Arctic Conditions*, Ottawa, Ontario, Canada, pp. 431-440.

Lau, M., Molgaard, J., Williams, F.M., and Swamidas, A. (1999). An Analysis of Ice Breaking Pattern and Ice Piece Size around Sloping Structures. *Proceedings of 18th International Conference on Offshore Mechanics and Arctic Engineering*, St. John's, Canada, pp. 1-9.

Lau, M. (2006). Discrete Element Modeling of Ship Maneuvering in Ice. *Institute for Ocean Technology (NRC/IOT) Report,* IAHR'06, Japan (CD).

Lau, M. (2007). Preliminary Modeling of Ship Manoeuvring in Ice Using a PMM. *Institute for Ocean Technology (NRC/IOT) Report*, TR-2006-02.

Lau, M., and Derradji, A. (2007). Phase IV Experimental Uncertainty Analysis for Ice Tank Ship Resistance and Manoeuvring Experiments using PMM. *Institute for Ocean Technology (NRC/IOT) Report*, TR-2006-03.

Lau, M., Liu, J.C., Derradji, A., and Williams, F.M. (2004). Preliminary Results of Ship Maneuvering in Ice Experiments Using a Planar Motion Mechanism. *Proceedings of the 17th International IAHR Symposium on Ice*, Saint Petersburg, Russia, pp. 479-487.

Lee, J., and Wang, Y.S. (1987). Vessel Transit Through Ridged Ice. *Proceedings of the 6th International Conference on Offshore Mechanics and Arctic Engineering (OMAE'87)*, Houston, USA, pp. 210-223.

Lewis, J.W., and Edwards, R.Y. (1970). Methods for Predicting Icebreaking and Ice Resistance Characteristics of Icebreakers. *SNAME*, Vol. 78, pp. 213-249.

Lewis, J.W., and Edward, R.V. (1989). Principles of Naval Architecture, Volume III, Motions in Waves and Controllability. Published by *The Society of Naval Architecture and Marine Engineers (SNAME)*, Jersey City, NJ, USA.

Lewis, J.W., Deford, F.W., and Butat, V. (1982). Resistance and Propulsion of Ice-Worthy Ships. *TRANS. SNAME,* Vol. 90, pp. 249-276.

Lindqvist, G. (1989). A Straightforward Method for Calculation of Ice Resistance of Ships. *Proceedings of the 10th International Conference on Port and Ocean Engineering under Arctic Conditions (POAC'89)*, Lulea, Sweden, pp. 722-735.

Lindstrom, Carl-Anders. (1990). Numerical Simulation of Ship Manoeuvring Motion in Level Ice. *Proceedings of POLARTECH'90,* Copenhagen Denmark, pp. 198-208.

Lindstrom, Carl-Anders. (1991). Numerical Estimation of Ice Force Acting on Inclined Structures and Ships in Level Ice. *Proceedings of 22nd Offshore Technology Conference,* OTC 6445, Houston, Texas, pp. 209-216.

Liu, J., Lau, M., and Williams, F.M. (2006). Mathematical Modeling of Ice-Hull Interaction for Ship Manoeuvring in Ice Simulations. *International Conference and Exhibition on Performance of Ships and Structures in Ice*, Banff, Alberta, Canada, ICETECH06-126-R0, (CD).

Liu, J., Lau, M., and Williams, F.M. (2007a). Mathematical Modeling of Ice-Hull Interaction for Real Time Simulation of Ship Manoeuvring in Level Ice. *Institute for Ocean Technology (IOT) Report*, LM-2007-06.

Liu, J., Lau, M., and Williams, F.M. (2007b). Software of IHI Model for Simulating Ship Manoeuvring in Level Ice. *Institute for Ocean Technology (IOT) Report*, LM-2007-07.

Liu J., Lau, M, and Williams F.M., (2008). Numerical Implementation and Benchmark of Ice-Hull Interaction Model for Ship Maneuvering Simulations, Proceedings of the 19th International IAHR Symposium on Ice, Vancouver, Canada, pp215~226.

Liukkonen, S. (1988). Friction Panel Measurement in Full-Scale and Model-Scale Icebreaking Ship Tests. *Proceedings of the 7th International Conference on Offshore Mechanics and Arctic Engineering*, Houston, Vol. IV, pp. 255-262.

Majid, I and Menon B., (1983). Investigative Study of Simulation Techniques and Navigation Problems for the Arctic Marine Environment, Prepared for Transportation Development Centre, TP 4339, Transport Canada, Montreal by Arctec Canada Ltd, Ottawa, Report No. FR964C.

Manual of MATLAB R. (2007a). Version 7.2.0.232, the Mathworks Inc.

Marineering Limited. (1997). The development and commissioning of a large amplitude planar motion mechanism for maneuvering of ships in ice and open water. *Institute for Ocean Technology (IOT) Report*, CR-1997-05.

Marton, C.G. (2000). Ice Navigation Simulation – Phase II. *Prepared for Transportation Development Center*, Transport Canada, by PhiloSoft Inc, Quebec, TP 13676E

Marton, C.G. (2001). Ice Navigation Simulation – Phase III. *Prepared for Transportation Development Center*, Transport Canada, by PhiloSoft Inc, Quebec, TP 13790E

Mckenna, R. (1993a). Ice Wedge Dynamics and Local Crushing. *Proceedings of 12th International Conference on Port and Ocean Engineering under Arctic Conditions (POAC'93)*, Hamburg, pp. 85-96.

Mckenna, R. (1993b). Scaling Relations for Icebreaking based on Analysis of a Simple Wedge. *Proceedings of 12th International Conference on Port and Ocean Engineering under Arctic Conditions (POAC'93)*, Hamburg, pp. 85-96.

Menon, B., Edgecombe, M., Tue-fee, K., and Glen, I. (1986). Manoeuvring Tests in Ice Aboard USCGC Polar Star in Antarctica 1985, *Maritime Administration,* Department of Transportation 400 Seventh Street, S.W. Washington D.C., 20590, Arctec Canada Limited, 311 Leggett Drive, Kanata, Ontario, Canada K2K 1Z8.

Menon, B., Glen, I., Steele, M., and Hardiman, K. (1991). Investigation of Ship Maneuverability in Ice-Phase I. *Transport Canada*, TP 10922E.

Menon, B., Steele, M., Samwel. L. (1988).Development of a Canadian Arctic Bridge Navigation Simulator: Validation of a Ship-handling Model. *Prepared for the Transportation Development Centre of Transport Canada*, Fleet Technology Limited, Arctec Canada Limited, 311 Leggett Drive, Ontario, Canada.

Michel, B. (1978). Ice Mechanics. *LES PRESSES OF L'UNIVERSITE LAVAL*, Quebec, Canada.

Milano, V.R. (1973). Ship Resistance to Continuous Motion in Ice. *SNAME Transactions*, Vol. 81.

Milano, V.R. (1975). Variation of Ship/Ice Parameters on Ship Resistance to Continuous Motion in Ice. *Proceedings of Ice Tech 75*, pp. B1-B26.

Milano, V.R. (1980). A Re-analysis of Ship Resistance When in continuous motion through solid ice. *Proceedings Intermaritec Symposium*, Hamburg, pp. 456-475.

Molyneux, W.D., and Williams, F.M. (1999). Ship Powering Performance in Multiple Layers of Broken Ice. *Proceedings of 18th International Conference on Offshore Mechanics and Arctic Engineering (OMAE'99)*, July 11-16, St. Johns, Newfoundland, Canada, pp. 1-9.

Molyneux, D, Williams, F.M., and Lam, C. (1998). Evaluation of Performance Limitations for Ships Navigating to and from VOISEY's Bay Part 2; Effect of Draft on Bulk Carrier Resistance and Propulsion. *Institute for Ocean Technoloyg (NRC/IOT) Report*, TR-1998-03.

Molyneux, D., Williams, F.M., and Hoffmann, K. (1998a). Evaluation of Performance Limitations for Ships Navigating to and from Voisey's Bay Part 4; Effect of Friction Coefficient on the Resistance and Propulsion of the R-Class Icebreaker. *Institute for Ocean Technoloyg (NRC/IOT) Report*, TR-1998-06.

Molyneux, D, Williams, F.M., and Hoffmann, K. (1998b). Evaluation of Performance Limitations for Ships Navigating to and from Voisey's Bay Part 5; Maneuvering Experiments in Level, Pack and Rubble Ice. *Institute for Ocean Technoloyg (NRC/IOT) Report*, TR-1998-07.

Molyneux, D, Williams, F.M., and Hoffmann, K. (1998c). Evaluation of Performance Limitations for Ships Navigating to and from Voisey's Bay Part 6;

Summary of experiment data. *Institute for Ocean Technoloyg (IOT) Report*, TR-1998-08.

Murray, J., and Spencer, D. (1997). A Simulation Model for a Turret Moored Tanker in Pack Ice Cover. *Proceedings of the 16th International Conference on Offshore Mechanics and Arctic Engineering/14th International Conference on Port and Ocean Engineering under Arctic Conditions (Joint OMAE/POAC Conference)*, Vol. IV, pp. 135-146.

Naegle, J. (1980). Ice-Resistance Prediction and Motion Simulation for Ships Operating in Continuous Mode of Icebreaking. *Ph. D. Thesis*, University of Michigan, Ann Arbor, USA.

Nevel, D. (1958). The Narrow Infinite Wedge on an Elastic Foundation. *U.S. Army Snow Ice and Permafrost Research Establishment*, Corps of Engineers, Technical Report 56.

Nevel, D. (1963). Circular Plates on Elastic Sealed Foundation. *U. S. Army Cold Regions Research and Engineering Laboratory*. Report 118,

Nevel, D. (1965). A Semi-Infinite Plate on an Elastic Foundation. *U. S. Army Cold Regions Research and Engineering Laboratory*, Report 136,

Nevel, D. (1966). Time Dependent Deflection of a Floating Ice Sheet. *U. S. Army Cold Regions Research and Engineering Laboratory*, Report 196,

Nevel, D. (1992). Ice Forces on Cones from Floes. *Proceedings of 11th IAHR International Symposiums on Ice,* Vol. 3, Banff, pp. 1391-1401.

Newbury, S. (1988). Icebreaking Experiments with 1:20 and 1:40 Scale Models of the CCG R-class Vessel. *Institute for Ocean Technology (IOT) Report*, TR-AVR-10.

Newbury, S. (1989). A Study of Ship Resistance in Pack Ice. *Institute for Ocean Technology (IOT) Report*, CR-1989-29.

Newbury, S. (1991). Modelling Techniques for Icebreaking Hull Forms. *Institute for Ocean Technology (NRC/IMD) Report*, LM-1991-10.

Newbury, S. (1992). Repeatability of Resistance Experiments in Ice with a 1:20 Scale Model of the Canadian R-Class Icebreaker. *Proceedings of American Towing Tank Conference (ATTC)*, New Orleans.

Newbury, S., and Williams, F. (1986a). R-Class Icebreaker Model Experiments. *Proceedings First International Conference on Ice Technology*, Springer-Verlag, Berlin, Boston, pp. 333~348.

Newbury, S., and Williams, F. (1986b). R-Class Icebreaker Model Experiments Results. *Institute for Ocean Technology (NRC/IOT) Report*, LM-AVR-04.

Patterson, A. (2002). Simulation and Modeling in Innovation. *Presented at Annual General Meeting of the International Marine Simulator Forum*, Keelung, Taiwan.

Patterson, A. (2003). Human Resource Issues in the Marine Transportation Industry. *Presented at the Ocean Innovation Conference*, St. John's, Canada.

Peirce, T.H., and Peirce, J.C. (1987). A Survey of the Potential for Improving the Maneuverability of Ice-transiting Vessels. *Transport Canada*, TP 8434.

Poznyak, I., and Lonov, B. (1981). The Division of Icebreaker Resistance into Components. *The Society of Naval Architects and Marine Engineers (SNAME)*, No. 19, Ottawa, Ontario, Canada, pp. 249-252.

Puntigliano, F.M. (1997). On the Ship Resistance Under the Design Waterline in the Continuous Model of Icebreaking in Level Ice. *Proceedings of the 16th*

International Conference on Offshore Mechanics and Arctic Engineering (OMAE'97), Vol. IV, Arc/Polar Technology, pp. 73-82.

Riska, K. (1987). On the Mechanics of the Ramming Interaction between a Ship and a Massive Ice Floe. *Dissertation for the degree of Doctor of Technology*, Mechanical Engineering Series No. 43, Helsinki University of Technology, Espoo, Finland.

Riska, K. (2006). Factors Influencing the Development of Routes for Regular Oil Transport from Dikson. *The 7th International Conference and Exhibition on Performance of Ships and Structures in Ice (ICETECH'06)*, Banff, Canada, ICETECH06-153-RF.

Riska, K., and Frederking R. (1987). Ice load Penetration Modeling. *Proceedings of the 7th International Conference on Port and Ocean Engineering under Arctic Conditions (POAC'87)*, Vol. 1, Fairbanks, Alaska, pp. 317-328.

Riska, K., Leiviska, T., Nyman, T., Fransson, L., and Lehtonen, J. (2001). Ice Performance of the Swedish Multi-Purpose Icebreaking Tor Viking II. *Proceedings of the 16th International Conference on Port and Ocean Engineering under Arctic Conditions (POAC'01),* Ottawa, Canada. pp. 849-865

Riska, K., Lohi, P., and Eronen, H. (2005). The Width of the Channel Achieved by an Azimuth Thruster Icebreaker. *Porceedings of the 18th International Conference on Port and Ocean Engineering under Arctic Conditions (POAC'05)*, pp. 647-662.

Riska, K., Patey, M., Kishi, S., and Kamesaki, K. (2001). Influence of Ice Conditions on Ship Transit Times in Ice. *Porceedings of the 16th International Conference on Port and Ocean Engineering under Arctic Conditions (POAC'01)*, Ottawa, Ontario, Canada, pp. 729-745.

Riska, K., Rantala, H., and Joensuu, A. (1990). Full Scale Observations of Ship-Ice Contact. *Faculty of Mechanical Engineering*, Laboratory of Naval Architecture and Marine Engineering, Helsinki University of Technology.

Roderick, K. and Edwards, J. (1979). Modelling the Interaction between Ice and Ships. *Physics and Mechanics of Ice, International Union of Theoretical and Applied Mechanics*, Symposium Copenhagen, Berlin Heidelberg, New York.

Rupp, K., and Jans, P. (1993). Shallow Draft THYSSEN/WAAS-Icebreaker. *10th International Conference on Port and Ocean Engineering under Arctic Conditions (POAC'93)*, pp. 227-237.

Sand, B., and Horrigmoe, G. (1998). Finite element analysis of breaking ice forces on conical structures. *Proceedings of the 14th International Symposium on ice*, Ed. Shen, H T, Vol 1, pp 475 - 482.

Sand, B., and Horrigmoe, G. (2001). Simulation of Ice Ridge Forces on Conical Structure. *Proceedings of the 11th ISOPE Conference*, Vol. 1, Stavanger, Norway, p754-760.

Sanderson, T. (1988). Ice Mechanics---Risks to Offshore Structures. *BP Petroleum Development Ltd*, Graham and Trotman Limited, London.

Shi, Y. (2002). Model Test Data Analysis of Ship Maneuverability in Ice. *Master Degree Thesis*, Faculty of Engineering and Applied Science, Memorial University of Newfoundland, St. John's, Canada.

Shkhinek, K., and Uvarova, E. (2001). Dynamics of the Ice Sheet Interaction with the Sloping Structure. *Proceedings of the 16th International Conference on Port and Ocean Engineering under Arctic Conditions (POAC'01)*, Ottawa, Canada, pp. 639-648.

Sinder, D. (2005). Ice Navigation in the Northwest Passage. *Presented at Ocean Innovation Conference*, Rimouski, Quebec.

Soininen, H. (1998). A Propeller-Ice Contact Model. *Dissertation for the degree of Doctor of Technology*, Helsinki University of Technology, Espoo, 116p.

Sorensen, C. (1978). Interaction between Floating Ice Sheet and Sloping Structures, *Institute of Hydrodynamics and Hydraulic Engineering*, Technical University of Denmark, Lyngby, Denmark, Series Paper 19, 175p

Spencer, D. (1992). A Standard Method for the Conduct and Analysis of Ice Resistance Model Tests. *Institute for Ocean Technology (IOT) Report*, IR-1992-12.

Spencer, D. (1993). Model Ice Resistance Database: A Tool for Designers. *Institute for Ocean Technology (IOT) Report*, IR-1993-26.

Spencer, D. (1998). Development of a New Large Amplitude Planar Motion Mechanism at IMD. *Proceedings of the 15th American Towing Tank Conference*, Iowa City, IA, USA, pp. 6-13-6-18.

Spencer, D., and Hardiman K. (1993). Effect of Lateral Ice Pressure on Ship Resistance. *Proceedings of the 12th International Conference on Port and Ocean Engineering under Arctic Conditions (POAC'93)*, pp. 272-279.

Spencer, D., Harris, C., and Williams, F.M. (1992a). Open Water Ship – Model Correlation of CCGS SIR JOHN FRANKLIN and Model 327. *Institute for Ocean Technology (IOT) Report*, LM-1992-06.

Spencer, D., and Timco, G. (1990). CD Model Ice- A Process to Produce Correct Density (CD) Model Ice. *IHAR Ice Symposium,* Espoo, pp. 756-755.

Spencer, D., Williams, F.M., and Newbury, S. (1992b). Model-scale/full-scale ice resistance correlation for the CCG R-class icebreakers. *Institute for Ocean Technology (IOT) Report*, LM-1992-20.

Spencer, D.S., Jones, J., and Colbourne, D.B. (1992c). A Proposed Standard Method for Conduct and Analysis of Ice Resistance Model Tests. *Institute for Ocean Technology (IOT) Report*, LM-1992-01.

Spencer, D., and Jones, J. (2001). Model-Scale/Full-Scale Correlation in Open Water and Ice for Canadian Coast Guard 'R-Class' Icebreakers. *Journal of Ship Research*, Vol. 45, pp 249-261.

Swamidas, A., Jordaan, I.J., Jones, S.J., and McKenna, R.F. (1991). Modelling of the ice failure processes in ship-ice interaction. *Proc. 11th. Intl. Conf. on Port and Ocean Engineering under Arctic Conditions*, Vol. 2, St. John's, pp. 685-703.

Tatinclaux, J. (1985). Level Ice Breaking by a Simply Wedge. *US Army Corps of Engineers Cold Regions Research & Engineering Laboratory (CRREL) Report*, 85-22.

Thomas, V., Andrew, V., and John, N. (1983). Predicting Ship Performance in Level Ice. *SNAME Transaction*, Vol. 91, pp. 329-349.

Timco, G. (1980). Mechanical Properties of Saline-doped and Carbamide (Urea)-Doped Model Ice, *Cold Regions Science and Technology*, Vol. 3, pp. 45-56.

Timco, G. (1984). Discussion of a Fine Grain Model Ice. *Proceedings of IAHR International Symposiums on Ice, Hamburg*, Germany, Vol. II, pp. 553-554.

Timco, G. (1985). Flexural Strength and Fracture Toughness of Urea Model Ice. *Proceedings of 4th International Conference on Offshore Mechanics and Arctic Engineering (OMAE'85)*., Dallas, TX, USA, Vol. II, pp. 199-208.

Timco, G. (1986). EG/AD/S: A New Type of Model Ice for Refrigerated Towing Tanks, *Cold Region Science and Technology*, Vol. 12, pp. 175-195.

Tryde, P. (1977). Intermittent Ice Forces Acting on Inclined Wedges. *U.S. Army Corps of Engineers Cold Regions Research and Engineering Laboratory (CRREL) Report*, 77-26.

Tucker, J., Patterson, A., Fiander, G., Harris, C., and Spencer, D. (2006). Simulation and Modeling of Navigating in Ice. *Proceedings of International Navigation Simulator Lecturers' Conference (INLSC-14)*, Genoa, Italy.

Tue-Fee, K., and Keinonen, A.J. (1986). Full Scale Maneuvering Tests in Level Ice of CANMAR KIGORIAK and ROBERT LEMEUR. *Marine Technology*.

Tue-Fee, K., et al. (1987). Model for Predicting the Steady Turning Performance of Conventional icebreakers in Level Unbroken Ice. *Proceedings of the International Conference on Ship Maneuvrability*, Paper No. 12.

Valanto, P. (1987). Model Test on the Icebreaking Cycle in Two Dimensions. *Report D64*, Wartsila Arctic Research Center, Helsinki.

Valanto, P. (1989). Experimental Study of The Icebreaking Cycle in 2-D. *Proceedings of the 8th International Conference on Offshore Mechanics and Arctic Engineering (OMAE'89),* Hague, pp. 343-349.

Valanto, P. (1993). Investigation of the Ice-Breaking Pattern at the Bow of the Ib Kapitan Sorokin on the Yenisei River Estuary in May 1991. *Proceedings of the 12th International Conference on Offshore Mechanics and Arctic Engineering (OMAE,93)*, Vol. IV, Glasgow, Scotland, pp. 127-134.

Valanto, P. (1997). On the Icebreaking Forces and Resistance of a Ship Advancing in Level Ice. *Proceedings of the 16th Int. Conference on Offshore Mechanics and Arctic Engineering*, Vol. IV, Arc/Polar Technology, pp. 63-71.

Valanto, P. (2001a). On The Cause and Distribution of Resistance Forces on the Ship Hulls Moving in Level Ice. *Proceedings of the 16th International Conference on Port and Ocean Engineering under Arctic Conditions (POAC'01)*, Ottawa, Ontario, Canada, pp. 803-813.

Valanto, P. (2001b). The Resistance of Ships in Level Ice. *SNAME Transactions*, Vol. 109, pp. 53-83.

Valanto, P. (2006). On the Ice Load Distribution on Ship Hulls in Level Ice. *International Conference and Exhibition on Performance of Ships and Structures in Ice*, Banff, Alberta, Canada, ICETECH06-110-RF, (CD).

Vance, G.P. (1975). A scaling system for ships modelled in ice. *Proceedings of SNAME Ice Tech. Symposium*, Montreal, Paper H1, 28 p.

Varsta, P. (1983). On the mechanics of Ice load on Ships in level ice in the Baltic Sea. *Phd thesis*, Technical Research Centre of Finland, Espoo, Finland.

Varsta, P., and Riska, K. (1977). Failure process of ice edge caused by impact with a ship's side's Ice. *Ships and Winter Navigation Symposium*, Symposium in Oulu University, Oulu, Finland, pp. 235-262.

Vinogradov, O.C. (1986). Simulation Methodology of Vessel-Ice Floes Interaction Problem. *Proceedings of the 5th International Conference on Offshore Mechanics and Arctic Engineering (OMAE'86)*, Japan, Vol. 4, pp. 601-606.

Waclawek, P. (1997). Maneuvers in Ice of CCGS Henry Larsen performed during the 1997 Voyage to Voisey's Bay. *Institute for Ocean Technology (NRC/IOT) Report*, TR-1997-20.

Waclawek, P., Molyneux, D., and Woodward, J. (1998). Ship Maneuvring using the PMM: A Numerical Analysis. *Institute for Ocean Technology (NRC/IOT) Report*, LM-1998-18.

Wadhams, P. (2000). Ice in The Ocean. *Gordon and Breach Science Publishers*, Copyright by 2000 Overseas Publishers Association (OPA).

Wang, J., Akinturk, A., Foster, W., Jone, S.J., and Bose, N. (2004). An experimental model for ice performance of Podded Propellers. *27th American Towing Tank Conference*, St. John's, Canada, pp. 1-7.

Wang, S. (2001). A Dynamic Model for Breaking Pattern of Level Ice by Conical Structure. *PhD dissertation*, Helsinki University of Technology, Department of Mechanical Engineering, Ship Laboratory, Finland, FIN-02015-HUT.

Williams, F.M. (1987). Resistance and Self Propulsion Tests in Ice of High Friction R-Class Model. *Institute for Ocean Technology (IOT) Report*, TR-AVR-04.

Williams, F.M., and Parsons B.L. (1993). Size Effect in the Flexural Strength of Ice. *Institute for Ocean Technology (IOT) Report*, IR-1993-27.

Williams, F.M., Snellen, J.B., and Bell, J.M. (1987).The Effect of Surface Friction on Ship Model Resistance in Level Ice. *Institute for Ocean Technology (NRC/IOT) Report*, TR-AVR-02.

Williams, F.M., Spencer, D., Mathews, S.T., and Bayly, I. (1992). Full Scale Trials in Level Ice with Canadian R-Class Icebreaker. *SNAME Transactions*, Vol. 100, pp. 293-313.

Williams, F.M., Spencer, D., Parsons, B., Hackett, P., Gagnon, B., Everard, J., and Butt, S. (1991). Full-Scale Ice Breaker Trials CCGS Sir John Franklin Indian Arm/Little Burnt Bay 1991, *Institute for Ocean Technology (NRC/IOT) Repo*rt, TR-1991-03.

Williams, F.M., and Waclawek, P. (1998). Physical Model Tests for Ship Maneuvering in Ice. *Proceedings of the 25th American Towing Tank Conference*, Iowa, pp. 9-11-9-16.

Williams, F.M., Waclawek, P., and Hyunsoo, K. (1996). Simulation of Maneuvering in Ice; *IMD-SAMSUNG Collaborative Project Status Report, Institute for Ocean Technology*, St. John's, Canada (Protected), TR-1996-28.

Yamaguchi, H., and Kato, H. (1994). Hydrodynamic Effect of Ship Advance on Ice Flexural Failure. *Proceedings of the 4th International Offshore and Polar Engineering Conference*, Osaka, Japan, pp. 592-595.

Yamaguchi, H., Toyoda, M., and Nakayama, H. (1997a). Influence of Floe Shape on Behavior of Ice Floes around a Structure. *Proceedings of the 16th International Conference on Offshore Mechanics and Arctic Engineering/14th International Conference on Port and Ocean Engineering under Arctic Conditions (Joint OMAE/POAC Conference)*, Vol. IV, pp. 461-468.

Yamaguchi, H., Suzuki, Y., Uemura, O., and Kato, H. (1997b). Influence of Bow Shape on Icebreaking Resistance in Low Speed Range. *Proceedings of the 16th International Conference on Offshore Mechanics and Arctic Engineering/14th International Conference on Port and Ocean Engineering under Arctic Conditions (Joint OMAE/POAC Conference)*, Vol. IV, pp.51-61.

Appendix A Brief Instruction of IHI Model Software

The complete instructions of the generated m-files are provided in IOT report (Liu et al., 2007a). The details of the running of the software are also provided in IOT report (Liu et al., 2007b).

A.1 List of Created M-Files for IHI Model Software

The whole IHI model software consists of three layers, Parameters Input Layer (**PIL**), Core Calculation Layer (**CCL**) and Results Output Layer (**ROL**).

The IHI model software consists of a collection of m-files as follows:

- Trim_chann.m
- Simpl_model_calcu.m
- Shear_mode.m
- Secti_two_line.m
- Secti_ice_break_force.m
- Rank_cross_posit.m
- Prope_ice_calcu.m
- Point_close.m
- Param_input.m
- Output_motio.m
- Output_force.m
- Output_chann.m
- Navigation.m
- Movie_proce.m
- Motion_ship.m
- Monit_calcu.m
- Judge_contact_hull.m
- Ice_force_calcu.m
- Ice_force_initi.m
- Ice_clear_force.m
- Ice_buoya_force.m
- Ice_break_force.m
- Hull_ice_model.m
- Gener_chann.m

- Chann_width_calcu.m
- Chann_close.m
- Calcu_water_line_for_chann.m
- Calcu_water_line.m
- Calcu_p1_p2_force_densi_right.m
- Calcu_p1_p2_force_densi_left.m
- Calcu_cross_point.m
- Calcu_conta_area.m
- Calcu_chann_for_new_chann.m
- Break_horiz_unit_width.m

The **CCL** layer consists of the following routines:

- Trim_chann.m
- Simpl_model_calcu.m
- Shear_mode.m
- Secti_two_line.m
- Secti_ice_break_force.m
- Rank_cross_posit.m
- Prope_ice_calcu.m
- Point_close.m
- Judge_contact_hull.m
- Ice_force_calcu.m
- Ice_force_initi.m
- Ice_clear_force.m
- Ice_buoya_force.m
- Ice_break_force.m
- Hull_ice_model.m
- Gener_chann.m
- Chann_close.m
- Calcu_water_line_for_chann.m
- Calcu_water_line.m
- Calcu_p1_p2_force_densi_right.m
- Calcu_p1_p2_force_densi_left.m
- Calcu_cross_point.m
- Calcu_conta_area.m
- Break_horiz_unit_width

The **ROL** layer consists of the following routines:

- Monit_calcu.m
- Output_chann.m

- Output_force.m
- Output_motio.m
- Movie_proce.m
- Chann_width_calcu.m

A.2 IHI Model Software Running and Result Output

The IHI model simulation can be started through running the main routine, **Navigation.m**. As the present IHI software is designed as VCP (Visual Calculation Program), one figure monitoring the simulation process keeps appearing onscreen during the simulation process as shown in Figure A.1. The simulation progress as the percentage of the total simulation is shown in monitoring figure (Figure A.2) and DOS Command Windows (Figure A.1) instantaneously at the same time. From the monitoring figure, the user can instantaneously monitor simulation progress, surge force, sway force and yaw moment, ship motion and position, channel shape and position and unbroken level ice-ship contact.

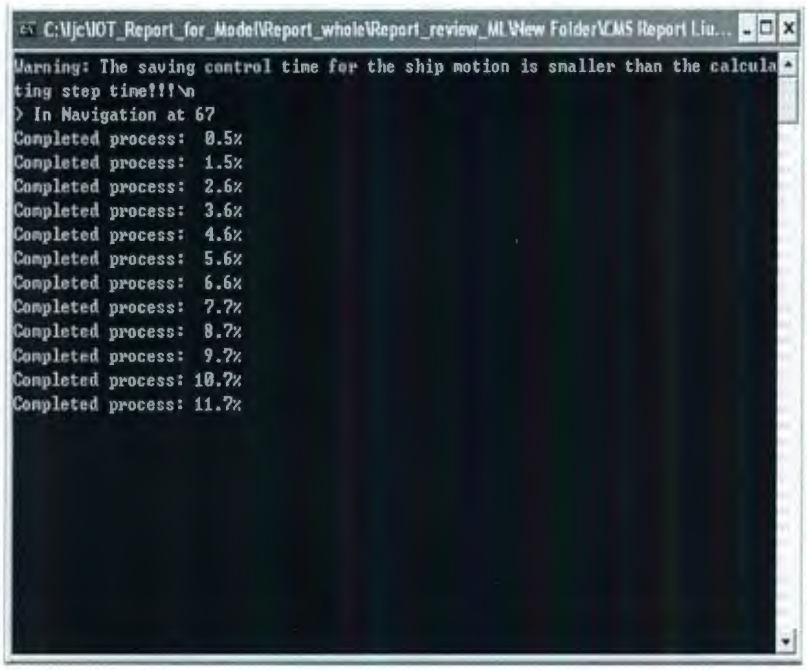

Figure A. 1 DOS window at one simulation run using IHI model software

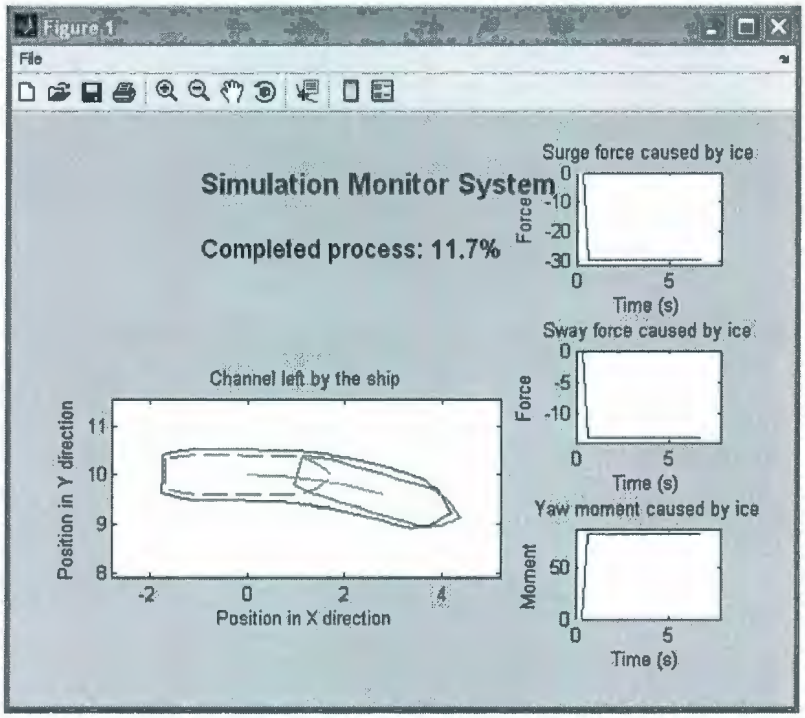

Figure A. 2 Monitor window at each simulation run using IHI model software

The present IHI model software is a working version for developing IHI model, therefore, comprehensive details of the calculation results are recorded and exported for later data check and model verification, those processes can be shut down to increase the model's simulation speed.

The following files recording the simulation results are generated during each simulation run: **Chann_number.dat** stores the shape and position of the ice edge and the ship's positions and stance at some specific moments during ship maneuvers; **Ice_force_each_point.dat** stores the ice forces computed at specified points on ship hull along the water line during the simulation; **Ice_force_global.dat** stores the global ice forces on the hull during ship maneuvers; **Ship_motion.dat** stores the ship's specified motions during the simulation.

Appendix B Movies of Selected Numerical Simulations Using IHI Model

B.1 List of Recorded Movies of the Selected Numerical Simulations

1) ArbitraryManoeuvre_TerryFox.avi

2) Resistance_TerryFox.avi

3) Backing_TerryFox.avi

4) Circle_r109_TerryFox.avi

5) Circle_r218_TerryFox.avi

6) Circle_r1090_TerryFox.avi

7) Circle_r218_dn3_TerryFox.avi

8) Circle_r218_dn10_TerryFox.avi

9) PureSway_TerryFox.avi

10) PureYaw_TerryFox.avi

11) 'Star'_TerryFox.avi

B.2 Brief Descriptions for the Movies

ArbitraryManoeuvre_TerryFox.avi

This movie records the simulated process of terry fox Icebreaker in an arbitrary manoeuvre run, in which the ship's motion is prescribed. The simulation showed that it is impossible to represent such a complicated manoeuvre using a simple analytical approach. The IHI model can satisfactorily simulates this arbitrary manoeuvre and correctly and accurately "feel" the ship motions and ice edge.

Resistance_TerryFox.avi

This movie records the simulated process of Terry Fox Icebreaker in a resistance run with 1.87 m/s velocity and zero drift angle. The simulation showed that only the bow directly contact the unbroken ice and the channel width kept constant.

Backing_TerryFox.avi

This movie records the simulated process of a simplified bare Terry Fox Stern breaking ice in a backing run with 1.87 m/s velocity and zero drift angle. The simulation showed that the IHI model worked well in this specific manoeuvre.

Circle_r5_TerryFox.avi

This movie records the simulated process of Terry Fox Icebreaker in constant radius run with –1.87 m/s tangential velocity, 109 m radius and zero drift angle. The simulation showed that the stern also directly contacts the unbroken level ice. The stern contacting ice is intermittent due to the straight waterline and curve ice edge.

Circle_r10_TerryFox.avi

This movie records the simulated process of Terry Fox Icebreaker in constant radius run with –1.87 m/s tangential velocity, 218 m radius and zero drift angle. The simulation shows that only the bow directly contacts the unbroken level ice.

Circle_r50_TerryFox.avi

This movie records the simulated process of Terry Fox Icebreaker in constant radius run with –1.87 m/s tangential velocity, 1090 m radius and zero drift angle. The simulation shows that only the bow directly contacts the unbroken level ice.

Circle_r10_dn3_TerryFox.avi

This movie records the simulated process of Terry Fox Icebreaker in constant radius run with –1.87 m/s tangential velocity, 218 m radius and -3.0° drift angle. The simulation shows that the aft-body of the hull intermittently directly contacts the unbroken level ice during the run.

Circle_r10_dn10_TerryFox.avi

This movie records the simulated process of Terry Fox Icebreaker in constant radius run with –1.87 m/s tangential velocity, 218 m radius and -10.0° drift angle. The simulation shows that the stern and mid-body continuously directly contacts the unbroken level ice during the running.

PureSway_TerryFox.avi

This movie records the simulated process of Terry Fox Icebreaker in pure sway run with 2.8 m/s tangential velocity, 933.8 seconds period, 54.5 m amplitude in Y direction and zero drift angle. The simulation shows that channel changes in a big

range and nearly one side of the hull from bow to stern directly contacts the unbroken level ice during the running.

Pureyaw_TerryFox.avi

This movie records the simulated process of Terry Fox Icebreaker in pure yaw run with 2.8 m/s tangential velocity, 933.8 seconds period, 54.5 m amplitude in Y direction and zero drift angle. The simulation shows that channel nearly keeps constant and only the bow directly contacts the unbroken level ice.

"Star"_TerryFox.avi

This movie records one prescribed maneuvers similar to the Terry Fox Icebreaker's "STAR" manoeuvre, in which the whole maneuver track consists of three same constant radius arcs tangentially connected with each other. The ship was prescribed with constant zero drift angle and constant tangential velocities. The pivot point was fixed at the mass center of the ship model. The simulation showed that the former channel left by the hull affects the late ice-hull contact, which leads to the continuous changing of the ice-hull contact and the global ice forces on the hull during the run.